Rheological behavior and modeling of waxy crude oils in transient flows

Rafael Mendes

▶ **To cite this version:**

Rafael Mendes. Rheological behavior and modeling of waxy crude oils in transient flows. Mechanical engineering [physics.class-ph]. Université Paris-Est, 2015. English. NNT : 2015PESC1062 . tel-01235326

HAL Id: tel-01235326
https://pastel.hal.science/tel-01235326

Submitted on 30 Nov 2015

HAL is a multi-disciplinary open access archive for the deposit and dissemination of scientific research documents, whether they are published or not. The documents may come from teaching and research institutions in France or abroad, or from public or private research centers.

L'archive ouverte pluridisciplinaire **HAL**, est destinée au dépôt et à la diffusion de documents scientifiques de niveau recherche, publiés ou non, émanant des établissements d'enseignement et de recherche français ou étrangers, des laboratoires publics ou privés.

UNIVERSITÉ PARIS-EST

ÉCOLE DOCTORALE SCIENCES, INGENIERIE ET ENVIRONNEMENT

THESIS

Submitted for obtaining the degree of

DOCTEUR DE L'UNIVERSITÉ PARIS-EST

Specialty: Fluid Mechanics

Presented by:

Rafael Mendes

Thesis subject:

RHEOLOGICAL BEHAVIOR AND MODELING OF WAXY CRUDE OILS IN TRANSIENT FLOWS

Jury:

M. Paulo R. de Souza Mendes	Reviewer
M. Jan Mewis	Reviewer
M. Philippe Marchal	Examiner
M. Guillaume Ovarlez	Examiner
M. Philippe Coussot	Thesis supervisor
M. Guillaume Vinay	Thesis co-supervisor

Presented the 05 June of 2015.

Abstract

Transporting waxy crude oils through long pipelines at low temperatures may be challenging, particularly the flow restart operation after a pipeline shut-in, due to the oil viscosity increase. The rheological behavior of a model waxy oil with macroscopic flow properties analogous to waxy crude oils is first analyzed using Magnetic Resonance Imaging velocimetry associated to stress measurements in a Couette geometry. While flowing at constant temperature, major irreversible structure break depending on the shear intensity are observed. Thus, the critical apparent shear stress, beyond which the material flows, depends on the thermal and flow histories of the oil. Next, the rheological behavior of two waxy crude oils is studied using rheometrical tests (creep tests, flow restarts, abrupt changes of shear rate and steady flow) after different flow histories, notably during the cooling process. Then, those experimentally observed trends are modeled. Additionally, a comprehensive study of the yield stress in function of flow and temperature histories is presented. It provides an approach for describing the yield stress field inside the pipeline at the flow restart moment. Finally, the entire rheological model is implemented in the computational code for simulating waxy crude oils flow restart in a real scale pipeline.

Keywords: waxy oils, rheological model, irreversible destructuring, yield stress fluid, flow restart, MRI velocimetry.

Résumé

Titre : Comportement rhéologique et modélisation des bruts paraffiniques en écoulements transitoires.

Le transport des bruts paraffiniques, et tout particulièrement leur remise en écoulement après un arrêt, dans de longues conduites sous-marines soumises à de basses températures, peut être difficile du fait de l'augmentation de leur viscosité. Le comportement rhéologique d´une huile paraffinique modèle, possédant des propriétés macroscopiques d'écoulement analogues à celles des bruts paraffiniques, est d'abord analysé en utilisant la vélocimétrie par imagerie par résonance magnétique associée à des mesures de contrainte de cisaillement au sein d'une géométrie Couette. Nous montrons que lors d'un écoulement forcé à température constante le matériau subit une déstructuration irréversible qui dépend de l'intensité du cisaillement. Ainsi la contrainte apparente critique permettant l'écoulement du matériau dépend de l'histoire thermique et d'écoulement subie par le matériau. Nous étudions ensuite le comportement rhéologique complet de deux bruts réels à partir de différents types de tests rhéométriques (fluages, redémarrage, régime permanent, changement brusque de vitesse) pour différentes histoires d'écoulement, notamment pendant la période de refroidissement. Le comportement détaillé du matériau en régime transitoire ainsi observé peut alors être modélisé. De plus les variations du seuil de contrainte en fonction de l'histoire thermique et de l'écoulement sont aussi décrites, ce qui nous donne le champ de contrainte seuil dans la conduite à l'état initial. Le modèle dans son ensemble est finalement implémenté dans un code de calcul pour simuler le redémarrage de l´écoulement d'un brut paraffinique dans une conduite réelle.

Mots clés : bruts paraffiniques, modèle rhéologique, déstructuration irréversible, fluide à seuil, redémarrage d'écoulement, vélocimétrie par IRM.

Résumé Substantiel

L'objectif de cette thèse est de développer une meilleure caractérisation rhéologique des bruts paraffiniques afin de prédire avec plus de précision les conditions de redémarrage des conduites de pétrole lorsque l´écoulement a été interrompu. La motivation et la pertinence du travail, ainsi que les principaux problèmes qui se posent, sont présentés dans le Chapitre 1.

Le Chapitre 2 donne un aperçu détaillé et critique de la littérature pertinente. Une attention particulière est posée sur les modèles de comportement thixotrope et les études rhéologiques des bruts en écoulement dans les conduites pétrolières. La définition de la contrainte seuil et des méthodes de mesure sont discutés. Des travaux antérieurs sur la modélisation de l´écoulement dans les conduites sont aussi discutés.

Deux bruts paraffiniques et un mélange d'une huile minérale avec de la paraffine ont été sélectionnés en tant que matériaux de test (Chapitre 3). Le chargement des échantillons et les procédures d'essais sont importants en raison de la forte incidence de l'histoire de cisaillement et de la température sur les résultats. Des procédures de test appropriées ont été sélectionnées pour s'assurer des résultats les plus représentatifs possibles. L'homogénéité thermique dans les échantillons au cours des expériences avec des changements de température a été vérifiée numériquement. La technique de vélocimétrie par IRM est présentée ainsi que les procédures opératoires pour réaliser les essais.

Dans le Chapitre 4, des tests rhéologiques préliminaires confirment que, dans la gamme de températures accessibles pour l'IRM, le comportement du fluide modèle est similaire à celui d'un brut paraffinique. Ces essais confirment également la lente reprise de ces matériaux une fois que leur structure a été détruite par cisaillement. Les mesures IRM sont particulièrement bien adaptées pour évaluer les profils de vitesse dans une géométrie Couette de gap 2 cm, à partir desquels les taux de cisaillement locaux sont calculés. Les couples correspondants sont mesurés séparément, permettant de calculer les viscosités instantanées locales. Les profils de viscosité ainsi générés sont un moyen de comparer les structures obtenues pour différentes histoires thermo-mécaniques. De cette manière, l'effet du taux de cisaillement pendant et après le refroidissement a été évalué, fournissant un aperçu plus détaillé de ces phénomènes. Le cisaillement imposé pendant le refroidissement affecte non seulement le niveau moyen de la structure, mais peut aussi créer un état de structure hétérogène dans le système. Il pourrait également être conclu que, après refroidissement, la vitesse de cisaillement maximale à laquelle l'échantillon est soumis détermine le comportement ultérieur, ce qui suggère donc une irréversibilité de l´état de structure de ces bruts paraffiniques. Un certain degré de réversibilité est détecté à des taux de cisaillement faibles. Ces résultats fournissent une base solide pour l'expérimentation et la modélisation ultérieure.

Afin d'obtenir des informations plus détaillées sur la réponse rhéologique induite par l'écoulement sur la structure du matériau, des expériences à contrainte imposée ou taux de cisaillement imposé sont présentées dans le Chapitre 5. Des test à contrainte imposée induisent un changement trop brusque de la structure pour être soumis à une analyse détaillée. Avec les

tests systématiques à taux de cisaillement constant, il est démontré que les effets de la déformation et du taux de cisaillement sur la réponse rhéologique du matériau peuvent être séparés, de façon indépendante pour les faibles déformations. L'effet de la déformation est confirmé par des expériences additionnelles où le taux de cisaillement imposé évolue par paliers. Une réduction irréversible de la viscosité après une augmentation du taux de cisaillement est confirmée par la réduction systématique du taux de cisaillement après qu´un état d´équilibre a été atteint.

Les conclusions des expériences donnent lieu à de nouvelles connaissances sur la rhéologie des bruts paraffiniques et fournissent également une base pour développer un nouveau modèle rhéologique, présenté dans le Chapitre 6. Le modèle proposé est basé sur un comportement à l'état d´équilibre obtenu en augmentant systématiquement le taux de cisaillement. Les viscosités obtenues dans ces conditions sont supposés être constantes pendant la réduction du taux de cisaillement, sous l´hypothèse d'une déstructuration irréversible. Dans l'équation cinétique décrivant l´évolution de la viscosité du matériau, les effets de la déformation et du taux de cisaillement sont séparés et pondérés par des coefficients. Le modèle est testé en comparant les prédictions avec des expériences d´écoulements transitoires qui n'ont pas été utilisées pour ajuster les paramètres du modèle. Ces comparaisons montrent des bons résultats. De plus, le modèle de Houska, qui suppose la réversibilité totale de l´état de structure du matériau, est aussi évalué.

Afin de calculer le redémarrage de la conduite rempli de brut paraffinique gélifié, il est impératif de prévoir l'impact de diverses conditions thermo-mécaniques sur la contrainte seuil lors de la gélification. Le Chapitre 7 présente différentes techniques pour mesurer la contrainte seuil. La méthode choisie pour mesurer la contrainte seuil consiste à imposer un faible taux de cisaillement constant, et observer la réponse en contrainte du matériau en définissant la valeur maximale mesurée comme la contrainte seuil. Cette méthode est systématiquement utilisée pour étudier l'effet sur la contrainte seuil des paramètres thermo-mécaniques pendant et après le processus de refroidissement. Le cisaillement lors du refroidissement provoque une baisse significative de la contrainte seuil. Le taux de cisaillement lors du refroidissement est jugé important, mais sa magnitude est importante uniquement pour des taux de refroidissement élevés. La déformation critique associée à la contrainte seuil est approximativement constante pour les différentes conditions d'essai. Toutes ces données sont utilisées pour modéliser la contrainte seuil après des différentes procédures de refroidissement.

Avec les résultats précédents un cas test pratique de redémarrage de l´écoulement dans une conduite avec un brut paraffinique est abordé dans le Chapitre 8. L´approche est basée sur la substitution du modèle rhéologique de Houska dans le simulateur numérique StarWaCS. La mise en œuvre numérique est discutée et les résultats des tests de redémarrage sont présentés pour la vitesse, la température et le champ de contrainte seuil reconstruit à partir des conditions de refroidissement du brut dans la conduite. Cela permet de tirer des conclusions nouvelles et intéressantes sur la façon dont l´écoulement d'un brut paraffinique redémarre selon les différentes situations de gélification.

Acknowledgments

I am thankful to a number of people that made this thesis possible. I first thank Guillaume Vinay, who supported the idea of this project from the beginning, supervising it, being always available for helping me with productive discussions and for his friendship.

I am grateful to my thesis supervisor Philippe Coussot, who has guided me through the research process, teaching me to look for what is scientifically relevant. With his experience and expertise, our discussions have made me sure that we would accomplish a nice work.

I have also had enlightening discussions with Guillaume Ovarlez, always with an intelligent idea to improve the work.

I have had a nice support at the laboratories from both IFPEN and UPE, thanks to Isabelle Hénaut, Brigitte Bétro and François Bertrand.

I thank Petrobras for financing this thesis.

I am grateful to the friends from Petrobras who have helped me to start this project. Many thanks to Marcelo, Roberto, Ziglio and José Roberto.

The colleagues from IFPEN have provided a great ambiance, making us feel at home in France. Thanks Philippe, David, Eléonore, Gilles, Florence, Martin, Véronique, Jean Christophe, Fred, Pauline, Laurent, Thierry, Manu, Navid, Nadège, Christelle.

Even being distant, my father, mother and sister were present with a word of care, believing in me more than myself.

My personal and professional accomplishments pass by the hands of my wife Luciana. I can always rely on her, she is always there. Thanks Lu for facing this challenge by my side. Together we are strong. Together, in this period in France, we gained experiences, culture and we had Arthur, the most important and the greatest joy of our lives.

CONTENTS

CHAPTER 1

INTRODUCTION

In offshore petroleum production, long subsea pipelines may be used for transporting crude oil to shore or another offshore facility. In this exporting model, after the petroleum primary processing in a production unit, the crude oil is pumped through a pipe to its destination. Subsea pipelines may be hundreds kilometers long in a cold environment, 4 °C when in deep waters, for example. Figure 1.1 depicts the oil exporting pipeline in an offshore petroleum production system. When dealing with a waxy crude oil, normally the oil is pumped at a temperature above its Wax Appearing Temperature – WAT – which is the temperature below which solid crystals of paraffinic components start forming. The pumps output pressure and power should be enough to keep the steady state flow condition. Along the flow, the oil loses heat to the environment, cooling, eventually below the WAT, and becoming more viscous. If, by any reason, the flow stops, the temperature in the entire pipe will decrease until reaching the equilibrium with the exterior. The entire pipe may become full of gelled oil, due to the solidification of its paraffinic components (see Figure 1.2). Roughly speaking, the oil gel is said to exhibit a yield stress.

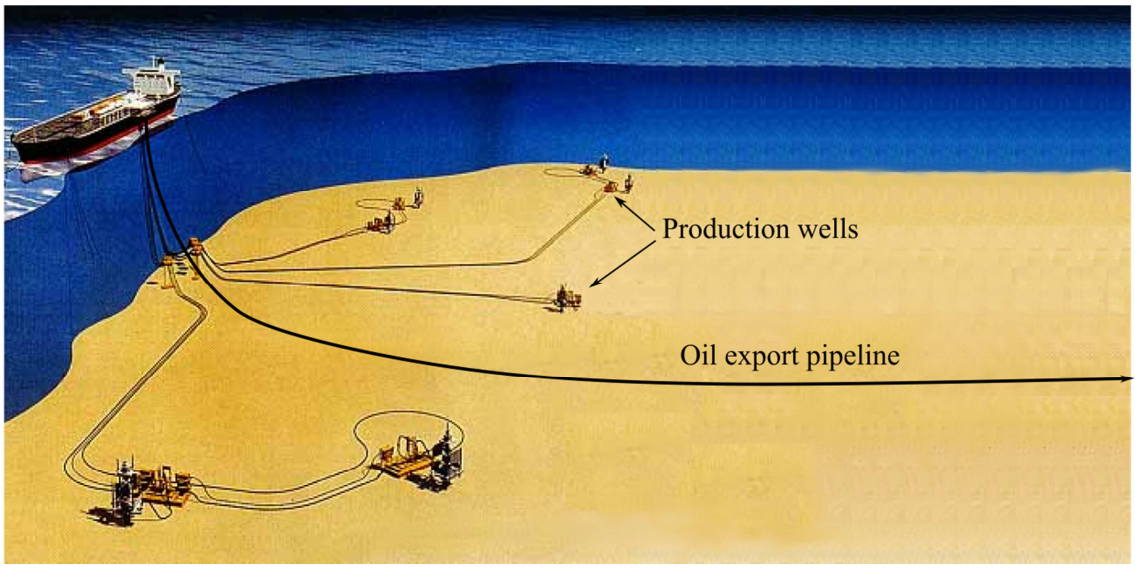

Figure 1.1. Sketch of an offshore petroleum production platform with its production wells and an oil export pipeline to shore. The pipeline lays on the sea floor and the vertical part of the pipe connecting it to the platform is called riser.

In that condition, the pumps maximum output pressure must be designed to overcome the additional resistance imposed by the gel and to resume the flow. The pressure for restarting a gelled pipeline is normally higher than the steady state operational pressure. In the scenario of a long pipeline, where steady state pump pressure may be as high as 80 bar, additional pressure requirements may become very expensive, if not prohibitive. Hence, it is important to have a

good estimation of the restart pressure for: First, being able to restart the flow and; Second, not being too conservative, avoiding unnecessary costs.

Thus, to resume the flow, the pressure drop imposed to the pipe must provide a local shear stress higher than the fluid yield stress. The classical way to calculate that pressure drop is through an integral force balance in the static fluid. The force imposed by the differential pressure must be higher than the force that the fluid exerts on the pipe wall. Thus, the minimum pressure drop is given by $\Delta P = 4L\tau_c/D$, where L is the pipe length, D is the pipe diameter, and τ_c is the fluid yield stress.

Figure 1.2. Waxy crude oil sample. When below its WAT, as in this image, it exhibits a yield stress.

Venkatesan and Creek [72] reported that the use of that classical expression is a highly conservative approach, overestimating the restart pressure by 3 or 4 times. In fact, that expression represents a static situation, which does not account for dynamic effects created by fluid properties heterogeneity, compressibility and thixotropic characteristics.

Different gel formation conditions may be present in one pipeline shut-in case. It will be seen throughout this work that the oil-gel properties are highly dependent on its thermal and flow histories. As an example of the heterogeneous conditions under which the gel is formed, Figure 1.3 shows a schematic representation of the section average temperature profile for a steady state flow and compares the fluid temperature history in two positions in the pipe. The oil enters the pipe at high temperature and loses heat to the ambient along the flow. When the flow stops, the fluid continues its cooling process at rest, or statically. So, the fluid far downstream from the entry of the pipeline is mostly cooled under shear and the region closer to the pipe entrance is mostly statically cooled. Different regions of the pipe will have cooled under completely different conditions, thus forming different gel properties. This simple exercise already demonstrates that, in order to avoid overestimations, the yield stress used in the minimum restart pressure calculation by static force balance should actually be a length averaged value, instead of a maximum value of one single flow history.

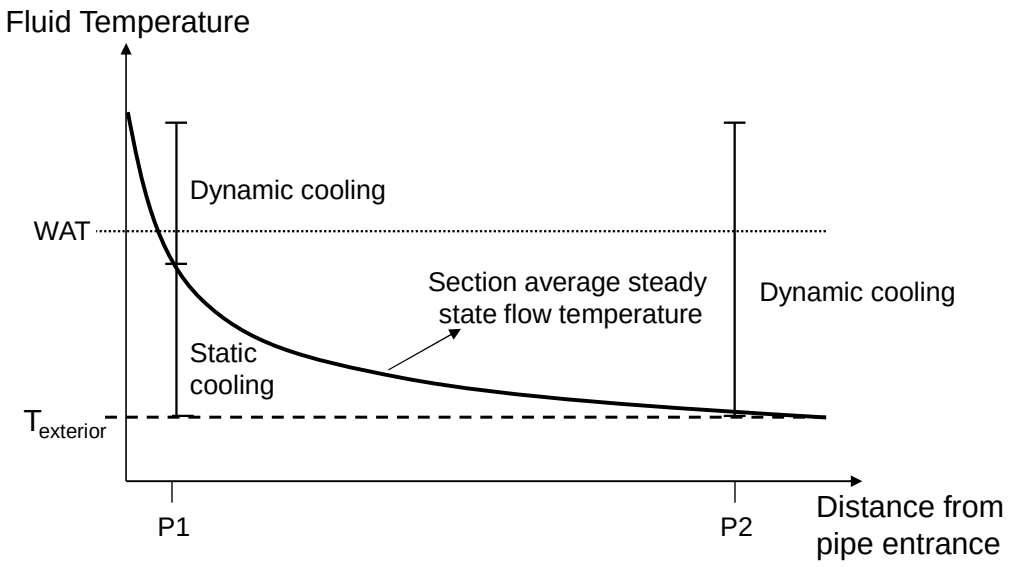

Figure 1.3. Scheme of different fluid temperature histories at two positions in the pipe. The fluid located at P1 has mainly undergone a static cooling, since it has cooled at rest while below the WAT. The fluid at P2, has mainly undergone a dynamic cooling, since it has cooled under flow.

Moreover, the different gel properties along the pipe shall give rise to different rheological behaviors once the flow has restarted. Predicting those rheological behaviors is important for evaluating the flow development and the time to reestablish steady state flow. Pipeline designers need to know how wax crystals affect the oil apparent viscosity, what parameters impact the yield stress development in a pipeline shutdown and how those properties will behave during the flow restart. Ekweribe et al. [20] report problems of transportation of waxy crude oils in 8 different regions in the world.

In general, a better understanding of this process is required and more reliable forecasts are needed to define project conditions of challenging scenarios, as:

- Long-distance oil export pipelines;
- Subsea petroleum production wells;
- Production systems with subsea gas-liquid separators, which need a long single phase pipeline for flowing the separated waxy oil until the production unit;
- Long tie-backs. An error of 20% in the estimation of the pressure required to initiate the flow in a 4 km long production pipeline should not be a problem, but such an error may be a serious issue for pipelines that are 10 times longer.

This work will focus on the offshore crude oil exporting pipelines scenario. In this scenario it is very difficult, or too expensive, to avoid the fluid temperature to drop. Hence, it is difficult to keep the flow above the WAT or avoiding gelling conditions when the flow stops. From the aspects discussed above, it is important to couple fluid properties with the flowing conditions, i.e. the dynamics involved in pipeline transient flow and thermal processes. Thus, it is essential to understand the behavior of the oil-gel flow properties under those conditions, measure the relevant ones and use them in an appropriate pipe flow calculation model.

Under this point of view, a general work plan comes up. This work starts by evaluating a model waxy oil rheological characteristics for different flow and cooling histories. Its rheological behavior is analyzed through the measurement of the local flow characteristics, delineating main rheological trends and acquiring data for a qualitative description. Next, quantitative measurements are performed with waxy crude oils on a standard commercial rheometer, paying attention to the specificities that this kind of fluid may present. At that point, a description of the crude oils physical behavior during complex flow histories shall be available.

The description provided by those analyses defines the characteristics of a rheological model. Thus, a mathematical model is proposed to represent those experimentally observed trends. According to this work plan and in contrast with most previous works in the field, the model is built without *a priori* assumptions based on any classical behavior of a certain class of fluids

The final part of the work applies the acquired knowledge and data in a pipe flow numerical simulation. That simulation shall allow assessing a typical case of pipeline flow restart with gelled oil. In order to provide a complete case study, a detailed analysis of the yield stress developed by a waxy crude oil is required. Thus, systematic yield stress measurements were performed in function of flow and thermal histories that the crude oil may be submitted to. All that rheological information was inserted in a suitable pipe flow model in order to execute complete pipeline flow restart simulations.

The literature review is presented in Chapter 2, gathering the elements involved in the general work plan described above. Then, the experimental materials and methods used in this work are presented in Chapter 3. The rheological behavior of a model waxy oil, with macroscopic behavior analogous to waxy crude oils, is discussed in Chapter 4. That analysis allows defining a new qualitative description of waxy oils rheological behavior. Next, Chapter 5 presents the study of waxy crude oils rheological behavior during complex flow histories. The main physical features identified in the two previous chapters are translated into a mathematical model presented in Chapter 6. In that chapter the predictions of developed model are compared to measured data. Chapter 7 explores a waxy crude oil yield stress behavior in function of different flow and cooling histories. A case study of the flow restart of a long crude oil exporting pipeline is presented in Chapter 8. That study combines all the physical concepts developed in this work. Finally, Chapter 9 presents the major conclusions and an outlook for future developments.

CHAPTER 2

LITERATURE REVIEW

2.1 Introduction

Waxy crude oil gelling occurs when growing paraffin crystals interlock and form volume-spanning links which entrain the remaining liquid oil. According to Visintin et al. [77] this process has been the object of studies for more than 80 years. General literature reviews on the subject may also be found in Rønningsen [55] and Ekweribe et al. [20]. In this literature review, more attention was given to works published in the last 10 or 15 years, since a lot of the previous knowledge was already incorporated in physical and numerical models developed by Rønningsen [55], Sestak et al. [56], and Vinay et al. [75], for example.

Section 2.2 presents the general chemical physics characteristics of the waxy crude oil gels. Then, after introducing some rheological definitions in Section 2.3, the waxy oils macroscopic rheological behavior is presented in Section 2.4. The objective here is to introduce this complex fluid, based on existing works. It will be presented the main parameters of waxy oils rheological behavior, mathematical models, thixotropic characteristics and gelling kinetics.

Next, Section 2.5 introduces the flow restart scenario adopted in this work. Mathematical pipe flow models are discussed under the light of the physical characteristics discussed in the previous sections. Section 2.5 also highlights the influence of the pressure and oil compressibility, where the literature is scarcer, and briefly comments some strategies used by industry while dealing with the gelling oil problem. Finally, Section 2.6 presents the conclusions of this literature review and delineates this research work program.

2.2 General chemical and physical characteristics of waxy crude oils

2.2.1 Chemical composition

A crude oil is a mixture of various hydrocarbons molecules. Its composition is normally divided in major groups of hydrocarbons: alkanes (also called paraffins), naphtenes, aromatics, resins and asphaltenes.

Alkanes and naphtenes (or cycloalkanes) are saturated hydrocarbon molecules. They present only single bonds between carbon atoms. While alkanes present linear (normal – n) or branched (iso) molecules structures, cycloalkanes present at least one ring of carbon atoms. Those two groups are called wax components of a crude oil.

The relative fraction of the major groups may widely vary from oil to oil. Those with higher fraction of alkanes, especially heavy alkanes, are called waxy crude oils. After refining, waxy oils produce valuable fuel products.

Typically, at the petroleum reservoir temperature, the high molecular weight paraffins are dissolved in the liquid matrix that constitutes the oil. But their solubility reduces drastically with the temperature decrease (Singh et al. [57]). So, during the petroleum exploitation they may solidify and form stable crystals. The temperature where the first wax crystals are noticed during the oil cooling is called the Wax Appearance Temperature – WAT.

The length of paraffin chains in solid deposits normally ranges from C16 to C65 (Srivastava et al. [58]), although they were already detected to be as long as C150 (Garcia et al. [23]). Normal-paraffins components are predominant in solid deposits in production and transportation, while the cycle and branched chains mostly contribute for tank bottom sludge (Misra et al. [36]).

Despite the studies done so far, not much can be said about the fluid macroscopic properties based directly on its composition. The amount of solid wax responsible for changing the oil flow behavior may be as low as 2% (Kané et al. [29], Venkatesan and Creek [72]).

Paso et al. [45] analyzed the crystallization process in mixtures of oils and paraffins and reported that the polydispersity of n-paraffins facilitates the gelation process. Rønningsen et al. [54] relate the thermal dependence of the waxy oil properties on the paraffins interaction with other components of the oil, as resins and asphaltenes. In fact, recent interesting studies evaluate the effect of asphaltenes on the wax crystal formation, as Tinsley et al. [68], Oh and Deo [39] and Alcazar-Vara et al. [3]. In global lines, those works conclude that asphaltenes only slightly change the WAT but dramatically depress rheological properties as viscosity and yield stress. The nature of the components is also important. Oils with shorter paraffins chains are more affected by aliphatic asphaltenes, while longer paraffins systems are more influenced by aromatic asphaltenes.

The variations and extremely complex composition of crude oils make very difficult to establish definitive analyses. The works cited above provide general trends. Thus, some degree of variation in physical behavior may be expected for different oils (Visintin et al. [77]).

2.2.2 Microstructure description

Solidification of paraffin follows classical nucleation and growth mechanisms. The appropriate thermodynamic conditions lead to the first crystals formation, which associate into particles (Dirand et al. [17], Paso et al. [45]). Those particles can later aggregate forming larger volume-spanning structures.

N-paraffins are said to crystalize usually into orthorhombic crystals (Dirand et al. [17]). It has been observed that two-dimensional platelets and “pine-cone” structures as the most common (Kané et al. [28]), getting to micrometer order of size in the main axis. Nowadays different visualization techniques can be used for evaluating paraffin crystals. Detailed descriptions of the oil gel crystals morphology may be found in recent works as Kané et al. [28], Paso et al. [45] and Rønningsen et al. [54].

Figure 2.1 presents an example of a microscopic image of a model waxy oil, i.e. a mixture of commercial mineral oil and 5% weight paraffin (details in the next chapter), 9 °C below its WAT. The sample was sheared after static cooling. Paraffin crystals are presented as dark needle-like shapes with length of the order of 10 μm. Individual crystals and cluster can be observed. A detailed analysis of paraffin crystals sizes using microscopic images can be found in Venkatesan et al. [71].

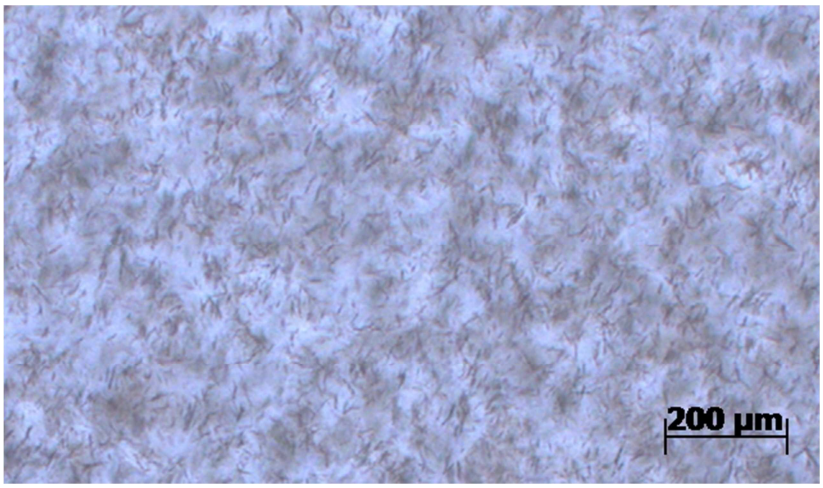

Figure 2.1. Microscope image of the model waxy oil, presented in the next chapter, at 23 °C (WAT is 32 °C) and cooled under shear. Crystals present needle shape with length of the order of 10 µm.

More detailed Images of a waxy crude oil gel microstructure using transmission electron microscopy (TEM) are provided by Kané et al. [28]. Figure 2.2 shows a replica of a fractured gelled crude oil. The sample was cooled at rest to 5 °C. It is possible to identify layers formed by small sub-units of disk-like shapes. According to the authors, the discs are supposed to result from the initial nucleation and from the crystallization at several places where nuclei merged in continuous layers.

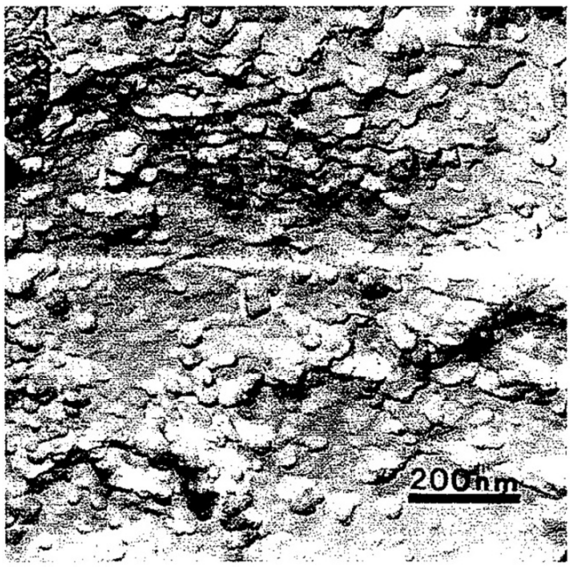

Figure 2.2. Fractured sample of a crude oil gelled at 5 °C after cooling at rest. The edges are serrated, showing disc-like sub-units. Source: Kané et al. [28].

The interaction between those structures would provide the oil with gel characteristics, as stopping the flow against the action of the gravity force, for example (Abdalla and Weiss [1]). Different works cite the action of London and van der Walls forces as responsible for attractive interaction (Abdalla and Weiss [1], Lopes-da-Silva and Coutinho [32]). Those types of forces would provide colloidal characteristics to the suspension of wax particles in the oil.

Since particles interact with each other, even forming larger aggregates, dynamic processes that affect particles formation or relative motion may affect their interaction and consequently the equilibrium of the system. The oil flow, creating shear forces, and cooling rate variations, acting on the solidification process, may modify that equilibrium. Venkatesan et al. [71] reported that shear and thermal histories affect the paraffin network, varying crystal sizes and agglomeration, thus affecting the gel macroscopic strength.

Kané et al. [28] did similar analysis as of Figure 2.2, but with sheared samples. In Figure 2.3(a) the crude oil was sheared at 10 °C, under shear rate of 10 s^{-1}. The formation of layers is less evident. However, some heterogeneous clusters or strings may be seen, as well as some individual discs. In Figure 2.3(b), presenting the same cooling condition but sheared at 500 s^{-1}, smaller discs forming large aggregates are observed. The authors conclude that high shears prevent the growth of large crystals and let their aggregates more spherical in shape and less distributed in size. They say this agrees with lower apparent viscosity measurements with the high sheared sample during cooling.

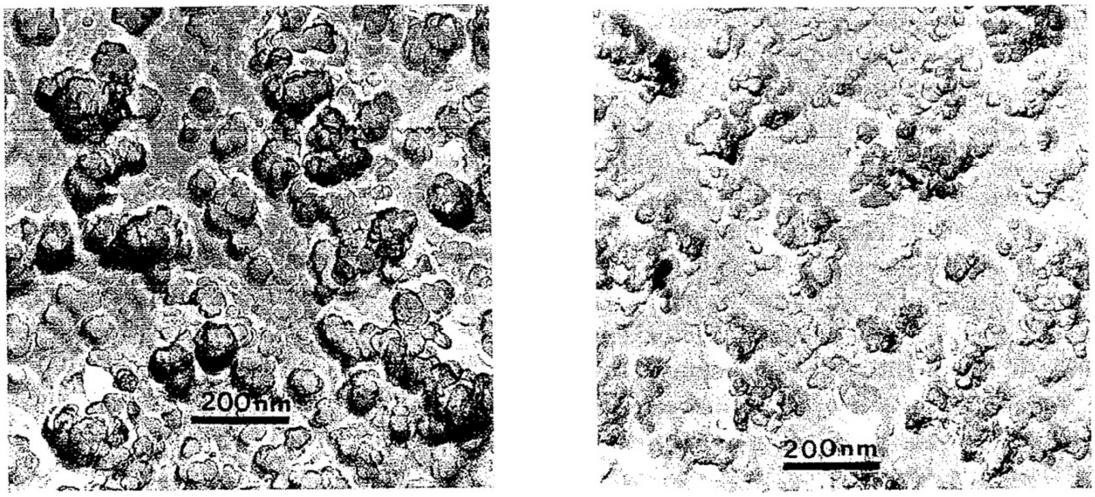

(a) (b)

Figure 2.3. Fractured sample of a crude oil gelled at 10 °C sheared at (a) 10 s^{-1} and (b) 500 s^{-1}.
Source: Kané et al. [28].

Although many works comment on the crystals size and form, the linkage between them, which is very important for understanding the overall structure strength, is not explored. In suspension flows, for example, it is not the size of the particles but how they interact that defines the mixture viscosity (Coussot [11]). In weakly flocculated dispersions, the size of the aggregates is not the only determinant parameter for viscosity determination (Dullaert and Mewis [18]). It seems that a better though global understanding can be obtained more directly from detailed rheometrical measurements, which is one of objectives of this work.

2.2.3 WAT, pour point and gelling temperature

As said in section 2.2.1, the WAT is the temperature where solid paraffin crystals are first noticed during the oil cooling. It is also called cloud point, due to the method of visual observation of the wax crystals appearance using a microscope. Currently, Differential Scanning Calorimetry (DSC) is mostly used for determining the WAT.

When the cooling rate is lower than the paraffin rate of precipitation, i.e. under equilibrium cooling, the measured WAT should be close the paraffin solubility limit, a thermodynamic property. Applying higher cooling rates will make the measured value a process dependent property.

The pour point is also a frequently mentioned property of a waxy crude oil. Its measurement is defined by the ASTM (American Society for Testing and Materials) method D-97. It basically consists in statically cooling the oil sample and evaluating if it flows under the gravity force in intervals of temperature. The lowest temperature where movement is observed is the pour point. It is a reference value for the industry, but of restricted application, since it is related to a specific measuring condition.

The gelation temperature, as defined by Venkatesan et al. [69], is the temperature below which the solid-like behavior takes predominance over the liquid-like behavior of the waxy oil. That comparison can be done by oscillatory rheometry (see Section 2.3). Since the shear and thermal history affect the paraffin network, the gelation temperature can be measured with respect to any cooling condition (cooling rate and applied shear). Thus, this is a more general property, which takes the cooling history into account.

2.3 Some rheological definitions

Before advancing into the macroscopic rheological behavior of waxy crude oils, it is important to define some rheological properties and flow variables.

2.3.1 Fundamentals

The interest in rheology is to determine the resistance to flow of a fluid from simple macroscopic measurements. In other words, determine the relation between stress and deformation of a material.

One way of establishing that relationship using few measurable variables is creating simple shear in the fluid, where fluid layers relatively move to each other under the action of tangential stress. Figure 2.4 presents a sketch of that type of flow between two parallel plates.

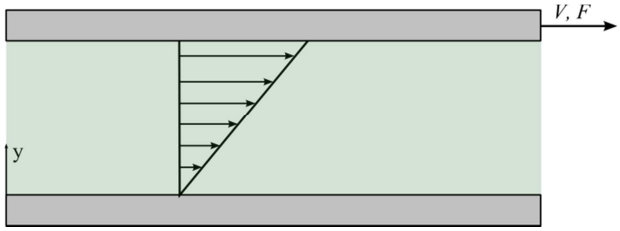

Figure 2.4. In simple shear between parallel plates (Couette flow) the shear rate is constant , so velocity profile is linear. This figure depicts the upper plate moving with velocity *V* under the action of a force *F*.

The upper fluid layer is in contact with the wall that has a velocity *V*, which is the same as the fluid by the no-slip condition. The lower layer is at rest. So, for a simple fluid, the fluid velocity may be written as $V = \dot{\gamma} y$, where $\dot{\gamma}$ is the constant shear rate. Thus, the fluid deformation or strain during a time interval Δt can be written as $\gamma = \dot{\gamma} \Delta t$.

In equilibrium, the tangential stress is constant throughout the fluid. The ratio between the shear stress and shear rate is called apparent viscosity: $\mu_{app}(\dot{\gamma}) = \tau/\dot{\gamma}$. That relationship between shear stress and shear rate represents the fluid rheological behavior.

The fluid rheological data is usually acquired using rheometers. For a given sample condition, they measure the flow in small gaps between rotating geometries, as parallel plates, cone-and-plate or concentric cylinders – Couette geometry. Controlled stress rheometers, for example, apply a torque to its rotating axe and measure the resulting rotational displacement. Through geometrical relations, they calculate the overall sample shear stress and shear rate, without measuring any local flow parameters.

For steady state flow, shear rates and their respective shear stresses are recorded in a certain range. Those data are called the material flow curve. Usually, it is plotted in a shear stress vs. shear rate graphic, and the slope of that curve is the fluid apparent viscosity.

The flow curve measurement aims the fluid steady state flow condition, which is the flow curve condition. For fluids with time-dependent behavior, it is necessary to wait for reaching the steady state condition at each shear condition in order to get the flow curve data points. A rough flow curve estimative may be obtained with increasing and decreasing shear ramps.

The material behavior may be also measured by imposing constant stress and observing the resulting deformation or strain rate. This procedure is called *creep test*. A series of creep tests using a wide range of shear stresses can indicate the fluid rheological behavior and the shape of the flow curve if the steady state flow is achieved. Creep tests may start from the same state of the material and capture its response to different imposed shear stresses. If the material exhibits some kind of internal arrangement or structure, as suspensions, the response of its evolution or destructuration under stress can be measured.

Interesting properties may also be evaluated without effectively flowing the fluid. In small amplitude oscillatory tests small deformations or stresses are applied to the fluid sample observing its response. If a small sinusoidal deformation $\gamma = \gamma_0 \sin(\omega t)$ of amplitude γ_0 and frequency ω is applied to a constant viscosity fluid the stress response will be out of phase with the imposed deformation: $\tau = \mu\dot{\gamma} = \mu\gamma_0\omega\cos(\omega t)$.

If the same oscillatory deformation were imposed to an elastic solid material, the response would be of the type $\tau = G\gamma = G\gamma_0 \sin(\omega t)$, where *G* is the shear elastic modulus.

Some fluids may present elastic behavior under small deformations. Pastes, emulsions or suspensions are typical examples. Small deformations should not affect the material internal organization if it does not exceed a critical value. Simple Kelvin-Voigt materials are modeled as $\tau = G\gamma + \mu\dot{\gamma}$ below the critical deformation, i.e. in the viscoelastic regime. Their response in stress to small oscillatory deformations is:

$$\tau = G\gamma_0 \sin\omega t + \mu\gamma_0\omega \cos\omega t = \tau_0 \sin(\omega t + \phi) \tag{2.1}$$

where ϕ is the phase angle between the imposed deformation and stress response, whose amplitude is τ_0.

This approach may be generalized to any type of viscoelastic material, where the oscillating response is not necessarily sinusoidal but stress amplitude and phase shift can be estimated.

Thus, the elastic (or storage) modulus and viscous (or loss) modulus may be defined, respectively, as

$$G' = \frac{\tau_0}{\gamma_0} cos\phi \text{ and } G" = \frac{\tau_0}{\gamma_0} sin\phi \quad (2.2)$$

Hence, those variables may give an idea of how “elastic” (solid) or “viscous” (liquid) the material behaves in that regime.

2.3.2 Special rheological properties

2.3.2.1 Types of fluids

Fluids may present different behaviors when submitted to shear. Figure 2.5 shows some special examples of flow curves. Those curves can be used to fit the rheological model parameters.

The fluids with viscosity independent of the shear rate and flow history are called Newtonian fluids. Their shear stress - shear rate relation is expressed by $\tau = \mu\dot{\gamma}$.

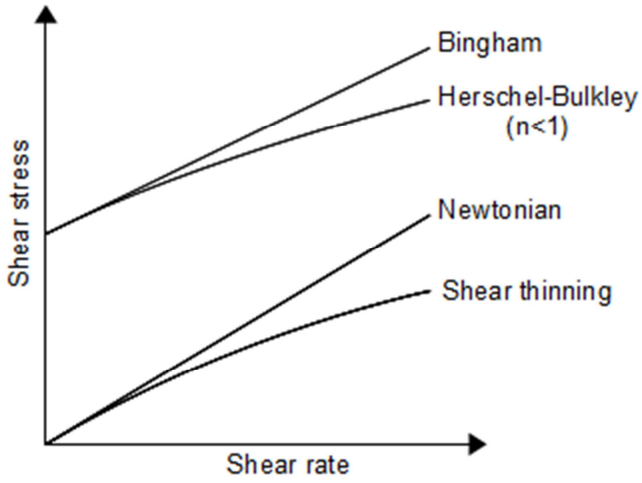

Figure 2.5. Flow curves of special rheological behaviors.

When the apparent viscosity varies with the shear rate the fluids are non-Newtonian. They can be represented by simple relations, as a power-law: $\tau = k\dot{\gamma}^n$, for example. Those who require a minimum stress to flow in simple shear, or a yield stress, can be modeled by the Herschel-Bulkley (HB) model: $\tau = \tau_c + k\dot{\gamma}^n$, where τ_c is that minimum or critical stress. When the exponent n is equal to 1, it is called the Bingham model.

2.3.2.2 Thixotropy

In practice, it may be difficult to measure the shear stress - shear rate relation. Fluid local heterogeneities may let simple shear hard to achieve, creating effects like wall slip (see Figure 2.6). Materials with long transients and flow history dependent fluids require careful experimental procedures. They may induce flow heterogeneities and respond differently to stress, thus disturbing the macroscopic measured data by presenting non-uniform local shear rate. This behavior is typically associated to a competition between an intrinsic restructuring capacity and destructuring effects proportional to the rate of deformation, where material may

require a higher shear stress to flow at lower shear rate. Figure 2.7 illustrates such phenomenon, that may induce the appearance of shear bandings.

Structure changes during flow are generally studied within the frame of thixotropy. This typically concerns materials made of colloidal particles in suspension in a liquid and able to form weak links as a result of colloidal interactions (Mewis and Wagner [35]). The basic rheological trends of such a behavior (see Figure 2.8) are a viscosity decrease in time during flow or increasing shear rate and viscosity increase at rest or decreasing shear rate. It may be characterized with different rheometrical procedures (see Coussot [9]). The fundamental property in that context is reversibility: The flow structure may be broken but will anyway recover its initial characteristics after an appropriate flow history.

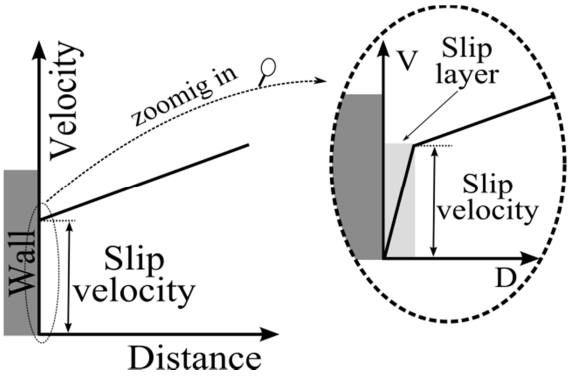

Figure 2.6. Material heterogeneities may create wall slip, where a thin fluid layer with lower viscosity forms between the wall and bulk fluid, giving the (macroscopic) impression that the bulk fluid has a slipping velocity with respect to the solid wall.

Thixotropic characteristics also include overshoot stress at start-up experiments at constant shear rate, followed by stabilization to the steady state stress (Mewis and Wagner [35]). The flow history before each test matters. In creep tests where a sequence of constant stress steps is applied, the apparent viscosity may have a complex behavior, with different delay times to achieve very different steady state values (Coussot et al. [10]).

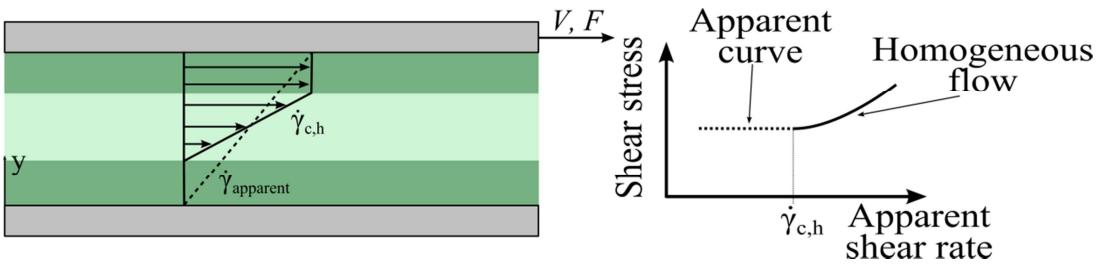

Figure 2.7. Fluids with unstable flow for an apparent shear rate below a critical shear rate $\dot{\gamma}_{c,h}$ induce heterogeneous velocity profile, as shear banding, creating an apparent flow curve.

Modeling such behaviors remains a very difficult task and a wide range of models have been suggested in literature (Coussot et al. [11]) but most of them contain a lot of parameters, which

have no obvious physical meaning or would need a long series of experimental tests to be measured. A similar situation is encountered in the field of waxy crude oil, i.e. various modeling approaches exist (see below), but the experimental data making it possible to fully check the validity of the models are even scarcer, in particular due to the difficulty to control at the same time the flow and temperature histories.

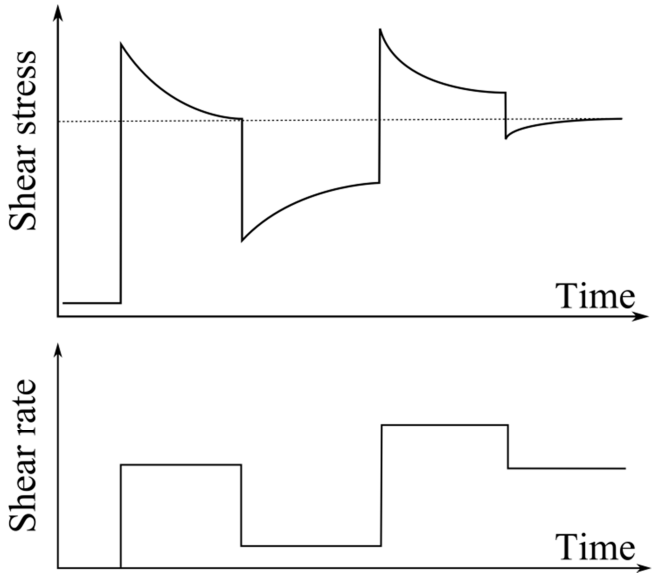

Figure 2.8. Typical thixotropic shear stress response to an imposed shear rate history.

The experimental approach of thixotropic behavior of usual concentrated colloidal systems is also complicated by the flow heterogeneities, such as shear-banding, which were shown to occur in Couette or cone-and-plate geometries (Ovarlez et al. [43], Pignon et al. [50], Møller et al. [38]).

2.3.3 Yield stress definitions

In the previous section, yield stress was presented as the minimum required stress by the fluid to flow. The fluid components may be arranged in certain way providing itself a structure capable of supporting external forces without continuous deformation. In fact, that is a very simple definition for a system that may exhibit complex solid-liquid transition when sheared beyond a critical deformation. That critical deformation corresponds to a critical stress, which also marks the transition from solid (or viscoelastic) regime to the liquid regime.

However, defining the yield stress also involves time-dependent effects. If a series of creep tests is performed, departing from the same material conditions, for shear stresses below the yield stress the material will increase its deformation with time until it stabilizes at a constant value. For shear stresses higher than the yield stress, the rate of deformation will increase until stabilizing in a constant strain rate. That kind of viscoelastic characteristic of the material may lead to long deformation equilibration times when the applied stress is close to the yield stress. Hence, it is time consuming to determine the yield stress experimentally by this method.

A faster but approximate method would be applying a shear stress or shear rate ramp. The beginning of the flow would be more difficult to define, as the material is deforming since the beginning of the test. If the imposed shear ramp is slow enough, a plateau may be observed in

the shear stress vs. shear rate curve. An alternative is to observe the decreasing ramp, looking for the minimum stress at which there was flow, just before the material comes to rest (when $\dot{\gamma} \to 0$). The special case of thixotropic fluids is discussed below.

Dynamic oscillatory tests may also be used to evaluate the yield stress. The oscillation amplitude can be increased with time and beyond a critical deformation the material viscous modulus should be higher than the elastic modulus. Below that critical deformation, the material would be in the solid regime, thus with higher elastic modulus. The oscillatory stress corresponding to the inversion between the moduli is said to be the yield stress. This is also a fast method for determining the yield stress, but submits the material to a complex deformation history.

Thixotropic fluids depend on the flow history, by definition. Thus, experimental procedures for determining its yield stress should take that characteristic into account, like the time at rest before the test and characteristic restructuring and destructuring times *versus* experiment duration. The shear rate or shear stress ramps, for example, should present a hysteresis between the increasing and decreasing ramps. In the increasing shear ramp the fluid presents a more structured state at the test beginning, thus presenting higher yield stress and apparent viscosity at the flow startup. As a result of the destructuring flow, the decreasing ramp may present lower apparent viscosity and the minimum stress to keep the flow should also be lower than the estimated yield stress from the increasing ramp. The yield stress determined from the increasing ramp is also called *static yield stress* and the yield stress from the decreasing ramp is the *dynamic yield stress*.

2.4 Macroscopic rheological behavior of waxy crude oils

2.4.1 General rheological characteristics

At temperatures above the WAT, the waxy crude oil has typically a Newtonian behavior. Its viscosity is independent of both shear rate and flow history and no yield stress is observed.

At temperatures lower than the WAT, the wax crystals network is generally assumed to be at the origin of its non-Newtonian properties. According to Rønningsen [55] the oil exhibits a shear thinning behavior and a yield stress due to the existence of a network of bond linkages. It means that higher the shear rate imposed to the fluid, lower its viscosity, and for starting the flow, a minimum stress must be applied. Even if the yield stress concept may be questioned on a definition basis, for engineering applications it is a very useful concept and represents a reference number that fits well in the time scale of a pipeline restart and related field operations.

Rønningsen [55] also showed time-dependence behavior of waxy crude oils, indicated by a hysteresis loop during a stress ramp test, where the fluid is submitted to an increasing and then decreasing shear stress (this type of test will be discussed in details in Chapter 4). When the analyzed oil is sheared after being cooled at rest, the gel structure breaks down with time, reducing its yield stress and the hysteresis loop amplitude between the stress ramp cycles. So, the flow history has also a strong influence on the gelled oil rheological properties. Its instantaneous properties depend on the experienced flow.

That time-dependency recalls a thixotropic behavior, where the fluid apparent viscosity evolves in time due to the fluid structure changes. Though the classical concept of thixotropy states that

it is a reversible effect, Rønningsen [55] found that in some cases the recovery was not complete after having broken down the structure.

Thixotropic properties associated to structure breakdown and buildup were also described by Kané et al. [29]. Waxy oil structure buildup was also analyzed by Visintin et al. [77], who showed gel properties evolution while holding the fluid at rest at low temperature after different cooling rates and proposed a model for that evolution.

According to Lopes-da-Silva and Coutinho [32], the gel elastic modulus evolution during the holding time after cooling, which in their case lead to higher yield stress, is related to the gel structure development, where crystals reorganize or rearrange bonds.

In addition to those characteristics that may be observed at constant temperature below the WAT, the gel properties are affected by variations in the dynamic process of solids formations. As a result of solidification of some components in a multi-component fluid (as seen in section 2.2.1) and crystals aggregation, the gel properties are affected by the variables of that process. Namely, the solidification rate, whose kinetics is a result of the cooling rate and the shear forces imposed to the crystals during and after their formation. Many works indicate that the typical waxy oil behavior is the decrease of the gel strength with the cooling rate increase and shear rate increase while cooling, independently (Lin et al. [31], Lee et al. [30], Venkatesan et al. [71], Visintin et al. [77]).

The studies presented by Kané et al. [29] and Visintin et al. [77] provide clear evidences of that process dependency, showing that it is imperative to keep the proper tracking of the shear and thermal history of waxy oils to estimate its rheological properties.

Lin et al. [31] and Venkatesan et al. [71] revised studies with different conclusions on the gel properties regarding cooling rate and holding time after cooling. Some discrepancies in the behavior of those properties, as yield stress variations, may be attributed to impurities (Lin et al. [31]) and others to experiments procedures (Chang et al. [5], Venkatesan et al. [71]). Kané et al. [29] reported experiments with waxy oils with poor reproducibility and the possibility of having non-uniform shear at shear rates lower than 10 s^{-1} with cone-and-plate geometry. Dimitriou et al. [14] analyzed a waxy oil by Particle Image Velocimetry in a rheometer and found, for a steady imposed shear rate, fluctuating periods of flow with wall slip and structural erosion, breaking the oil gel progressively in smaller fragments. A comprehensive analysis of waxy crude oils sample preparation and possible sources of problems in rheological measurements can be found in Marchesini et al. [34].

Finally, the picture of a waxy crude oil cooling process may be rather complex: There is a solidification process, which has its own kinetics due to the different paraffin molecules; Then, forming a colloidal-type gel (Lopes-da-Silva and Coutinho [32]), where solids in suspension present interaction forces; In a fluid that may be in motion, with shear between different fluid layers, changing the solids relative position and the formation of aggregates. So, at the end of cooling and phase change, the system may still be out-of-equilibrium, letting place to structure rearrangements. Therefore, the resulting rheological behavior of the gel is function not only of the oil composition but of what happens during and after the cooling process.

2.4.2 Rheological models

2.4.2.1 Yielding model

The waxy oils yielding characteristics was investigated by Chang et al. [5]. They define three yield stresses to characterize the initial yielding of a waxy crude oil: τ_e, the elastic-limit yield stress, below which the fluid exhibits a linear elastic response; τ_s, the static yield stress, the stress at the starting point of immediate fracture or flow; And τ_d, the dynamic stress, an extrapolated shear stress at zero shear rate obtained from the flow curve or from an instantaneous flow curve corresponding to a given sheared state.

According to the same authors, the creep condition, where yielding and plastic deformation start to occur, happens between the elastic and static yield stresses. It means that flow may occur at a shear stress below the static limit if sufficient time is given to the action of this imposed shear stress.

Chang et al. [5] and Chang et al. [6] present graphics of controlled stress and controlled shear tests in linear and log scale and also compare them with oscillatory tests, identifying the stresses limits in each graphic, as in Figure 2.9, for example. The fluid used was a waxy crude oil. All dynamic variables must be carefully controlled, to reduce the difficulty in measuring and defining those stresses in practice, as argued by Møller et al. [37].

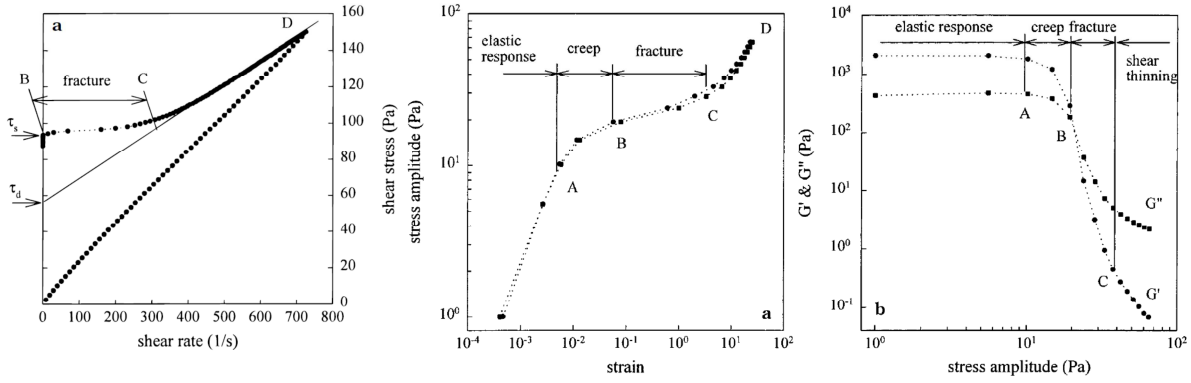

(a) (b) (c)

Figure 2.9. (a) Difference between static and dynamic stresses in a controlled stress test at 16 °C; (b) stress vs. strain relationship in an oscillatory test at 20 °C and (c) storage, G', and loss, G", moduli. Source: Chang et al. [5], p. 1552 and 1557.

Both the elastic and static yield stresses are dependent on the strength of the network of wax crystals in the oil, while the dynamic yield stress is related to the concentration, size and arrangement of the wax particles during the structure shear. It is important to note that the elastic and static stresses are highly dependent on thermal and shear history and on the stress loading rate. It implies that for direct application of those values on pipeline restart, the measurement must account for those histories.

For engineering proposes, the static yield stress is of most interest for determining the pump capabilities for restarting the gelled oil flow. Designing a pipeline restart based on the creep condition is considered nowadays much riskier. It would require high confidence in the fluid rheological model and a robust pipe flow model, properly relating the dynamic, creep and

compressibility effects for calculating the restart time and predict the behavior of the flow rate with time.

Several works in the literature were devoted to characterize waxy oils yield stress after different cooling histories. As said in the previous section, typically, lower cooling rates, lower shear rates and longer holding times at rest give rise to higher yield stresses, when analyzed independently (Venkatesan et al. [71], Lin et al. [31], Zhao et al. [83]). The oil-gel shear stress response at low deformations, as in creep and recovery tests, with the objective of analyzing its detailed yielding characteristics were also studied by Chang et al. [5], Kané et al. [29], Magda et al. [33] and Oh et al. [40], for example. More details on the yield stress measurement will be presented in Chapter 7.

2.4.2.2 Constitutive equations

Waxy crude oils below the WAT are described to be yield stress shear thinning fluids. A classical and efficient model for describing that type of fluid is the Herschel-Bulkley model. Indeed, the rheological behavior of waxy oils in steady state flow was already satisfactorily modeled using the Herschel-Bulkley model, but also Casson model, Cross model or Roberts-Barnes-Carew model (Rønningsen [55], Chang et al. [6], Dimitriou et al. [14] and Visintin et al. [77]). Those models are fitted on steady state flow data and represent the fluid rheological response in steady state to a certain flow and temperature history.

Transient models for representing the rheological behavior of waxy crude oils based on different strategies may be found in the literature. Generally, they were not specially developed for waxy crude oils, but inherited from other applications, as from food industry. Basically, three classes of models may be distinguished (Mewis and Wagner [35]): (1) The continuum mechanics approach, that introduce time-dependent function in existing models, as the Bingham model; (2) The microstructural models, that deduce macroscopic properties from the microscopic interactions between the material components and; (3) The structural kinetics models, where the fluid structure evolution is characterized by one parameter, that envelops the microstructural features, to be considered in the constitutive equation.

The first class of models was applied for waxy crude oils in, perhaps, its simplest way. The work of Rønningsen [55] used that strategy. In that work, Herschel-Bulkley and Casson models were fitted to waxy oils flow curves and a dumping function was used for reducing the rheological model parameters in order to account for destructuring flow. Later, Chang et al. [6] applied the same model for the flow restart of a pipeline with waxy crude oil, also treating the time evolution of the fluid apparent viscosity from results of viscosity decay experiments, where the apparent viscosity change was measured with time for various constant stress tests. Then for a given time of destructuring flow, one point of each constant stress test forms an "instantaneous" flow curve. Those various instantaneous flow curves were fitted by a time-dependent Bingham equation of the form:

$$\tau = \tau_c(t) + \eta\dot{\gamma}, \qquad \text{for } \tau > \tau_c(t)\,, \tag{2.3}$$

$$\tau_c(t) = \frac{\tau_c(0) - \tau_c(\infty)}{1 + kt} + \tau_c(\infty) \tag{2.4}$$

The equations above describe one single flow and cooling history according to the experiments used to fit the parameters of the model. The function $\tau_c(t)$ represents the yield stress while the

material is in the solid state, but in the liquid state it is only a mathematical fitting function of the instantaneous flow curve, without much physical meaning. It is similar to the curve parameter τ_d in Figure 2.9(a).

Dimitriou et al. [14] and Visintin et al. [77] presented similar approaches by fitting the strong variations of apparent viscosity in equilibrium states (steady state) obtained from imposed shear stress tests. That class of models has the advantage of directly fitting the oil rheological behavior. However, physical processes are let to a second plan, thus experiments must be very close to field conditions to which the model will be applied.

The second class of models, the microstructural one, relies on the physics of the interaction mechanisms of the material components. Such modeling approach, applied to waxy crude oils, based on fractal clusters, was proposed by Kané et al. [29]. They showed the thixotropic behavior of waxy oils during creep, recovery and transient imposed shear rate experiments. The common point with other classes of models is that they have also adjusted the unknown parameters of the model with the gelled oil flow curves (i.e. the apparent viscosity), but for different temperatures below the WAT. They have related those data to oil-gel structural observations of a previous work (Kané et al. [28]) in a fractal description of the media. One of the conclusions, however, stated that it was not entirely possible to relate the phenomenological parameters of the model for flow description with the structural features of the gel networks.

Considering the structural kinetic models, the third class, numerous models have appeared lately (see Mewis and Wagner [35]). However, few studies describe the flow evolution of waxy crude oils beyond yielding and its representation by pertinent rheological models. In literature this has been mostly done through modeling. A work of reference in that field is that of Houska [26] (applied in pipeline flow models by Sestak et al. [56], Cawkwell and Charles [4] and Wachs et al. [79]), who described the rheological behavior by a model in the range of classical thixotropic models for colloidal dispersions (see Coussot [9], Mewis and Wagner [35]). That model is the result of an evolution of representing thixotropic flows by generalizing the Bingham model. It includes a first equation, Eq. (2.5), of the Herschel-Bulkley type with yield stress and viscous coefficients depending on a structure parameter - λ, and a second (kinetic) equation, Eq. (2.6), describing the evolution of the structure parameter as a function of flow history, at constant temperature.

$$\tau = \tau_{y0} + \lambda\tau_{y1} + (k + \lambda\Delta k)\dot{\gamma}^n \tag{2.5}$$

$$\frac{d\lambda}{dt} = a(1-\lambda) - b\lambda\dot{\gamma}^m \tag{2.6}$$

In this description the yield stress can vary from a low value corresponding to a fully destructured fluid ($\lambda = 0$) to a high value for a fully structured material ($\lambda = 1$). The structure parameter evolves according to a kinetic equation with destructuring and restructuring terms. So a more structured fluid would have a higher yield stress and consistency coefficient, thus higher apparent viscosity. Under shear, the structure parameter reduces its value with time, representing a destructuration, thus reducing the yield stress and apparent viscosity.

The determination of the Houska model parameters is done by rheometry, exploring different shear values and structure parameter evolutions (see Cawkwell and Charles [4], Hénaut and

Brucy [24], Vinay [73], Wang and Huang [80]). However, it is very difficult to find in literature a discussion of the quality of this model to describe the effective rheological behavior of such materials obtained from careful and systematic rheometrical data. The work of Wang and Huang [80] advanced in that direction.

A version of the Houska model involving more parameters and a second structure parameter was proposed by Ding et al. [16]. Their proposition has the objective of account for a partial reversibility of thixotropic phenomena, but without presenting effective results improvement.

The model proposed by Dullaert and Mewis [19], Eqs. (2.7)-(2.9), was recently applied for representing elastic and thixotropic behavior of a waxy crude oil by Ahmadpour and Sadeghy [2]. The model successfully represented fitted measured data of stepwise increasing shear rate and an up-and-down shear rate ramp. With respect to the Houska model, the Dullaert-Mewis model explicitly considers the elastic stress, with an evolution equation for the elastic strain taking into account aggregates relaxation after stress reduction and stretching after stress increase. The kinetic equation of the structure parameter λ features a shear-induced build-up term proportional to the square root of the shear rate.

$$\tau(\lambda,\dot{\gamma}) = \lambda G_0 \gamma_e(\lambda,\dot{\gamma}) + \lambda \eta_{st,0}\dot{\gamma} + \eta_\infty \dot{\gamma} \tag{2.7}$$

$$\frac{d\lambda}{dt} = \left(\frac{1}{t^\beta}\right)[-k_1\dot{\gamma}\lambda + k_2\dot{\gamma}^{0.5}(1-\lambda) + k_3(1-\lambda)] \tag{2.8}$$

$$\frac{d\gamma_e}{dt} = \left(\frac{k_4}{t}\right)^\beta [\tau(\lambda,\dot{\gamma})\gamma_c - \tau_{ss}(\dot{\gamma})\gamma_e] \tag{2.9}$$

Some other recent works also provided more sophisticated modeling approaches of the behavior of thixotropic materials, relying on interesting physical arguments. De Souza Mendes [59] used a shear stress equation with the form of a linear viscoelastic Maxwell constitutive equation, but with variable parameters, that depend on a structural parameter. The kinetic equation for the structure parameter includes a characteristic relaxation time and the shear stress is the driving force for the structure breakage.

In that model, the steady state (*ss*) viscosity function η_{ss}, which represents the flow curve, is a fairly generic function, designed to fit non-monotonical flow curves. De Souza Mendes [60] further develops the model to the form of Jeffreys viscoelastic materials. This last version is presented in Eqs. (2.10)-(2.13).

$$\tau + \theta_1\dot{\tau} = \eta_v(\dot{\gamma} + \theta_2\ddot{\gamma}) \tag{2.10}$$

$$\eta_v = \left(\frac{\eta_0}{\eta_\infty}\right)^\lambda \eta_\infty, \quad \theta_1 = \left(1 - \frac{\eta_\infty}{\eta_v}\right)\frac{\eta_v}{G_s}, \quad \theta_2 = \left(1 - \frac{\eta_\infty}{\eta_v}\right)\frac{\eta_\infty}{G_s}, \quad G_s = \frac{G_0}{\lambda^m} \tag{2.11}$$

$$\frac{d\lambda}{dt} = \frac{1}{t_{eq}}\left[(1-\lambda)^a - (1-\lambda_{ss})^a\left(\frac{\lambda}{\lambda_{ss}}\right)^b\left(\frac{\tau}{\eta_v\dot{\gamma}}\right)^c\right] \tag{2.12}$$

$$\lambda_{ss} = \frac{\ln\eta_{ss} - \ln\eta_\infty}{\ln\eta_0 - \ln\eta_\infty}, \quad \eta_{ss} = \left[1 - \exp\left(-\frac{\eta_0\dot{\gamma}}{\tau_0}\right)\right]\left[\frac{\tau_0 - \tau_{od}}{\dot{\gamma}}e^{-\dot{\gamma}/\dot{\gamma}_{od}} + \frac{\tau_{od}}{\dot{\gamma}} + K\dot{\gamma}^{n-1}\right] + \eta_\infty \tag{2.13}$$

On another side, Teng and Zhang [66] represent the material stress response by adding an elastic and a viscous tress term. In the elastic stress the shear modulus is assumed to vary

proportionally to a structural parameter and a nonlinear damping function. The viscous stress term is proportional to a structure-dependent consistency parameter and a completely unstructured one, similar to the Houska model. The kinetic equation for the structure parameter assumed a characteristic time that depends on the structure parameter itself and the driving force for the structure breakage is the flow energy dissipation – ϕ, that is the product shear stress times shear rate.

$$\tau = \lambda G_0 h(\gamma_e)\gamma_e + (1-\lambda)(k + \lambda\Delta k)\dot{\gamma}^{n_1} \tag{2.14}$$

$$h(\gamma_e) = 1/(1 + p_1\gamma_e^{p_2}) \tag{2.15}$$

$$\frac{d\lambda}{dt} = \frac{1}{1+\gamma^{n_2}}[a(1-\lambda) - b\lambda\phi^m] \tag{2.16}$$

$$\frac{d\gamma_e}{dt} = \left[g_1 - (1-g_1)s\dot{\lambda}\right]\dot{\gamma}, \qquad \text{with } g_1 = e^{-p_1\gamma^{p_2}} \tag{2.17}$$

The parameters of the model were fitted to stepwise increasing shear rate tests, while the stepwise decreasing part of the test was not modeled. The predictions of this model were successfully compared with experimental data for flow start after static cooling. In fact, besides the good agreement with experiments, what also makes this work interesting is the comparison with waxy crude oil rheometrical data that was not used to fit the model parameters.

At last, Dimitriou and McKinley [15] developed a rheological constitutive equation that captures the main features observed in LAOS (Large Amplitude Oscillatory Shear) experiments with a model waxy oil. In that work, the material deformation was modeled in two separated components, a linear viscoelastic and a plastic deformation. The concept of isotropic-kinematic hardening is applied by allowing a plastic deformation only when the shear stress is higher than a yield stress added to a back stress. The later tracks the location of the center of the material yield surface with the stress direction. The elastic part of the deformation is modeled with constant parameters, thus carrying the strong assumption that G' and G" do not vary with changes in the material structure. The authors leave the choice of the visco-elastic model open. If a linear Maxwell-like behavior is considered, the proposed model is given by:

$$\gamma = \gamma^{viscoelastic} + \gamma^{plastic} \tag{2.18}$$

$$\gamma^{plastic} = \begin{cases} 0 & if\ |\tau - CA| < k_3\lambda \\ \dfrac{\tau - CA}{|\tau - CA|}\left(\dfrac{|\tau - CA| - k_3\lambda}{\mu_p}\right) & if\ |\tau - CA| \geq k_3\lambda \end{cases} \tag{2.19}$$

$$\gamma^{viscoelastic} = \gamma^v + \gamma^e \text{ with } \gamma^e = \tau/G \text{ and } \dot{\gamma}^v = \tau/\eta \tag{2.20}$$

$$\frac{dA}{dt} = \dot{\gamma}^{plastic} - (q|A|)^m sign(A)\left|\dot{\gamma}^{plastic}\right| \tag{2.21}$$

$$\frac{d\lambda}{dt} = k_1(1-\lambda) - k_2\lambda\left|\dot{\gamma}^{plastic}\right| \tag{2.22}$$

where A and λ are internal variables, representing the material structure state. Experimentally measured stress overshoots and a negative slope in a local shear stress vs. local shear rate were well predicted by the model.

The analysis in the work of Dimitriou and McKinley [15] is focused on the physical behavior of the model waxy oil in its slurry state, i.e. before the tests the sample was highly sheared at the test temperature, erasing stronger gel characteristics that would be obtained from static cooling, for example. By doing so, they could model and predict thixotropic phenomena around the flow curve of the material. Hence, a structure state equivalent to $\lambda = 1$ in this model completely different condition than the $\lambda = 1$ state in the Houska model. In the later, that would be a strong gel state after static cooling.

Actually, in view of describing the flow characteristics during startup, there is a strong issue with the descriptions of the models presented in this section: They implicitly assume that the material exhibits reversible rheological properties, which somewhat restricts the range of evolution of the structure parameter and does not allow to fit the model to experimental data obtained after different cooling histories, which in particular may show a strong decrease of the apparent viscosity.

It should also be kept in mind that most rheological models were developed for a fixed temperature. It may be fine for restart pipeline flows where the oil gel is pushed out of the pipe at constant temperature. However, there are cases where the temperature is not uniform at the flow restart moment. Additionally, the pushing fluid may enter in the pipe at higher temperature, thus changing the temperature of the gel, with a strong dependence on the fluids interface extent.

2.4.3 Gelling kinetics at constant temperature

Lopes-da-Silva and Coutinho [32] reported studies on the kinetic behavior of isothermal crystallization-induced gelation of waxy crude oils under quiescent conditions. They noticed a storage modulus (*G'*) increase at constant temperature after cooling. The storage modulus was measured by performing oscillatory rheometry, where very low amplitude deformations are applied, inside the linear elastic response of the material. Higher storage modulus means stiffer material. That rheological response of the gelled oil was interpreted as a consequence of structure development generated by the crystalline morphology, clusters formation and interaction with the liquid phase. Thus, the fluid structure evolution was related to the increase in elastic modulus. Eq. (2.23) was adjusted to experimental data, representing that relation:

$$\frac{G' - G'_0}{G'_\infty - G'_0} = 1 - \exp(-(k_a\,(t - t_0))^n) \tag{2.23}$$

where G'_∞ and G'_0 are the equilibrium and initial storage modulus, t_0 is an induction time, *n* is a constant and k_a is the Avrami rate constant, given by

$$k_a = Aexp(-E_a/(RT)) \tag{2.24}$$

where *A* is the Avrami pre-exponential factor, E_a is the activation energy, *R* is the universal gas constant and T is the temperature. For a fixed temperature, with zero induction time, the Eq. (2.23) becomes equivalent to the solution of Eq. (2.6) with zero shear rate, assuming that the fluid structure parameter varies linearly with the elastic modulus.

The gelation kinetics was also evaluated by Ekweribe et al. [20], where the model of Lopes-da-Silva and Coutinho [32] was applied, fitting its parameters to the measured properties of a

commercial waxy oil. Visintin et al. [77] and Lin et al. [31] also used similar kinetic model to fit the evolution of storage modulus of waxy crude oils.

That evolution at rest and constant temperature indicates the gel stiffening, that may lead to higher yield stress. From the works above, only Visintin et al. [77] explicitly presented the yield stress increase with the holding time at constant temperature.

It is worth noting that the cooling rate also defines the gel structure. Different cooling rates lead to different levels of storage modulus (also verified experimentally in the works cited above). For cooling at rest, lower cooling rates resulted in higher storage moduli, that evolve less with time. Higher cooling rates resulted in lower storage moduli with more important increase during holding time. However, that difference in the temporal evolution did not change the initial tendency observed just after the cooling phase. Lin et al.[31] and Venkatesan et al. [71] found, for the oils that they have analyzed, that if the oil is sheared while cooling the behavior is the opposite.

Thus, according to literature, the gel evolution at constant temperature after cooling may affect sensibly the gel strength and hence the overall pipeline restart pressure. Pipeline restart calculations and the oil rheological evaluation should evaluate the importance of this effect.

2.5 Flow restart scenario

2.5.1 Presentation

In view of the waxy crude oils rheological characteristics presented above, an analysis of the pipeline flow restart scenario shall reveal the important aspects to be taken into account. The main questions to be answered are: What is the minimum pressure gradient to restart the flow? And how will the transient flow develop afterwards?

As the oil-gel rheological behavior is strongly dependent on its cooling conditions, it is necessary to know the fluid flow and thermal histories once its temperature is below the WAT. From a fluid mechanics point of view, the following comments can be drawn about long oil exporting pipelines.

As said in Chapter 1, typically, in offshore crude oil exporting pipelines the oil enters the pipe at a temperature above the WAT. Constant inlet and outlet pressures keep the flow rate constant. The pipe may have external insulation layers, depending on the flow assurance strategy adopted. Long transportation pipes typically do not have high insulation, once the temperature shall fall anyway. In deep waters, the ambient temperature is around 4 °C. For single-phase flows the terrain does not interfere in main flow characteristics as friction pressure drop and heat transfer.

All those conditions characterize a steady state operating condition that is the flow condition prior to the shut-in. So, knowing steady state temperature and velocity fields is essential for being able to describe the oil shear and thermal histories.

From a rheological point of view, for performing steady state flow calculations, it is necessary to know the oil apparent viscosity behavior with the temperature in the range of shear and cooling rates of the flow.

When the flow is stopped, velocity goes to zero and the fluid will cool from its steady state flow temperature towards the ambient temperature. Whether it will achieve the exterior temperature depends on the duration of the shutdown. In this phase, heat diffusion is considered to be the main heat transfer mechanism in the oil (Vinay [73]). So, temperature history will vary with the axial and radial positions in the pipe. The exception is for the part of the flow that was above the WAT at shut-in time. That region was sheared only above the WAT, but in what concerns the wax crystals formation, the cooling process was static. Additionally, oil thermal shrinkage may be responsible for the appearance of gas bubbles, that would change the fluid overall compressibility and terrain configuration may also play a role (see Section 2.5.4).

At restart time, pressure shall be increased at the pipe entrance, typically pushing the oil-gel by simpler and with lower viscosity fluid. As the flow rate should be slow until the complete expulsion of the gelled oil, temperature in the pushing, or incoming, fluid may rapidly fall. Thus, a lower viscosity fluid (as diesel oil) to push the gel is preferable to keep pressure drop as low as possible.

If the overall fluid compressibility is low, pressure wave shall travel fast and a pressure profile will be rapidly established, promoting gel breakage where the shear stress is higher than the yield stress. The shear stress is higher at the pipe walls and the gel is weaker where it was highly sheared while cooling. If compressibility is high, pressure profile evolution in time must be carefully calculated in order to obtain reliable shear stress field predictions.

During almost all the gel expulsion phase, the oil-gel will flow at approximately constant temperature, i.e. without much influence of the heat brought by the incoming fluid. Heat transfer between the two fluids will become important only when the incoming fluid flow rate increases and if the interface between the fluids increases.

In summary, the interest in predicting the steady state flow and pipe shut-in phases is to know the flow and thermal histories to assess the oil-gel structure state at restart time and predict the yield stress field in the pipe. In the flow restart phase, the rheological model plays a major role in the pipe flow models, which should also be able to capture other fluid dynamics phenomena to increase the accuracy of its predictions.

2.5.2 Pipe flow numerical models

Lab scale experiments of pipe flows, based on classical force balance model, cannot be extrapolated directly to real field condition without avoiding conservative estimative (Yusof et al. [81]). The scale of pressure and temperature variations in the real pipeline should be carefully taken into account and compared with lab scale, since gel properties are sensible to history of those variables. This reasoning supports the importance of appropriate mathematical pipe flow models for doing the correct “translation” from oil rheological data to overall pipe behavior.

The restart model presented by Sestak et al. [56] in 1987 considered an isothermal integral pipe model, where a thixotropic yield stress fluid (gelled oil) was pushed out of the pipe by an incoming Newtonian fluid. The gel rheology was modeled with the Houska model. The use of this 1D model for calculating the restart pressure is the same as doing the static force balance on the gelled oil. The gel structure parameter is considered to be uniform in the pipe cross-section and, at restart, the pipe is considered to be full of completely structured gel. An average shear rate is considered for destructuring the gel after flow restart.

Chang et al. [6] presented a 1D pipeline restart model where the outgoing fluid, modeled as thixotropic non-Newtonian fluid, may have different structure states in the pipe radial direction. It allows calculating the shear rate radial variation, resulting in an improved prediction of the destructuring flow once the flow was restarted. They considered as well the possibility of a delayed startup, due to the creep when the applied shear stress value is between the static and the elastic yield stresses. As in the previous model, fluid properties are considered to be uniform in the pipe prior to restart.

Davidson et al. [12] developed a similar model but including the fluids compressibility. Section 2.5.4 introduces the compressibility effects Pipe models normally use that feature also for accounting for the average fluid compressibility increase due to the possible appearance of small gas bubbles during the oil cooling process. Davidson et al. [12] confirmed the tendency of lower pressure required for the flow restart and a more rapid increase of the mass flow rate when compressibility is taken into account. In one calculation example they noticed a pipeline clearance time 16% higher when compressibility is not considered. Results like that (as in Wachs et al. [79]) show that the fluid compressibility help reducing the required restart pressure, but they also show that the fluid yield stress is the most important variable in the pipeline restart problem.

Later, Davidson et al. [13] continued improving the model by taking into account gas pockets separating oil-gel liquid slugs. That would be the scenario of a multiphase production pipe, where terrain may provide the creation of large gas pockets at higher regions of the pipe. Those gas pockets help reducing the restart pressure due to its high compressibility. Despite modeling the restart with gas pockets, they did not model the gel formation in this scenario.

De Souza Mendes et al. [61] have presented an one-dimensional, incompressible pipe flow model where a gelled oil can be displaced by an incoming fluid. Despite being one-dimensional, the use of the rheological model as presented by de Souza Mendes [60] allows having a radial description of the fluid structure state. As said in Section 2.4.2.2, in that model the structuring level is a function of the shear stress, which has a known radial profile.

A similar rheological model (de Souza Mendes and Thompson [62]) was very recently applied in a pipe flow model by Oliveira et al. [42]. But the focus of this work was on compressibility effects. They introduced a compressible one-dimensional model where two flow restart time scales are evaluated, namely, the pressure wave propagation and the material response time.

Vinay et al. [74] presents a transient two-dimensional flow model based on more complete version of Navier-Stokes equations, using a Bingham fluid model, solved by finite volume method. Lagrangian multipliers techniques and augmented Lagrangian/Uzawa methods are employed for the precise tracking of unsheared regions in the pipe. Later, Vinay et al. [75] improved the model by taking compressibility into account. They also presented cases where the flow rate prediction at restart is more accurate due to compressibility effects. Vinay et al. [76] simplified that model by turning it into a one-dimensional model and analyzed the different physical phenomena that may occur in different dimensionless parameter regimes. The parameters evaluated were Reynolds and Bingham numbers, dimensionless compressibility and pipe length.

Wachs et al. [79] modify the model presented by Vinay et al. [76] proposing a 1.5-dimension model, i.e., only the axial velocity, temperature and fluid properties (as the structure

parameter), are calculated along the pipe radius. That simplification reduces considerably the calculation time, "from days to hours", without losing accuracy when compared to the previous model of Vinay et al. [76]. Another improvement done by Wachs et al. [79] is the use of the Houska model for representing the fluid rheological behavior. All those features make this last model one of the most complete models for pipeline restart found in literature so far.

Independently of the pipe flow model used, an essential information for a successful estimative of restart pressure is to obtain a good estimative of the gel structure along the pipe at the end of the shut-in process. After the shut-in, a very heterogeneous gel structure may form inside the pipe. This makes difficult to have a precise estimative of the length averaged yield stress to use in the classical force balance model, or any other model, for calculating the restart pressure. An incorrect characterization of the restart initial condition is believed to be the major source of error in the restart pressure calculation, but authors of pipe flow models usually do not present specific studies on this subject.

2.5.3 ColdStart methodology

A methodology called ColdStart was developed at IFP Energies nouvelles, to provide practical guidelines to operators to handle the waxy crude oil flow restart problem. That methodology is fully described in the Patent [47]. It is a 5 step procedure as follows:

1. Determination of the rheological model parameters;
2. Description of the temperature field at the pipeline shutdown;
3. Thermal calculations during the holding time;
4. Description of the initial state;
5. Simulation of the flow restart process.

The Step 1 consists in choosing an appropriate rheological model and determining its parameters from experimental data. The methodology employs the Houska model. Steps 2 and 3 aim to describe the flow and temperature histories of the oil at each position in the pipe in order to evaluate its influence on the yield stress, which is calculated in Step 4. Step 5 is the pipeline restart simulation itself using a numerical pipe flow model called StarWaCS, essentially described by Wachs et al. [79].

Perhaps the most interesting approach used in the methodology is in Step 4, where it is assumed that the material structure state is linearly proportional to the elastic modulus G' of the gel for any cooling and flow history. This assumption allows performing rheometrical experiments with different types of cooling procedures measuring G' without effectively flowing the sample and breaking the gel. That can be done once the G' of a reference state is related to the structure parameter λ of that state. That reference state is conveniently chosen as a highly structured state corresponding to a given static cooling procedure. Thus, the structure parameter is given by

$$\lambda = \frac{G'}{G'_{ref}} \tag{2.25}$$

Furthermore, the measurement of G' while cooling allows relating the structure parameter to the temperature for a certain cooling process. Thus, a direct relation between the resulting structure state and cooling procedure can be established. Therefore, the structure parameter at each region of the pipe can be estimated with the data calculated in steps 2 and 3.

The use of G' to calculate the structure parameter in the Houska model was first presented by Hénaut and Brucy [24] and later described by Vinay [73]. That idea of assessing the material structure state by evaluating the elastic modulus with small amplitude oscillatory tests was also used by Lopes-da-Silva and Coutinho [32], as presented in Section 2.4.3, and Visintin et al. [77], for example.

2.5.4 Pressure effects

There are two main aspects when considering the pressure on the restart of pipelines with gelled crude oil. First, the pressure effect on the gel properties themselves. Second, the additional flow phenomena caused by the pressure action over a compressible yield stress fluid.

It is known that crude oil viscosity usually increases with pressure. But there is very few data in the literature about the pressure effect on crude oil gel properties. Ekweribe et al. [20] was the only work found that explicitly presents measured data on the subject. They observed, by the use of oscillatory rheometric tests under pressure, that elastic properties of the gel decrease at elevated pressures, supposedly forming a weaker gel. Only model wax – oil mixtures were analyzed.

Some more data are available for a different scenario: The live oils. The objective would be the analysis of production pipes, from a petroleum production well head to the platform, where there is multiphase flow of oil and miscible natural gas. Suppiah et al. [64] reported a reduction of 70% in yield stress and restart pressure of recombined live oil at 2,200 psi over the dead oil, using a model pipeline test. Recombining an oil and gas means to artificially try to recover in the laboratory the same gas-oil ratio under pressure as in the pipeline. Robertson et al. [52] reported a reduction in the gel yield stress by measuring with a rheometer the impact of incorporated gas in the crude oil at 200 psi. The reductions in the yield stress compared to crude oil varied from 52% to 63%, depending on the oil and the amount of gas incorporated. Thomasson [67] also presented similar results of the dissolved gas on gel strength.

When pressure exhibits substantial variations in the pipeline, the oil compressibility also may influence restart conditions reducing the necessary restart pressure (see Figure 2.10). During the restart, when the pipe inlet pressure increases, the region closer to the pipe entrance will be compressed, causing a shear stress that may break the gel structure at that region only. As the rupture advances downstream the pipe, the broken gel behind it offers lower resistance to flow, leading to a pipeline restart pressure lower than the pressure estimated when the flow is considered incompressible. For taking that phenomenon into account when modeling the gel compressibility, it is also important to model the fluid thixotropic behavior, because once the gel structure has broken it offers no more the same resistance to flow.

The oil-gel compressibility does not depend only on itself, but also on the pipeline geometry and its flow stop conditions. According to Philips et al. [49], during the cooling, the oil specific mass increases, reducing the overall pipe pressure and giving rise to flow towards the lower regions of the pipeline. If, in any region of the pipe, pressure falls below the crude oil vapor-liquid equilibrium, then vapor bubbles, composed by the oil lighter fractions, will form. It is important to note that, at rest, when temperature falls and a yield stress appears in the oil, it starts acting against the shrinkage flow and the migration of the bubbles to high regions in the pipe, contributing for the formation of small bubbles in different regions of the pipe (for measurements report see also Hénaut et al. [25]).

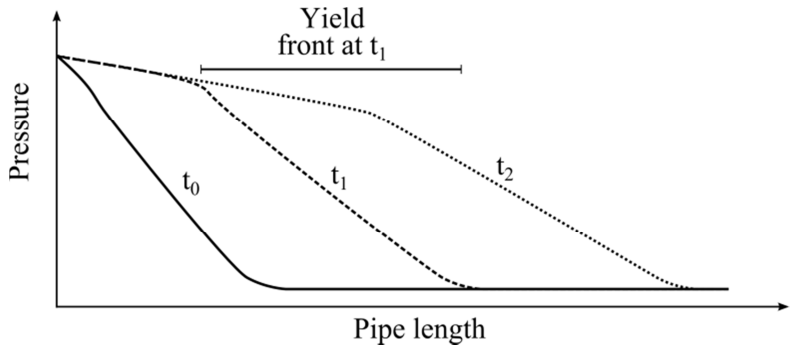

Figure 2.10. Pressure profile along the pipe main axis representing the compression flow in three instants. Fluid compressibility acts reducing the minimum required restart pressure by concentrating the pressure gradient in a shorter region of the pipe.

This effect would also lead for "trapped" pressure gradients, generated by shrinkage and supported by the fluid yield stress (Philips et al. [49], El-Gendy et al. [21]). As a side effect of the bubbles, the fluid overall fluid compressibility increases (Philips et al. [49], Hénaut et al. [25]), Lee et al. [30]).

Lee et al. [30] reported that the effect of hydrostatic head on the restart pressure was significant, as the gel breaking pressure decreased 50% when their model pipeline was restarted without a hydrostatic head during the cooling and aging period. The additional pressure in the pipeline created by the hydrostatic head, as in a pipeline riser (see Figure 1.1), prevented the formation of gas bubbles during cooling, which were considered to be responsible for the reduction in the restart pressure.

Thinking of multiphase flow pipelines (pipes from well head to platform, for example), i.e. a case of much higher gas fraction than the above description, Thomasson [67] suggested that the insertion of artificial high points in the line could reduce the restart pressure by separating oils slugs by big gas pockets, thus helping in restarting the pipe flow by parts.

In summary, the experimental data on gelling oil is still very limited. Complex flow phenomena may be created from the oil volume contraction with the temperature decrease and pressure increase. Their relative importance was not yet sufficiently analyzed. Despite the studies about the bubbles influence on the fluid overall compressibility, only single works were found regarding different aspects of the pressure effects.

2.5.5 Gelling in the presence of water-in-oil emulsion

The transport of crude oil may happen in the presence of water, generally forming a water-in-oil emulsion. That would probably not be the case of long oil exporting pipelines. Since the viscosity water-in-oil emulsion is much higher than that of the crude oil alone, it would hardly be a project scenario. Although, it may be the scenario of a producing well flowline, where the oil has not arrived to the first treatment facility yet. There are not many works in the literature on this subject. Here, only general conclusions are commented.

The global tendency reported in the literature is that the formation of wax crystals in the presence of water-in-oil emulsion increases the gel strength. The work of Visintin et al. [78] suggests that wax crystals form on the emulsion liquid-liquid interface, increasing emulsion stability. They also reported pour point increases in different water-in-oil emulsion, up to 5 °C.

De Oliveira et al. [41] also reported that waxy crude oil with low viscosity can produce very stable and viscous emulsions that increase gel strength. Their measurements showed that apparent viscosity increases one order of magnitude with 70% water cut.

The recent work of Sun et al. [63] analyzed the yield stress of the gel formed in the presence of water-in-oil emulsion and reported the yield stress increase of one order of magnitude when water cut evolves from 0 to 60%. Looking at the flowing characteristics of those types of mixtures, Paso et al. [46] measured stress vs. deformation curves in controlled shear rate experiments. They concluded that the shapes of the measured curves are similar with and without water-in-oil emulsion.

The gel formation in the presence of water-in-oil emulsion remains a topic to be explored. The focus scenario would be that of production flowlines and, particularly, long tie-backs, where there is less room for incertitude.

2.5.6 Pipelines operators mitigation strategies

Increasing the pipe inlet pressure is not the only method for dealing with a gelled oil pipeline. Some works in the literature report pipeline operators´ strategies for solving or mitigating this problem.

One mitigation method for the oil gelation problem is the use of pour point depressants – PPD, chemical additives that interfere the wax crystals growth. Robertson et al. [52] reported its use as an option for a field already developed in Vietnam coast, presenting data of yield stress reduction of 30% for a PPD concentration of 100 PPM, and 65% reduction for 250 PPM. During design phase, aiming for a robust project, PPD is normally not an option. Its cost (the product itself, injection facilities, logistics, etc) are typically high, normally not suited for continuous use. PPD costs, as any other solution, should be compared with the usual solution of increasing pump capacity, which leads to extra pumping costs and, eventually, the additional cost of raising the pipe maximum allowable working pressure.

Robertson et al. [52] also reported the strategy of pumping water into some pipelines to displace the oil prior to gelling. That should be feasible for pipelines where the facilities downstream are prepared for treating the water. Oil-based fluids, as simply Diesel, should be easier to deal with, but if very high volumes are necessary, logistics (mainly offshore) may be a problem. Emergency situations are more difficult for replacing fluids, as there may be no time for executing the operation.

Thomasson [67] reports that if the gel does not break with the applied pressure, an easy first approach is to apply pressure to the gel and wait, "there have been field reports of the gel breaking after several hours of exposure to pressure". It is probably related to transient phenomena as thixotropy, creeping, and/or compressible effects.

Since the gel strength is sensitive to temperature, heating the pipeline prior to restart, or only its critical areas where the gel is stronger (Yusof et al. [81]), is also a solution to the gelation problem.

2.6 Conclusions from the literature review

The literature on the flow restart of a pipeline containing gelled oil reinforces the idea presented at the introduction of a complex physical situation. The texts on the oil rheological characterization show that the waxy crude oil gel formation is governed by a large number of parameters. The physics behind the non-Newtonian and time-dependent behavior presented by this colloidal gel is not completely understood. It is very difficult to obtain quantitative rheological information from the fluid microstructure. Better results with global understanding can be obtained more directly from detailed rheometrical measurements.

Nevertheless, rheological models for crude oils remain somewhat restricted to the data they were developed or fitted to. There is still a need to get more experimental data concerning waxy crude oil flows for well-controlled flow histories. The fluid dynamic behavior under transient flow is not explored in details. Most destructuring flow experiments start from fully structured gels at only one given condition and most flow inducing parameters are held constant during the experiment. Thus, there is also a lack of qualitative and quantitative data on the transient flow of gelled waxy crude oils, considering different gel formation conditions.

Based on the information assembled from literature, a more detailed work plan can be delineated in order to improve the understanding of the gel formation and flow restart. Qualitative rheological behavior can be assessed with a model waxy oil, where non-Newtonian and time-dependent effects are created by the artificial presence of the paraffins. Next, with waxy crude oil samples, the gelled oil behavior shall be mapped regarding different transient flow aspects.

Initially, the waxy crude oil basic rheological characteristics shall be evaluated. Its apparent viscosity behavior with shear rate and temperature can indicate basic non-Newtonian characteristics and its thermal dependence. That kind of data is also an essential information for pipeline flow simulations.

Then, transient rheological measurements at constant temperature starting from a strong gel state shall provide information on the presence of yield stress before and after flow start and assess time-dependent aspects as flow start, destructuring flow and restructuration capacity. Experiments imposing shear rate ramps can be used for evaluating those aspects and getting an overview on how the waxy oil should behave in a flow restart.

The rheological behavior measured with those basic rheometrical tests may also be found in model waxy oil. Thus, detailed flow transients will be evaluated with a model waxy oil using local flow measurements, in order to avoid the problems caused by flow heterogeneities. The use of MRI velocimetry techniques shall provide effective instantaneous flow curves data, allowing the observation of the fluid behavior during cooling at different shear rates and the fluid evolution during flow restarts and velocity step changes. There is no data in the literature concerning waxy oils instantaneous flow curve evolution during the cooling process and transient flows. Nor on the heterogeneities of flow velocity profiles that may be caused by local phenomena.

After evaluating the major qualitative behavior of a waxy oil from different flow histories, rheometrical tests shall measure the destructuring flow in order to provide data for modeling purposes. In that aim, a complete rheometrical analysis of two waxy crude oils will be carried out, including start flow tests at different velocities, abrupt changes of velocity level, steady

flow, sweep tests, for different cooling and flow histories. With all those data, it shall be possible to set up a model describing the different trends observed at each step of this rheological study.

Additionally, of particular interest is the oil-gel yield stress for different cooling conditions. Yield stress measurement methods will be compared and its behavior will be mapped in function of the main parameters indicated in the literature, namely, the cooling rate, shear rate while cooling and holding time at rest after cooling. A panorama of yield stress order of magnitudes in function of those parameters will be drawn.

Finally, all the knowledge gathered during the above described studies can be used to simulate a complete pipeline flow restart case. Such case study will show how to use the measured rheological data in a consistent methodology for calculating the minimum restart pressure and transient flow development.

In the next chapter the materials and methods employed in this work are presented. Then, the above work plan starts being developed in Chapter 4, exploring the local flow characteristics associated to rheometrical measurements in transient tests under different gel formation conditions.

CHAPTER 3

MATERIALS AND METHODS

3.1 Materials

Three different fluids were used in this work: One model fluid and two waxy crude oils.

The model fluid is a mixture of a commercial mineral oil (Sigma-Aldrich CAS Number 8042-47-5) relative density 0.84 with 5% weight of wax (Sigma-Aldrich CAS Number 8002-74-2, melting point 58 – 62 °C). The model fluid WAT is 32 °C, which is useful for experiments at ambient temperature, where it exhibits qualitative rheological behavior similar to the crude oil at 4 °C, as it will be seen later. Before being charged in the rheometer, the model fluid was heated to 40 °C, for 20 minutes, in order to sample the fluid above its WAT.

The waxy crude oils were named A and B. Crude oil A has density 27 °API (American Petroleum Institute gravity) and WAT of 22 °C. Crude oil B has density 31 °API and WAT of 30 °C. Both oils were sampled from larger containers after mixing and stored in small flasks. No solid deposits were observed at any time in the containers. Before being collected for the rheometry tests, the flasks were heated to a temperature above the WAT. Once loaded in the rheometer, the oil was heated to 60 °C and sheared for erasing any thermal memory before the beginning of the experiment.

The WAT of the oils were measured with a differential scanning calorimeter Mettler Toledo DSC1.

3.2 Rheometry

Conventional rheometry tests were performed with a TA Instruments AR2000, a controlled stress rheometer, equipped with a Peltier plate and a 40 mm diameter serrated plate geometry. A trap sitting on the Peltier plate covers the geometry and sample leaving a small opening to the ambient. The gap between the parallel plates was set to 0.6 mm for the model fluid and crude oil A and 1 mm for the crude oil B.

A smaller gap for crude oil A made the gap filling easier. Such gaps are thought to be in the appropriate range according to recommendations of Marchesini et al. [34], allowing to minimize shrinkage effects (as the conclusions of Hénaut et al. [25] suggest) and optimize temperature control. Smaller gaps are better for the temperature control but wider gaps contribute to reduce the probability of flow heterogeneities (see Coussot [9]) and to obtain gap independent results (see Marchesini et al. [34]).

3.2.1 Sample loading

Although the crude is a dead oil, it may still lose its light ends (low molecular weight) components due to evaporation to the ambient. That evaporation changes the oil composition along the experiments, mainly at high temperature steps, as 60 °C. This composition change precludes keeping the same material during a series of tests. It was found that the oil apparent

viscosity always increased when comparing two or three successive thermal cycles using the same sample. The repeatability of the rheometry experiments was obtained only if the sample loaded in the rheometer was changed after each thermal cycle. It means that after loading the oil in the rheometer, heating it to 60 °C for erasing any thermal memory before the beginning of the experiment and then cooling it down to experiment conditions (usually 4 °C, to simulate pipeline conditions), the plates were cleaned and a new sample was taken from the flask for the next experiment. Any additional thermal treatment with the crude oil was avoided in order to try to keep its original composition as constant as possible.

Section 7.3.2.1 presents a comparison between two experiments, one using the trap covering the rotating geometry and other using a hermetic cell, which prevents any oil component from escaping to the atmosphere. Results show that the use of the trap can provide similar results as with an hermetic cell.

There were no composition stability issues with the model fluid. It was loaded in the rheometer at 40 °C and experiments started at 50 °C, with 5 minutes holding between thermal cycles.

3.2.2 Rheometrical tests and sample cooling conditions

The rheological measurements of the oil shall be made, *a priori*, at 4 °C. As it was seen in the previous chapter, the cooling process has direct impact on the waxy oil properties. The main variables affecting the gel final strength are the histories of temperature and shear. Those two variables may have multiple combinations during and after the cooling and generate numerous fluid structures at the equilibrium temperature.

Figure 3.1 shows an example of how those histories of temperature and shear may vary and present different combinations during the gel formation. When the oil is cooled at rest (continuous line) with a low cooling rate ($\dot{T}_0$) it is expected to develop a relatively high strength. In addition, when it is let at rest and at constant temperature after cooling, its structure should further develop (vertical dashed lines), increasing the gel strength. But if the cooling process happens under shear the gel strength is not expected to be so high. So, in Figure 3.1, $\dot{\gamma}_2 > \dot{\gamma}_1$. That figure also shows that the cooling could be mixed, i.e., part under shear and part at rest. While cooling at rest, literature supports that lower cooling rates originate stronger gels, so $\dot{T}_2 > \dot{T}_1$.

Finally, Figure 3.1 highlights that the same waxy oil at the same temperature may present an infinite variation of gel strengths, depending on its temperature and flow history.

In order to simplify all the possible combinations, shear and cooling rates will be treated separately. For each rheological experiment, they will be fixed at a constant value during the cooling. So, the oil will be tested at 4 °C after cooling at a constant cooling rate below the WAT, constant shear rate and let at rest after cooling for a given holding time. Between the different experiments the values of cooling rate, shear rate while cooling and holding time will be changed to create different gels properties.

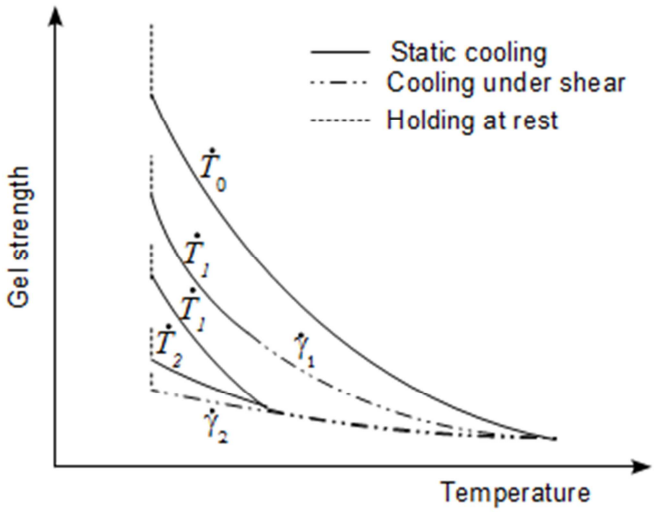

Figure 3.1. Schematic example of the resulting gel strength in function of different possible variations and combinations of cooling rate, shear rate and holding time at rest at constant temperature. Typical behavior expected for the shear rates $\dot{\gamma}_1 < \dot{\gamma}_2$ and cooling rates $\dot{T}_0 < \dot{T}_1 < \dot{T}_2$.

Figure 3.2 presents the behavior of the controlled parameters during one rheological test with crude oil A. For all tests, the initial condition is the oil at 60 °C, where it is a Newtonian liquid. Next, all the experiments start by applying a cooling rate of -1 °C/min from 60 °C to 25 °C (3 °C above its WAT). For crude oil B, the cooling rate of -1 °C/min was applied until achieving 35 °C.

Next, the cooling rate may be changed to a slower value ($\dot{T}$). Tests showed that the cooling rate used above the WAT did not influence the rheological measurements below the WAT. Experiments were designed in that way in order to reduce their duration when slower cooling rates are applied. After cooling to 4 °C at $\dot{T}$ the shear and cooling rates are set to zero and the cooling phase is finished. During the cooling phase, different experiments may use different constant shear rates values ($\dot{\gamma}_{cooling}$), including zero for simulating static cooling.

Then, during the holding time, the sample is let at rest at 4 °C. When the desired holding time is reached, some rheological tests may be executed, as performing shear ramps or measuring the yield stress, for example.

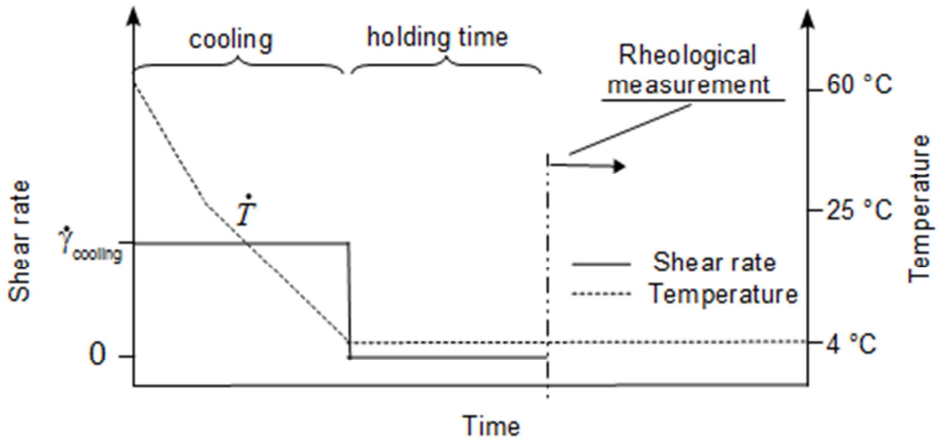

Figure 3.2. Scheme of cooling rate, shear rate while cooling and holding time used in rheological measurements of crude oil A.

In fact, rheological characterization measurement may be executed at any time of the scheme in Figure 3.2. If the shear rate is non-zero in the cooling phase, apparent viscosity can be measured. When the fluid is not being sheared, during holding time or cooling at rest, small amplitude oscillatory tests can measure the gel elastic and viscous moduli behavior with time, for example.

However, even with those simplifications, the number of possible test conditions is still large. Thus, the oil basic characteristics will be first assessed under some fixed parameters conditions. In a first moment, in Chapter 4, an apparent viscosity evaluation with temperature will be done at one cooling rate and four shear rates. Then, transient flows will be performed with shear rate increasing and decreasing cycles after cooling at rest with one cooling rate and one holding time duration. As it will be seen along this work, the cooling rate of -1 °C/min and holding time of 20 min will be the most used values for those parameters. A large number of tests were performed to evaluate different flow histories departing from the same initial oil-gel structure state.

3.2.3 Analysis of the heat transfer in the oil sample

In rheometrical tests presented here with the plate-plate geometry, the temperature control is done by controlling the lower plate temperature, i.e. the Peltier plate. The oil sample temperature is, in fact, the result of the net heat transfer between the sample and both plates, if border effects are neglected. The upper plate temperature is not controlled and exchanges heat with the ambient, that is approximately 20 °C.

As there is a cooling phase involved in all rheometrical tests, it is important to evaluate the sample thermal response to the imposed cooling rates at the Peltier plate. Thus, the objective of this analysis is to estimate the sample temperature in function of the cooling rate and the gap size between the plates.

The heat transfer in the oil sample was modeled as a transient one-dimensional process in the perpendicular direction of the plates plan (see Figure 3.3). Only heat conduction is considered, since flow is perpendicular to heat transfer direction. The governing equation is

$$\frac{\partial T}{\partial t} = \alpha_T \frac{\partial^2 T}{\partial y^2} \tag{3.1}$$

where α_T is the thermal diffusivity and y is the perpendicular direction to the Peltier plate.

The Peltier plate has a prescribed temperature that varies from 60 to 4 °C according to a given cooling rate. The sample is bounded in the upper side by the second plate, made of steel, 3 mm thick, which exchanges heat by natural convection with the air above. The natural convection heat transfer coefficient between the upper plate and the air is estimated at 5.4 $Wm^{-2}K^{-1}$. The oil thermal diffusivity was considered to be 7.49×10^{-8} m^2s^{-1}.

Cooling rates from -5 to -0.1 °C/min were evaluated. Figure 3.4 shows the calculated temperature profiles in the oil layer when the Peltier plate has achieved 4 °C for two different gaps of 0.6 and 1 mm.

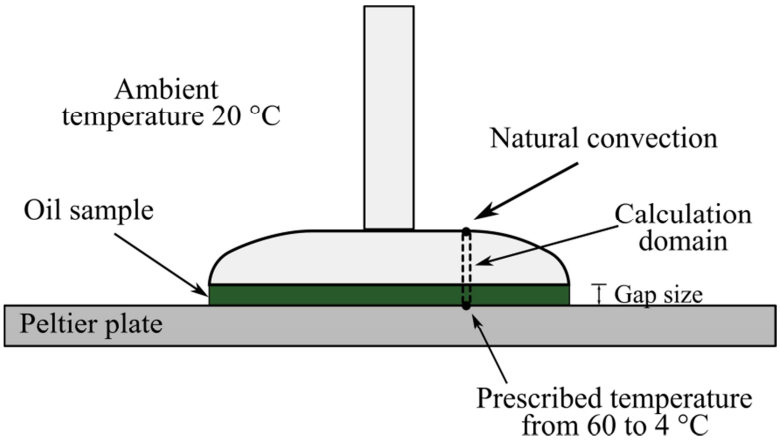

Figure 3.3. Schematic draw of oil sample in the plate-plate geometry in the rheometer. The heat transfer calculation domain is represented by the dashed region with circles at the boundary conditions points.

Results show that, when the final temperature is achieved, for cooling rates lower than -0.5 °C/min for a 1 mm gap the temperature difference between the oil at upper plate and at Peltier plate is less than 1 °C. For a 0.6 mm gap the sample temperature control is better. The temperature difference between the oil at upper plate and at Peltier plate is less than 1 °C for cooling rates lower than -2 °C/min.

Although such cooling rate values are large when compared to practical application (as it will be seen in Chapter 8), analyses of the cooling rate impact on the oil rheological behavior should consider the sample late temperature evolution with respect to the Peltier plate. If larger gaps are used, the cooling rate should be reduced in order to keep a good temperature control of the oil sample.

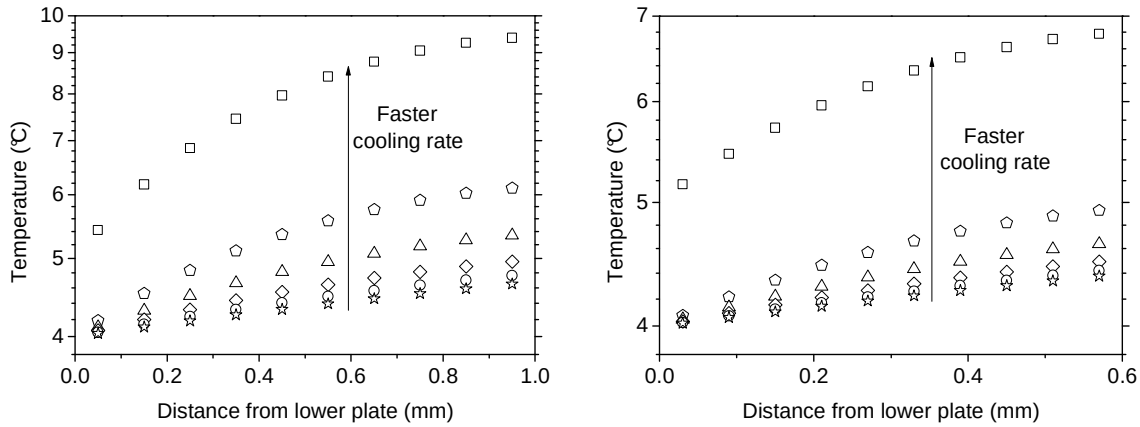

Figure 3.4. Calculated temperature profiles in the gap of the plate-plate geometry when the Peltier plate (lower plate) achieves 4 °C for the cooling rates of -5 (squares), -2 (pentagons), -1 (triangles), -0.5 (diamonds), -0.25 (circles) and -0.1 °C/min (stars). (a) 1 mm gap and (b) 0.6 mm gap.

3.3 MRI velocimetry

3.3.1 Principles

MRI velocimetry tests were conducted in a Couette geometry with inner cylinder radius of 4 cm, external cylinder radius of 6 cm and 11 cm height. The MRI velocity data provide a direct information on the local flow characteristics which, if associated with stress measurement, give the effective constitutive equation of the material. So, the idea is to use the MRI to measure the fluid tangential velocity radial profile with time – $V(r,t)$ – for various imposed inner cylinder speeds. With the velocity profiles in this 2 cm gap, the shear rates – $\dot{\gamma}(r,t)$ – can be calculated as follows

$$\dot{\gamma}(r,t) = r\frac{\partial(V(r,t)/r)}{\partial r} \tag{3.2}$$

Then, the same experiment procedure is reproduced with the same geometry, in the conventional rheometer to measure the torque – $\Gamma(t)$, which is not available in the MRI apparatus. From the torque, the shear stress in each radial position can be calculated by the expression

$$\tau(r,t) = \frac{\Gamma(t)}{2\pi r^2 H} \tag{3.3}$$

where *H* is the fluid height along the internal cylinder. From Eqs. (3.2) and (3.3) it can be deduced the effective instantaneous flow curve $\tau(r) = f_t(\dot{\gamma}(r))$, where f_t is a time-dependent function.

(a) (b)

Figure 3.5. (a) The MRI apparatus with the sample container lowered. (b) Couette geometry mounted in the rheometer.

The principles of MRI velocimetry can be found in Coussot [9]. The MRI setup and procedures are the same as described by Raynaud et al. [51] and Rodts et al. [53]. Here, just the main trends of such measurements are recalled. The magnetic resonance imaging was performed with a

Bruker setup equipped with a vertical 0.5 T magnet Magnex Scientific, fitted with shielded gradients, leaving a free bore of 25.5 cm and delivering a gradient of 50 mT/m with a rise time of 500 µs. The signal was collected within a linear birdcage coil of 24 cm length and 20 cm diameter. The measurement volume has 2 cm height and is located at center of the cylinders axe so that edge effects would remain negligible. The inner cylinder rotation ranged from 0.2 rpm to 200 rpm during the tests. The velocity profiles acquisition was carried with an enhance signal to noise by accumulation, obtaining one profile each minute, except for the 0.2 rpm where the profiles obtained each 2 min for further reducing the noise induced by low velocities. The radial resolution allows measuring 35 points inside the 2 cm gap.

The MRI measurement works by imposing magnetic pulses to the sample that will "mark" the fluid according to its position and in second moment the new position is measured and the fluid angular velocity component is calculated. In the frame of classical mechanics, the atomic nuclei exhibit a magnetic moment (spin, that also depends on mass distribution) that may be altered when in a magnetic field. That alteration happens with a free precession with a relaxation time (t_1) proportional to the magnetic field intensity. In addition to that, if a second oscillatory perpendicular field is also imposed, the nuclei magnetic moment may resonate (according to the first field intensity and the perpendicular field oscillation frequency). When this second field is released there will be a return to the previous precession with a different relaxation time (t_2).

The signal sequence used for measuring the angular velocity profile is showed in Figure 3.6(b). Two radiofrequency pulses select a measuring region in the Couette geometry (see Figure 3.6(a)). A first magnetic gradient in z-axis direction proportional to *r* is imposed to the sample. Then a second perpendicular oscillatory field is applied, thus "marking" the fluid in the measuring region. A lecture gradient parallel to that region makes complexes magnetizations profiles on it. A pair of "coding" gradients, of amplitude *G*, with duration δ and separated by a time interval Δ allows to establish a phase difference $\varphi(r)$ that is proportional to the angular velocity $V_\theta(r)$: $\varphi(r) = \psi G \delta \Delta V_\theta(r)$, where ψ is the gyromagnetic ratio of the proton.

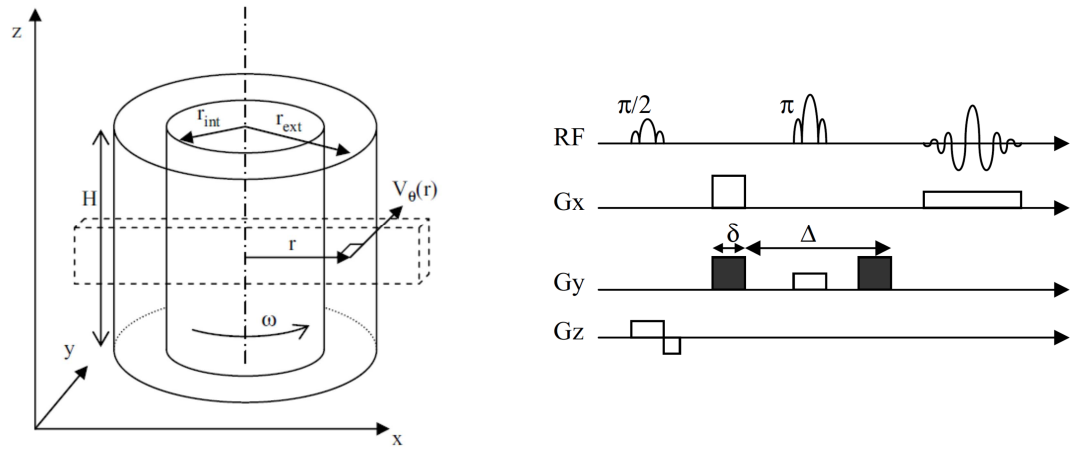

(a) (b)

Figure 3.6. (a) Angular velocity measurement region in the Couette geometry. Magnetic gradients in z and y-axis mark the fluid. (b) Temporal sequence of signals used for measuring the angular velocity profile in the selected region of the Couette geometry. Source: Rodts et al. [53].

The velocity measurement is done by two consecutives magnetization profiles measurements, with and without the *coding* gradients, and then comparing for each radial position the phase difference of the two measured profiles.

3.3.2 Sample temperature

There is no direct temperature control in the Couette geometry inside the MRI, but the room temperature is kept between 20 and 23 °C. The reproducibility and consistency of the measured data suggest that the possibility to have slightly different temperatures in this range had a negligible impact on the tests.

The experimental procedures start with the model fluid being heated between 38 and 40 °C, then loaded to the test geometry and let cool down by natural convection with the ambient air. Under such conditions a critical question concerns the homogeneity of the temperature inside the fluid volume. Figure 3.7 presents the calculated temperature profiles in the test geometry each 5 min for 165 min of cooling period.

Those profiles were obtained by numerical solution of the transient one-dimensional heat diffusion equation in the radial direction through the oil (radius 4 to 6 cm) and the internal cylinder (made of PMMA – acrylic, radius 0 to 4 cm). The heat transfer at the top and bottom of the Couette geometry was not considered in the simulation. The ambient is assumed to be at 20 °C. The air is considered to exchange heat directly with the oil external layer at radius 6 cm, with a heat transfer coefficient of 4 $Wm^{-2}K^{-1}$. The external cylinder wall was not considered in the calculation, it is a thin wall with very low heat capacity when comparing to the mass of oil that it is in contact with. The thermal diffusivities employed in the calculations were 7.49×10^{-8} and 1.14×10^{-7} m^2s^{-1} for the oil and the PMMA, respectively. Those calculated profiles give an estimative of the overall temperature behavior, since no measured temperature data is available inside the fluid sample.

The viscous dissipation typically is not taken into account in temperature calculations on this type of flow. The Brinkman Number, that relates the work dissipated in the fluid to the diffusion heat transfer, is low, around 10^{-2}, and justifies that choice as it will be seen later. It's defined by

$$Brinkman\ Number = \frac{\mu U^2}{k_T(T_{fluid} - T_{exterior})} \tag{3.4}$$

where U is the fluid velocity (here the inner cylinder linear velocity), μ is the fluid apparent viscosity, k_T is the fluid thermal conductivity and T_{fluid} and $T_{exterior}$ are the fluid and ambient temperatures.

At the end of this cooling period the minimum temperature in the fluid is 23.8 °C and the maximum is 25.5 °C. Over the same duration beyond this period one expect the minimum temperature of the fluid to be 22.0 °C and the maximum to be 23.0 °C. As will be seen later this is sufficient to ensure that temperature variations after the cooling period are small enough for limiting their influence on the velocity profiles or torque values.

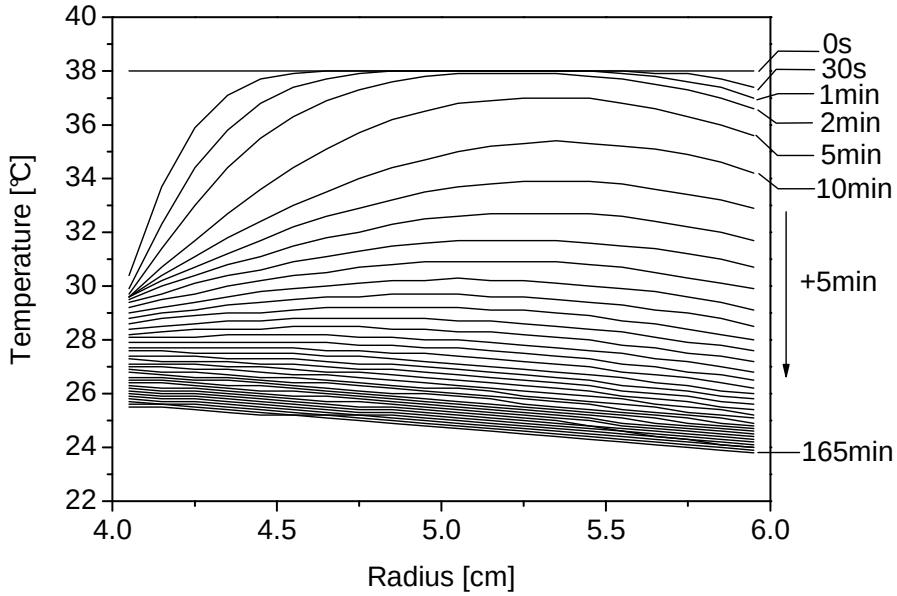

Figure 3.7. Calculated temperature profiles in the oil inside the Couette geometry each 5 min. for 165 min. Initial fluid temperature was 38 °C and 20 °C for the inner cylinder, at radius 4 cm.

3.3.3 MRI and rheometry tests procedures

Different experimental procedures with the model fluid were conducted in the MRI apparatus. In all of them the model fluid is heated between 38 and 40 °C before being loaded in the Couette geometry and inserted in the MRI. In each test the model fluid was allowed to cool down under different shear conditions and after cooling different sets of rotation velocities were imposed over time. The same Couette cell used with the MRI was also mounted in the conventional rheometer. Next, exactly the same experimental procedures were followed, charging the fluid in the rheometer at the same temperature as at the MRI and executing the same inner cylinder velocity steps, but now measuring the torque time evolution.

A wide variety of temperature and flow histories could be studied and corresponding data would be difficult to analyze. In order to progress in the understanding of the rheology of such materials it is first necessary to study relatively simple histories. More precisely, here the focus is on procedures which partly separate material evolutions due to temperature and flow rate variations. The temperature is first decreased under a given shear rate until it is fully established in the whole sample. Then, the shear rate is varied over time in a wide range. Interestingly, such procedure is rather close to the temperature and flow histories undergone by such fluids in pipelines. It should be noted that in the Couette geometry only the apparent shear rate is imposed, by the rotation velocity of the inner cylinder.

Three different protocols were employed, with the objective of distinguishing the basic interplay between temperature and flow histories. All three tests were performed with the same temperature history with different shear rates while cooling. The principles of these protocols are as follows (see Figure 3.8):

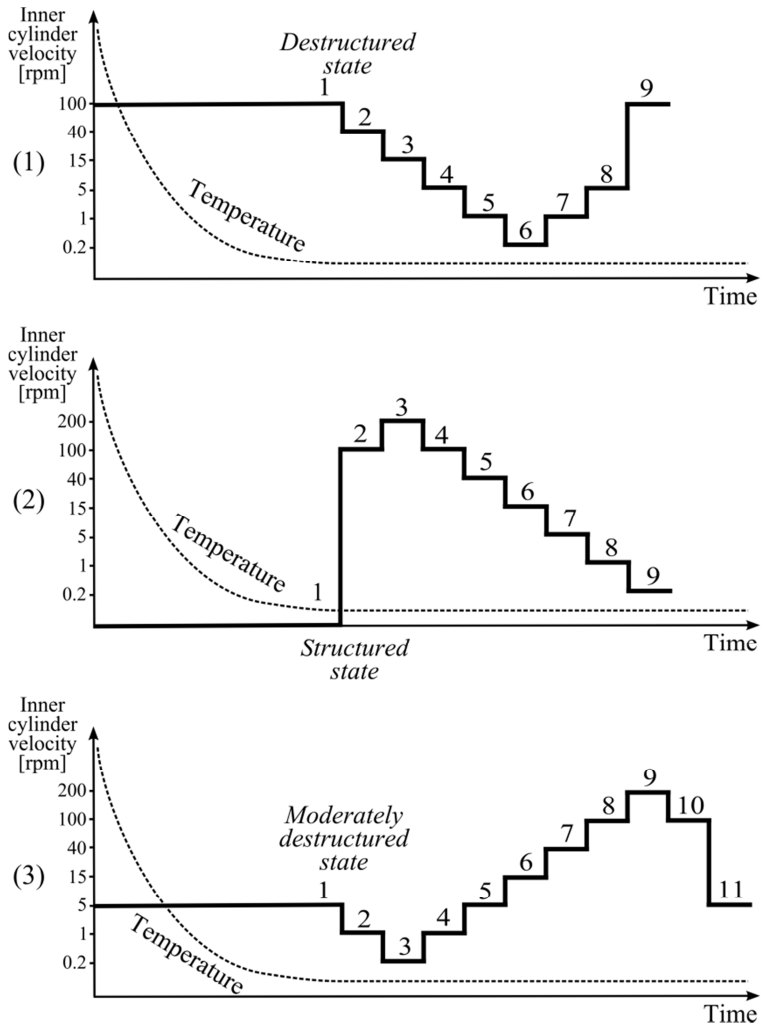

Figure 3.8. Couette inner cylinder velocity and temperature histories in the three tests performed with MRI velocimetry associated to conventional rheometry.

- Protocol 1: **Cooling under high shear**. In this first case the inner cylinder velocity was set to 100 rpm during the cooling phase, causing a relatively high shear. Thus, after this stage the fluid is expected to be in a highly destructured state. The rheological properties of the fluid are studied with particular focus on its time and shear dependent behavior. It is done by imposing a decrease to very low shear rates followed by an increase back to the initial high shear level. In practice, the velocity is changed in steps, first descending to very low level as 0.2 rpm and then increasing it again.
- Protocol 2: **Cooling at rest**. In this case the cooling is supposed to bring the material to a well-structured state. Then, the evolution of the material properties are followed, in particular observing possible destructuring and restructuring effects under shear. This is done by imposing a ramp of increasing shear rates followed by a ramp of decreasing shear rates.
- Protocol 3: **Cooling under low shear**. In this case, it can be considered that the material is in a "partially" structured state. The fluid rheological properties are first analyzed as in Protocol 1, i.e. with a decreasing shear rate ramp. *A priori*, it avoids further material destructuring. Then the shear rate is increased far beyond the level imposed while cooling, in order to observe the effect of a possible further destructuration.

CHAPTER 4

STUDIES COUPLING MRI AND RHEOMETRY

4.1 Introduction

The literature review has showed that there is a lack of transient flow data of waxy oils for different cooling histories. Moreover, it was seen in Chapter 2 that the complex phenomena of flow destructuring and restructuring may lead to unstable flow conditions, with negative slopes in the transient flow curves. For facing the problems that may arise from those characteristics, as wall slip and shear bandings, Magnetic Resonance Imaging – MRI – velocimetry technique is applied here.

MRI velocimetry allows evaluating complex flow situations in a large Couette geometry, directly measuring the fluid velocity profile. With that technique, it is not required to assume a velocity profile in the geometry gap as in conventional rheometrical tests. The use of wide gap in a Couette geometry is interesting because it may reveal flow characteristics caused by a non-homogeneous shear stress field that would be difficult to notice in a conventional rheometer.

The MRI velocimetry tests presented in this chapter were carried out under simple experimental conditions, using the model waxy oil presented in the previous chapter. This model waxy oil will be shown to have a rheological behavior similar to a waxy crude oil, although in a different temperature range (see Section 4.2.4). The transient and steady state behavior of the oil is studied after different histories of cooling, mainly with or without shear while cooling, observing the fluid structure break and build up as a result of flow velocity variations.

The objective here is to analyze the qualitative rheological behavior of a waxy oil. That analysis starts by investigating the macroscopic rheological behavior of a waxy crude oil. Crude oil A samples were used in this evaluation. The next section presents some simple rheometrical tests in order to assess the oil thermal dependence, behavior under shear rate ramps test and recovery after shear. An analogous rheological behavior is showed to be found in the model waxy oil.

Section 4.3 discusses the MRI velocimetry measurements coupled with assisting rheometrical tests. Measurements performed with the three protocols discussed in Section 3.3.3 are presented and analyzed in details. Finally, the last section of this chapter draws the major conclusion and presents an evaluation of crude oil A in order to check the behavior observed with the model waxy oil.

4.2 Macroscopic measurements with conventional rheometry

4.2.1 Apparent viscosity thermal dependence

For calculating pipeline flows with crude oils, where the oil enters the pipe at a given temperature and then loses heat to the ambient, it is necessary to know the oil rheological behavior with the temperature. In a first moment, knowing the oil apparent viscosity in function

of temperature is a basic requisite for many flow models. The apparent viscosity is a useful information that may encapsulate complicated rheological phenomena. It is a simple relation between shear stress and shear rate at a given condition. Newtonian fluids are independent of the shear rate and flow history. Newtonian crude oils are known for typically increasing exponentially with the temperature decrease. One simple experiment for mapping the oil apparent viscosity with temperature consists in charging a rheometer with the oil, heating the sample to an initial test temperature and reducing the sample temperature with a chosen shear rate and measure the shear stress during the cool down. This test can be repeated for various shear rates and if, at the same sample temperature, the apparent viscosity is the same for various shear rates, it reflects a Newtonian fluid behavior at that temperature.

This type of test was performed with the waxy crude oil, cooling it from 60 °C to 4 °C with the cooling rate of -1 °C/min. Constant shear rates of 10, 50, 100 and 500 s^{-1} were used. Figure 4.1 presents the apparent viscosity measured. It can be seen that from 60 °C until around 19 °C the curves for all shear rates superimpose. They increase linearly with the temperature reduction in a semi-log scale. From 19 °C to 4 °C the slopes of the curves change, not superimposing each other anymore. The slopes are steeper when the shear rate is lower and the shear stress – shear rate relation is no longer linear.

This test indicates that the oil present a Newtonian behavior until the temperature is above the WAT minus 3 °C. Below that temperature apparent viscosity is lower for higher shear rates, indicating a non-Newtonian shear thinning behavior. In dealing with a waxy crude oil, the fact that this effect appeared at 3 °C below the WAT may be a result of two phenomena: (1) The crystallization kinetics, i.e., crystals take time to form and when their effect was noticed the temperature had already decreased (see Venkatesan et al [69]) or; (2) A minimum amount of wax crystals is necessary for changing the oil rheological properties (see Kané et al. [29]).

The oscillations exhibited by the 10 s^{-1} curve in Figure 4.1 may be due to the difficulty of the rheometer control system in keeping a constant shear rate at low torque (around 1 μNm).

As the oil rheology depends on the thermal history, Figure 4.1 presents only one particular dynamic picture. The cooling rate of -1 °C/min is probably too fast when compared with most subsea scenarios, mainly for thermally insulated pipelines. The thermal history of the fluid depends also on its radial position inside the pipe.

This type of data is typically used in the oil industry for calculating steady state and transient flow in pipes. Even if it does not correspond to the exact physical condition in the pipe, it gives satisfactory results, keeping in mind the uncertainty in many other pipeline flow calculation variables, as flow boundary conditions (flow rate and pressure), temperature of the fluid at the pipe entrance, ambient temperature, pipe roughness (that may be influenced by corrosion or solid deposits), etc. The data in Figure 4.1 may be used to fit apparent flow curves at various temperatures or simply translated into a table format for getting directly the apparent viscosity at given shear rate and temperature.

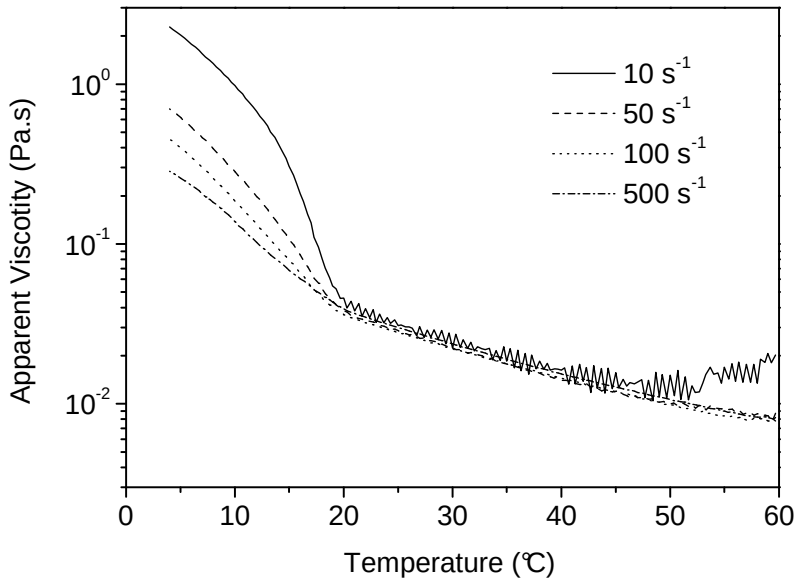

Figure 4.1. Apparent viscosity versus temperature measurements for different shear rates, cooling from 60 °C to 4 °C at -1 °C/min. For each curve a new crude oil sample was used.

However, this kind of measurement allows only a restricted view of the fluid properties. Its behavior must be still evaluated under different gel formation conditions with more appropriate transient tests. One of those tests is presented in the next section. A more complete dynamic analysis is the subject of Chapter 5.

4.2.2 Shear rate ramp test

The basic rheological behavior of the crude oil A was first evaluated with conventional rheometry, at 4 °C, which is the temperature of interest for this work scenario. The test performed was a shear sweep test. The oil was charged in the rheometer and again cooled from 60 °C to 4 °C at the cooling rate of -1 °C/min and zero shear stress (static cooling). Once the 4 °C temperature was achieved, it was left at rest for a holding time of 20 minutes. Then, a logarithmic increasing shear rate ramp until 1,000 s^{-1} with duration of 5 minutes was performed, followed by an analogous decreasing ramp (see Figure 4.2), forming an up-and-down shear cycle. Such test is used for estimating the flow curve of fluids as a first approximation.

For simple behavior liquids the increasing and decreasing curves superimpose and it provides the effective flow curve of the material. For simple yield stress fluid the increasing curve includes a first part with a steep slope associated with the solid regime, then a plateau and a further increase of the stress with the shear rate. The decreasing curve mostly follows the increasing curve, but at low shear rate it follows the plateau extrapolated towards low shear rates. For a thixotropic yield stress fluid the decreasing curve is situated below the plateau of the increasing curve, a phenomenon associated with the destructuring of the fluid (see Coussot [9]).

Figure 4.3 presents the shear stress measured in this test. During the shear rate increase, the fluid exhibits a local maximum shear stress at very low shear rate, i.e. an apparent yield stress. In this case, the fluid required a shear stress of 241 Pa to start flowing. When that value was

achieved the sample strain was 0.18 and shear rate 0.02 s^{-1}. While the shear rate is further increased, the shear stress decreases before starting to increase again with the shear rate. The shear stress measured in the descending ramp is well below the curve in the increasing ramp. Such a difference between the two curves indicates that the fluid structure was completely changed by the flow during the increasing ramp. At the end of the descent the fluid exhibits a slight tendency to a yield stress three orders of magnitude lower than at the ramp up. This hysteresis recalls the behavior of thixotropic fluids, again suggesting a structure network break, strongly reducing the apparent viscosity. A striking phenomenon is the stress decrease during the increasing ramp, which reflects the fact that the apparent viscosity of the material immediately drops beyond the yield stress. Such an effect might induce, or be related to, some flow instability leading to shear-banding (see Pearson [48] and Coussot et al. [7]).

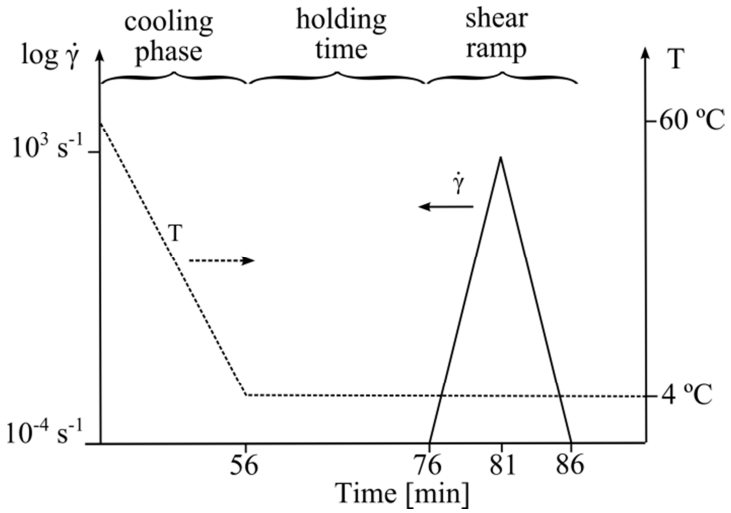

Figure 4.2. Schematic temperature shear rate versus time in shear sweep tests.

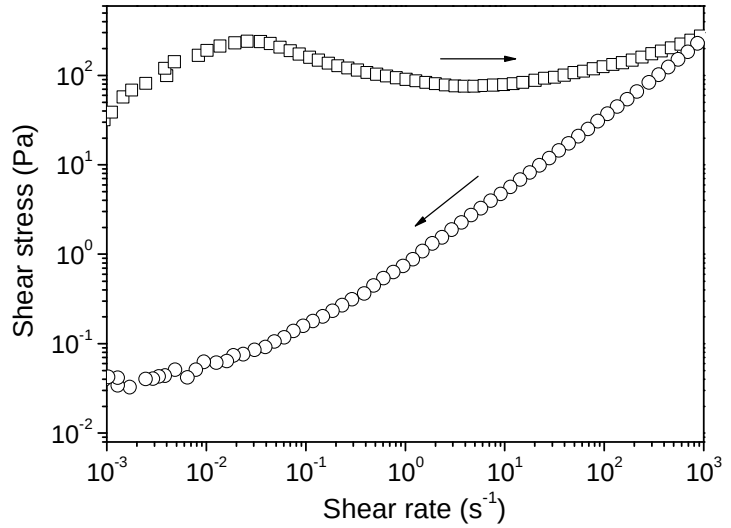

Figure 4.3. Shear stress measured in shear sweep test with the waxy crude oil after static cooling from 60°C to 4°C at -1°C/min and holding at 4°C for 20min.

4.2.3 Recovery after shear

As said before, the reversibility of the fluid structure changes is a typical characteristic of thixotropic fluids. Thus, after being sheared, the fluid structure may recover to its initial state as in a classical thixotropic fluid.

Crude oil A recovery capacity at rest was evaluated by repeating the same sweep cycle with different holding times between the cycles (see Figure 4.4). At the end of the first cycle the fluid was held at rest, still at 4 °C, during 0, 10, 20, 60 and 360 minutes. It means that five tests were performed, each with two sweep cycles and a different holding time between them, always changing the oil sample after each test for getting good repeatability.

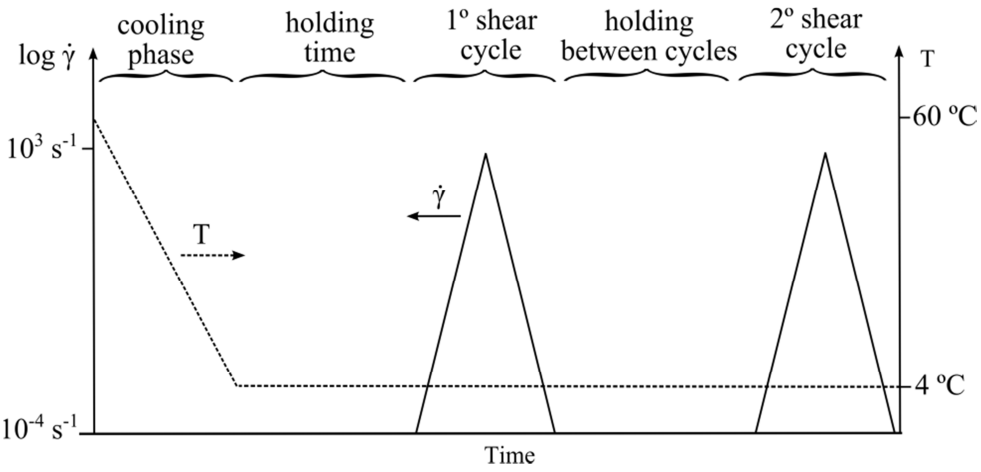

Figure 4.4. Schematic temperature and imposed shear rate for analyzing the fluid recovery capacity after shear. In all four tests the cooling rate was -1 °C/min, 20 minutes of holding time after cooling. The holding time between cycles was changed in each test, from 0 to 360 minutes.

Figure 4.5 presents only the shear increasing steps (the ramp ups) of the first and second shear cycles of each test. It shows that for the first cycle, executed after the initial cooling, the curves superimpose themselves, indicating good repeatability in this experiment. The ramp up in the second shear sweep cycle without holding time between cycles (squares) is very similar to the previous ramp down. The curves for holding times of 10, 20, 60 and 360 min present the same initial slope, but the shear stress increase happens progressively at lower shear rates. Increasing intermediate regions with lower slopes are observed. As the shear rate increases, the curves finally superimpose.

It is possible to observe in Figure 4.5 that crude oil A exhibits a very slow restructuring process. In order to quantify it, the apparent yield stress of the ramp up of the second shear cycle was evaluated in function of the holding time at rest between cycles (see inset of Figure 4.5). The apparent yield stresses were inferred through the change in slope of the increasing curves. Specifically, two regions are fitted using a straight line and their intersection point is taken as the yield stress. The apparent yield stress increases as a small power-law of the time at rest and it is still 30 times smaller than the initial yield stress after 6 h at rest.

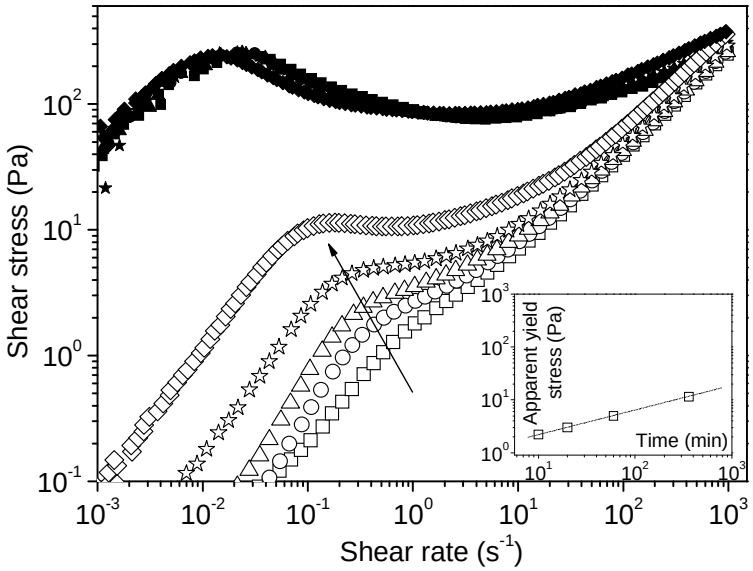

Figure 4.5. Measured shear stress of crude oil A for holding times of 0 (squares), 10 (circles), 20 (triangles), 60 (stars) and 360 min (diamonds). Only the up curves are shown, filled symbols correspond to the first ramp, open symbols to the second one.

Moreover, an extrapolation the line fitted to the data in the inset of Figure 4.5 indicates that the recovery of the initial yield stress would need about 9,000 h at rest, about one year. However, such long time scale may suggest that the observed restructuring effect is not associated with the evolution of the interactions between the particles but rather some significant aging of the particles themselves. Additionally, such a time of rest can also be considered quite unrealistic. Within the framework of crude oil exporting pipelines, realistic time scales would not be larger than several tens of hours. Hence, restructuring will remain small in terms of apparent yield stress. In practical terms, for a pump system that is able to start the flow overcoming the apparent yield stress of the first ramp up, restructuring in terms of apparent yield stress would not be a problem.

4.2.4 Similarity between the model fluid and the crude oil

The objective of exploring the rheological characteristics of a model waxy oil is to verify if it presents an analogous behavior to waxy crude oils in a different temperature, namely at room temperature. It would then allow performing experiments using the model fluid without specific thermal control. In fact, the quantity of paraffin added to the commercial oil was chosen in order to obtain that similarity.

When performing a shear sweep test with the model fluid, using an analogous procedure presented in Figure 4.2 but changing only the cooling step, from 50 °C to 23 °C, the behavior is qualitatively similar to the crude oil, as shows Figure 4.6.

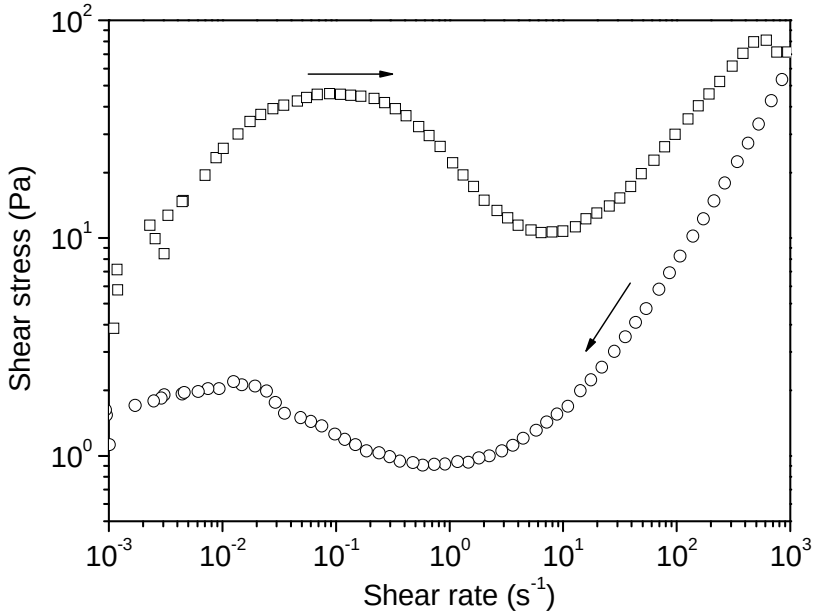

Figure 4.6. Shear stress measured in shear sweep test with the model fluid after static cooling from 50 °C to 23 °C at -1 °C/min and holding at 23 °C for 20 min.

The same basic characteristics observed with the crude oil are also present in the model fluid. Shear stress increases up to a maximum, then decreases and finally again increases. The decreasing curve is well below the increasing one. The exact values of stress variations differ, which may be explained by similar processes but with different destructuring characteristic times. In addition, in the decreasing curve it seems that the material tends to restructure leading to a curve similar to the increasing one with a minimum. This may be explained by a restructuring process faster than for the crude oil.

Finally, the conclusion is that the two fluids have, in their own temperature range, a similar qualitative macroscopic rheological behavior with different characteristic times of structure changes. This justifies studying the model oil with more sophisticated tools (MRI) to get further insight in the behavior of way crude oil.

4.3 MRI study

4.3.1 Cooling under high shear

In Protocol 1, the inner cylinder velocity was set to 100 rpm during the cooling period. Then, once the temperature is assumed to be constant, the rotational velocity was decreased, in steps, to 40, 15, 5, 1 and to 0.2 rpm (see Figure 4.7). Those velocities allowed covering shear rates from 40 s^{-1} until rest, with some overlaps between the different cylinder velocity steps. Then the inner cylinder velocity was again increased to 1, 5 and 100 rpm. The duration of the steps was between 10 and 30 min, until the velocity profile seemed no longer change. Hence, transient and steady state data of each step were recorded. Such test provides information on the rheological behavior of a waxy oil that goes through a pipeline in a cold environment under relatively high shear.

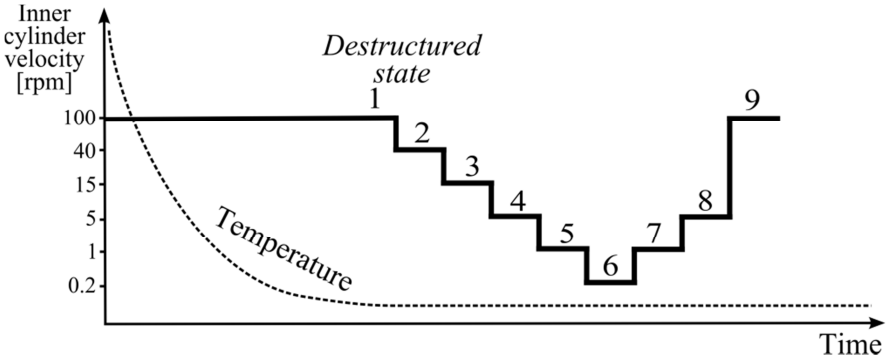

Figure 4.7. Protocol 1 inner cylinder velocity sequence. During the cooling the velocity is 100 rpm (step 1).

4.3.1.1 Cooling Phase

In this test the fluid cools down dynamically, with inner cylinder velocity of 100 rpm. Figure 4.8 presents the velocity profile and the torque evolution during the cooling phase. In the first 30 min of cooling the velocity profile presents a non-uniform slope, possibly due to temperature variations. With time, temperature gets more uniform and the velocity profile becomes similar as for a Newtonian fluid, i.e. as if it had a constant viscosity. Although the velocity profile does not seems to change, the torque measurements during this cooling step shows the apparent viscosity increase for at least 2 h. The velocity profile in a large Couette flow does not depend on the viscosity value itself, but on its relative variation with the radial position, as the velocity at borders are given by the cylinders.

The instantaneous flow curves based on those measurements, showed in Figure 4.9, are calculated with Eqs. (3.2) and (3.3). As time passes, the slope of the curves increases, indicating the apparent viscosity increase with the cooling. A linear relation between shear stress and shear rate can be noticed. So, after the cooling phase, shear rates were observed to be between 20 and 40 s^{-1}, where the fluid exhibited Newtonian behavior, after being cooled under this same range of shear.

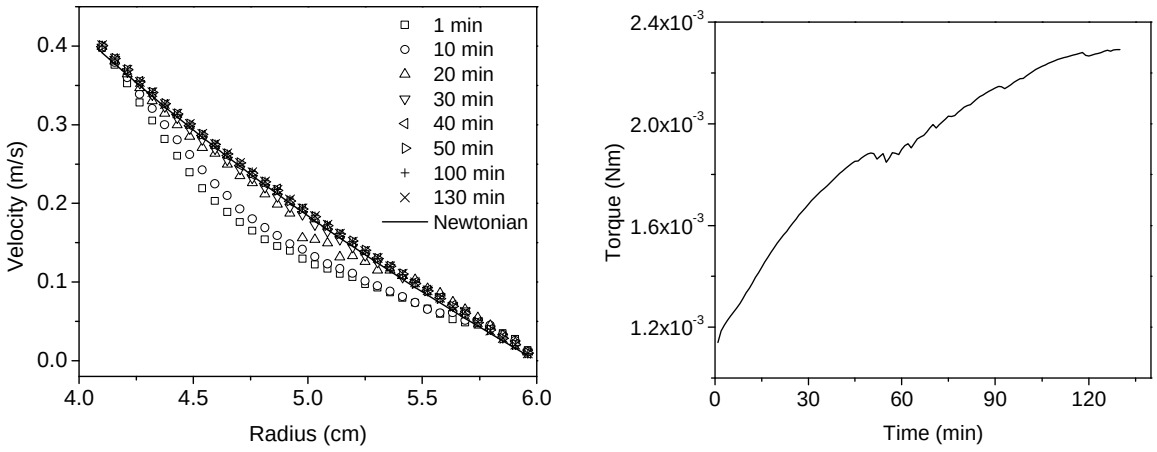

(a) (b)

Figure 4.8. (a) Velocity profiles in Step 1 of Protocol 1, waxy oil cooling at inner cylinder velocity of 100 rpm. (b) Torque measured with time during this step.

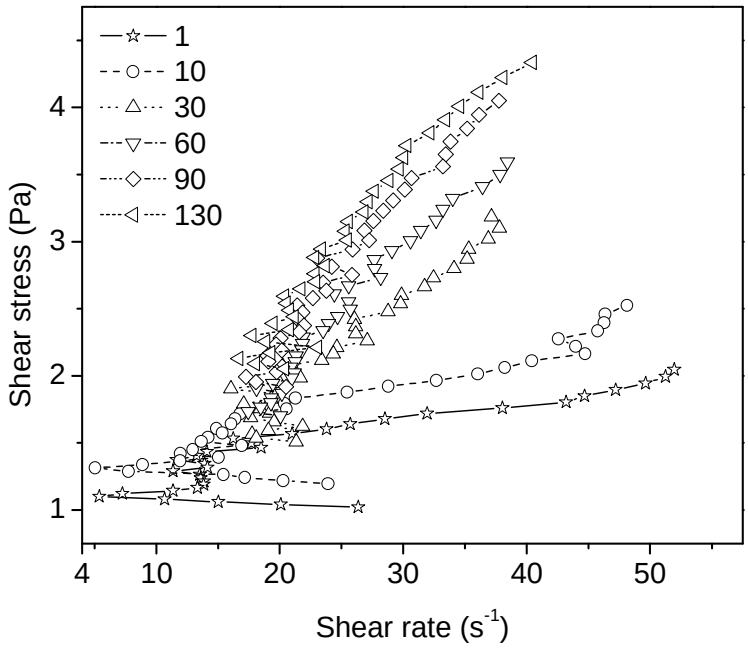

Figure 4.9. Instantaneous flow curves measured during cooling at 100 rpm in Step 1 of Protocol 1.

4.3.1.2 Inner Cylinder Velocity Decrease

In the next steps of Protocol 1, with the inner cylinder velocity decrease, the fluid shear rate also reduces. At lower velocities, the velocity profiles started to gain a curvature, presenting a reduction of shear rate at the outer region of the Couette geometry. Figure 4.10(a) shows, as an example, the velocity profiles measured in Step 4. A small velocity profile evolution in time can be observed, as a profile curvature slight increase, getting more distant from the Newtonian behavior observed in Step 1.

It was also observed that the time for achieving the steady state flow is longer as the inner cylinder velocity reduces. As a result, the final flow curves presented at the end of those lower velocity steps, although close, are not exactly the steady state ones (see below). The lack of time for achieving the steady state condition starts notably happening for inner cylinder velocities below 5 rpm (Step 4), where shear rate is lower than 3 s^{-1}. Figure 4.10(b) shows that torque wasn´t constant at the end of the Step 4. As the temperature no longer exhibited significant variation with time, the torque increase may be attributed to the fluid structure buildup resulting in a higher apparent viscosity at low shear rates.

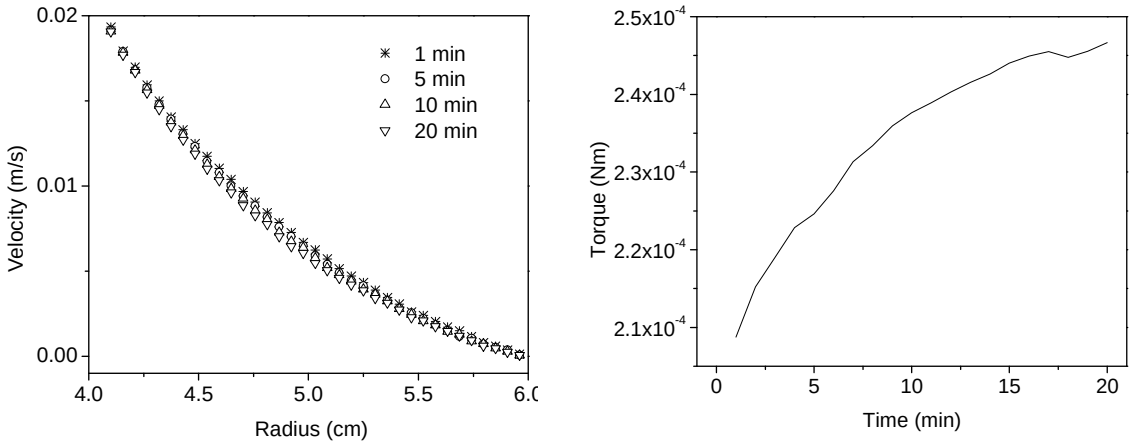

(a) (b)

Figure 4.10. (a) Velocity profiles in Step 4 of Protocol 1. The inner cylinder velocity was reduced from 15 to 5 rpm. (b) Torque evolution during the same step.

This can be better noticed when looking at the instantaneous flow curves measured during Step 4, presented in Figure 4.11. At the lower shear rates the instantaneous flow curves present slight higher slopes, indicating the apparent viscosity increase. The apparent flow curves evolution in time show that higher shear stresses are required for keeping the same shear rate. This reflects the torque curve increase in time.

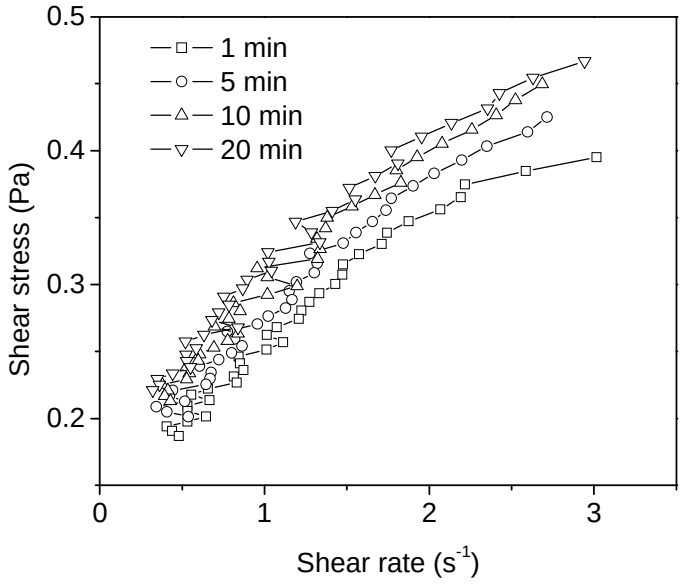

Figure 4.11. Instantaneous flow curves during Step 4 of Protocol 1. Fluid starts showing high flow curve slopes at lower shear rates.

At lower velocities, starting at 1 rpm (Step 5), the flow stopped at the outer region of the Couette geometry, as shows Figure 4.12(a). The velocity profiles show a progressive flow stop coming towards the low radii during the 20 min duration of this step. The profile measured in

the first minute already showed no flow beyond the 5.6 cm radius. The zero velocity region increased until the 5.2 cm radius, approximately. The flow that comes to rest indicates the presence of a yield stress.

The instantaneous flow curves evolution in Step 5 is presented in Figure 4.12(b). It can be seen that the curves' slopes did not increase, but they shifted upwards with time. Although fluctuating, the instantaneous flow curves point to a minimum shear stress, apparently in the order of 0.15 Pa at end of the step.

The same phenomenon of flow region reduction was observed in Step 6 (0.2 rpm), not shown in graphics here. The zero velocity region increased until the 4.5 cm radius, approximately.

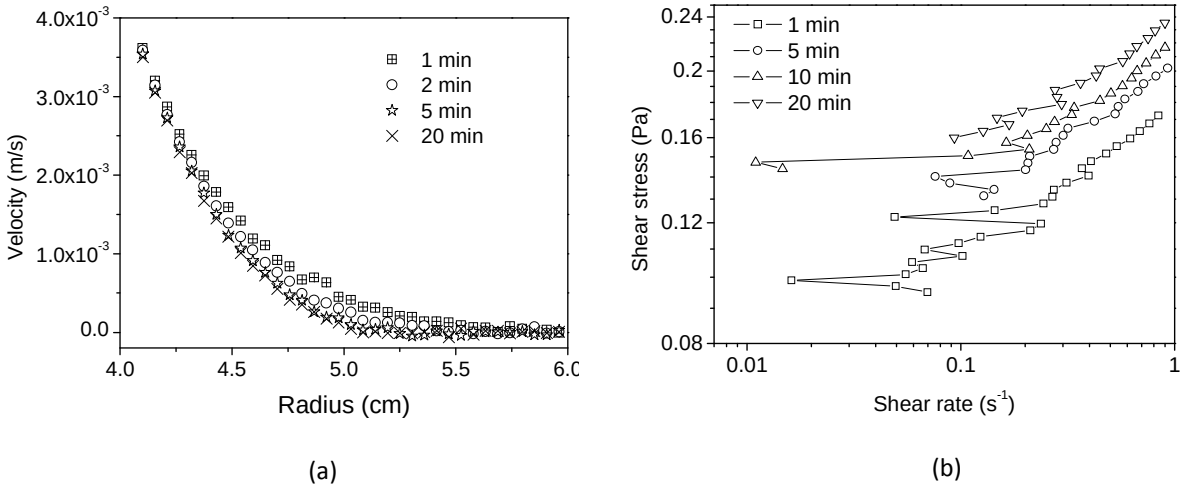

Figure 4.12. (a) Velocity profiles in Step 5 of Protocol 1, inner cylinder velocity coming from 5 to 1 rpm. The flow stopped at the outer region. (b) Instantaneous flow curves of this same step. Although fluctuating, the curves start showing a tendency to a minimum shear stress.

4.3.1.3 Inner Cylinder Velocity Increase

The decrease of the inner cylinder velocity in steps allowed observing the fluid structure build up inside each step. In the next steps of Protocol 1, the inner cylinder velocity is again increased, passing by the same velocities as before (see Figure 4.7). The flow speeds up, increasing the shear rate and promoting the fluid structure break, as it will be seen below.

When the shear rate is changed, the fluid takes time to reach the new structure state. Its structure evolution can be seen as a transient process in each step. When shear rate is reduced, structure builds up, but when shear rate is increased, it breaks.

Figure 4.13(a) shows the velocity profiles and torque evolution during Step 8, where the inner cylinder velocity was increased from 1 to 5 rpm. The profiles evolve in the direction of increasing the flow region. As the first stage of this step the fluid structure was stronger, that structure was progressively broken with the shear increase. The behavior of the velocity curves is analogous to Figure 4.12(a), but in the opposite direction.

Although the inner cylinder velocity was 5 rpm, as in Step 4, the final velocity profile of Step 8 is still not the same as in Step 4 (see Figure 4.10(a)). That difference may be originated by the still changing fluid structure. The fluid started the Step 8 at a well-structured state, because it was flowing at low shear in the previous step, with part of it at rest. The torque curve with time continued to evolve, decreasing, at the end of the step, as showed in Figure 4.13(b). According to the curve tendency, a much longer time should be given to observe the flow stabilization.

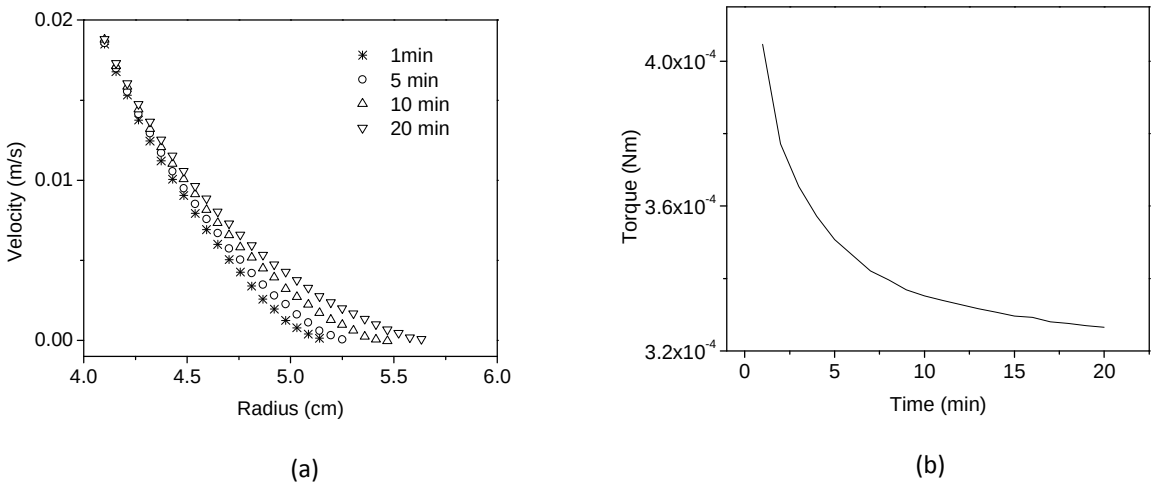

Figure 4.13. (a) Velocity profiles in Step 8 of Protocol 1. The inner cylinder velocity was increased from 1 to 5 rpm. (b) Corresponding torque evolution with time.

Figure 4.14 shows the corresponding shear stress *versus* shear rate curves during those two transient processes in Steps 4 and 8. Two inner cylinder velocity changes are compared. The lower side of the graph shows the transient flow curves after the inner cylinder velocity reduction from 15 to 5 rpm (Step 4), where the fluid structure builds up. The upper side shows the curves after a velocity increase, from 1 to 5 rpm (Step 8), thus increasing the shear rate and bringing the fluid to a lower structure state, reducing its apparent viscosity with time. Both evolutions where observed for 20 min, what was not enough to achieve the steady state since their torque curves continued to change in time.

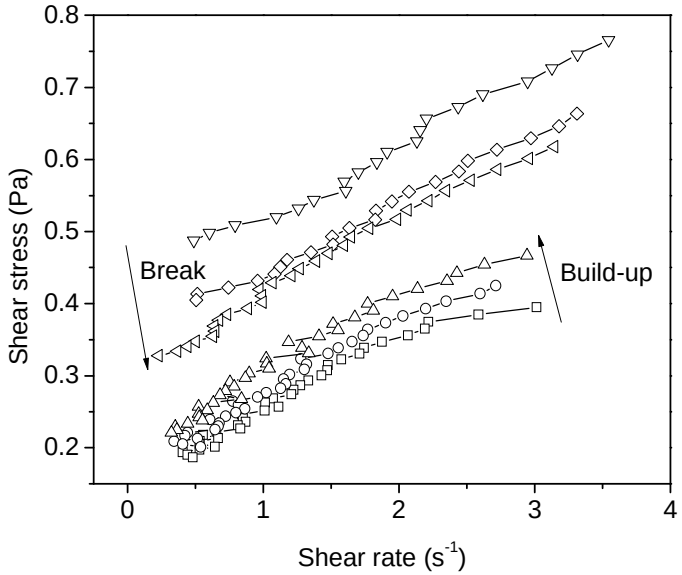

Figure 4.14. The *transient* or *apparent* flow curves during their evolution after step changes in Protocol 1. The fluid structure build up happened in Step 4 (15 to 5 rpm) and the break in Step 8 (1 to 5 rpm).

4.3.1.4 General Behavior

The fluid structure changes were observed to be reversible in Protocol 1. When the velocity is again increased, the measured flow curves present the tendency to superimpose the preceding ones. Presented in Figure 4.15, all the apparent flow curves at the end of each step in Protocol 1 depict the general flow curve of the model fluid. The fact that the torque curves were still changing at the end of the low velocity steps is in fact at the origin of the small gaps between the flow curves at low shear rates in Figure 4.15. Actually, it was observed that lower the shear rate, longer the time to reach the steady state.

To sum up this case of cooling under high shear, where the waxy oil flows below the shear rate imposed during the cooling phase, shear thinning and yield stress are observed. In addition, thixotropy is observed at low shear rates where this transient process is much slower. As in the classical meaning of thixotropy, those changes were observed to be reversible.

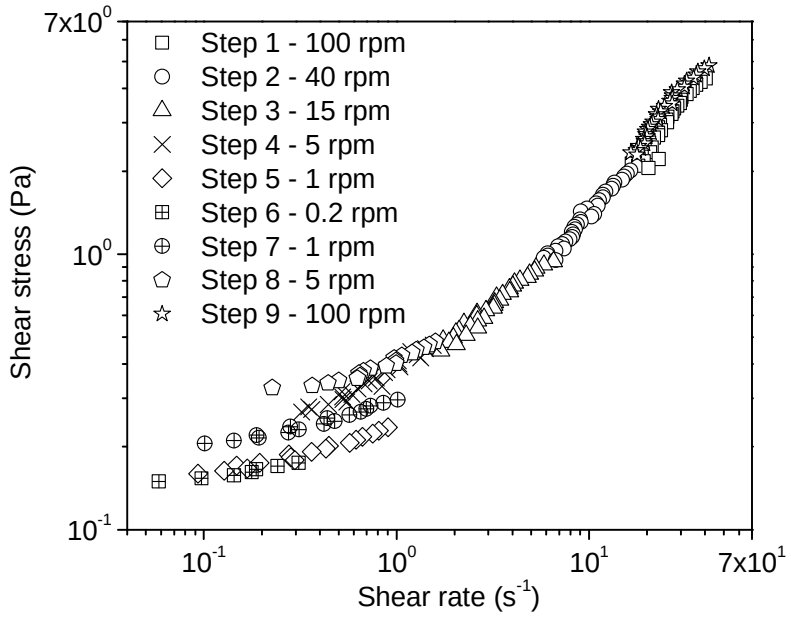

Figure 4.15. Flow curves measured at the end of each step in Protocol 1.

4.3.2 Cooling at rest

In Protocol 2 the fluid was cooled at rest and the flow was then started by setting the inner cylinder velocity to 100 (step 2) and then 200 rpm (step 3), as shows the scheme in Figure 4.16. The velocity was then reduced following the same steps as in the previous test until 0.2 rpm. This test represents the field case of flow restart, where the oil cooled at rest when temperature dropped below the WAT. Starting the flow from a completely gelled oil may indicate how the velocity profile can develop in the pipeline.

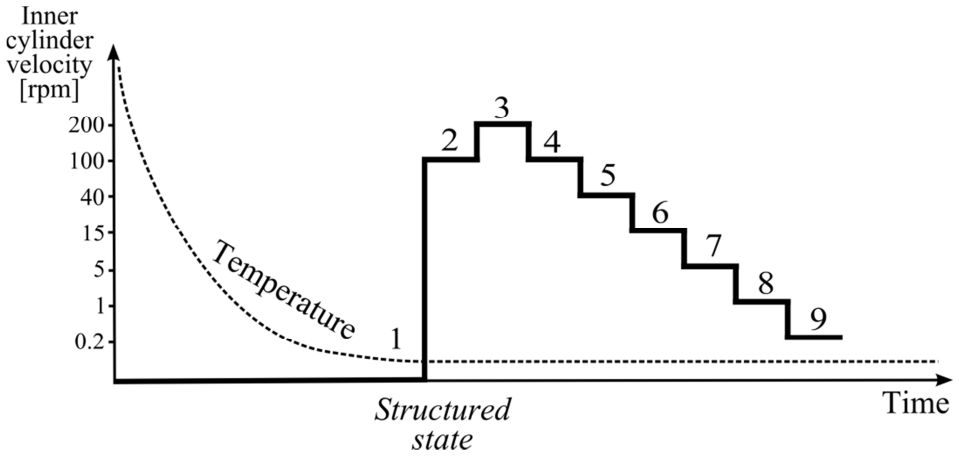

Figure 4.16. Protocol 2 inner cylinder velocity sequence. The model fluid is cooled at rest.

The flow restart at 100 rpm in Protocol 2, Step 2, after the fluid was cooled at rest, resulted in a completely different velocity profile from Protocol 1. Not all the fluid inside the Couette was brought to flow, as shows Figure 4.17. The fluid at the outer region continued at rest.

That happened because the shear stress field acting in the fluid is heterogeneous (according to Eq. (3.3)). When the fluid in the region closer to the inner cylinder starts flowing, the torque required to keep the inner cylinder velocity at 100 rpm decreases, due to the structure break close to the inner cylinder, so decreasing the entire shear stress field. It becomes lower than the high yield stress developed by the fluid under static cooling, being insufficient to bring to flow the fluid closer to the outer cylinder.

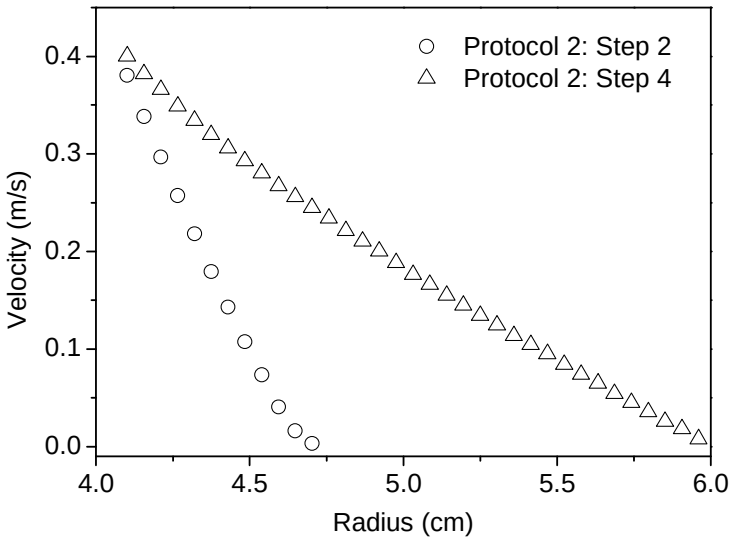

Figure 4.17. Velocity profiles at 100 rpm in Protocol 2. The circles are the measured values for the first equilibrium profile after flow restart. The triangles represent the velocity profile after highly shearing the sample.

Only after 20 min of high shear at inner cylinder velocity of 200 rpm in Step 3 that all the fluid in the Couette geometry was brought to flow. Consequently, in the next step, Step 4, when the inner cylinder velocity was again set to 100 rpm, the velocity profile matched the profile of Protocol 1 (see Figure 4.8(a)). The high shear in Step 3 was responsible for the fluid structure break, leaving the fluid in similar condition as at the end of the cooling at 100 rpm in Protocol 1.

The flow curves corresponding to those two 100 rpm velocity profiles (steps 2 and 4 of Protocol 2) are presented in Figure 4.18. The inner cylinder velocity is the same for the two curves, but in the Step 2 the shear rates are higher due to the smaller flowing region. Despite the heterogeneous fluid structure in the Step 2, both curves seem to have the same slope and represent the same rheological behavior. The region that is at rest in Step 2 does not appear in the flow curve, since it has zero shear rate.

It is interesting noting the shear stress near linear behavior with the shear rate in the two curves. That is a Newtonian fluid characteristic. However, part of the fluid in Step 2 is still at rest, thus presenting a yield stress. It shows how heterogeneous the flow restart of a waxy oil can be. A non-uniform shear stress acting on the fluid may create fluid regions with completely different rheological behaviors. But after the shear is imposed to all the domain until the equilibrium is reached, the flow becomes homogeneous again, with the same rheological characteristics. This kind of analysis shows the importance of measuring the flow with local velocimetry.

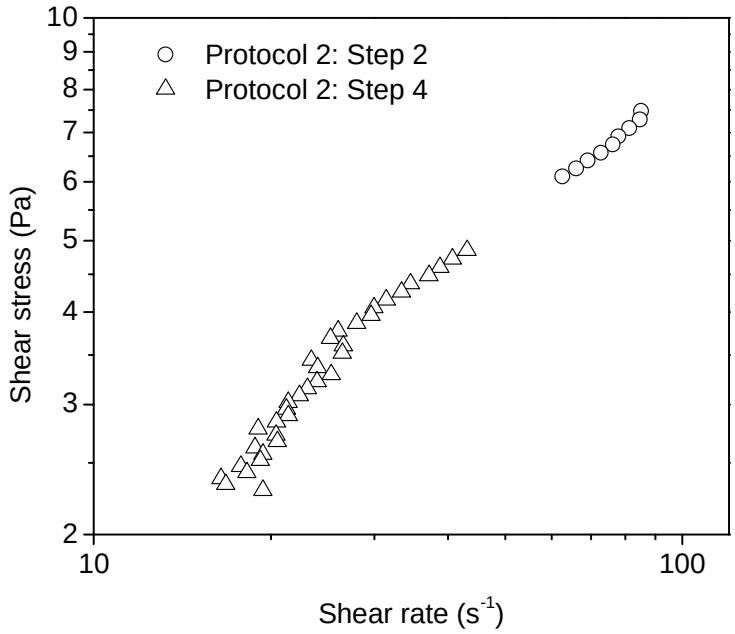

Figure 4.18. Flow curves corresponding to the velocity profiles in Figure 4.17.

The next steps of Protocol 2 presented the same behavior as the velocity decreasing steps in Protocol 1, in terms of velocity profiles and torque values. It is not possible to say that the fluid structure after highly shearing a waxy oil cooled at rest is effectively the same as cooling under high shear, but the resulting local velocity and mechanic behaviors are the same.

4.3.3 Cooling at low shear rate

In Protocol 3 the cooling was under low shear condition, with inner cylinder of 5 rpm. After the cooling phase, the velocity was reduced to 1 and 0.2 rpm and then increased, up to 200 rpm, passing by the same steps as the previous protocols. Then two more steps were performed, 100 and 5 rpm, for allowing direct comparison with the previous tests at the same velocity after high shear. The steps performed in Protocol 3 are presented in Figure 4.19. The Protocol 3 presents similar conditions to field cases of pressure ramp up in pipelines, for example. The fluid is forced to flow in a shear rate higher than the shear rate imposed while cooling.

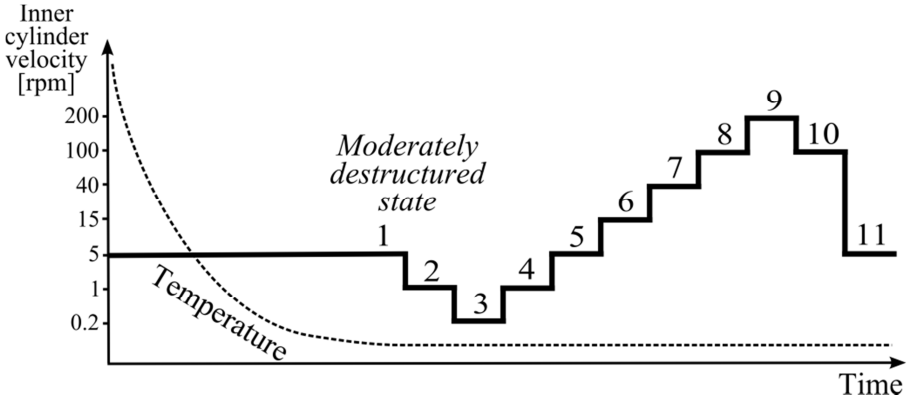

Figure 4.19. Protocol 3 velocity procedure. The fluid was cooled at low shear, under inner cylinder velocity of 5 rpm.

4.3.3.1 Cooling Phase

In this test the fluid was cooled at low shear, 5 rpm inner cylinder velocity. The velocity profiles evolution during that cooling process is presented in Figure 4.20. In the first minutes, while still at high temperature, the fluid exhibited a Newtonian-like behavior, with a velocity profile qualitatively similar to the first step of Protocol 1.

As temperature decreases, so decreases the velocity at the outer region of the Couette, until coming to rest. It can be seen that at 30 min the outer 5 mm of the gap were already at rest, showing zero velocity, and so remained until the end of the step. Meanwhile, in the inner side, where the fluid was flowing, the slope of the velocity profile has progressively increased. It has increased to compensate the reduction of the flow region, as the inner cylinder velocity, at radius 4 cm, was constant.

With the flow coming to rest at the outer region of the gap in the early stages of the cooling process, that region made most of its cooling at rest. It had a similar cooling process as Protocol 2. This allowed the development of a strong gel structure in that region.

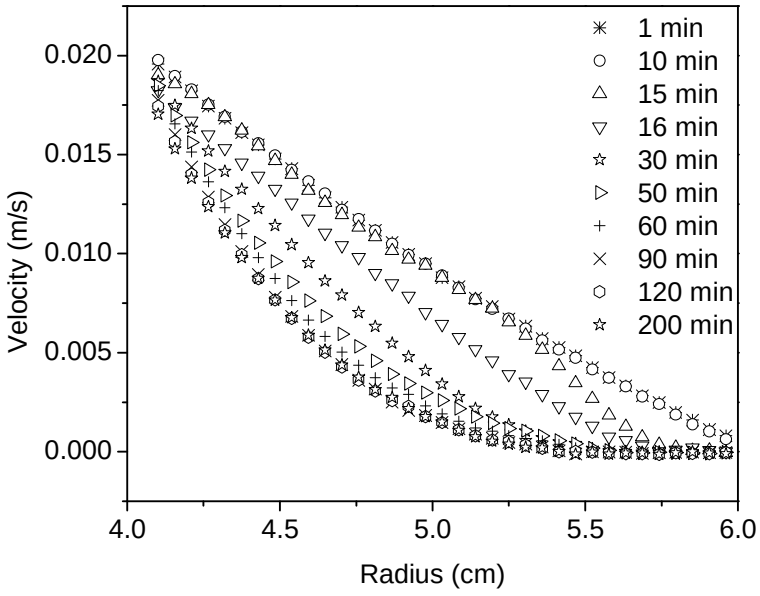

Figure 4.20. Velocity profiles in Step 1 of Protocol 3, where the fluid was cooled at inner cylinder velocity of 5 rpm.

The next velocity decreasing steps did not show any new physical behavior regarding the previous tests. On the other hand, the following velocity increasing steps revealed that outer region of the Couette geometry, which came to rest while cooling, developed a strong resistance to flow, as it will be seen next.

4.3.3.2 Inner Cylinder Velocity Increase

When the inner cylinder velocity was set to 100 rpm in Step 8 of Protocol 3, not all the fluid in the geometry came to flow, as shows the steady state velocity profile of that step in Figure 4.21.

That is a similar behavior to the previous test, Protocol 2, where the first 100 rpm step also didn´t bring the entire fluid domain to flow.

Then, in Step 9, the inner cylinder velocity was set to 200 rpm as in Step 4 of Protocol 2, but instead of shearing the fluid for 20 min, only 9 min of high shear were applied. With this lower shearing time, the resulting velocity profile at 100 rpm in the next step (Step 10 of Protocol 3) showed two distinctive slopes. The first corresponds to the high shear region, with steeper inclination, and the second corresponds to the region of the fluid that was cooled mostly at rest (see Figure 4.20), which probably suffered an incomplete structure break with respect to Step 4 in Protocol 2 (see Figure 4.17). It clearly evidences the fact that the gel structure depends on the type of cooling, as mentioned earlier in this text.

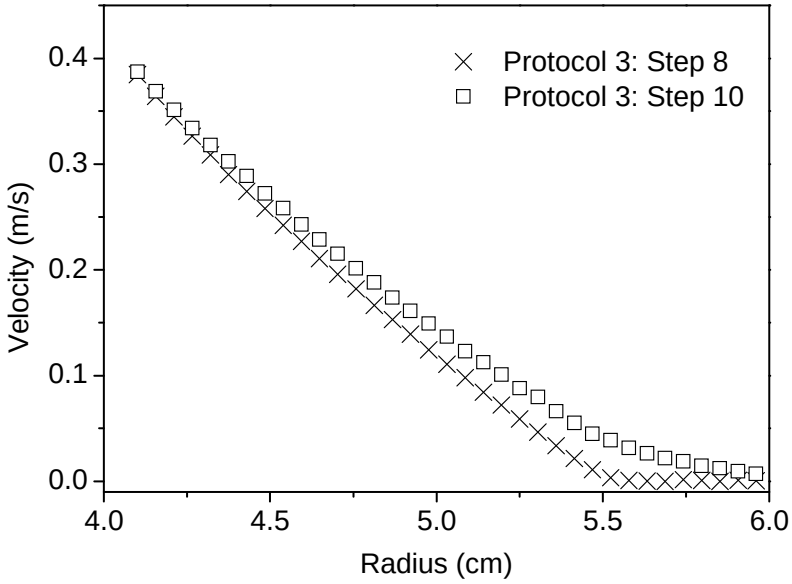

Figure 4.21. Velocity profiles at 100 rpm in Protocol 3. The crosses represent the first profile at equilibrium at 100 rpm in Protocol 3. The squares represent the velocity profile at 100 rpm after shearing the fluid with 200 rpm for 9 min.

4.3.3.3 Velocity Decrease after High Shear

In the final step of Protocol 3, the inner cylinder velocity was again reduced to 5 rpm. The objective of this final velocity decrease was to evaluate the fluid behavior at the same velocity it has cooled, but after passing by several shear conditions, particularly those higher than the shear imposed while cooling.

Figure 4.22 presents the comparison between the flow curve at 5 rpm in the last step of Protocol 3 and the flow curve measured just after cooling, end of Step 1. After 20 minutes of flow at 5 rpm, the measured flow curve in Step 11 was fairly below the flow curve at the end of the 5 rpm cooling step, Step 1. The curves have analogous shape but the curve of Step 11 shows lower apparent viscosity, and a tendency to a yield stress one order of magnitude lower than the Step 1 curve.

The difference between the curves shows that the high shear rates imposed to the fluid between those two 5 rpm steps changed irreversibly the fluid. The fluid restructuring capacity was not enough to achieve the same apparent viscosity it had just after cooling (before of being highly sheared) for the same inner cylinder velocity. This is an analogous behavior to the crude oil presented in Section 4.2.3 (see Figure 4.5), indicating the partial structure recovery.

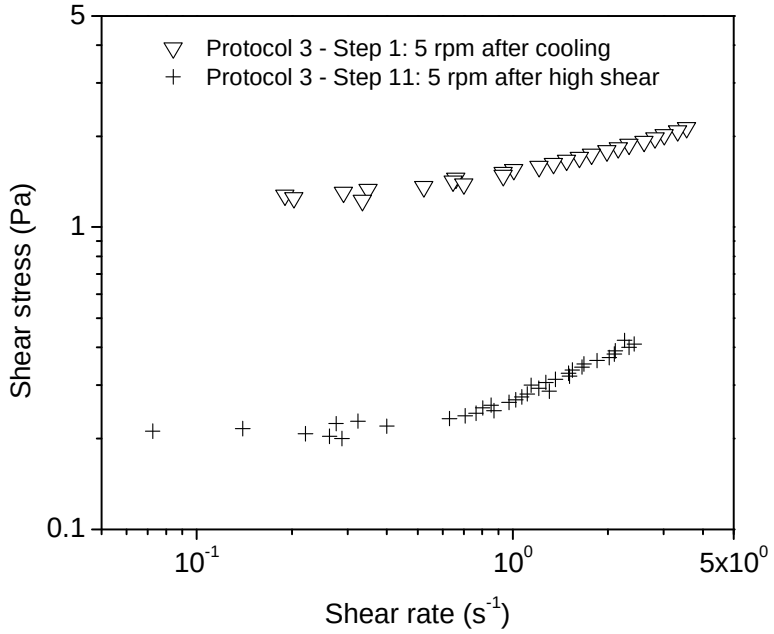

Figure 4.22. Flow curves at inner cylinder velocity of 5 rpm in Protocol 3. The triangles are the flow curve at the end of the cooling step. The flow curve with crosses is the last step measured, after the fluid suffered high shear.

4.3.4 Comparing fluid responses for the different flow histories

From Protocol 1, where the fluid was cooled under high shear, it is possible to notice the apparent viscosity increase while reducing the shear rate. That happens through a transient process at each inner cylinder velocity step down. The appearance of a yield stress promotes the flow stop in the outer region of the Couette geometry. When the velocity is again increased the inverse process occurs, the fluid apparent viscosity reduces and the fluid apparent flow curve evolves towards the same curve it had before at the same inner cylinder velocity.

Protocols 2 and 3 showed that according to the cooling process, the velocity profile at the same inner cylinder velocity can be very different. The sequence of velocity profiles at 100 rpm presented in the previous sections demonstrates how heterogeneous the flow may present itself according to its shear history. More interesting, the different rheological characteristics of the fluid were created by the cooling conditions and the non-uniform shear stress field to which it was submitted.

Figure 4.23 presents four selected flow curves corresponding to four steps of 100 rpm in the three tests. This graphic allows comparing different flows with the same boundary conditions, but with different starting points. Figure 4.18 already showed the flow curves measured in Protocol 2. Here, it is possible to notice that those curves correspond to the same flow curve

measured at the 100 rpm step of Protocol 1, where the fluid was cooled under that inner cylinder velocity.

In addition, Figure 4.23 also shows the flow curve measured at Step 10 of Protocol 3, where the velocity profile presented two slopes (see Figure 4.21). Those two slopes also appear in the corresponding flow curve: One related to the high shear region, superimposing the other 100 rpm flow curves and; A second slope at lower shear rates, which is a result of a high shear imposed to the sample that has not attended the equilibrium condition.

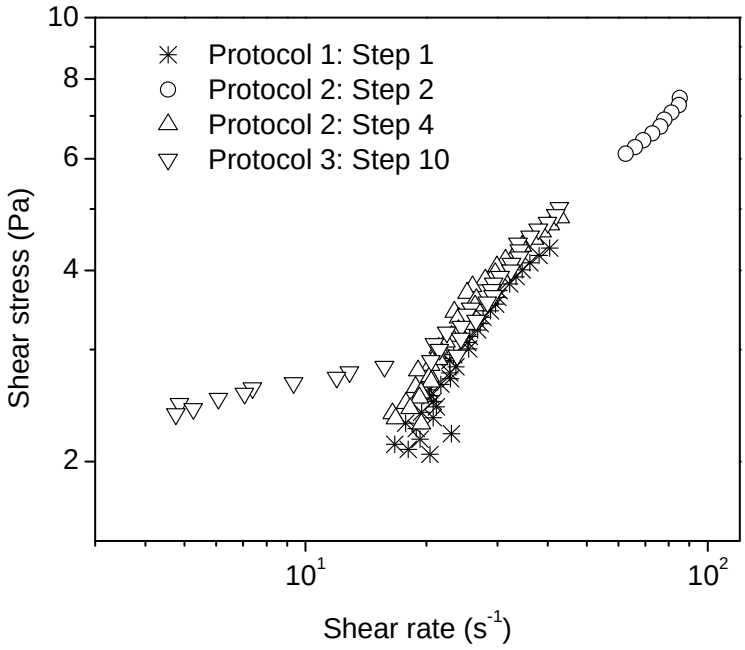

Figure 4.23. Flow curves at the starting 100 rpm steps of Protocol 1 (stars) and 2 (circles), and after high shear in Protocols 2 (up triangles) and 3 (down triangles).

Despite the fact that in the three tests the same cooling rate occurred under different shear conditions, it can be said that after the fluid had been strongly sheared it obeys the same flow curve independently of its starting structure state. In Protocols 2 and 3, the fluid structure is not homogenous in the Couette geometry, since the outer region remains at rest in the case of Protocol 2, Step 2 and a second slope can be observed in the instantaneous flow curve of Protocol 3, Step 10.

Figure 4.24 compares four other flow curves measured at 5 rpm with those flow curves at 100 rpm in Figure 4.23. The objective of this comparison is to observe the general fluid behavior after three different cooling conditions and shear histories.

The first 5 rpm curve is the flow curve at the end of the cooling process of Protocol 3. That flow curve presents a much higher apparent viscosity than the flow curves of the 100 rpm steps. This is an expected result, because cooling waxy oils at low shear rates allows the development of stronger structure network than cooling under high shear rates.

But when the flow curve measured at 100 rpm after the cooling process at 5 rpm is plotted in the same graphic, as discussed above, it is interesting noting that it superimposed the others 100 rpm curves. It indicates that the high shear strongly reduced the fluid apparent viscosity.

Then, when the velocity is reduced to 5 rpm in all tests the fluid behavior is the same, the flow curves are practically coincident, presenting an apparent viscosity much lower than the flow curve measured just after cooling at 5 rpm. In the case of Protocol 3, the high shear changed the fluid irreversibly, i.e. if the fluid is not heated and cooled again it will never have the same flow curve as just after cooling at 5 rpm. After the high shear it followed the same general flow curve depicted in Figure 4.15, as it also did in Protocol 2 after being strongly sheared.

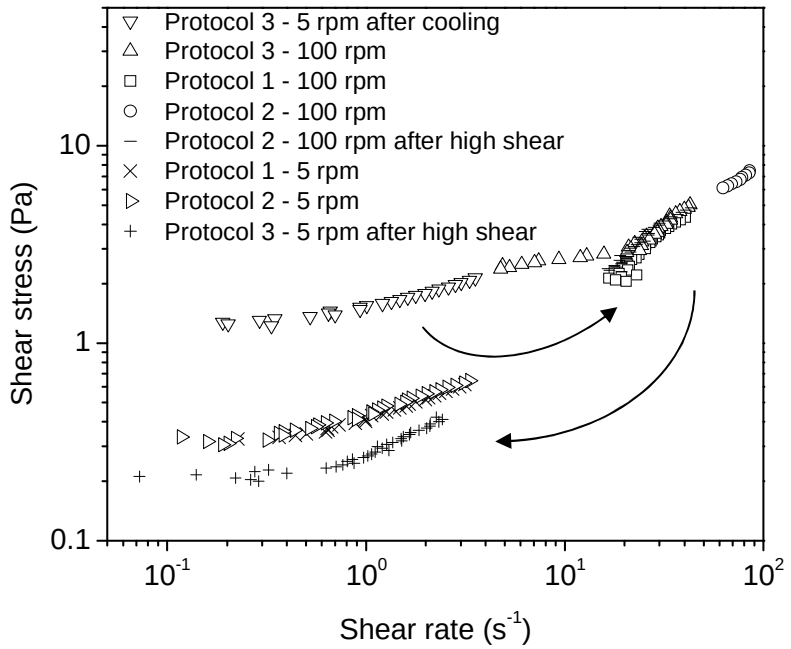

Figure 4.24. Apparent flow curves at the end of selected steps: At the end of the cooling period at 5 rpm (down triangles); 100 rpm after high shearing the fluid cooled at 5 rpm (up triangles); 100 rpm after cooling at rest (circles); At the end of the cooling period at 100 rpm (squares); At 100 rpm in Protocol 2 after high shear (crosses); 5 rpm after high shear in Protocol 1 (stars); 5 rpm after high shear in Protocol 2 (right triangles) and; 5 rpm after high shear in Protocol 3 (plus).

That comparison shows that the same structure state may be achieved by cooling the fluid under high shear or by breaking the structure formed under lower shear conditions while cooling.

As a conclusion from the behavior observed in Figure 4.24, it can be said that the fluid rheological behavior is defined by the maximum shear it was submitted after temperature stabilization. In other words, if at a certain moment the fluid is submitted to a shear higher than its historical maximum after the cooling period, that new maximum shear will change the fluid behavior, by breaking its structure, defining a new steady state flow curve with new reversible thixotropic behavior. The magnitude of this change will depend on the duration of this high shear, if it achieved steady state or not. Later on, if this new shear maximum value is not exceeded the fluid will always follow these same behavior. This changing in rheological behavior

by a new maximum shear is irreversible. The previous behavior can only be obtained if the fluid is again heated and cooled following the same flow history as before.

4.4 Conclusions

4.4.1 Reversible and irreversible structure breakup

The transient features described in this chapter define two different thixotropic characteristics of the waxy oil. One reversible, that acts mainly at the low shear rates driving the fluid towards the steady state flow curve. Another irreversible, that acts breaking the structure formed in the cooling period and redefining the fluid rheological parameters if the shear rate goes over its historical maximum, once temperature is stable.

That irreversible structure break redefines the fluid flow curve. Figure 4.25 illustrates this reasoning. When the cooling process has ended and temperature is stable, every time a new maximum shear rate - $\dot{\gamma}_{max}$ - is achieved the corresponding shear stress is located on the state curve drawn in black in Figure 4.25. That state curve at $\dot{\gamma}_{max}$ is a one direction path, because every time a new $\dot{\gamma}_{max}$ is achieved there is an irreversible break in the fluid structure, which becomes weaker. Then, for $\dot{\gamma} < \dot{\gamma}_{max}$, it follows the corresponding dashed flow curve from the respective $\dot{\gamma}_{max}$. If a new maximum is not achieved, the fluid will exhibit reversible thixotropic behavior and follow the dashed flow curve. If a new $\dot{\gamma}_{max}$ occurs, a new flow curve will take place, with a lower apparent viscosity than the previous one.

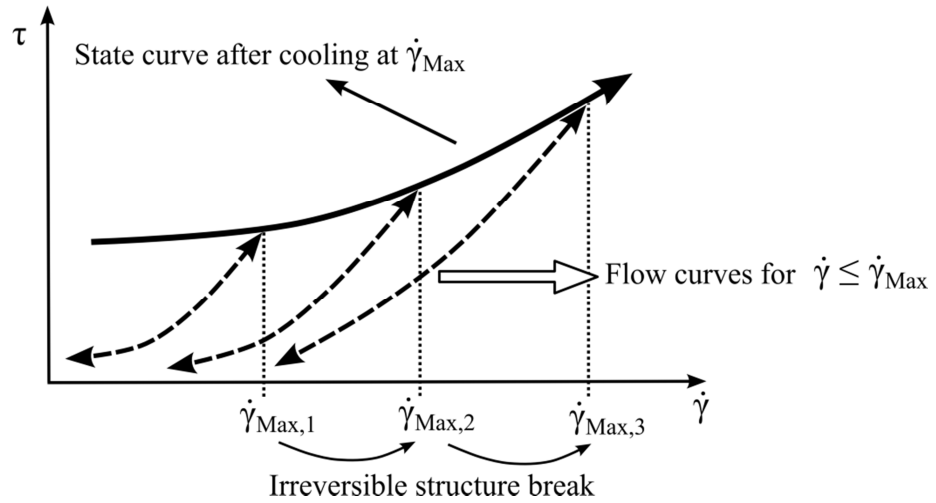

Figure 4.25. Sketch of the waxy crude oil behavior with irreversible structure breaks represented by the state curve in black and flow curves defined by the maximum shear rate suffered by the fluid.

4.4.2 Comparing to waxy crude oil behavior

The behavior depicted in Figure 4.25 can be checked with conventional rheometry experiments for the model fluid and the waxy crude oil by executing the sequences of shear rate variations of Figure 4.26 after the cooling process. In these experiments the oils samples are loaded in the rheometer and cooled at 1 s^{-1}. The model fluid was cooled from 50 °C to 23 °C at -1 °C/min and the crude oil from 60 °C to 4 °C, with cooling rates of -1 °C/min until 25 °C and -0.5 °C/min from 25 to 4 °C. The oils were then held at constant temperature, shearing at 1 s^{-1} for developing the flow and get close to a steady state condition. Next, a descending shear rate ramp, with duration

of 3 min, was imposed until 10^{-4} s^{-1}, followed by an increasing shear rate ramp until 5 s^{-1} to the crude oil and 10 s^{-1} to the model fluid. This shear rate stage was kept constant during one hour, waiting again for shear stress stabilization. Then analogous processes were performed with shear rate increases until 100 s^{-1}, as shown in Figure 4.26.

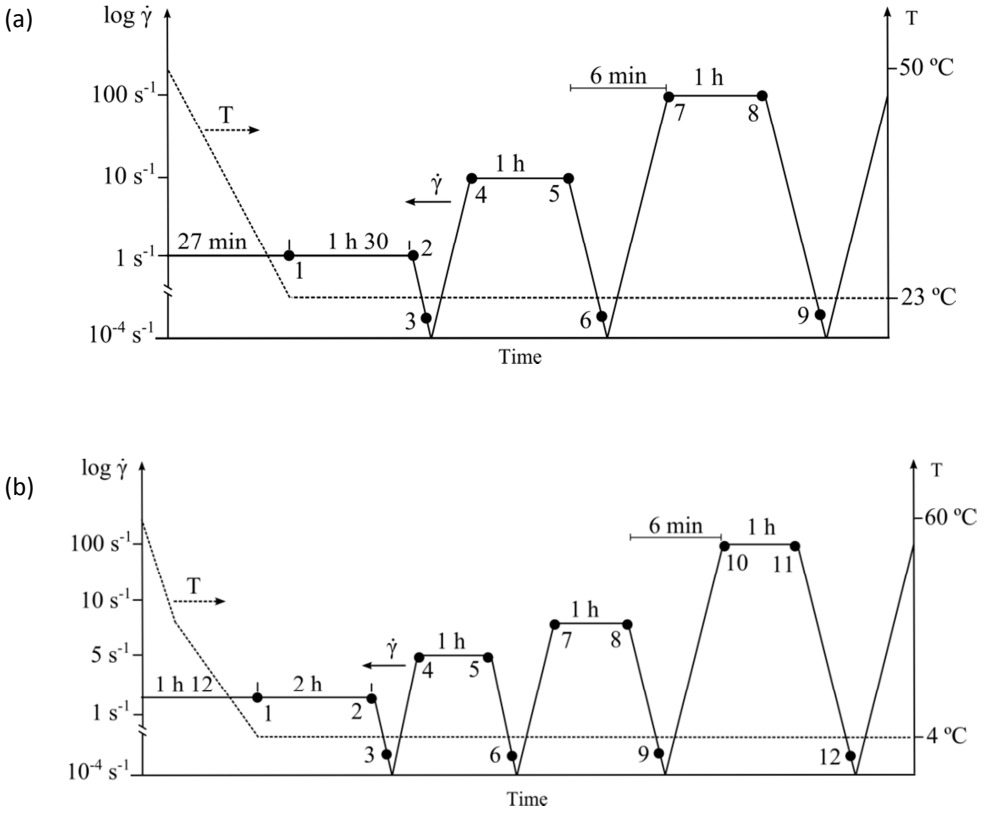

Figure 4.26. Scheme of shear rate behavior with time imposed to the (a) model fluid and the (b) waxy crude oil for testing its structure break after the cooling period. Numbered bullets mark special points.

The results in terms of shear stress vs. shear rate in time along this procedure are quite interesting. When the fluid has been presheared at a given shear rate level (here 1 s^{-1}) while cooling, the increasing and decreasing instantaneous flow curves practically superimpose if the shear rate remains below the imposed value during the preshear. When the shear rate is again (rapidly) increased, beyond the preshear value, the shear stress vs. shear rate curve is in the continuity of the flow curve obtained previously. But, waiting for a sufficient time at a shear rate higher than the maximum level in preshear the stress decreases (dotted lines in Figure 4.27), a new steady state level is reached after some time. A new state of structure is achieved, which is again stable as long as the shear rate imposed does not overcome the maximum level of the previous shear. The next decreasing and increasing flow curves are superimposing (see Figure 4.27). A similar result is successively obtained for higher maximum shear rate levels. Finally, exactly the same trends are found as those observed from the MRI tests with the model oil and schematically represented in Figure 4.25: The state of the material is governed by the maximum shear rate it has undergone after cooling.

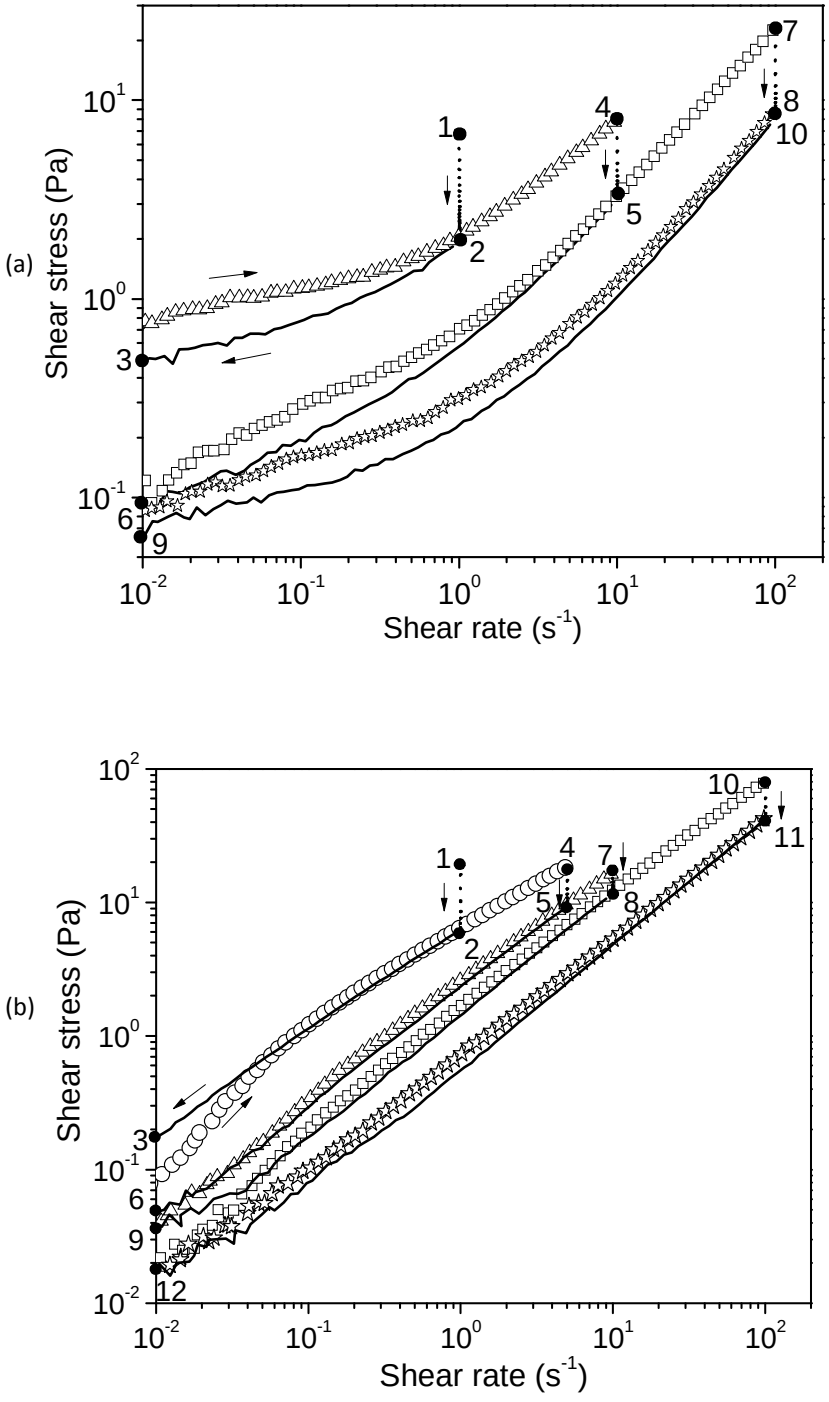

Figure 4.27. Shear stress measured with imposed shear rate scheme of Figure 4.26 starting at the end of the cooling period at an apparent shear rate of 1 s^{-1} for the (a) model fluid and (b) the crude oil. Continuous curves correspond to decreasing shear rates and symbols to increasing shear rates. The vertical dashed lines are the stabilization steps: At 1 s^{-1} (a) 1.5 h for the model fluid and (b) 2 h for the crude oil and; 1 h for the succeeding steps. Numbered bullets indicate the time sequence as in the previous figure.

CHAPTER 5

RHEOLOGICAL STUDY OF THE DESTRUCTURING FLOW

5.1 Introduction

The shear rate ramp test presented in Section 4.2.2 illustrates the complex rheological characteristics of a waxy crude oil statically cooled to a temperature below its WAT. When that fluid is submitted to an up-and-down shear rate ramp, first, it is observed a rapid increase of the stress with the shear rate, as for a yield stress fluid in the solid regime. Then, beyond a maximum value which likely corresponds to a solid-liquid transition, the stress falls despite the increasing shear rate, indicating an important destructuring process. With further shear rate increase the stress finally increases again, forming a non-monotonic transient shear stress vs. shear rate curve during this flow start. Finally, when the shear rate is decreased the stress is significantly below the ramp-up curve.

At first sight, the trends observed in that test suggest that waxy crude oil A exhibits a yield stress and a common thixotropic behavior, due to the important hysteresis in the up-and-down curves. In this case, the local minimum in the stress vs. shear rate curve, which cannot correspond to homogeneous steady flows (Tanner [65], Coussot [9]), is consistent with observations for strongly thixotropic fluids (Coussot et al. [7], Pignon et al. [50], Møller et al. [38]).

However, those results also show intriguing trends:

- The decreasing ramp reveals a linear fluid behavior in a limited range of shear rates with negligible yield stress with respect to the increasing curve;
- It strongly departs from the increasing curve since the stress level is situated three orders of magnitude below;
- With such a difference between the two curves the question is open as to whether the material behavior is reversible, i.e. is it possible to recover the ramp-up shear stress level waiting sufficient time at a given shear rate at some point in the ramp-down curve?

The conclusions from the analyses in Chapter 4 using Magnetic Resonance Rheometry provided some explanations to these observations and showed that the thixotropic characteristics observed in waxy crude oils differ from the classical concept. The fluid steady state flow curve critically depends on its flow history at the temperature achieved after the cooling process. Each time the waxy oil is submitted to a shear rate higher than it has ever seen, an irreversible degradation of the fluid rheological parameters takes place, redefining its steady state flow curve.

In this chapter those different aspects are further investigated, namely, the relation between the start flow characteristics after different cooling and flow histories and the subsequent

rheological behavior (possibly thixotropic) and the question of the reversibility of the destructuring process. In that aim, complete rheometrical analyses of two waxy crude oils were carried out. Initially, crude oil A samples are analyzed in details. Then, crude oil B is tested for the same characteristics observed with crude oil A.

In Section 5.2 the results from creep tests with crude oil A are presented. Those are flow start cases under constant imposed shear stress after static cooling. Next, Section 5.3 discusses flow start cases where a constant shear rate was imposed to the samples. In Section 5.4, the rheological response to abrupt shear rate changes during the destructuring flow are evaluated. Sections 5.5 and 5.6 show relevant aspects of the rheological behavior when the oil is highly sheared, i.e. close to its steady state flow condition. In Section 5.8, crude oil A flow curves are evaluated for different temperatures, completing the necessary elements for calculating flow properties in steady state conditions. Section 5.9 presents a general evaluation of crude oil B, assessing its destructuring flow properties, transient responses to shear rate changes and behavior at equilibrium flow. Section 5.10 summarizes the conclusions of this chapter.

It is not expected here that those two crude oils represent all possible waxy crude oil rheological behaviors, since each crude oil may have a particular characteristic. As it is not possible to define a representative waxy crude oil in a global sense, though, this work goes beyond the analysis of model waxy oils by investigating two crude oils.

As a large number of experiments was performed, a relatively fast cooling protocol was chosen to reduce the total duration of the experiments. Samples of crude oil A were statically cooled from 60 to 4 °C under the cooling rate of -1 °C/min and followed by a holding time of 20 min at rest at 4 °C, except for the tests presented in Section 5.7 and 5.8. For crude oil B, the cooling rate was -1 °C/min from 60 to 35 °C and then -0.5 °C/min until 4 °C, followed by a holding time of 60 min. These values were chosen based on the heat transfer analysis presented in Section 3.2.3.

5.2 Creep tests

The creep test allows evaluating the yielding characteristics of the fluid, namely, a series of different imposed shear stresses. If the stress is below a minimum yield stress limit, after an initial deformation, no flow should be observed. If the applied shear stress is higher than that critical stress, the oil sample should start flowing within some time, depending on the applied stress magnitude.

A set of tests was performed after cooling the oil sample A at rest from 60 °C to 4 °C at -1 °C/min and holding time of 20 min. Next, a constant shear stress is applied and the shear rate is measured with time. After an initial deformation, the shear rate corresponding to a stress of 150 Pa apparently tends to zero, indicating that this stress value is too low to start the flow (see Figure 5.1). On the contrary, for stresses equal or larger than 200 Pa, it can be observed a dramatic increase of the shear rate, that reaches a value of the order of 10^3 s^{-1} after a sharp increase.

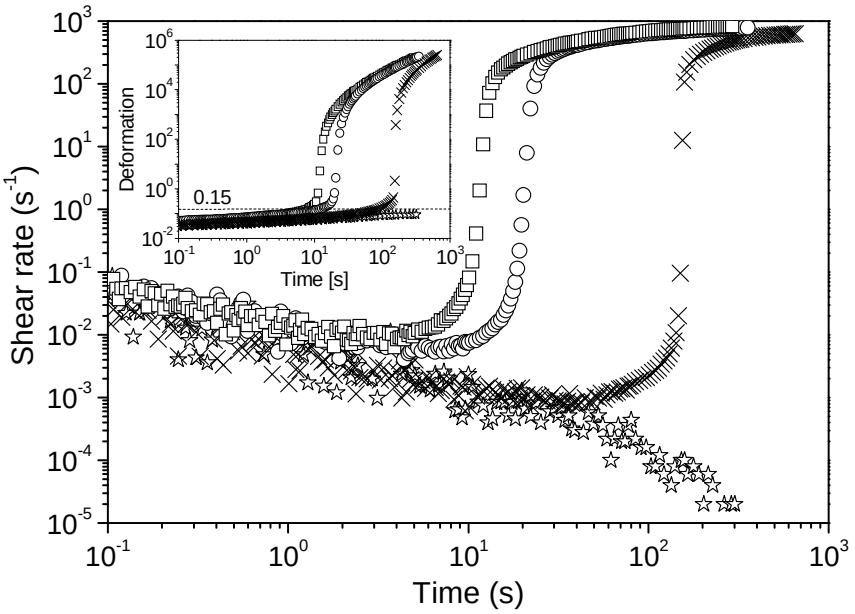

Figure 5.1. Shear rate vs. time for different constant stresses (150 (stars), 200 (crosses), 225 (circles) and 250 Pa (squares)) applied to crude oil A cooled at rest. The inset shows the corresponding deformation vs. time curves with the deformation of 0.15 represented by a dashed line.

Qualitatively, such behavior, i.e. no flow below a critical stress and rapid flow beyond this stress, is similar to the viscosity bifurcation effect observed for colloidal dispersions (see Coussot et al. [8]). However, here the effect is stronger: The shear rate reached for a stress just above the yield stress (here situated between 150 and 200 Pa) is very high. It is worth noting that this behavior is consistent with the observations of Figure 4.3: The flow starts for a stress in the order of 200 Pa and the shear rate rapidly reached a high value since no stable flows at lower shear rates can be obtained under the given stress.

It is worth noting that for the different stress values the abrupt increase of the shear rate, associated with the transition to the liquid regime, occurs for the same critical deformation (around 0.15). That means that the material first undergoes a creep flow in its solid regime and falls in the liquid regime when it has reached its critical deformation. Here, it is considered that at the solid-liquid transition, yielding affects the initial solid structure configuration by irreversibly breaking it. Then, in the liquid state, plastic effects take place (see Coussot [9]). The shear rate in the creep flow decreases when the stress approaches the yield stress. It means that the time before reaching the liquid regime will increase at the approach of the yield stress, which complicates the exact determination of the yield stress value in practice.

5.3 Constant shear sate tests

In the creep tests presented in Section 5.2, it was noticed an abrupt increase of the shear rate during the transition from the solid to the liquid regime. This rapid destructuring flow presents itself as an additional difficulty for studying the flow properties. Thus, controlled shear rate tests may be preferable for analyzing the liquid regime.

Fluids exhibiting the viscosity bifurcation effect discussed in Section 5.2 also exhibit shear banding in steady state when a shear rate is imposed below a critical value reached at a stress just above the yield stress (Ovarlez et al. [43]). In that case the thickness of the shear localization band decreases with the apparent shear rate value and the shear rate along the interface between the solid and the liquid regions is finite and can even be constant if the stress distribution is homogenous. This effect results from the competition between destructuring and restructuring processes in these thixotropic fluids (Coussot et al. [8]).

The MRI-rheometry study of Chapter 4 using the model waxy oil suggests that the situation for waxy crude oils strongly differs from that for thixotropic colloidal suspensions. Indeed, for that model waxy oil a qualitatively similar macroscopic behavior was observed (strong hysteresis in a sweep test as in Figure 4.3). However, it was shown that after the initial breakage of the structure requiring a high stress, the fluid can steadily flow in a wide range of shear rates without exhibiting shear banding. This suggests that for waxy oils the restructuring process is negligible in those experiments and irreversible destructuring process plays a major role. That also means that, in general, controlled shear rate tests should not be affected by shear banding.

A series of constant shear rate values is imposed to oil-gel samples that were submitted to the same cooling history, originating the same gel structure. The samples were all cooled from 60 °C to 4 °C at -1 °C/min and held at 4 °C for 20 min. Next, a constant shear rate was imposed. That procedure was repeated for shear rates ranging from 0.01 to 100 s^{-1} and the shear stress response of the material was measured with time. In this test, the critical deformation, where the solid structure collapses, will be achieved in different times, according to the magnitude of the impose shear rate. The measured data is presented as shear stress vs. strain evolutions for the different shear rate levels in Figure 5.2. It is worth noting that since a controlled stress rheometer is used, it is not able to impose a stable velocity in the beginning of the flow, especially when the apparent viscosity rapidly varies. For the shear rates of 3 and 100 s^{-1}, for example, the rheometer could keep them constant only after deformation values of 1 and 10, respectively. It was possible to see the importance of this effect from the velocity measurements and observe that in general the velocity becomes stable and equal to the constant imposed value just after the stress peak, so that this effect should not affect the data analysis beyond the peak.

The first clear trend that may be observed in the measured data is that the stress vs. deformation curves for low deformations (say below 0.05) approximately fall along the same curve (see Figure 5.2). This means that the rate of shear does not play a significant role here, which indicates that the material is deformed in the solid regime. The stress then reaches a maximum value (peak) which depends on the shear rate and finally continuously decreases. The stress peak thus likely marks the transition from the solid to the liquid regime. The fact that the critical deformation associated with this transition (position of the peak) increases with the shear rate is possibly due to a stronger role of viscous effects at higher shear rates.

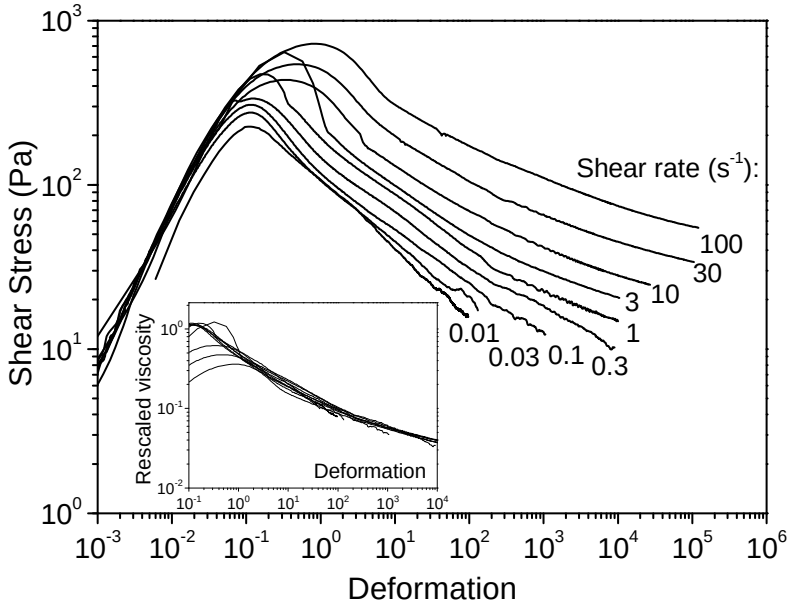

Figure 5.2. Shear stress vs. deformation response of crude oil A cooled at rest for different imposed shear rate values. The inset shows the apparent viscosity rescaled by arbitrary factors as a function of the deformation.

In the liquid regime the shear stress undergoes an impressive decrease of up to two orders of magnitude, and it apparently achieves stable levels for high shear rates. Long transient periods were also observed by Rønningsen [55] and Zhao et al. [83]. This strong shear stress decrease indicates the rapid and significant material destructuration.

It is worth noting the similarity of the stress vs. strain curves in logarithmic scale, which means that they could be superimposed by an appropriate, essentially vertical, translation. Also note that, since the apparent viscosity vs. deformation curves are obtained by dividing the stress curves by a constant factor, a similar analysis applies with such curves, as shown in the inset of Figure 5.2. Those arbitrary factors, used only to show the similarity between the curves, are power-law of the shear rate (numerically, the apparent viscosity was multiplied by $0.002\dot{\gamma}^{0.75}$).

This suggests that the viscosity level is given by the applied shear rate but the evolution of this viscosity depends only on the total deformation undergone by the fluid from the test beginning. For such a series of tests, starting from the same initial state, this means that the structure state does not depend on the shear rate but evolves only with the deformation. A higher shear rate will change the material structure state faster only because it deforms the material faster, but the “quantity of deformation” needed to go from a high structure state to the equilibrium is independent of the shear rate level. That point shall be confirmed by the apparent viscosity analysis discussed in details in Section 5.4.

5.4 Sudden shear rate changes

The above assumption concerning a single structure state associated with a given deformation can be tested by imposing sudden shear rate variations and looking at the variations in apparent

viscosity. Considering the similarity of the apparent viscosity curves (see inset of Figure 5.2) the fluid should respond to a velocity gradient change by directly evolving (by a vertical translation) from the viscosity vs. deformation curve associated with the initial shear rate to that associated with the new shear rate value.

In order to verify that hypothesis, additional tests were performed by first imposing a given shear rate and then changing it in two steps, one increasing of one decade and a second one returning to the initial shear rate. During the first stage the viscosity vs. strain curve is the same as the constant shear rate curve previously obtained, thus demonstrating the reproducibility of the data (see Figure 5.3). Then, for each step of shear rate, an excellent agreement with the above assumption is observed as long as the deformation is not too large. The dotted or dashed lines instantaneously follow the viscosity curve associated with a constant (higher) shear rate from the flow beginning and then follow this curve (see Figure 5.3). This apparently tends to confirm that the state of structure reached at a given deformation under a flow at a small shear rate is the same as that reached for the same deformation under higher shear rate flow.

Although, for large deformation, say more than about 100 strain units, after a sudden change in shear rate the viscosity does not immediately reach the upper or lower curve. This effect progressively increases for larger deformation, as in the case of shear rate reductions from 100 to 10 s^{-1}. Here the apparent viscosity tends to remain approximately constant despite deformation increase, and it is at a level significantly below the continuous curve associated with the correspondent constant shear rate curve. That means that the structure will *a priori* never recover that associated with a steady flow at the smaller shear rate, even after a very long time of flow.

In Figure 5.3, another interesting behavior can be observed at large deformations. At the shear rate change from 10 to 100 s^{-1} at 10^4 strain units, for example, the apparent viscosity exhibited an instantaneous reduction, similar to the low deformation step changes but without achieving the corresponding curve of the new shear rate level. That instantaneous jump was followed by a much slower progressive viscosity evolution, apparently towards the curve of constant shear rate of 100 s^{-1}.

Those results mean that the structure state evolution essentially depend on deformation at sufficiently small deformations and significantly depends on the shear rate for large deformations. The latter effect is typical of thixotropy: In a shear rate step the viscosity takes time before reaching steady state (see Mewis and Wagner [35]). However, here the process seems different: After a large deformation at a high shear rate (e.g. 100 s^{-1}) and a jump to 10 s^{-1} the viscosity rapidly reaches a plateau which is very distant from the curve of constant shear rate at 10 s^{-1} and would hardly join it even after very long time of flow. Thus the intense shear at 100 s^{-1} has irreversibly destructured the material, which presents a negligible restructuring capacity with respect to the overall viscosity change during that experiment.

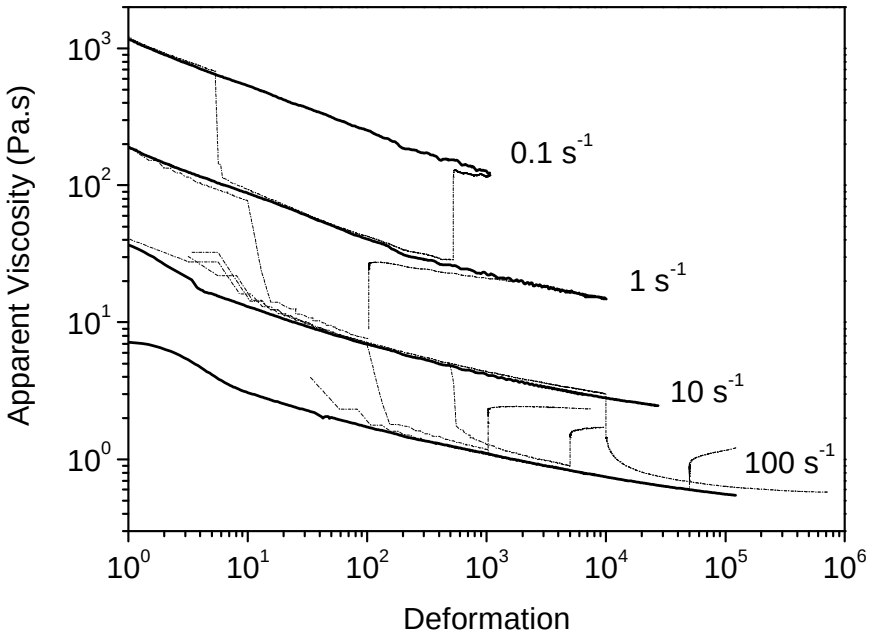

Figure 5.3. Apparent viscosity vs. deformation for the tests of Figure 5.2 at different imposed shear rates (continuous lines). The dashed, dotted or dashed-dotted lines correspond to independent tests of stepwise changes in shear rate.

The experiments of step changes in shear rate revealed that there is a same systematic response of the same structure state to different shear rates only at low deformations. However, at high deformations shear rate and deformation cannot be treated as independent variables, as the material does not follow anymore the constant shear rate destructuring curves.

5.5 Obtaining the equilibrium states

It was seen above that the fluid is progressively destructured when submitted to a constant shear rate. Nevertheless, the equilibrium structure, i.e. that associated with a steady state flow, is not reached even after 10^5 strain units. Here, it is considered that the material has achieved the equilibrium state, for a given shear rate, when the shear stress does not change with time. In order to approach faster to the effective equilibrium state of each shear rate level, the conclusions of the previous chapter will be applied. It was shown that the equilibrium state for a given temperature history is independent of the flow history when the shear rate is the maximum shear rate experienced by the material. It suggests that a single experiment is sufficient to find the equilibrium states of various shear rates levels if the shear rate is stepwise increased. Thus, a solution for achieving faster the equilibrium state could consist in starting by imposing a flow at low shear rate during the cooling process. Such test was carried out by first imposing a low shear rate (namely 0.1 s^{-1}) during the cooling phase from 60 to 4 °C at -1 °C/min and then keeping that shear rate at the constant temperature of 4 °C for a significant time (3 h, see schematic procedure in Figure 5.4(a)).

After that procedure the steady state flow condition seems to be reached (see Figure 5.4(b)), i.e. the stress has reached a plateau. If now the shear rate is increased in steps, at each equilibration step that will be the maximum historical shear rate, hence independent of the previous flow. Indeed, when the shear rate is increased after equilibrium in the previous level, the stress first increases and then progressively decreases towards a new equilibrium state. This process repeats itself at each shear rate stepwise increase. For those new shear rate levels the time of flow, although already large in practice, does not make it possible to reach the exact equilibrium state. It is always difficult to decide whether the equilibrium has been reached, which often leads to arbitrary criterion (e.g. variations smaller than 5% over three successive periods of 30 s as used by Dimitriou and McKinley [15]). Hence, another approach is followed here, based on the observation that the shear stress vs. time curves obtained after the different steps of shear rate have apparently a similar shape (see Figure 5.4(b)).

Thus, the relative viscosity difference to the equilibrium, i.e. $(\eta - \eta_{eq})/(\eta_0 - \eta_{eq})$, where η is the apparent viscosity, η_0 is the apparent viscosity at the initial time (starting at the new shear rate level) and η_{eq} is the (unknown) apparent viscosity at equilibrium, can be plotted in function of time, as presented in the inset of Figure 5.4(b). So, here it is assumed that $(\eta - \eta_{eq})/(\eta_0 - \eta_{eq})$ is a function of time only, and the values of η_{eq} at each shear rate level can be fitted in a way that the curves effectively fall along the same master curve (see inset of Figure 5.4(b)). The values for η_{eq} obtained by that procedure are typically on the order of 10% smaller than the last value measured at the end of each step.

The equilibrium apparent viscosity values obtained with the above described procedure correspond to equilibrium shear stress values, given by $\tau_{eq} = \eta_{eq}\dot{\gamma}$. The equilibrium shear stresses obtained from a cooling under shear can be compared to the shear stress values obtained when the flow was started by imposing a shear rate after cooling the sample at rest. Since there are strong variations (of more than one order of magnitude) of the stress with the deformation (see Figure 5.2), it is interesting to look at the stress reached for each shear rate after different deformations. It is remarkable that the shear stress vs. shear rate curves obtained after different deformations exhibit a similar shape, as shown in Figure 5.5. That is a consequence of the apparent similarity of the stress vs. deformations curves observed in Figure 5.2. Those curves shift downwards when the deformation increases.

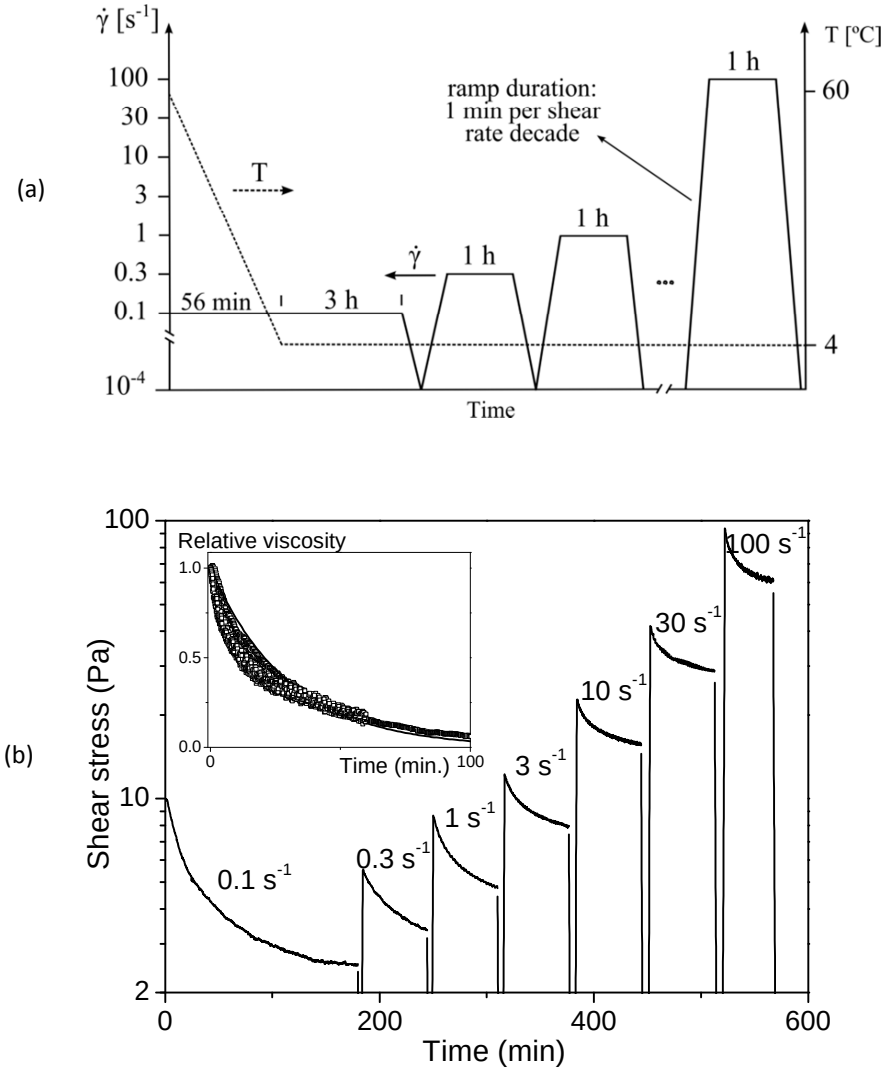

Figure 5.4. (a) Schematic procedure for imposing shear rate at 4 °C after the end of the cooling period. The cooling was under a shear rate of 0.1 s^{-1}. The shear rate is stepwise increased after a flow at the previous level. (b) The measured shear stress of crude oil A from the end of cooling period. The inset shows the relative viscosity difference to the equilibrium (see definition in text) variations as a function of time for the different shear rate steps (symbols). The continuous dark line is a model of the type $d\eta/dt = -(\eta - \eta_{eq})/t_0$, where t_0 is a characteristic time.

Under those conditions it seems that the stress vs. shear rate curve will get very close to the curve representing the equilibrium states after cooling under shear, which is apparently situated at a relatively short distance below the largest iso-deformation curve deduced from the measurements (see Figure 5.5). In a first moment, there could be the suspicion that the very different flow and temperature history would induce a structure different from that obtained by cooling at rest followed by shear. It does not seem to be the case here. Such a conclusion is also supported by the experiments presented in Chapter 4, where it was showed, using MRI velocimetry, that for the model waxy oil about the same steady state flow curve is obtained after a long time of flow following a cooling under shear or a cooling at rest.

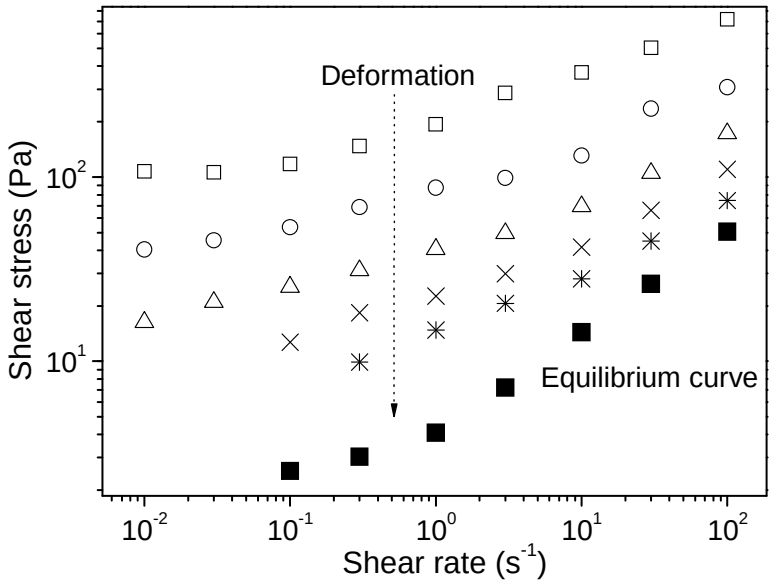

Figure 5.5. "Iso-deformation" shear stress vs. shear rate curves measured at constant shear rate. Open symbols correspond to data of Figure 5.2 at different total deformations: 1 (squares), 10 (circles), 100 (triangles), 1,000 (crosses) and 10,000 (stars). Full squares are the equilibrium values determined from data at equilibrium condition of Figure 5.4 (see text).

5.6 Behavior at equilibrium

It was suggested above that the destructuration at high shear rates after a long period of flow (large deformations) could be partly irreversible, i.e. the viscosity being unable to get back to its equilibrium level at a lower shear rate (see Figure 5.3). This aspect can be clarified by analyzing the rheological behavior of the fluid when it has reached its equilibrium state. In that aim, between each increasing step at higher shear rate in the experiment showed in Figure 5.4 (after cooling under shear) the shear rate was reduced to a very low value before being increased again up to the next step level (see procedure in Figure 5.4(a)). Those down-and-up ramps starting at each equilibrium state, corresponding to a historical maximum shear rate, shall reveal the fluid behavior while the shear rate is below that historical maximum. As the ramps rate of decrease and increase may play a role in the measured behavior due to reversible restructuring effects, an additional experiment (discussed after the analysis of the shear ramps) was set to evaluate the material restructuring capacity during equilibration steps at lower shear rates and during aging at rest.

First, following the procedure in Figure 5.4(a), the shear rate ramps for values below the corresponding shear rate equilibrium point result in an apparent simple liquid behavior (see Figure 5.6). The shear stress monotonically decreases with the shear rate reduction and the curves do not exhibit a yield stress, but follow a nearly Newtonian behavior. Moreover, the increasing shear rate curves superimpose to the respective decreasing curves, without changing the fluid behavior within the duration of the ramps (1 min per shear rate decade). Those results show that after having reached the equilibrium condition at a given shear rate, the fluid behaves mostly as a simple liquid, without showing important thixotropic effects, as it will be discussed

next. Furthermore, a new liquid behavior, associated with a smaller viscosity, is reached at each new shear rate level. That means that this behavior of the fluid depends on the level of the maximum shear rate experienced by the fluid, but only if the fluid is sheared at a higher shear rate and kept for sufficient time so that it can reach a more liquid (lower viscosity) state.

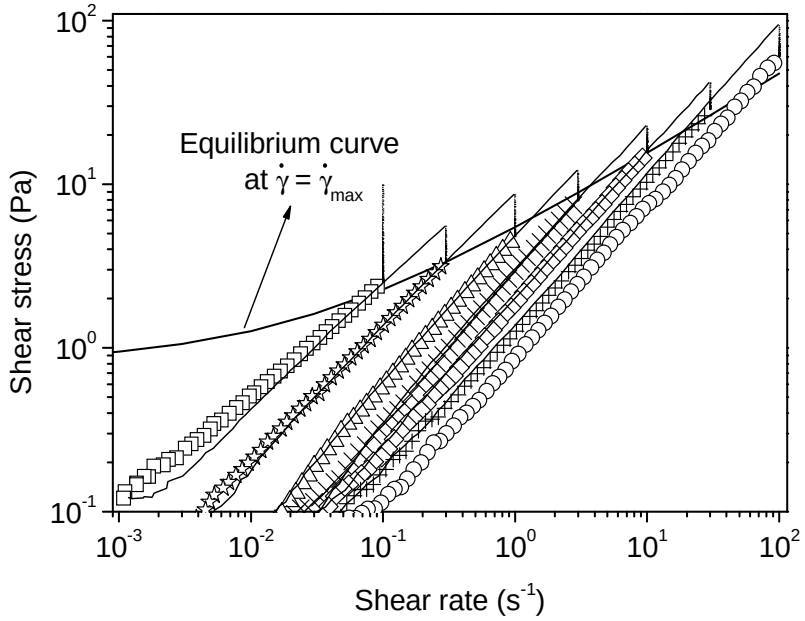

Figure 5.6. Shear stress measured with imposed shear rate from the end of the cooling period at an apparent shear rate of 0.1 s^{-1}. Continuous curves correspond to increasing shear rates and symbols to decreasing shear rates. The vertical dashed lines are the stabilization steps. Same data as in Figure 5.4.

The superimposition of the decreasing-increasing stress vs. shear rate curves around some equilibrium suggests that thixotropic effects are weak when it has reached its equilibrium state associated with a given shear rate. It confirms the observations done in Section 4.2.3, where tests evaluated the effect of time at rest after strong shear. Those tests showed that the fluid structure recover at rest is very slow.

In order to confirm the weakness of thixotropic effects, additional tests were carried out to look at restructuring effects after strong shear. In that aim, intermediate equilibration steps were performed during a shear rate ramp down test departing from the equilibrium state at 100 s^{-1}, i.e. an unstructured state. At the equilibration steps the restructuring flow at different shear rate levels was measured. The experimental procedure of this test consists in cooling a crude oil A sample from 60 to 4 °C at -1 °C/min under shear rate of 100 s^{-1}. This shear rate was kept constant for more 75 min after the sample reached 4 °C in order to achieve a stable shear stress value. Next, the shear rate was decreased with a continuous ramp to 10 s^{-1}. The shear rate was then kept constant at this new level waiting for equilibration of the shear stress value. This process continued to the shear rates of 1 and 0.1 s^{-1}. After the last equilibration step the shear rate was ramped down to 10^{-4} s^{-1}.

The results presented in Figure 5.7 compare the shear stress measured with the procedure above with the shear rate ramp down (ramp rate of 1 min per decade) from 100 to 10^{-4} s^{-1}

presented in Figure 5.6, represented by circles in both figures. The first aspect to be highlighted in this comparison is that both shear rate ramps starting at 100 s^{-1} are very similar over the four decades of shear stress, despite having completely different flow histories. Important differences appear only for shear stress and shear rate below 0.1 Pa and 0.1 s^{-1}, the lowest decades. This confirms the concept that the equilibrium state at the historical maximum shear rate experienced by this material is independent of the flow history. It can be also seen in Figure 5.7 that the oil restructuring capacity is negligible at the 10 and 1 s^{-1} steps. The inset in Figure 5.7 shows the evolution of the shear stress with time in the equilibration steps at constant shear rate. The most significant structure recover was observed at the shear rate of 0.1 s^{-1}, where the shear stress approximately doubled its value before achieving stable flow at around 6,000 s.

Finally, the decreasing shear rate ramp seems a good approximate method for assessing the oil-gel steady state flow curve for shear rates below a given state of equilibrium. Good agreement is obtained during the ramp down until the shear rate of 1 s^{-1}. The most important relative difference was measured at 0.1 s^{-1}, which was of the order of 0.1 Pa. This means that restructuring during flow (after a decreasing step of shear rate) is generally negligible, mainly when compared to the structure state presented by the material just after static cooling.

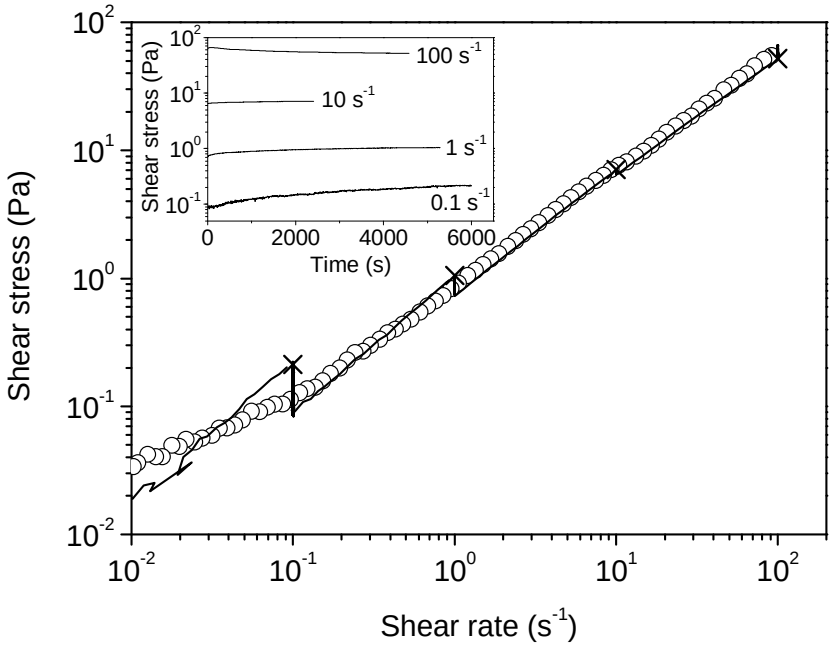

Figure 5.7. Comparison between the shear rate ramp down starting at 100 s^{-1} of Figure 5.6 (circles) and a ramp down test also starting from the equilibrium condition at 100 s^{-1} but with intermediate equilibration steps at 10, 1 and 0.1 s^{-1}. The shear stress variation during the equilibration steps is shown in the inset

5.7 Destructuring from other cooling conditions

In sections 5.2 to 5.4 the destructuring flow of crude oil A was evaluated after a cooling process at rest, with a cooling rate of -1 °C/min and holding time of 20 min at 4 °C. As the presence of shear while cooling influences the resulting gel strength, it is interesting analyzing the

destructuring flow after some different cooling conditions. Thus, the objective of this section is to evaluate the destructuring flow starting from different cooling conditions.

The results of three other cooling processes are evaluated. The following experiments protocols were performed (always cooling the sample from 60 to 4 °C):

1. Dynamic cooling at 1 s^{-1} and -1 °C/min with holding time of 20 min, followed by constant shear rate of 10 s^{-1};
2. Dynamic cooling at 10 s^{-1} and -1 °C/min with holding time of 60 min, followed by constant shear rate of 100 s^{-1};
3. Mixed cooling at -1 °C/min with dynamic cooling at 1 s^{-1} until the temperature of 8 °C followed by static cooling from 8 to 4 °C. The holding time at rest at 4 °C was 20 min and the destructuring flow at 1 s^{-1};

The above protocols involve shear during the wax crystals formation. In protocol 3 the sample has the final part of the cooling process at rest, thus a mixed cooling condition.

In Figure 5.8, the measurements from the four protocols are compared in terms of apparent viscosity behavior. Additionally, the viscosity values measured for the static cooling at -1 °C/min and holding time of 20 min for destructuring flows at 1, 10 and 100 s^{-1} (same data as in Figure 5.3) are plotted in Figure 5.8.

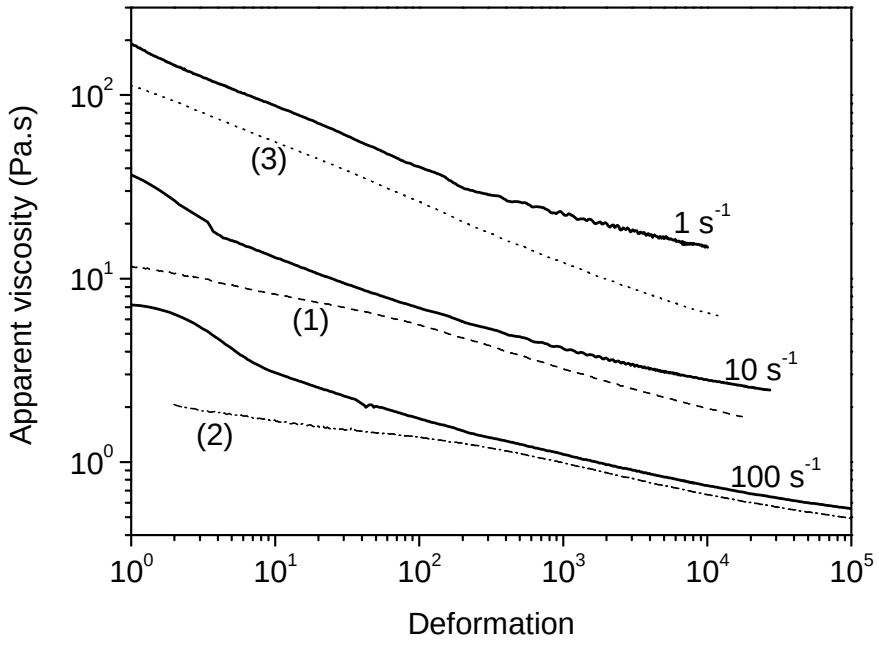

Figure 5.8. Comparison of apparent viscosity behaviors at 1, 10 and 100 s^{-1} measured with the four protocols. The continuous lines are the same data as in Figure 5.3

The presence of shear while cooling resulted in lower apparent viscosity than the destructuring flow measured after static cooling with the same imposed shear rate value.

For low deformations, indeed, it is expected that the viscosity presents lower values than the respective static cooling curve, since weaker waxy oils gels are formed under shear while cooling. At very high deformations, towards the steady state condition, curves with the same shear rate are expected to superimpose, since the viscosity at the equilibrium condition are expected to be the same. In that sense, the apparent viscosity for protocols 1 and 3 seem to be still far from that convergence. Although the viscosities of the respective curves for static cooling are still evolving.

Finally, destructuring flows departing from different cooling conditions can be considered to be analogous to the destructuring flows studied in Section 5.3, where only destructuring after static cooling was analyzed. Lower viscosities are observed at low deformations and destructuring rates present the same trends.

5.8 Equilibrium flow curves at higher temperature

The waxy crude oil equilibrium flow curves at higher temperatures are important rheological data for calculating flow properties. Those properties, as velocity and shear rate, are used to describe the flow and temperature histories prior to the flow restart moment. They constitute essential information for describing the cooling process experienced by the waxy oil.

The equilibrium curves at higher temperatures were obtained using the same procedure as in section 5.5 for 4 °C. Crude oil A was cooled under low shear rate and when it reached the target temperature, the shear rate was stepwise increased, waiting for the equilibrium condition at each shear rate step.

As expected, higher temperatures result in lower shear stresses for the same shear rate (see Figure 5.9). The equilibrium curves obtained for the different temperatures in the range from 4 to 16 °C are similar, i.e. they may be superimposed by a vertical shift. This suggests that the evolution of the structure for these systems is analogous. Non-Newtonian effects seem to disappear around the temperature of 20 °C, where the equilibrium curve is close to a Newtonian fluid flow curve (see Figure 5.9).

In order to evaluate the rheological behavior at temperatures higher than the WAT, an additional series of tests were carried out according to the following procedure. A sample was charged in the rheometer, heated to 60 °C and a shear rate ramp up and down cycle from 10^{-4} to 100 s^{-1} in 6 min was performed. Next, the oil was cooled at rest until 50 °C at -1 °C/min, then left 5 min at rest for temperature equilibration and another shear rate ramp cycle was performed. That procedure was continued to the temperatures of 30 and 20 °C.

The ramps up and down at all temperatures superimposed each other, as expected for a simple liquid behavior. These curves have a slope value of 1 in logarithmic scale, indicating a Newtonian behavior (see Figure 5.9). For the temperature of 20 °C, it can be seen in Figure 5.9 that the two measurement methods originated curves that are almost superimposing. The main differences between them can be seen at low shear rates, where wax crystals, already present in a small quantity at that temperature, may be the cause of the emerging time-dependent effects.

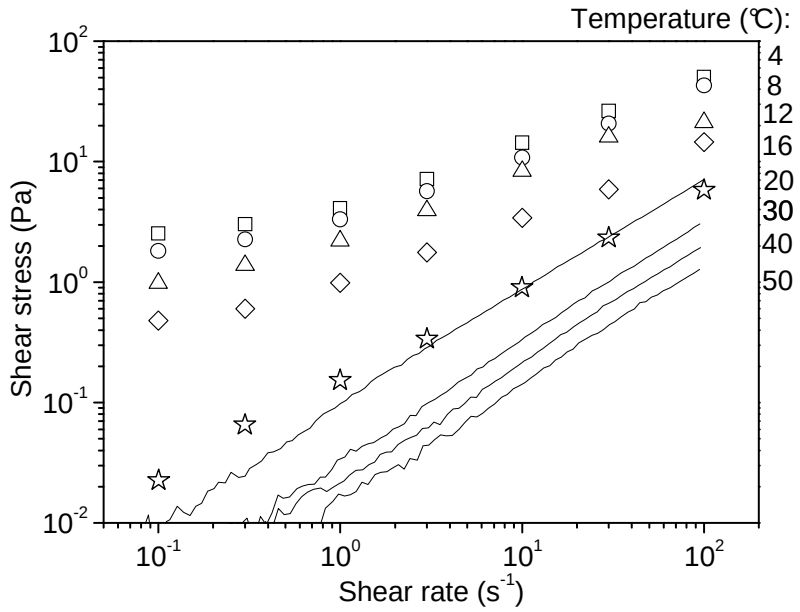

Figure 5.9. Equilibrium curves for crude oil A after cooling to different temperatures, indicated in the right side. Symbols are measured values for temperatures below the WAT. For the temperature of 20 °C and higher (continuous lines) the data were obtained from sweep tests.

5.9 Evaluation of crude oil B

The characteristics of the destructuring flow of crude oil B at 4 °C were also evaluated. With the studies developed so far in this and in the previous chapter, the analysis was more objective, looking for main features of the rheological behavior. The measurements performed with crude oil B was measured applied the same systematic protocol as for crude oil A.

Figure 5.10 shows the shear stress response vs. deformation for imposed constant shear rate. The same characteristics observed with crude oil A are present here, although at higher shear stresses.

The increasing part of the curves, the solid regime, is independent of the shear rate for deformations lower than approximately 0.01. The critical deformation, marking the solid-liquid transition, seems to converge to 0.1 as the shear rate reduces. Next, the decreasing part of the curves show analogous behavior with respect to the shear rate when the shear stress is plotted *versus* the deformation.

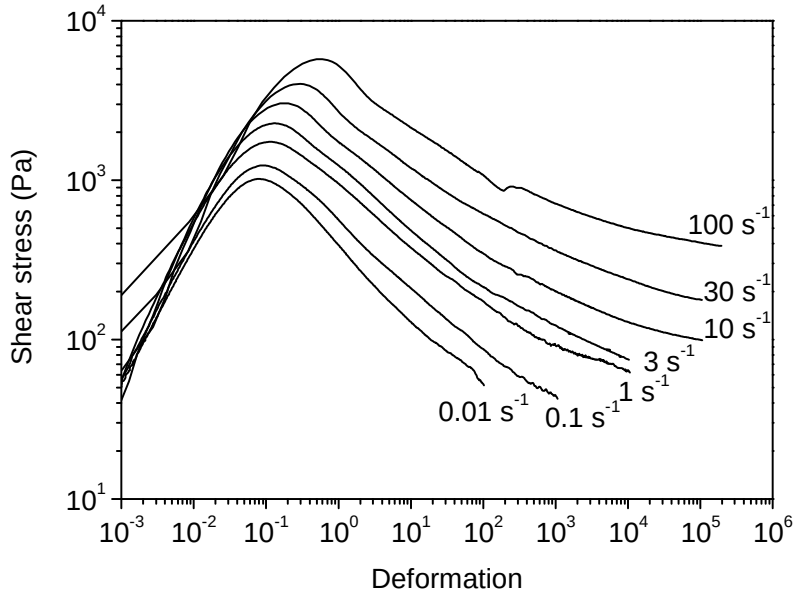

Figure 5.10. Shear stress vs. deformation for imposed constant shear rate tests with crude oil B.

The apparent viscosity behavior, presented in Figure 5.11, for the constant shear rate tests reflects the important destructuration as deformation evolves. Additionally, Figure 5.11 shows the viscosity behavior for destructuring flows with step changes of one order of magnitude in the shear rate (discontinuous curves).

The number of tests performed here is lower than those executed with crude oil A, but general characteristics also show that for sufficiently small deformations viscosity step changes are practically instantaneous and jump from one constant shear rate curve to another. For large deformations, the viscosity step changes lose intensity and the approximation to the correspondent constant shear rate curve happens progressively. For decreasing shear rate steps at high deformations there is not an increasing progressive viscosity evolution. Only a local jump to an intermediate point between the constant shear rate curves, used here as reference curves, is observed.

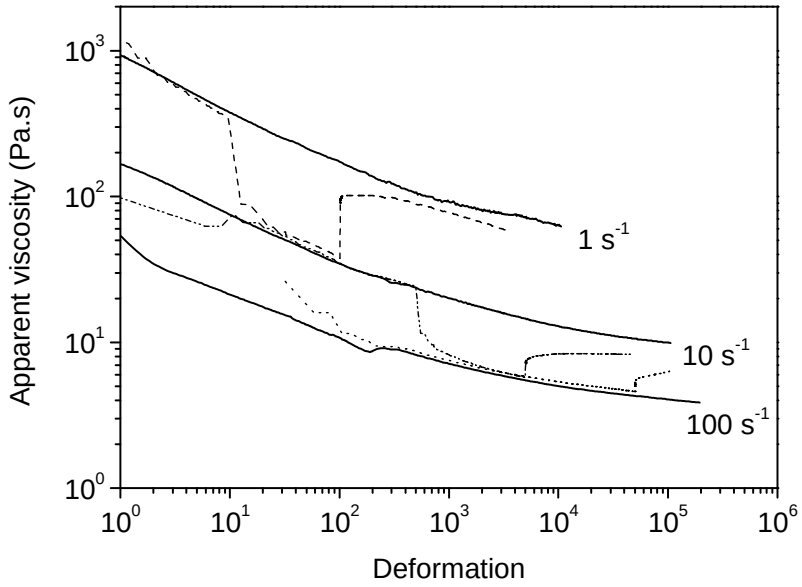

Figure 5.11. Apparent viscosity behavior with the deformation for selected data of Figure 5.10 (continuous lines) and for destructuring flow with step changes in shear rate at different deformation levels (discontinuous lines).

Following an analogous protocol as in Figure 5.4(a), the crude oil B responses to shear rate ramps departing from the different steady state conditions are shown in Figure 5.12. It can be seen that for shear rates lower than the previous equilibrium step (which is the maximum historical shear rate), the behavior is essentially that of a simple liquid if the fluid is not sheared beyond that maximum historical shear rate. As the shear rate increases the viscosity reaches lower values, which do not recover to previous levels within the ramps duration.

Finally, this short analysis indicates that the same overall characteristics found with crude oil A can be observed with crude oil B. Its responses in terms of shear stress and viscosity are about one order of magnitude higher than crude oil A.

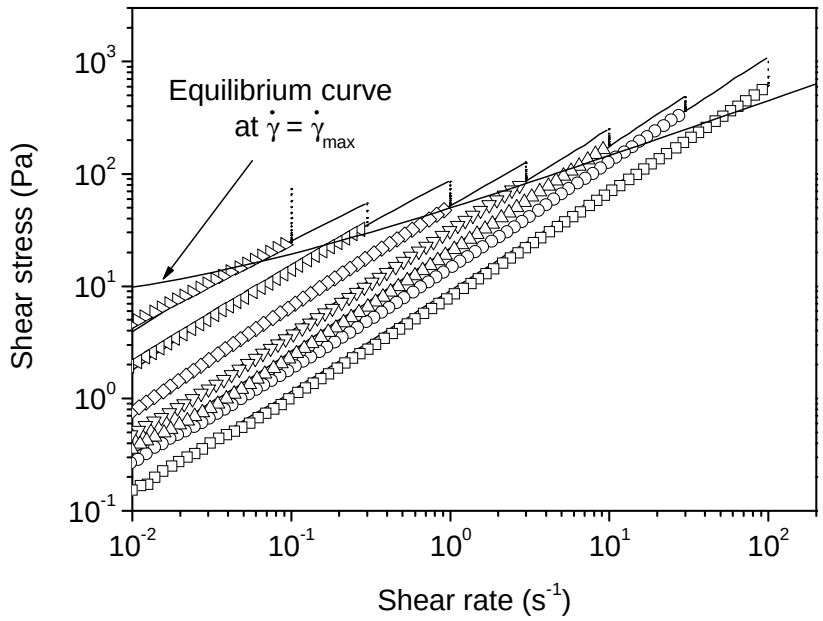

Figure 5.12. Shear stress response to imposed shear rate ramps after reaching the equilibrium at each shear rate level. Data start from the end of the cooling period at the apparent shear rate of 0.1 s^{-1}. Continuous curves are increasing shear rates and symbols to decreasing shear rates. The vertical dashed lines are the stabilization steps.

5.10 Conclusions

Creep tests showed that for different constant imposed shear stress values there is an abrupt increase of the shear rates associated with the transition from solid to liquid regime. That destructuring flow under constant shear stress is difficult to be analyzed due to flow properties rapid evolution. For all imposed shear stress values, it was noticed that the transition from solid to liquid regime occurs around the same critical deformation.

Results from constant shear rate tests showed shear stress decreases of two orders of magnitude during the destructuring flow. Additionally, shear stress vs. deformation curves are similar for various imposed shear rate, from 0.01 to 100 s^{-1}. It indicates that the destructuring process is proportional to the amount of deformation imposed to the sample.

Step changes in shear rate during the destructuring flow revealed that at low deformations shear rate and deformation act as independent variables in the fluid shear stress response. A step change in shear rate creates step changes in fluid viscosity as well. It means that, for low deformations, the state of structure is directly linked to the level of deformation, whatever the shear rate value. However, at higher deformations, after an increasing step in shear rate there is a progressive viscosity decrease tending to the fluid viscosity response presented at the same deformation when destructured at constant shear rate. But it was also noticed that, if a decreasing step in shear rate is done at high deformations, only a lower magnitude step increase in viscosity is observed, without important progressive changes afterwards, as if the viscosity

were upper bounded by the destructuring experienced so far. In other words, the restructuring under shear rate is limited for this material.

When the shear rate is decreased departing from an equilibrium state, the viscosity remains constant. Moreover, equilibrium states achieved at higher shear rates present lower viscosities.

Two facts observed in the rheometrical tests are interpreted as analogous responses: (1) The viscosity did not increase during the shear rates reductions departing from an equilibrium state and; (2) The limited viscosity increases observed after step decreases in shear rate during the destructuring flow at large deformations. They indicate the weak restructuring capacity of the evaluated waxy oils.

Thus, the equilibrium flow curve depends on the flow history and it is tuned by the maximum shear rate experienced by the fluid. That physical characteristic should be taken into account in rheometrical procedures, as waiting for flow stabilization in stepwise increasing shear rates, in order to match the history of each layer of the fluid in a pipeline laminar flow.

The material flow curves at temperatures higher than 4 °C were also measured. They show that non-Newtonian effects disappear from temperatures around the WAT. Above the WAT only classical Newtonian fluid responses were observed.

The complex features first analyzed using crude oil A samples were also found with crude oil B. This oil presents shear stresses almost one order of magnitude higher than crude oil A for the same shear rate levels. Although, the qualitative behavior is same with respect to equilibrium condition and destructuring flow tests.

CHAPTER 6

MODEL DEVELOPMENT

6.1 Introduction

The rheological behavior of waxy crude oils as observed in the various tests presented in Chapter 5 seems rather complex and does not belong to a class of materials exhibiting a well-known type of constitutive equation. In particular, it clearly does not correspond to the usual thixotropic behavior, since one major trend is that, when starting from a cooling at rest, a strong and almost irreversible destructuration of the material is observed. Under these conditions, only the fundamental rheological characteristics of these materials will be kept as they have been identified so far and are expressed as follows:

- Once the oil-gel structure is broken from rest, by achieving a critical shear stress or a critical deformation, a strong destructuring flow takes place, irreversibly changing the fluid structure state;
- In a first stage, this destructuring essentially depends on the deformation undergone by the fluid from its solid-liquid transition and; In a second stage, it also depends on the flow characteristics, i.e. shear rate history;
- After being sufficiently sheared, an equilibrium state is achieved for a given shear rate. This equilibrium state depends on the maximum shear rate experienced by the fluid;
- From that equilibrium state the behavior can be essentially considered as that of a simple liquid if the fluid is not sheared beyond that maximum “historical” shear rate.

This chapter is focused on modeling the rheological features observed in Chapter 5. The list above resumes a complex fluid behavior. It describes the major physical phenomena that shall be mathematically represented by the developed model. In contrast with most previous works in this field, this modeling approach will thus be carried out without any *a priori* assumption based on classical behavior of a class of fluids.

The description of the model development starts in Section 6.2, with a simple approach for the solid behavior. Section 6.3 presents the modeling of the flow curves and near equilibrium destructuring flow. Major destructuration process is evaluated in Section 6.4. Section 6.5 presents a mathematical representation for the transient responses that follow shear rate changes. Comparisons between the results of the proposed model and experimental data of crude oils A and B are shown in Section 6.6. In Section 6.7, selected tests are also compared with results provided by the Houska model, that nowadays is the most used model for describing waxy crude oils. In Section 6.8, predictions of the proposed model are compared to data of destructuring flows departing from different cooling conditions than those used to fit the model parameters. The equilibrium flow curves for temperatures higher than 4 °C are modeled in Section 6.9. Finally, Section 6.10 discusses the conclusions of the modeling work presented in this chapter.

6.2 Solid state

In this work, the behavior in the solid regime will not be considered in detail. It is simply assumed that in the solid state, the material is a viscoelastic solid, i.e. the stress is proportional to the deformation and shear rate: $\tau = G\gamma + \mu_S \dot{\gamma}^n$. Additionally, it turns into a liquid for a critical deformation γ_c, so that it presents a yield (critical) stress $\tau_c = G\gamma_c$ when the deformation rate tends to zero. In this approach the critical parameter is the yield stress, which is the stress to be overcome for starting the flow.

The critical deformation, which here appears to be around 0.15 (see Figure 5.1 and Figure 5.2), is also a relevant parameter of the fluid. It can be determined from the position of the stress peak at low shear rates. Here no further details of the solid regime will be explored, assuming it does not play a major role in the startup flow since this concerns deformations much smaller than 1.

However, it is possible to study or model in more detail the behavior in the solid regime, as done in the works of De Souza Mendes et al. [60] and Dimitriou and McKinley [15].

6.3 Near-equilibrium behavior

In the liquid regime the behavior is described by the apparent viscosity, η. At steady state the fluid may be considered in a first approximation as Newtonian, i.e. η is constant, in a range of shear rates which depends on the flow history. Moreover the steady state value of η depends on the flow history. A complete mapping of this viscosity value as a function of flow history would be difficult. Nevertheless, reference may be done to the equilibrium behavior obtained after a very long flow under a given shear rate that is also the maximum shear rate undergone by the fluid after it has started cooling below the WAT. The viscosity corresponding to that equilibrium behavior may be represented by a Herschel-Bulkley (HB) model (see Figure 5.6):

$$\eta_{eq} = (\tau_{0,eq} + k_{0,eq}\dot{\gamma}_{max}^{n})/\dot{\gamma}_{max} \tag{6.1}$$

where $\tau_{0,eq}$, $k_{0,eq}$ and n are constants for the given temperature. In that equilibrium state the fluid exhibits a constant viscosity defined by Eq. (6.1) as long as the shear rate remains lower than $\dot{\gamma}_{max}$. So, for $\dot{\gamma} < \dot{\gamma}_{max}$ the following relation holds: $\tau = \eta_{eq}(\dot{\gamma}_{max})\dot{\gamma}$. As a consequence, despite the same format, it cannot be said that the crude oil follows a HB model, since in the Eq. (6.1) each shear stress vs. shear rate pair is associated with a specific irreversible state of destructuring, whereas for a usual HB behavior it is possible to move along that curve by increasing or reducing the shear rate.

The parameters of Eq. (6.1) can be obtained from the equilibrium curve when $\dot{\gamma} = \dot{\gamma}_{Max}$ showed in Figure 5.6. Furthermore, from the analysis of the fluid behavior observed in Figure 5.4(b), the master curve of the viscosity decreasing process at constant shear rate indicates that the viscosity η variations with time from one equilibrium condition to another can be modeled by kinetic equation of the form

$$\left.\frac{d\eta}{dt}\right|_{near\ equilibrim\ at\ \dot{\gamma}_{cst}} = -\frac{1}{t_0} Sup\{0, (\eta - \eta_{eq})\} \tag{6.2}$$

where t_0 is an inherent characteristic time of the viscosity variations from one equilibrium state to another and η_{eq} is given by Eq. (6.1). The $Sup\{\}$ function assumes the higher value between zero and viscosity difference to the respective shear rate equilibrium value. It models the

observed behavior that the fluid structure state does not evolve if the current shear rate is lower than the historical maximum one, i.e. the destructuration is mostly irreversible and the fluid behaves as a simple liquid when below $\dot{\gamma}_{max}$.

6.4 Constant shear rate destructuring flow

In view of describing the transient characteristics of this fluid, some aspects of the destructuring flow can be highlighted. It was observed that during a first phase of flow there is a similarity of the shear stress vs. deformation curve (see Figure 5.2), which was confirmed by the similarity of the stress vs. shear rate curves at fixed deformation (see Figure 5.5).

In addition, it is considered that the shear stress tends towards an equilibrium value for sufficiently large deformations. As a consequence, the evolution of the difference $\tau - \tau_{eq}$ can be actually viewed as a function of the deformation. It appears that for the different shear rates the different $\tau - \tau_{eq}$ vs. γ curves are parallel in a logarithmic scale. This means that $\tau - \tau_{eq}$ is proportional to γ^{-m} (where m is a positive constant) by a factor that depends on the shear rate. As the shear stress vs. shear rate curves for iso-deformations in Figure 5.5 can be represented by HB-type equations, that factor may be expressed in the form $\tau_0 + k\dot{\gamma}^n$.

In Figure 6.1 it can be observed that the $(\tau - \tau_{eq})$ vs. γ curves effectively fall along a single curve when rescaled by that factor. Finally, for a deformation between 1 and 10^4 (roughly) the apparent viscosity may be represented by the following expression, valid within 20% when a constant shear rate is applied (continuous lines in Figure 6.1):

$$\eta = \eta_{eq} + (\tau_0 + k\dot{\gamma}^n)\gamma^{-m}/\dot{\gamma} \tag{6.3}$$

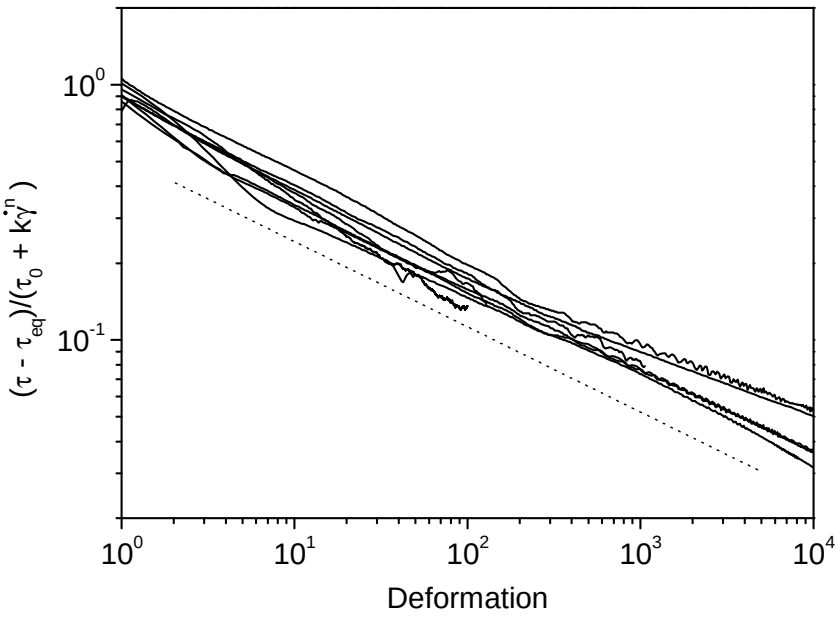

Figure 6.1. Variation of the relative stress distance from the equilibrium state, scaled by the factor $\tau_0 + k\dot{\gamma}^n$ as a function of deformation for start up flows after static cooling at different shear rates (data are the same as in Figure 5.2).

It is worth emphasizing that, as it has been defined, Eq. (6.3) only describes the rheological behavior of the fluid when a constant shear rate is applied after the cooling period when the material has reached a gel behavior, which is obviously not the general case. The simplest approach for generalizing that model would assume that this equation gives the instantaneous apparent viscosity under a given shear rate after any flow history leading to a total deformation γ. This approach would be the equivalent of considering that the material reaches a given structure state that depends only on the total deformation and this structure state has an impact on the shear stress through the factor γ^{-m}, as in Eq. (6.3). This description seems to be in agreement with data for strong shear rate variations (up or down) as long as the deformation is sufficiently small (see Figure 5.3).

6.5 Varying the shear rate

As the deformation increases and if the shear rate varies, the above description does not correspond any more to the observations (see Section 5.4). In that case, the fluid only progressively tends to the viscosity given by Eq. (6.3) (see Figure 5.3 and Figure 5.4(b)), as if it was an attractor point. For cases of very large deformation and shear rate decreases, the viscosity may even never reach the viscosity predicted by Eq. (6.3), remaining at a smaller value. It is a similar behavior to the decreasing shear rate ramps of Figure 5.6, where the viscosity does not increase with shear rate reductions.

Hence, the complex rheological behavior revealed by the experiments discussed in Chapter 5 may be summarized as: At low deformation, for complex flow histories, the fluid viscosity changes almost instantaneously towards the value predicted by Eq. (6.3); As the deformation increases, if the shear rate is changed, viscosity takes some time to evolve towards the value predicted by Eq. (6.3) for the new shear rate level. But when that level has been reached, the viscosity once again evolves with deformation according to the prediction of Eq. (6.3) as long as the shear rate is kept constant. At large deformations, if the shear rate is increased, the time for reaching the equilibrium is very long but follows a simple kinetics represented by Eq. (6.2). Additionally, at large deformations, close to the equilibrium, if the shear rate is decreased the fluid now tends to keep its apparent viscosity.

Finally, the behavior of the fluid depends on the flow history in a complex way, while the experimental observations necessarily concern simple flow histories. This has several consequences. First, it appears convenient to use the viscosity expression given by Eq. (6.3) as a reference behavior and describe the fluid viscosity evolution. That expression in particular means that the steady state behavior expected after a long flow under a given shear rate (i.e. more precisely, a very large deformation) corresponds to a Newtonian behavior with a viscosity defined by Eq. (6.1) for a shear rate below $\dot{\gamma}_{max}$. Then, in order to describe the time variations of the viscosity as a function of the flow history, it is convenient to represent it in function of two variables, here considered to be independent, namely, the deformation and the shear rate. This means that the viscosity evolution equation may be written as:

$$\frac{d\eta}{dt} = \frac{d\eta(\gamma,\dot{\gamma})}{dt} = \dot{\gamma}\left.\frac{\partial\eta}{\partial\gamma}\right|_{\dot{\gamma}} + \frac{d\dot{\gamma}}{dt}\left.\frac{\partial\eta}{\partial\dot{\gamma}}\right|_{\gamma} \tag{6.4}$$

At this stage the simplest approach for the first term in the RHS of the above equation assumes a behavior as that observed at the approach of the equilibrium curve under constant shear rate (see section 6.3), but now with a target viscosity defined by Eq. (6.3), that will be written as $\eta_{ref}(\gamma, \dot{\gamma})$, and a characteristic time t_0 varying with the distance to the equilibrium condition.

For the second term on the RHS of Eq. (6.4), there is not much information available from the experimental data. It will be assumed that in this expression the variation of η with $\dot{\gamma}$ is equal to the variation of η_{ref} with $\dot{\gamma}$ times a factor α depending on the distance to the equilibrium, i.e. $\alpha = 1$ at the solid-liquid transition and $\alpha = 0$ at the equilibrium condition of the corresponding shear rate. This choice is motivated by the behavior observed in: (1) Figure 5.6, where close to the equilibrium condition, the increases in shear rate beyond the historical maximum value does not promote instantaneous viscosity changes and; (2) In Section 5.4, where at low deformations instantaneous variations in the shear rate promoted instantaneous variations in the viscosity (increasing or decreasing) and shear rate variations during the destructuring flow only promoted partial viscosity variations with respect to the values predicted by Eq. (6.3), i.e. η_{ref}.

Finally, by substituting the terms in Eq. (6.4), the following kinetic equation is obtained:

$$\frac{d\eta}{dt} = -\frac{1}{t_0} Sup\{0; (\eta - \eta_{ref})\}_{\dot{\gamma}} + \alpha \frac{d\dot{\gamma}}{dt} \frac{\partial \eta_{ref}}{\partial \dot{\gamma}}\bigg|_{\gamma} \tag{6.5}$$

It is worth noting that the *Sup{}* function in the first term in the RHS ensures that the viscosity will remain constant if the new imposed shear rate is below the state of reference which has been reached at that time. Finally, convenient expressions for α and t_0 are as follows:

$$\alpha = \left[\frac{\ln(\eta/\eta_{eq})}{\ln(\eta(\gamma_c)/\eta_{eq})}\right]^{a} \tag{6.6}$$

$$t_0 = 1 + K\alpha^{-M} \tag{6.7}$$

where α is limited between 0 and 1 and t_0 is bounded by the characteristic time $t_{0,max}$ associated to highly sheared states near the equilibrium condition, as observed in Figure 5.4. K, M and a are positive constant parameters that may be fitted to the data in asymptotic cases (very close or very far from the equilibrium) and for transient flows associated with jumps of shear rate, notably those presented in Figure 5.3.

It is also worth noting that while the first term in the RHS of Eq. (6.5) predicts the viscosity behavior at constant shear rate (such as the continuous lines in Figure 5.3 or the viscosity variations in Figure 5.4(b)) and bounds its growth in reducing shear rate cases (Figure 5.3), the second term allows predicting viscosity instantaneous changes as a result of shear rate instantaneous changes, for both increasing and decreasing shear rate cases (as the viscosity instantaneous variations observed in Figure 5.3).

In summary, the model proposed here may be written as in the following equations:

$$\tau = G\gamma + \mu_S \dot{\gamma}^n \qquad \text{if } \gamma < \gamma_c \tag{6.8}$$

$$\tau = \eta\dot{\gamma} \qquad \text{if } \gamma \geq \gamma_c \tag{6.9}$$

$$\frac{d\eta}{dt} = -\frac{1}{t_0} Sup\{0; (\eta - \eta_{ref})\}_{\dot{\gamma}} + \alpha \frac{d\dot{\gamma}}{dt} \frac{\partial \eta_{ref}}{\partial \dot{\gamma}}\bigg|_{\gamma} \tag{6.10}$$

$$\eta_{ref} = (\tau_{0,eq} + k_{0,eq}\dot{\gamma}^n)/\dot{\gamma} + (\tau_0 + k\dot{\gamma}^n)\gamma^{-m}/\dot{\gamma} \tag{6.11}$$

$$\alpha = \left[\frac{\ln(\eta/\eta_{eq})}{\ln(\eta(\gamma_c)/\eta_{eq})}\right]^a, 0 \leq \alpha \leq 1 \tag{6.12}$$

$$t_0 = 1 + K\alpha^{-M}, t_0 \leq t_{0,max} \tag{6.13}$$

where $\tau_{0,eq}$, $k_{0,eq}$, τ_0, k, n, m, γ_c, a, K, M and $t_{0,max}$ are constant positive parameters of the model.

The model can be used for simulating imposed shear rate cases, for example, as follows: While in the solid regime, the shear stress is calculated by the viscoelastic solid model given by Eq. (6.8). The deformation γ is known from the integration of the shear rate with time. When the critical deformation γ_c is achieved the material becomes liquid and its first apparent viscosity value is assumed to be equal to η_{ref}, given by Eq. (6.11). Thus, now in the liquid regime, the shear stress is calculated by Eq. (6.9) and the viscosity η evolves in time according to Eq. (6.10).

It is interesting to note that the critical stress for the solid-liquid transition appears in the model by substituting Eq. (6.11) in Eq. (6.9), taking $\gamma = \gamma_c$ and the limit $\dot{\gamma} \to 0$: $\tau_c = \tau_{0,eq} + \tau_0 \gamma_c^{-m}$. So, in order to have the stress continuity in the solid-liquid transition, the solid viscoelastic parameters may be calculated as $G = \tau_c/\gamma_c$ and $\mu_S = k_{0,eq} + k\gamma_c^{-m}$.

6.6 Comparison to experimental data

6.6.1 Parameters fitting

The structure of the proposed model was basically deduced from the experimental observations and most of the parameters are fitted to data associated to simple flow histories. By construction the model shall fit all the data gathered with the destructuring flow experiments presented in the previous chapter.

The parameters $\tau_{0,eq}$, $k_{0,eq}$, and n were determined from the equilibrium curve for $\dot{\gamma} = \dot{\gamma}_{max}$ in Figure 5.6 (also shown in Figure 5.5 as black squares). The destructuring flow data at constant shear rate of Figure 5.2 were used to find the parameters τ_0 and k. With the appropriate values all curves shall have the same relative stress distance to equilibrium, as shown in Figure 6.1. This figure provides the value of the deformation exponent m. The parameter a was fitted to provide the best average magnitude of the viscosity instantaneous variations due to instantaneous shear rate changes at the discontinuous lines in Figure 5.3.

The parameters M and K were chosen to fit the progressive viscosity evolution that follows that shear rate change. The characteristic time of that evolution is bounded by a maximum value

$t_{0,max}$ found to be the same for all constant shear rate curves of Figure 5.4(b) (destructuring flow close to equilibrium). The critical deformation γ_c was defined from the maximum shear stresses observed in Figure 5.2 (confirmed by creep tests shown in Figure 5.1). Table 6.1 presents the parameters of the model for crude oils A and B.

Table 6.1. Parameters of the model measured for crude oils A and B.

Parameter	Crude Oil A	Crude Oil B
$\tau_{0,eq}$ (Pa)	0.66	8.5
$k_{0,eq}$ (Pa.s^n)	4.3	39
n	0.5	0.5
τ_0 (Pa)	103	330
k (Pa.s^n)	76.3	400
m	0.4	0.5
M	12	4.3
a	0.3	0.7
K (s)	0.1	0.05
$t_{0,max}$ (s)	1800	2000
γ_c	0.15	0.1

The destructuring flow data of Figure 5.3 used to fit the model parameters is compared to the model predictions for those six experiments in Figure 6.2 and Figure 6.3. The simulated apparent viscosities are represented by the continuous lines. For each case a sample of crude oil A was cooled at rest from 60 to 4 °C at -1 °C/min and held at 4 °C for 20 min before start the tests. In Figure 6.2, the following tests are presented: (1) Start at 0.1 s^{-1}, change to 1 s^{-1} at 10 strain units, back to 0.1 s^{-1} at 500 strain units; (2) Start at 10 s^{-1}, change to 100 s^{-1} at 100 strain units, back to 10 s^{-1} at 1,000 strain units and; (3) Start at 100 s^{-1} and change to 10 s^{-1} at 50,000 strain units. Figure 6.3 shows the comparison between the following procedures: (1) Start at 1 s^{-1}, change to 10 s^{-1} at 10 strain units, back to 1 s^{-1} at 100 strain units; (2) Start at 10 s^{-1}, change to 100 s^{-1} at 1,000 strain units, back to 10 s^{-1} at 5,000 strain units and; (3) Start at 10 s^{-1} and change to 100 s^{-1} at 10,000 strain units.

According to the model construction features, the global trends observed in those experiments are captured by the model. The parameters used to control the magnitude of the instantaneous viscosity changes in function of instantaneous shear rate changes, α in Eq. (6.12), and the characteristic time of the destructuring process at constant shear rate, t_0 in Eq. (6.13), may still be improved but the order of magnitude of viscosity jumps and long destructuring flows are in a good agreement with the experiments.

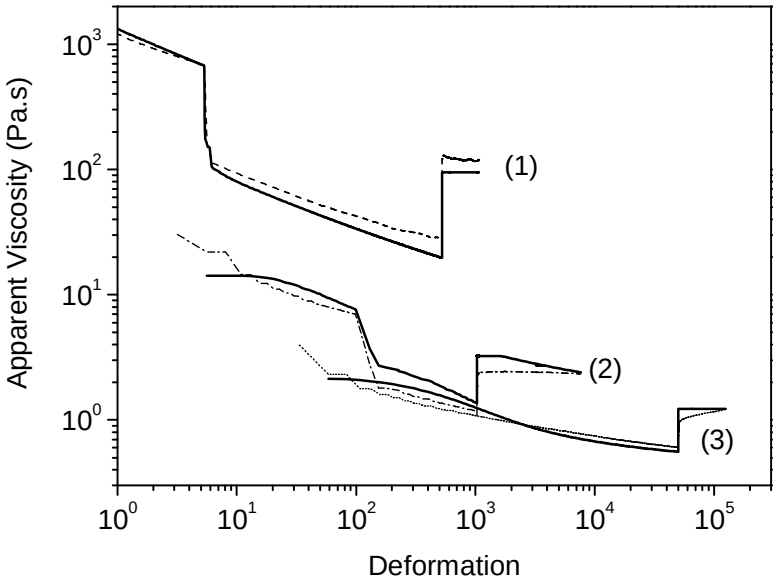

Figure 6.2. First group of data comparing simulated (continuous lines) and measured data for 3 shear rate step changes experiments presented in Figure 5.3.

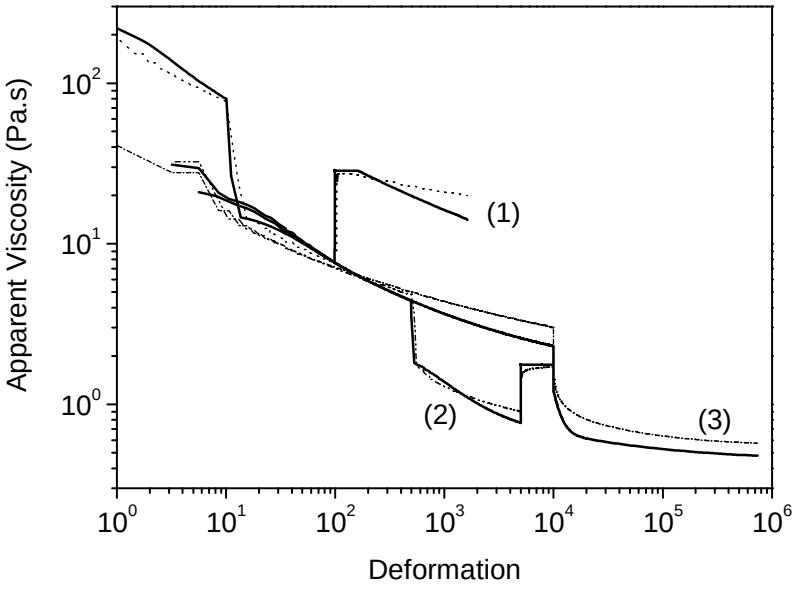

Figure 6.3. Second group of data on the comparison between simulated (continuous lines) and measured data for shear rate step changes experiments presented in Figure 5.3.

Figure 6.4 presents the comparison between model predictions and the fluid rheological behavior close to the equilibrium. The experiment procedure is that of Figure 5.4(a). The simulated data, represented by the continuous line, starts at the equilibrium condition at 0.1 s^{-1}

and follows the same imposed shear rate history as in the experiment. The up (dashed lines) and down (symbols) ramps of Figure 5.6 are repeated Figure 6.4. The inset shows the measured data (dashed lines) at the equilibration steps (constant shear rate steps) of Figure 5.4(b) in comparison to the simulated data (continuous lines).

The qualitative agreement between measured and simulated data is good. The most important differences are noticed for shear rates below 10^{-2} s^{-1} and at the destructuring flow of the increasing shear rate ramps from 10 to 30 s^{-1} and from 30 to 100 s^{-1}. Nevertheless, the general agreement is good for this comparison covering six decades of shear rate variations and about 6.5 h of flow.

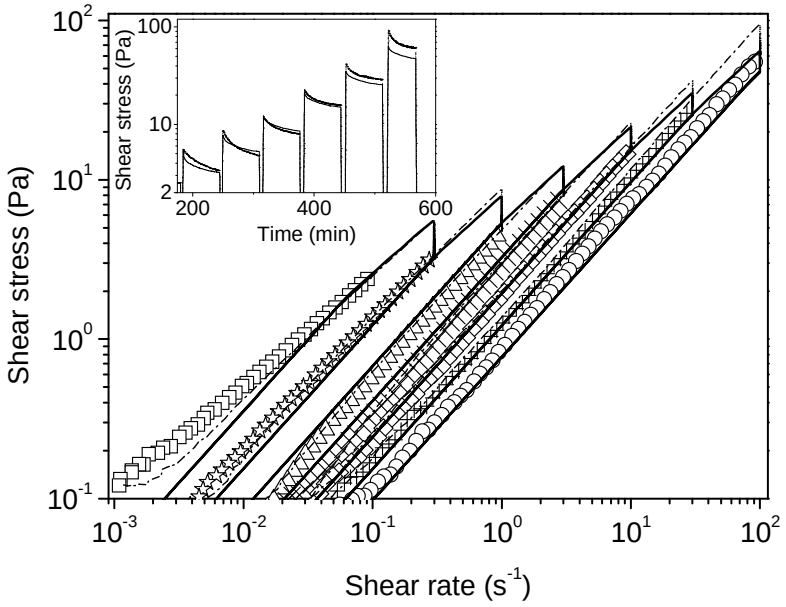

Figure 6.4. Comparison between simulated (continuous lines) and measured (symbols and dashed lines) data for the experimental procedure described in Figure 5.4(a), starting at the equilibrium condition at 0.1 s^{-1}. The inset presents the equilibration steps at constant shear rate.

6.6.2 Comparison to complex flow data

The comparisons presented in the previous section allows evaluating model predictions of the data used in the fitting procedure. It should more interesting to look at the predictions of the model in the case of more complex flow histories, notably not used as input of fitting parameters. The flow restart data measured with creep tests and progressive increasing shear rate are good examples.

Figure 6.5 shows the comparison between the model predictions and the creep tests presented in section 5.2. The material response below the critical deformation is captured by the model by calculating the final deformation when the imposed shear stress is below the critical value. For this crude oil, at the cooling conditions described for those tests, the critical stress is 224 Pa. For imposed shear stresses above the critical value, the material starts flowing. It begins with a very low shear rate followed by a rapid increase, capturing the impressive structure collapse. Then,

the shear rate will tend towards its equilibrium value. It is remarkable that the strong structure collapse will allow high shear rate equilibrium values for constant stress cases.

As discussed above, the minimum stress required to start the flow is given by $\tau_c = \tau_{0,eq} + \tau_0 \gamma_c^{-m}$. If that shear stress is left constant in time, at the equilibrium $\tau_c = \eta_{eq}\dot{\gamma}$, i.e. an equilibrium shear rate given by $\dot{\gamma} = \left[\tau_0 \gamma_c^{-m} / k_{0,eq}\right]^{1/n}$. According to the values of the fitted parameters, in Table 6.1, that equilibrium shear rate obtained when the critical stress is kept constant is 2,617 s^{-1}.

The final shear rates are predicted to be somewhat higher than the measured values, probably because they are far out of the range of shear rates in the data used to fit the model parameters at steady state flow, resulting in an underestimation of the power coefficient of the shear rate. Also in quantitative terms, the model seems to predict a slow onset of flow for the 250 Pa curve. In Figure 6.5, time equal to zero corresponds to the critical deformation, thus only the material behavior after the solid-liquid transition is compared. Finally, from a qualitative point of view there is a good overall agreement of the model predictions with the data.

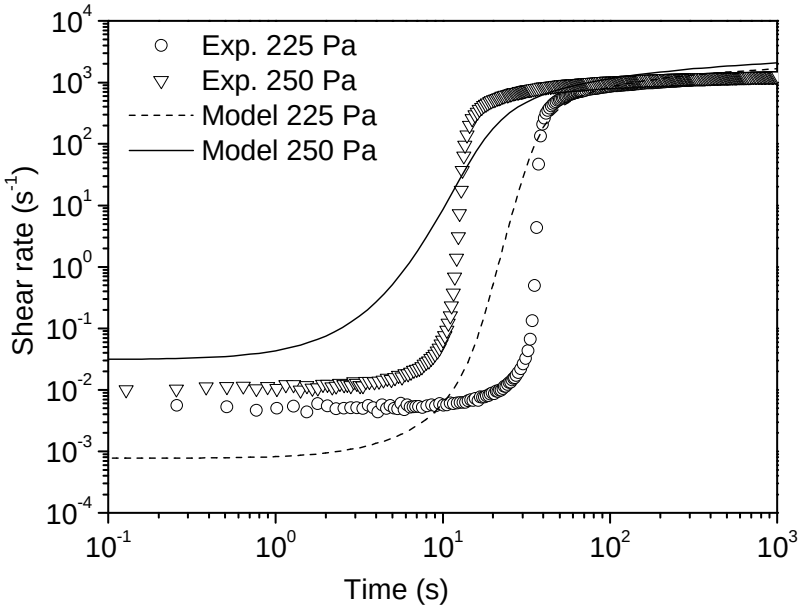

Figure 6.5. Model comparison to imposed shear stress experiments with crude oil A. Time is equal to zero at the critical deformation, which is considered to represent the solid-liquid transition and is the minimum of curves in Figure 5.1.

Comparisons to tests where the imposed shear rate is varied in time were also done. The first test of that type is the shear sweep test presented in Figure 4.3, in which the shear rate is increased from zero to a large value then decreased. It can be seen (see Figure 6.6) that the model (fitted to the data under simpler flow histories) is in good agreement with the experimental data obtained for this typical test. In particular, it is interesting to note that it represents the decreasing then increasing parts of the stress vs. shear rate curve during the increasing shear rate ramp, since it suggests that the model properly captures the timing for destructuring under complex flow histories.

In two other cases, starting from rest after static cooling, a given shear rate was imposed during 10 s and then decreased from to almost zero in 2 min. It is possible to see that once again that the model is in good agreement with experiments for the stress vs. shear rate curves during these transient flows. It confirms the above conclusions about its ability to properly reproduce the characteristic time of destructuring and the viscosity increase with shear rate reduction during the destructuring flow.

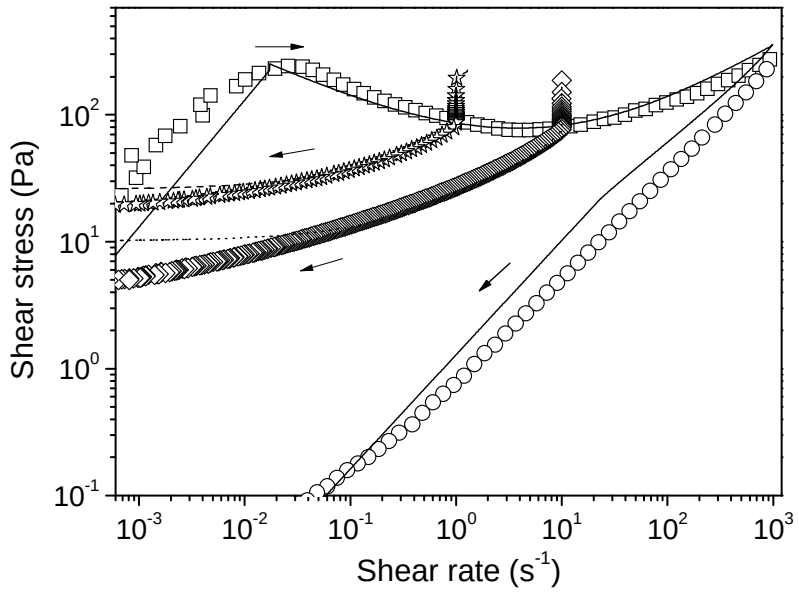

Figure 6.6. Experiments with imposed shear rate variations in time and comparison with the predictions of the model (continuous, dashed and dotted lines): Shear ramps test (squares and circles, data of Figure 4.3), constant shear rate during 10 s (1 s^{-1} (stars) or 10 s^{-1} (diamonds)) then logarithmic decrease down to 10^{-4} s^{-1} in 2 min.

The same conclusions apply when the above experiments are performed with crude oil B. Figure 6.7 presents the same shear rate ramp test as that of Figure 6.6, but with crude oil B. The inset shows the comparison of the creep test with crude oil B imposing a shear stress of 1,000 Pa.

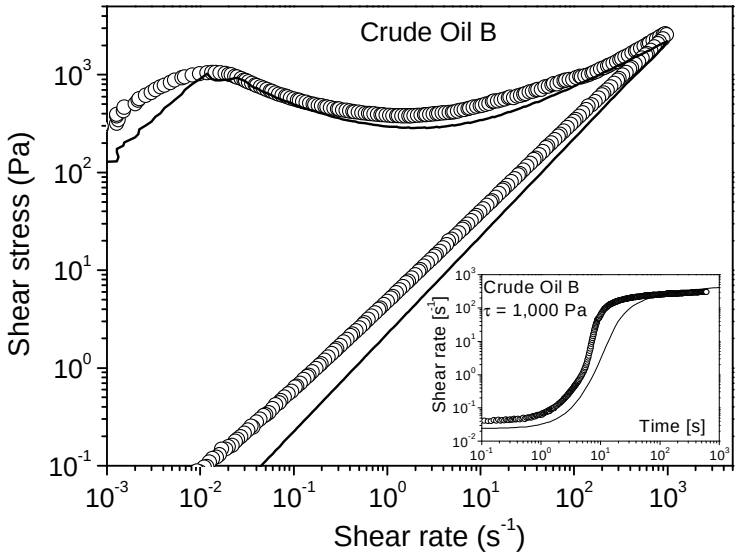

Figure 6.7. Comparisons between measured (symbols) and calculated data (continuous line) for crude oil B in the same experiments of Figure 6.5 (creep test, in the inset) and Figure 6.6 (shear ramp test).

6.7 Houska model evaluation

The Houska model was also fitted to measured data of crude oil A, according to the fitting procedure suggested by Cawkwell and Charles [4] and further developed by Hénaut and Brucy [24]. The Houska model is given by (recalling Eqs. (2.5) and (2.6))

$$\tau = \tau_{y0} + \lambda\tau_{y1} + (k + \lambda\Delta k)\dot{\gamma}^n \tag{6.14}$$

$$\frac{d\lambda}{dt} = a(1-\lambda) - b\lambda\dot{\gamma}^m \tag{6.15}$$

where τ_{y0} and τ_{y1} are the permanent and time-dependent yield stresses, k and Δk are the steady state and time-dependent consistency parameters, *n* is the power-law coefficient, *a* is the structure buildup coefficient, b is the break down coefficient and *m* is the adjusting parameter for shear rate dependence. λ is the structure parameter that is equal to zero when the oil-gel is in a completely destructured state and equal to 1 when the gel is at its strongest state.

6.7.1 Fitting procedure of the Houska model parameters

The fitting procedure consists of estimating τ_{y0}, k and *n* by measuring the oil flow curve when the crude oil is completely destructured, i.e., after cooling at -1 °C/min and 10 min of flow at 1,000 s^{-1} at the desired test temperature (4 °C). The parameters τ_{y1} and Δk are fitted from the maximum shear stresses measured from imposed shear rates tests from static cooled oil samples. Here, the maximum values of the curves in Figure 5.2 were used. The parameters *a*, *b* and *m* are fitted from partial destructured states, i.e. after 1 min of flow at different shear rate values. The use of more data points from the curves of Figure 5.2 did not improve the model predictions. Table 6.2 presents the values of the parameters found for crude oil A.

Table 6.2. Houska model parameters for crude oil A.

Houska model parameter	fitted value for crude oil A
τ_{y0} (Pa)	0
τ_{y1} (Pa)	224
k (Pa.s^n)	0.237
Δk (Pa.s^n)	180
n	0.96
a (s^{-1})	2.33×10^{-4}
b (s$^{1/m}$)	0.03
m	0.124

It is worth mentioning that the parameters values above represent the best fit over the given data set. It means that this is the best overall data representation, but particular cases may present serious problems. As an example, the restructuring parameter *a* indicates that if the fluid is let at rest after strong shear, it shall recover 95% of its yield stress value in about 3.5 h. According to Figure 4.5, after 6 h at rest only 5% of the yield stress value was recovered.

6.7.2 Houska model comparison to experimental data

Figure 6.8 presents the comparison of the data obtained with the Houska model with the same measured data of Figure 6.6 and Figure 6.7. Clearly this model is unable to predict the behavior of the material under such complex flow histories. The discrepancy on the stress values between the model predictions and the data is often larger than one order of magnitude.

(a)

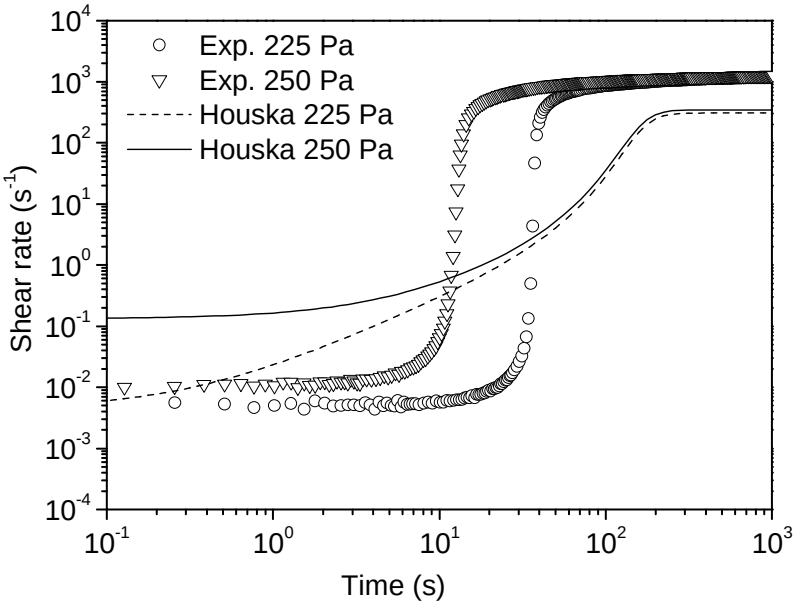

(b)

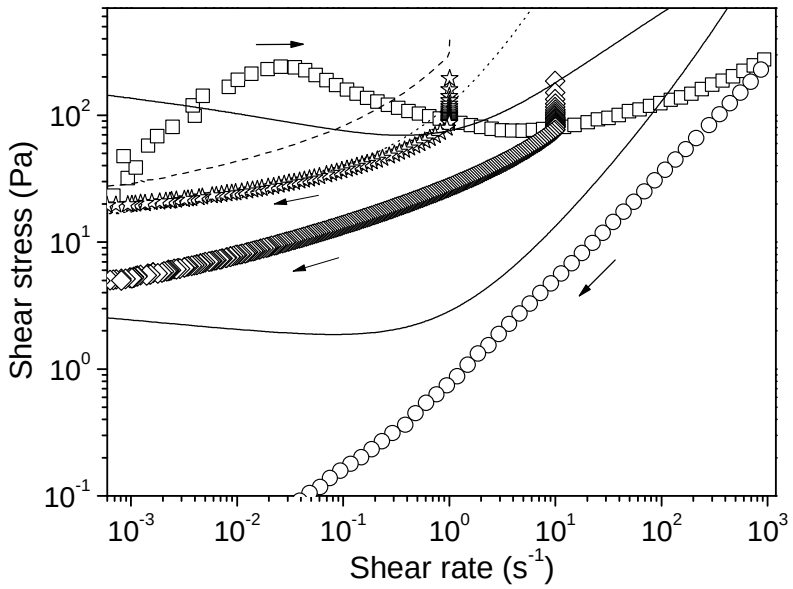

Figure 6.8. Houska model (lines) and experimental data (symbols) comparisons for the same imposed shear stress cases as in Figure 6.5. (b) Comparisons for the same imposed shear rate cases as in Figure 6.6.

6.8 Comparison for different cooling conditions

Section 5.7 presented destructuring flow experiments departing from different cooling conditions than those used to fit the parameters of the proposed model. The analyzed destructuring flows appear to be analogous to those measured after static cooling.

Following that analogy, the dimensionless shear stress measured for the destructuring flows of the four protocols in Section 5.7 can be plotted *versus* the deformation and compared to the

model prediction. The proposed model considers the dimensionless stress, as calculated in Section 6.4, given by $(\tau - \tau_{eq})/(\tau_0 + k\dot{\gamma}^n)$, as a power-law of the deformation (γ^{-m}).

Then, an appropriate linear shift in the curve that represents the model prediction shall match the initial viscosity presented by each destructuring flow. Such linear shift implicitly assumes that the destructuring rate with the deformation will remain the same and that the equilibrium condition given by the shear rate magnitude shall also be the same as for static cooling.

Figure 6.9 shows the dimensionless shear stress (with parameters given by Table 6.1) calculated for the destructuring flows (symbols) according the three protocols presented in Section 5.7. The prediction of the model is plotted as the bold dashed line. The shifted model curves that match the initial viscosity (or shear stress) value of each destructuring flow are shown as discontinuous lines.

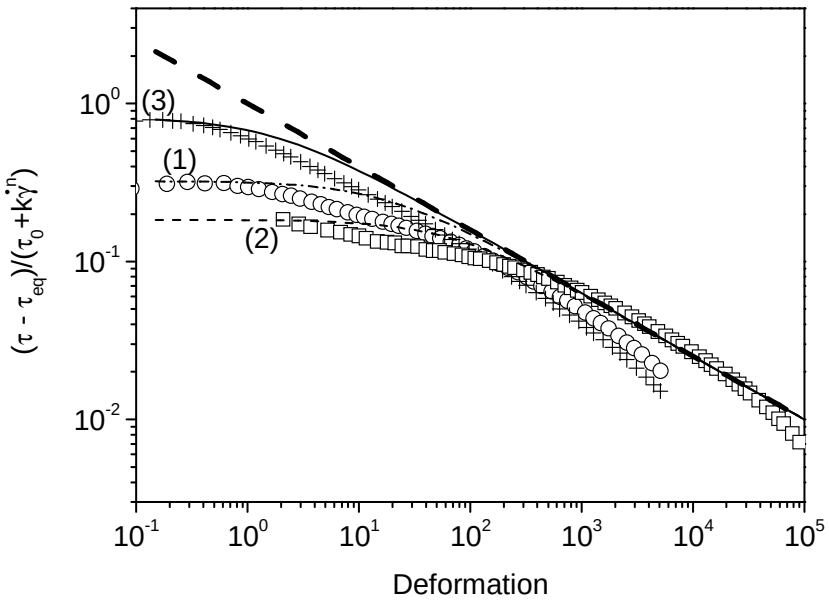

Figure 6.9. Comparison of the dimensionless shear stress between measured data (symbols) and predicted by the model (discontinuous lines) shifted for matching the initial measured stress value of each experiment protocol described in Section 5.7. The bold dashed line show the model predictions for the tests after static cooling of Section 6.4.

During the first 3 or 4 decades of deformation de agreement between the shifted model prediction and measured data is good. Beyond that point, the destructuring rate seems faster than predicted by the model for protocols 1 and 3.

Nevertheless, the overall predictions can be considered good, considering that they represent destructuring flows after completely different cooling processes. The only additional data for describing those flows is the shear stress at the solid-liquid transition.

6.9 Temperature effects

The equilibrium flow curves for higher temperatures presented in Section 5.8 can be represented by a HB model with temperature-dependent parameters. Figure 6.10 shows the measured data (already presented in Figure 5.9) and fitting curves of the form $\tau_{eq} = \tau_{0,eq}(T) + k_{0,eq}(T)\dot{\gamma}^{n(T)}$. The fitted parameters are presented in Table 6.3.

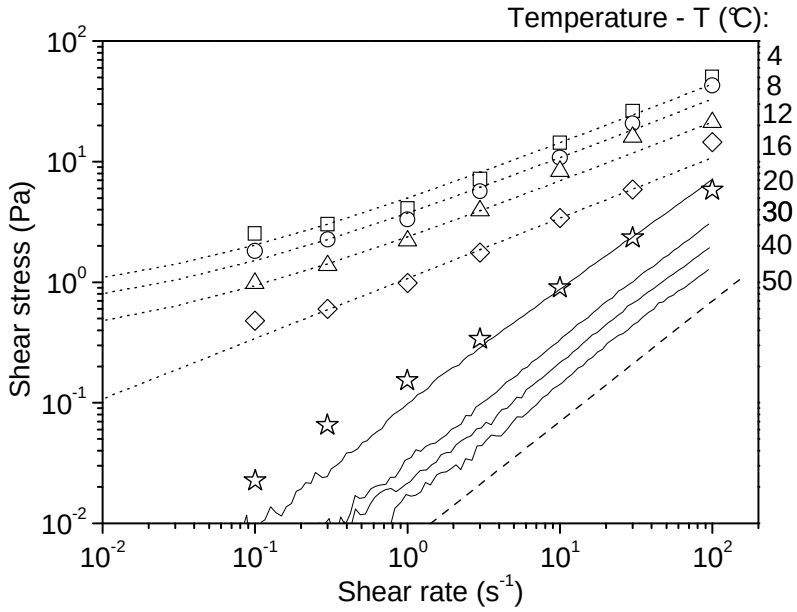

Figure 6.10. Comparison between measured data (symbols) and HB model (dotted lines) with temperature-dependent parameters for the equilibrium flow curves at different temperatures. Continuous lines are measured values above 20 °C. The dashed line shows the slope of a Newtonian fluid.

Table 6.3. HB parameters of crude oil A fitted to equilibrium curves of Figure 6.10.

Temperature (°C)	$\tau_{0,eq}$ (Pa)	$k_{0,eq}$ (Pa. s^n)	n
4	0.66	4.33	0.5
8	0.48	3.26	0.5
12	0.27	2.11	0.5
16	0	1.08	0.5
20	0	0.074	1
30	0	0.033	1
40	0	0.021	1
50	0	0.014	1

6.10 Conclusions

This chapter has presented the development of a model for predicting the complex rheological behavior of the analyzed waxy crude oils during destructuring flows and at steady state flow conditions.

The model is based on a constitutive equation that relies on the fluid apparent viscosity. That viscosity evolves in time according to the flow history towards an equilibrium flow curve. At this equilibrium condition the waxy oil is modeled as a Newtonian fluid if the shear rate is lower than the maximum shear rate experienced by the fluid. If the fluid is sheared at a higher shear rate, the equilibrium viscosity is irreversibly decreased. The curve that defines the equilibrium viscosity in function of the maximum historical shear rate is modeled by HB-type equation.

For destructuring flows at constant shear rate, the difference between the shear stress and its value at the equilibrium condition was shown to be proportional to the power of the deformation.

However, in order to take the flow history into account, variations in the shear rate during the destructuring flow are modeled considering two types of viscosity responses. First, instantaneous shear rate changes shall produce instantaneous viscosity changes, similarly as in non-thixotropic fluids. Then, those instantaneous changes are followed by a progressive viscosity variation towards the equilibrium viscosity.

Moreover, the intensity of those two responses depends on the relative structure state to the equilibrium condition. For more structured states, instantaneous viscosity changes represent almost all the viscosity variations. Shear rate changes at structure states closer to equilibrium produce low instantaneous viscosity changes and progressive viscosity variations with longer characteristic times. Those progressive viscosity variations occur only for increasing shear rates, where viscosity reduces with time.

That final format of the proposed model was built by steps, based on experimentally observed features of the studied waxy oils. The comparisons to experimental data not used in the fitting process of the parameters showed good quality predictions, for constant shear stress flows, shear rate up-and-down ramps and decreasing ramps during the destructuring flow where a yield stress is still present. Predictions of Houska model for the same tests did not succeed as the proposed model, mostly due to constraints of classical thixotropic characteristics assumptions.

The capacity of taking the flow history into account for determining the fluid rheological behavior at equilibrium state is an important improvement of the proposed model. In practice, the application of this model will also improve the transient flow prediction of a pipeline flow restart with gelled oil. The main features of the model were developed to account for the complex fluid responses experimentally observed. Compared to the Houska model, for example, predictions of flow rate changes and shut-in during destructuring flows shall be improved as well.

CHAPTER 7

YIELD STRESS AS A FUNCTION OF FLOW AND TEMPERATURE HISTORIES

7.1 Introduction

This chapter is focused on analyzing the yield stress of crude oil A. As the practical application in mind is the flow restart in pipelines, the yield stress is the most important fluid property to be taken into account in the minimum restart pressure calculation. As other rheological properties, the yield stress of a gelled oil depends on the flow and temperature histories. After a flow shutdown, there are particular flow histories for the different positions inside a long pipeline. Notably, the cooling and shear rates experienced since the pipe entrance.

Combining all possibilities of flow and temperature histories in the yield stress analysis would be a difficulty, as already discussed in the Section 3.2.2. In the study presented here, the different temperature histories were limited to a given set of cooling rates and the time during which the oil is hold at rest at the final cooling temperature before measuring the yield stress. The shear history while cooling was divided in three categories: Static cooling, where the oil is not sheared at all; Dynamic cooling, where the oil is sheared with a fixed shear rate while cooling and; Mixed cooling, which corresponds to the case where the oil was sheared from its initial cooling temperature until an intermediate temperature and then cooled at rest until achieving the final cooling temperature. Additionally, in the mixed cooing cases, the yield stress dependency on the limit temperature between the dynamic and static phases of the cooling procedure is also evaluated.

The practical objective here is to provide an approach for describing the yield stress field inside the pipeline at the flow restart moment. Furthermore, as an attempt to reduce the number of experiments required for accomplishing that task, the yield stress behavior in function of the parameters cited above is also compared to the oil-gel elastic modulus. This is a property commonly used to assess waxy oils structure state (see Section 2.4.2).

The next section evaluates yield stress measurements techniques and presents systematic measurements of the yield stress of crude oil A. Section 7.3 compares measured yield stress values with the oil elastic modulus, analyzing the relation between those properties. Section 7.4 presents the correlations established between yield stress and cooling process parameters. The final section concludes the yield stress analysis with a consolidated approach for estimating the waxy oil yield stress field in the pipeline at the restart moment.

7.2 Measuring the yield stress of a waxy crude oil

Measuring the yield stress of a viscoplastic material may be a hard task. The yield stress is the smallest shear stress that is capable of breaking the material solid structure and sustain the

subsequent flow, i.e. continuous deformation. There are different techniques developed for measuring the yield stress. A broad review on the subject is presented by Coussot [9].

Waxy crude oils are a special class of materials, with peculiarities that do not fit classical behaviors of thixotropic yield stress materials. As it was shown in the two previous chapters, maintaining the flow is generally not a problem once the solid structure was broken. It is due to the impressive structure collapse that the fluids studied here required a high shear stress to start flowing but a low shear stress in steady state flow.

Thus, the approach for measuring the yield stress of waxy oils consists in starting the tests with an oil sample in its solid state, instead of reducing the flow velocity gradient to observe the shear stress tendency towards very low shear rates or a critical shear rate value. The methods for measuring the yield stress differ in how the material is deformed, essentially the rate of deformation, until its critical deformation is achieved and the shear stress associated to the solid-liquid transition is measured.

The next subsections discuss some examples of yield stress measurement of a waxy crude oil and the behavior of that rheological property with respect to different cooling histories.

7.2.1 Measurement methods comparison

7.2.1.1 Creep test

As already discussed in Section 5.2, the creep test is perhaps the most direct method for assessing the yield stress value. A shear stress is imposed to the fluid and it is then observed if it flows or not. When a series of creep tests is performed, as shown in Figure 5.1, the yield stress, defined as the stress value below which there is no flow, can be estimated by successive approximations. But, as already commented, that value is of restricted practical application if the creep flow is too long and the time for start flowing the sample is too high compared to the envisaged application. Ideally speaking, at the yield stress the creep flow takes an infinite time. In order to avoid that, a maximum waiting time could be defined as a practical limit.

In the case of waxy crude oils, the sample preparation for rheometrical tests takes a certain time, as there is a cooling process associated to the definition of the sample initial condition. Thus, performing several tests is a time consuming task.

Alternatively, a first approximation could be obtained by imposing a shear stress ramp. Or, yet, by imposing stepwise increases in shear stress. By both ways, the stress value where the flow starts would be associated to the rate of stress increase and analyzing the creep flow would be more difficult since it would happen under variable shear stress.

Thus, despite its precision and the observation of the creep flow, which represents the material dynamics while it is in the solid state, the creep test is not a much practical method for determining waxy oils yield stress due to the time it takes to get to a good approximated value.

7.2.1.2 Oscillatory test

Oscillatory stress ramp

A second method to estimate the fluid yield stress consists in performing a oscillatory test, at a given oscillation frequency, measuring the elastic and viscous response of the material and

increase with time the amplitude of the movements, i.e. increasing the oscillatory stress. At the beginning of the test, if the material is in its solid state, the elastic modulus should be higher than the viscous modulus. As the amplitude of the oscillations increases, the elastic modulus decreases, eventually to a value lower than the viscous modulus. At that point the material is said to exhibit a more viscous than elastic behavior, characterizing a predominant liquid behavior. Thus the oscillatory shear stress at that crossing point is said to be the yield stress. Chang et al. [5] already applied this method for waxy crude oils.

The physics related to increasing oscillatory deformations is not intuitive when thinking of flow restart in a pipeline. Directly imposing a shear stress to the sample as in the creep test would be more similar physical conditions. Although, this method provides an apparent yield stress value with only one test. As an inconvenient, it may carry the influence of dynamic effects from the oscillation, as frequency and rate of increase of the amplitude of the movements.

This test was executed with the crude oil after the same cooling process as before. Oscillation frequency was set to 10 Hz and oscillatory shear stress increasing logarithmically from 1 to 10,000 Pa in 5 min.

Figure 7.1 presents the measurements done with this method for the crude oil A. At low oscillatory stresses, the elastic modulus is higher than the viscous modulus, characterizing a solid-like behavior. Both moduli present a constant plateau at low oscillatory stresses and start decreasing at some point. At 274 Pa the slopes present a sharp decrease but with higher intensity for the elastic modulus, which becomes lower. That crossing characterizes the yield stress limit of the material, since the viscous modulus becomes dominant and characterizes a liquid-like state. At the same time it can be seen a steep increase in the maximal oscillatory strain, or the amplitude of the oscillation. At the beginning of the test the strain amplitude showed a linear behavior with the stress, indicating the elastic response of the material at those stress levels.

The yield stress found with this technique is higher than the shear stress of 250 Pa required to start the flow in 8 s according to the creep test (see Figure 5.1). One possible reasoning for that result is that once the gel structure is compromised, at some point in the decreasing part of G' curve, no further increase in oscillatory stress would be necessary to continue the destructuration, it would be just a matter of time for the G’ to drop, similarly to the previous method.

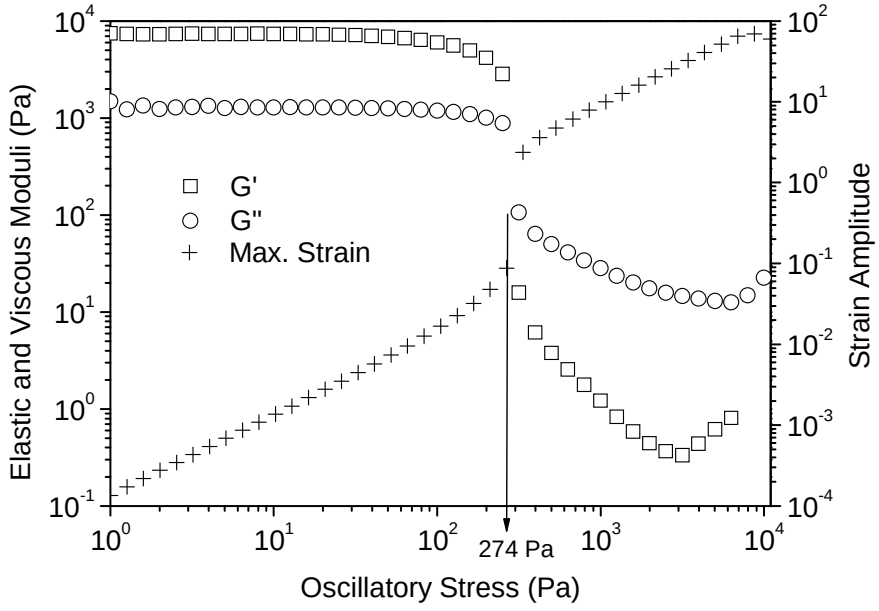

Figure 7.1. Oscillation test at 10Hz increasing stress with time.

Sensibility to frequency

The elastic modulus values may be sensible to oscillation frequency. An evaluation of that dependence was done by measuring the elastic modulus with oscillatory tests under variable frequency. The oscillation frequency was varied from 0.1 to 50 Hz with successive frequency increasing and decreasing ramps. The crude oil A sample preparation and cooling process was the same the previous creep tests. Two strain amplitudes were also tested, 0.04% and 1%. The first value is very low deformation, inside the material elastic regime, while the second is close to the beginning of the G' decreasing (Figure 7.1).

Figure 7.2 presents G' measurements changing strain amplitude with ramp up and down in frequency. It can be seen that G' always increases with frequency in the range analyzed. Although the G' variation with frequency is relatively simple, no plateau of constant G' value was found, differently from Chang et al. [5]. No important variation was observed with the frequency ramp direction or strain amplitude. The latter presents similar values to those in Figure 7.1 at the same strain amplitude.

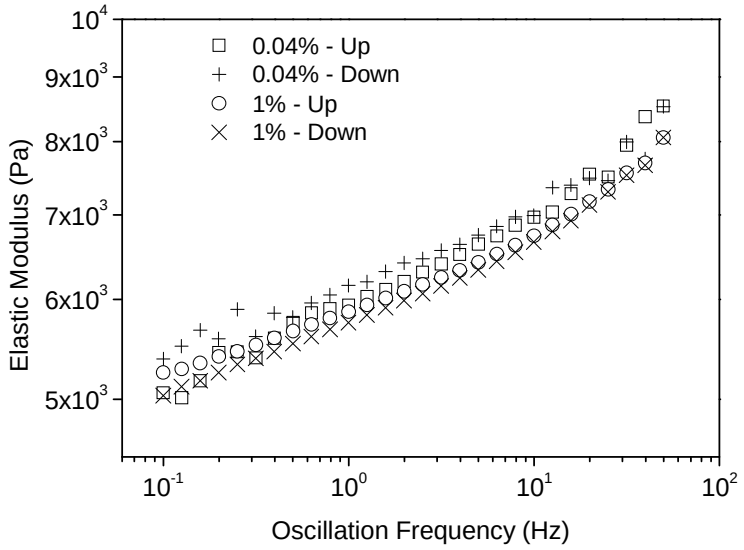

Figure 7.2. Oscillation tests to evaluate G' behavior with frequency and maximum deformation.

As the elastic modulus varies continuously with frequency, the oscillation test to estimate the yield stress was repeated with a oscillation frequency of 1Hz to evaluate its impact on the yield stress estimation. Despite that frequency dependence of G' values, a yield stress of 268 Pa was found, thus practically the same value as at 10 Hz. Chang et al. [5] found bigger variations, they measured lower yield stresses (around 20%) with frequency increase from 1 to 10 Hz.

7.2.1.3 Low shear rate test

This yield stress measurement method consists in imposing a very small and constant shear rate to the waxy crude oil and measure its maximum shear stress, which is considered to be the yield stress. The deformation increases slowly as well as the stress until reaching a critical deformation, beyond which the fluid exhibits lower resistance to deformation. The idea behind this test is to apply a very low shear rate to get very low viscous response of the material, thus measuring the yield stress as a local maximum stress in the shear stress vs. time or shear stress vs. strain curve. It should be comparable to the creep test, where constant shear stresses are applied. But in this case, only one test is needed to measure the yield stress.

With the same cooling conditions and holding time of the previous tests, the shear stress vs. deformation curve measured with a shear rate of 5×10^{-3} s^{-1} is presented in Figure 7.3. Initially, the shear stress increase at low deformations corresponds to the solid response, similarly to the higher shear rate cases presented in Section 5.3. The slope starts reducing for deformations higher than 0.05. The maximum stress measured was 224.9 Pa, at the critical deformation 0.21. Beyond that point, the shear stress decreases with the deformation.

In this low shear rate test, once the stress starts decreasing, it can be said the most important links between the wax crystals were broken. In a rheometer, it is not possible to be sure that this breakage happened throughout the sample and the deformation is uniform. Nevertheless, while in solid state, the material structure is expected to be more uniform, leading to a more uniform deformation distribution as well. Therefore, the maximum stress, marking the transition in the material structure, is retained as the yield stress.

The employed rheometer allows, for crude oil A, applying a reasonable constant (±20%) shear rate of 5×10^{-3} s^{-1}, due to its system of controlling the shear rate (rotational velocity) by the stress (torque) manipulation. The shear rate magnitude has an influence on the maximum shear stress value. Figure 7.4 shows the maximum shear stresses measured with constant shear rates already presented in Figure 5.2 and the value obtained with this new low shear rate experiment.

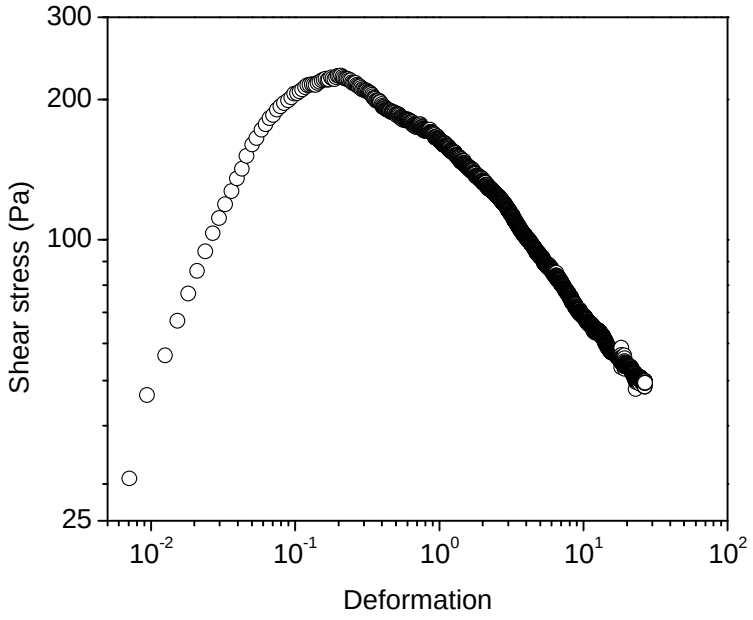

Figure 7.3. Shear stress measurements for a constant shear rate of 5×10^{-3} s^{-1}. This test was performed with the fluid cooled from 60 °C to 4 °C at -1 °C/min with a holding time at 4 °C of 20 min.

Despite the values for 1 and 3 s^{-1}, where the rheometer failed in keeping the shear rate constant close the maximum shear stress (5 and 22 s^{-1} were the respective instantaneous values), the maximum shear stress seems to start forming a plateau when the shear rate decreases. As a reference only, without specific physical meaning, the dashed line added to Figure 7.4 is a HB-type fitting of the measured data with yield stress 224 Pa.

The yield stress measured by this technique is an intermediate value between the creep and oscillatory tests. The creep test has indicated a yield stress somewhat lower than 200 Pa. The oscillatory stress ramp estimates the yield stress at 274 Pa. The difference between these values is big, higher than 30%. But the shear rate histories experienced by the material during each test are also very different.

The low shear rate test is the method retained in this work for measuring the fluid apparent yield stress. It requires the execution of one single cooling procedure and applies a monotonic increasing deformation to the material, as for pipeline flow restart cases.

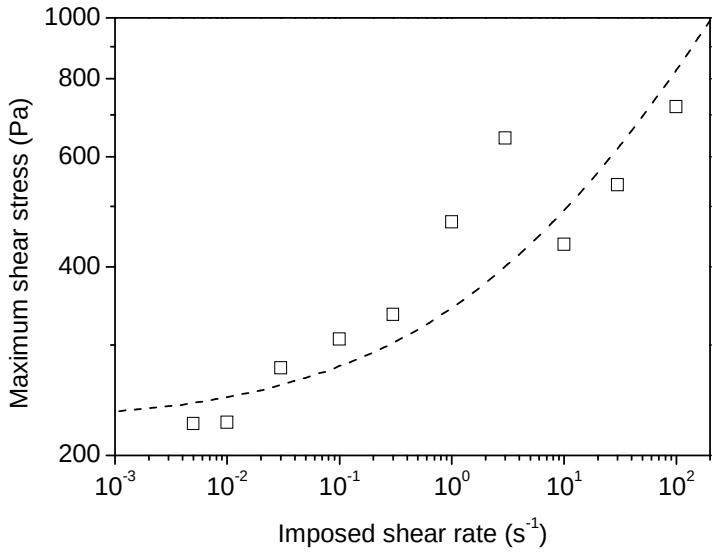

Figure 7.4. Maximum shear stresses (symbols) measured for different imposed shear rate values for crude oil A samples after the same cooling process. The dashed line is a HB-type fitting with yield stress of 224 Pa.

7.2.2 Yield stress after static cooling

The low shear rate procedure was used for estimating the yield stress in function of the oil cooling conditions. In this section, a systematic evaluation of the yield stress is performed changing two parameters, namely, the cooling rate and the holding time at rest after cooling. The samples were cooled from 60 °C to 25 °C at -1 °C/min and from 25 °C to 4 °C at cooling rates of -0.1, -0.25, -0.5 and -1 °C/min. The use of faster cooling until 25 °C, thus above the WAT of crude oil A, showed no difference when compared to slower constant cooling rates starting from 60 °C. The holding time at rest at 4 °C after cooling was varied from 1 to 180 min.

Figure 7.5 presents the yield stresses measured for static cooling varying the cooling rate and holding time after cooling. Each set of symbols represents a different cooling rate. It can be seen that for all cooling rates the yield stress increased with the holding time, though the -1 °C/min data set that apparently did not increase from the holding time of 40 to 180 minutes. The -1 °C/min cooling rate curve also presents systematic lower yield stress values. No specific order is observed for the other 3 cooling rates. The minimum measured value was 156 Pa (-1 °C/min, 1 min) and the maximum 336 Pa (-0.25 °C/min, 180 min).

The increase in the yield stress with lower cooling rates observed with different waxy oils was not observed in this set of data (Venkatesan [71], Lin et al. [31]). From -0.5 to -0.1 °C/min is not possible to observe a specific trend. The variation with the holding time shows that this may be an important parameter in the gelling process of crude oil A, allowing further gel structure development. From this data set, it is also not possible to say that the yield stress remains constant at long holding times, but the variation gets lower.

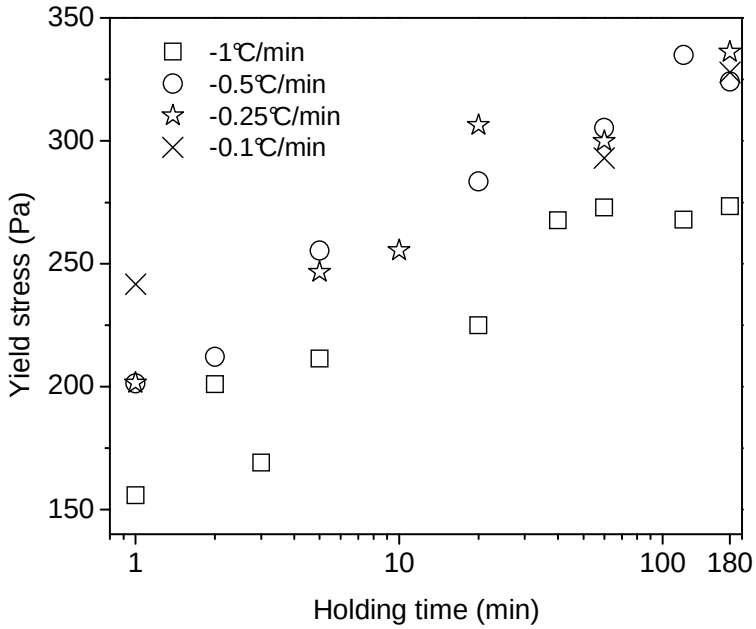

Figure 7.5. Apparent yield stress measured after a static cooling from 60 °C to 4 °C at four different cooling rates and holding times at 4 °C from 1 to 180 min.

Those data are complemented with the critical deformation, i.e. the strain value measured at the corresponding maximum shear stress, shown in Figure 7.6. The critical strain decreases with the holding time for all cooling rates. Unlike the yield stress data, the slower cooling rates present systematically lower critical deformations.

According to this result the material becomes more fragile with slower cooling rates, since the critical deformation is reached earlier. As the yield stress values are similar for cooling rates slower than -0.5 °C/min, at a given holding time, it indicates an average elastic modulus increase at slower cooling rates, i.e. the gel becomes more rigid.

Figure 7.6 also demonstrates that assuming a constant value of 0.15 for the critical deformation is a rough approximation of its variations with cooling rate and holding time. Nevertheless, improving its description to more detailed level would be a secondary improvement with respect to the yield stress prediction when thinking of calculating pipeline restart pressure or the transient destructuring flow at much higher deformations. More rigorous models would take those variations observed in Figure 7.6 into account.

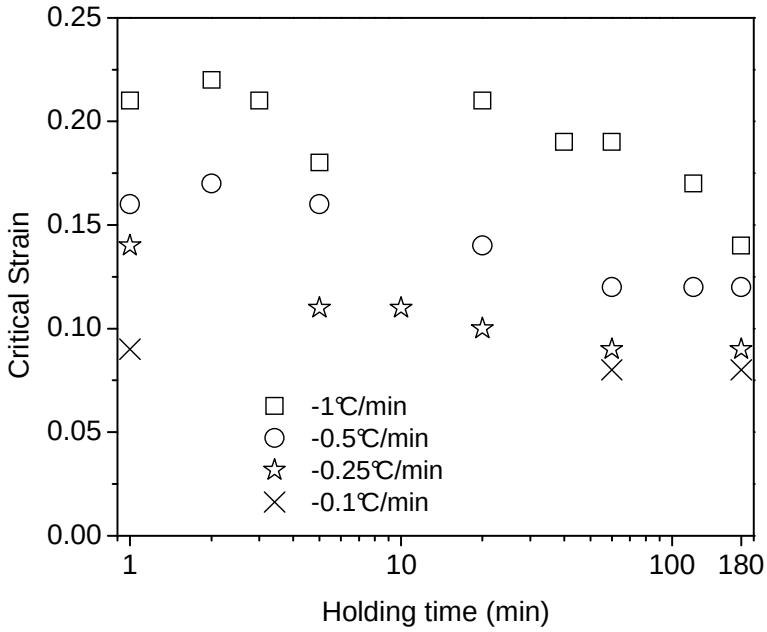

Figure 7.6. Strain measured at the maximum shear stress after a static cooling from 60 °C to 4 °C at four different cooling rates and holding times at 4 °C from 1 to 180 minutes.

7.2.3 Yield stress after dynamic cooling

The yield stress measurements done under dynamic cooling conditions, i.e. at shear rates of 1, 10 and 100 s^{-1} are presented in Figure 7.7. The cooling rates used were -0.25 and -1 °C/min.

It can be seen that the yield stress values are much lower, one or two orders of magnitude, than for the static cases presented in Figure 7.5. The yield stresses measured with the slower cooling rate, -0.25 °C/min, are systematically lower and less dispersed than for the cooling rate of -1 °C/min. For the -1 °C/min cases, it is possible to observe that lower the shear rate, higher the yield stress for all three holding times. The 1 s^{-1} case presented the most important yield stress increase with the holding time, from 20 to 36 and then to 48 Pa in 1, 60 and 180 min, respectively.

The cooling with shear rate of 1 s^{-1} exhibited clear tendencies of yield stress increase with the holding time, particularly for the -1 °C/min case, where the yield stresses were systematically well above the other (slower) cooling rate values (around 5 times). That is the opposite tendency as for static cooling. Some works in the literature try to explain that as a result of the shear action on the wax crystals size (see section 2.4.1). Nevertheless, the implicit difference between the two cooling rates is the higher shearing time for the slower cooling rate, which contributes for destructuring the fluid. So, for the slow cooling rate, the shear rate seems to be not very important to the yield stress value. Additionally, the yield stress values are lower, without a clear tendency of the cooling rate influence below values of 10 Pa. On the other hand, for the faster cooling rate, -1 °C/min, the shear rate influence is significant, mainly for long holding times.

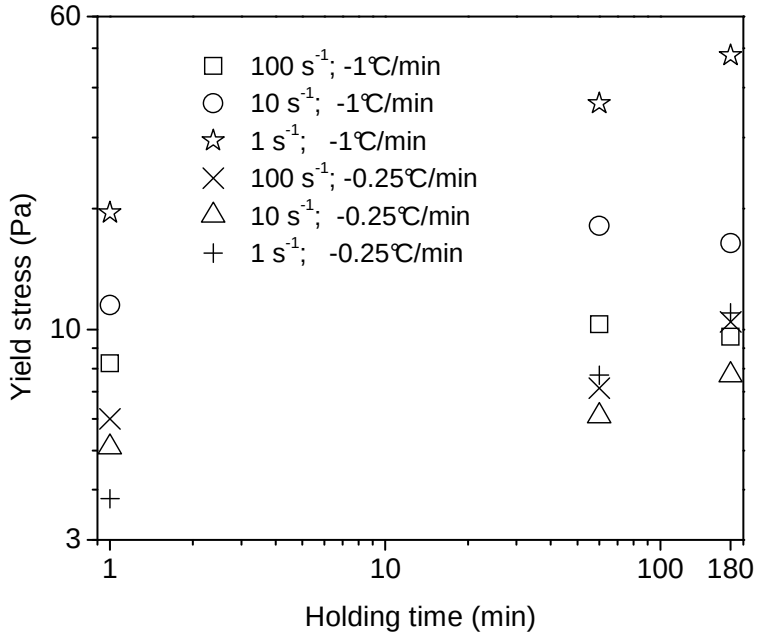

Figure 7.7. Apparent yield stress measured for dynamic cooling with 100 s^{-1}, 10 s^{-1} and 1 s^{-1} from 60 °C to 4 °C at cooling rates of -1 and -0.25 °C/min and holding times at 4 °C from 1 to 180 min.

So, for slow cooling rates, the sample has been sheared for a long period. It exhibits a low yield stress with a lower dependency on the shear rate magnitude during the cooling. For faster cooling rates, the sample has been sheared for a shorter period of time. The corresponding yield stress presents a stronger dependency on the shear rate during cooling.

Figure 7.8 shows the yield stress behavior with the shear rate applied while cooling for samples that were cooled at -1 °C/min and statically held at 4 °C for 1 min after cooling. Additionally to the data already presented in Figure 7.7, the yield stress after shearing at 0.1 s^{-1} was added to the data set. The yield stress after static cooling was also plotted in order to keep the global perspective.

A monotonic decrease of the yield stress with the shear rate while cooling can be observed in Figure 7.8. The influence of the shear rate in the cooling period is so strong that even a small shear rate of 0.1 s^{-1} is enough to reduce the yield stress of one order of magnitude, comparing to the static case. The inset in Figure 7.8 shows the tendency in log-log scale. Even if there are only four points, the tendency seems clear and confirm the results observed by Zhao et al. [82].

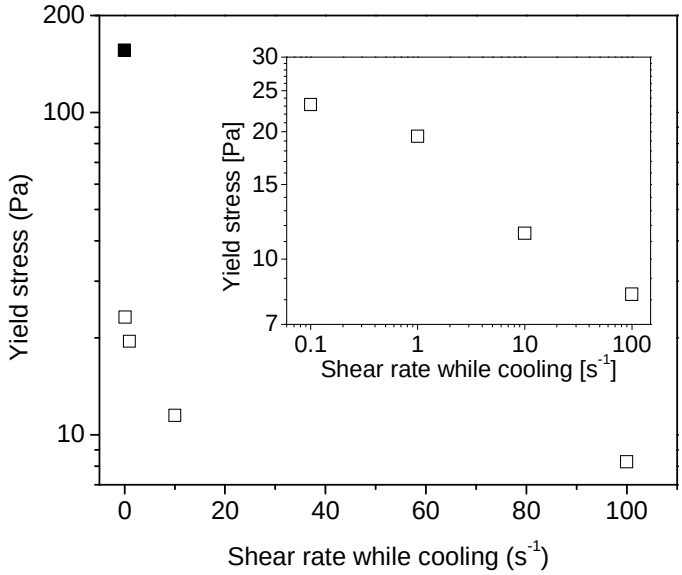

Figure 7.8. Yield stress variation with the shear rate while cooling. For all points the cooling rate was -1 °C/min and holding time of 1 min. The points corresponding to static cooling (full square) and cooling at 0.1 s^{-1} where added to the data already presented in Figure 7.7. The inset shows the same data but in a log-log scale, where the tendency can be clearer seen.

7.2.4 Yield stress after mixed cooling

Here the term "mixed cooling" makes reference to an intermediate cooling condition, where the oil is cooled under flow until a given temperature - T_{stop} - below the WAT and then cooled at rest. It corresponds to the oil that was still cooling while flowing in the pipeline at the shut-in moment and finished its cooling period at rest. Hence, it was partially cooled under shear and partially at rest.

The first part of the yield stress analysis after mixed cooling consisted in varying the temperature limit between the dynamic and static cooling condition and observe its effect on the yield stress measured at 4 °C. In this analysis the cooling rate and holding time after cooling were constant for all tests, at -1 °C/min and 20 min, respectively.

Figure 7.9 presents the yield stress vs. the temperature limit between dynamic and static cooling for two data sets. The squares correspond to a shear rate of 1 s^{-1} during the dynamic part of the cooling and the circles to the shear rate of 100 s^{-1}. As the yield stress is measured at the temperature of 4 °C, the values for the transition temperature of 4 °C are in fact the same as a scenario of dynamic cooling only. The star, at 22 °C, corresponds to a static cooling condition, because that is the oil WAT. If the waxy crude oil was not shear below the WAT, that corresponds to a static cooling.

The yield stress decreases with the increasing of the shearing part of the cooling procedure. The same trend is observed for the shear rates of 1 and 100 s^{-1}, but the yield stress values for the lower shear rate are systematically higher. So, shearing the oil while cooling, even if only during part of the cooling, will affect the final yield stress at 4 °C. Shear reduces the yield stress value proportionally to the duration of the dynamic part of the cooling.

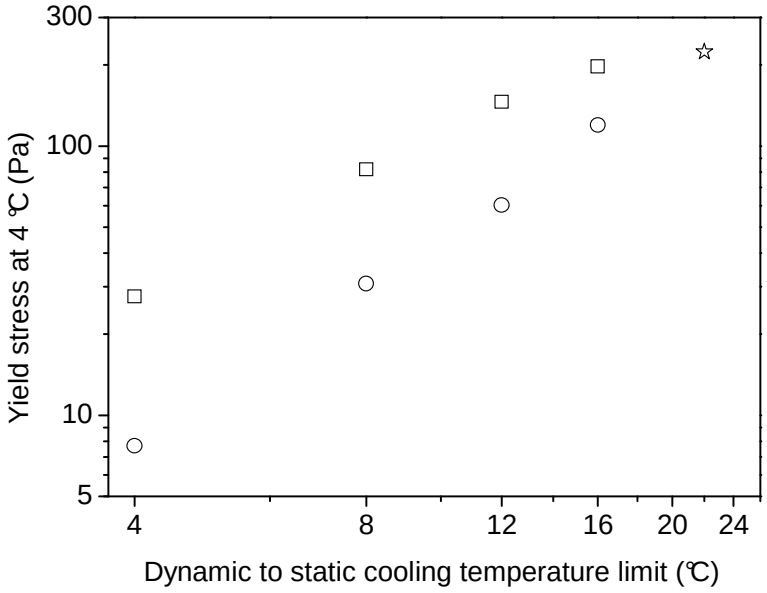

Figure 7.9. Yield stress measured at 4 °C in function of the limit temperature between dynamic and static cooling. The cooling rate is -1 °C/min, with shear rates of 1 s^{-1} (squares) and 100 s^{-1} (circles) while the temperature is above the dynamic to static cooling temperature limit. The star corresponds to the static cooling case and it's referenced to the WAT of 22 °C of crude oil A.

The same tests were also performed for the cooling rate of -0.25 °C/min and holding time of 180 min. The idea was to observe the influence of the shear rate after longer periods of shear while cooling and longer holding time. That condition in the static cooling case created the stronger gel. Figure 7.9 presents the measured results.

The tendency with respect to the temperature limit where the shear was stopped is the same as observed in the previous case of faster cooling rate: There is an apparently linear dependency of the yield stress at 4 °C with T_{stop} in a log-log scale. However, the shear rate influence is not clearly noticed here. The data for 1 and 100 s^{-1} practically superimpose each other. This is in accordance with the observations for dynamic cooling cases in the previous section.

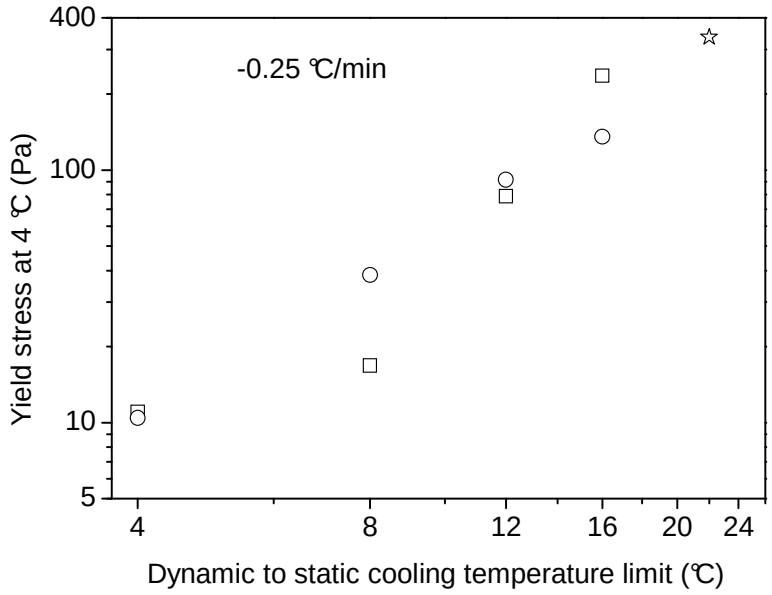

Figure 7.10. Yield stress measured at 4 °C in function of the limit temperature between dynamic and static cooling for the cooling rate of -0.25 °C/min and holding time of 180 min. Squares correspond to the shear rate of 1 s^{-1} and circles to 100 s^{-1}.

The third analysis performed in the mixed cooling scenario evaluates the yield stress values for different cooling rates. Here the temperature limit between dynamic and static cooling was fixed to 12 °C. While cooling above that temperature the oil was sheared with different shear rate values from 0.1 to 100 s^{-1}. The rest of the cooling, from 12 to 4 °C, was at rest, followed by a holding time of 20 min, for all cases. The cooling rates used were -1 and -0.25 °C/min.

The measured yield stresses are presented in Figure 7.11. General trends are the same as observed in the completely dynamic cooling cases (see Figure 7.8) for both cooling rates. The yield stress is reduced with the shear of the sample. Although, it is remarkable that for the cooling rate of -1 °C/min the yield stress reduction with shear rate is more gradual than for the -0.25 °C/min. The fact that the sample was sheared with 0.1 s^{-1} above 12 °C reduced the yield stress from 306 to 85 Pa, for the cooling rate of -0.25 °C/min.

The yield stress measurements showed that when the cooling rate is slow and there is a shear rate acting during the cooling phase, the oil-gel structure state is weaker. Longer the time spent under shear while cooling, lower the gel strength and lower the influence of the shear rate magnitude.

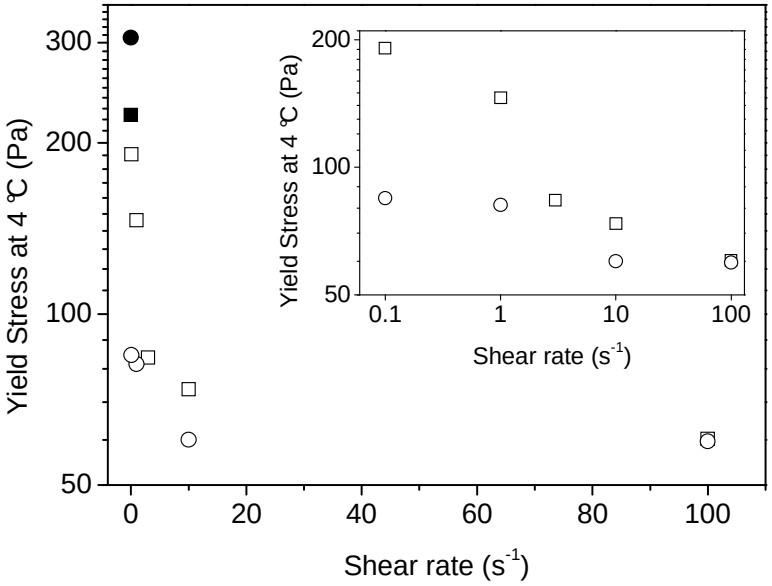

Figure 7.11. Yield stress at 4 °C for mixed cooling condition. The dynamic part of the cooling was from 60 to 12 °C and the static part from 12 to 4 °C. Cooling rates of -1 °C/min (squares) and -0.25 °C/min (circles). Full symbols, plotted as references, correspond to the completely static cooling. The inset shows in details the influence of the shear rate for the two cooling rates.

7.2.5 Yield stress behavior with temperature

In order to complete the description of the yield stress with cooling parameters, additional tests were carried out to evaluate its behavior with the temperature. The yield stress and the critical deformation were measured from low shear rate tests after static cooling at -1 °C/min. Figure 7.12 presents the measured values.

The yield stress continuously decreases as the temperature increases and tends to zero around 16 °C, which means that beyond that temperature the material is mostly a liquid without yield stress. In most of the range where a yield stress exists the critical deformation remains around 0.15.

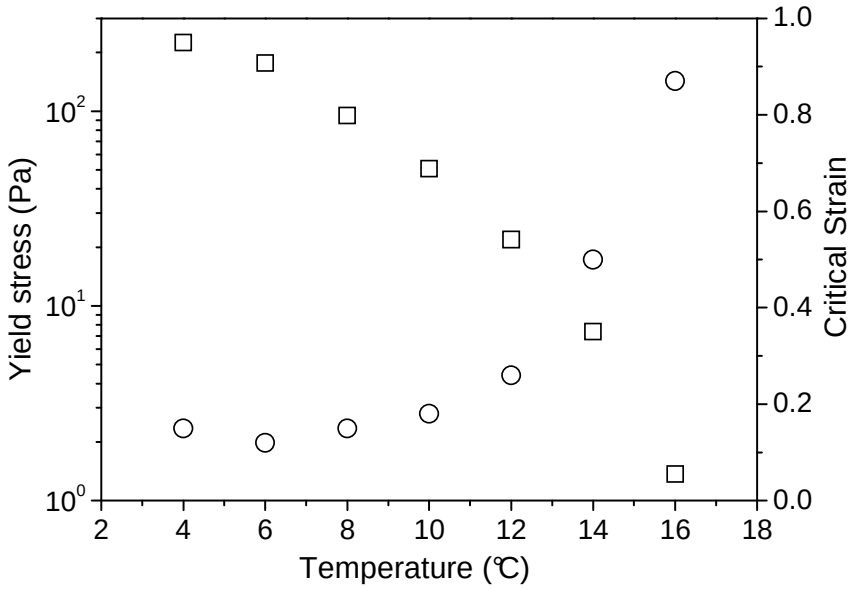

Figure 7.12. Yield stress (squares) and critical deformation (circles) as a function of temperature for crude oil A.

7.3 Elastic modulus evolution

Small amplitude oscillatory tests have been carried in order to evaluate whether the trends observed on the yield stress could be as well observed on the elastic modulus of the gel while cooling and during the holding time after the cooling. Oscillations amplitude was set to 0.04%

As presented in Section 2.3.1, the elastic modulus (G') is related to solid-like characteristics of the gel. Thus, following the behavior of G' with time could provide an indication of the oil-gel yield stress behavior. The gel strength was already related to G' measurements by Lopes-da-Silva and Coutinho [32], Ekweribe et al. [20] and used to determine waxy crude oils yield stress in the patented ColdStart methodology (see Patent [47]).

The practical objective in following the elastic modulus evolution is to use it as a gel structure state indicator. If a relation between G' and yield stress can be drawn, it can be used as a method for reducing the number of experiments to detect yield stress tendencies with respect to some cooling parameter.

7.3.1 Cooling phase

The small amplitude oscillatory tests performed during static cooling and holding time of the yield stress measurements presented in Section 7.2.5 measured the G' behavior prior to the yield stress measurements. Figure 7.13 presents the elastic modulus evolution with temperature and during hold time at constant temperature. The yield stress data already showed in Figure 7.12 is plotted in the same graphic. Convenient scales were adopted to qualitatively compare both properties.

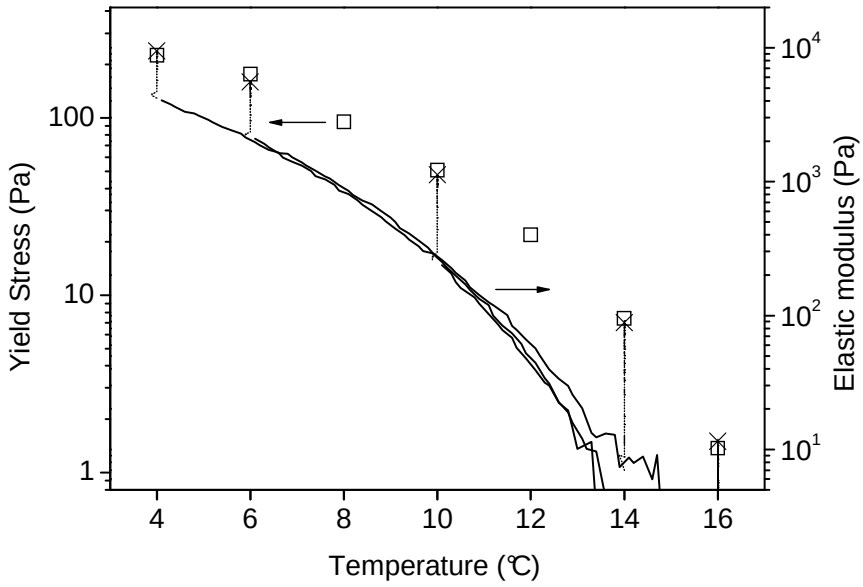

Figure 7.13. Comparison of crude oil A elastic modulus qualitative behavior, measured during static cooling (continuous lines) and holding time of 20 min (vertical dashed lines), with the yield stress measured at the same experiment (squares), already showed in Figure 7.12. The last G' value measured before the yield stress measurement is indicated by the crosses.

The elastic modulus during static cooling increases with the temperature decrease, as show the continuous lines in Figure 7.13. The superimposing continuous curves show the good repeatability of the data. After cooling, the gel elastic modulus evolution during the holding time, the vertical dashed lines in Figure 7.13, suggests a gel structure development that matches the corresponding yield stress measured in the sequence. The last G' value measured before the yield stress measurement is indicated by the crosses. The G' evolution during the holding time acts "shifting" the G' curve measured during the cooling period.

Hence, for those static cooling conditions it can be said that the G' has analog behavior to the gel yield stress development. Once a reference point is taken between G' and τ_c for a given condition, the G' evolution could be used to estimate τ_c in other conditions.

A similar analysis can also be done for the mixed cooling cases. In Figure 7.14 the yield stress data presented in Figure 7.9 and Figure 7.11 are plotted *versus* the respective G' values measured immediately before the yield stress measurements. This comparison shows that the linear relation between those two properties is not so clear as in the previous cases of static cooling scenarios. Although, the global tendency continues showing that higher the elastic modulus, higher the yield stress.

The complexity of the various fluid structure states obtained from different cooling processes cannot be expressed only by two macroscopic properties as the yield stress and elastic modulus. They only allow approximate correlations. Nevertheless, that simple correlation is a starting point to assess the yield stress of the variety of cooling processes inside a pipeline.

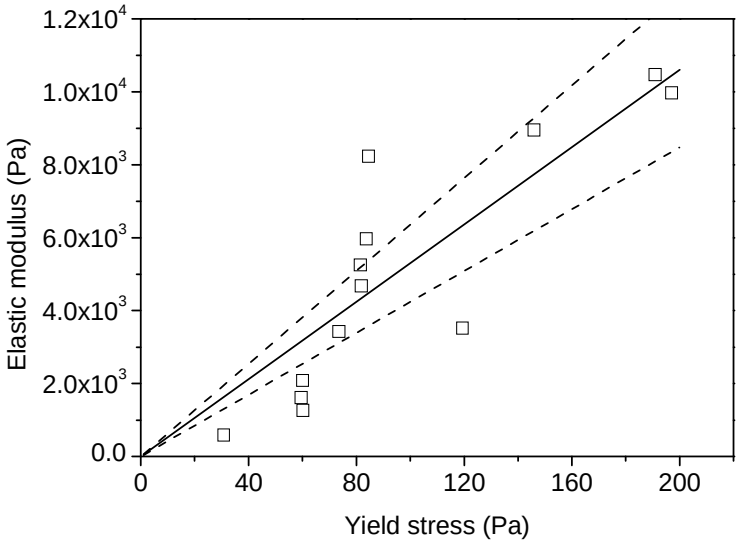

Figure 7.14. Elastic modulus measured immediately before the respective yield stress measurement for the mixed cooling scenarios of Figure 7.9 and Figure 7.11. The continuous line represents a linear relation between the two properties with the +/- 20% reference given by the dashed lines.

7.3.2 Holding time

The yield stress evolution with the holding time is also going along with the elastic modulus increase. Figure 7.15 shows the G' evolution during the holding time for some selected yield stress evaluation tests. The G' is plotted for the cases of static and dynamic cooling of 1 and 100 s^{-1} and cooling rates of -1 and -0.25 °C/min.

The higher relative increases of G' happen after a cooling under shear, however, the most important (absolute) augmentations are after a static cooling, where an already high value increases further. The shapes of the curves are the same as obtained by Lopes-da-Silva and Coutinho [32] and Lin et al. [31]. It is also worth noting that the slower cooling rates cases present much less relative G' evolution during the holding time than the cases where the oil was cooled faster. It may indicate that the gelling process was more "out-of-equilibrium" at the end of cooling when faster cooling rates are applied than when the oil is more slowly cooled, letting time for structure arrangements.

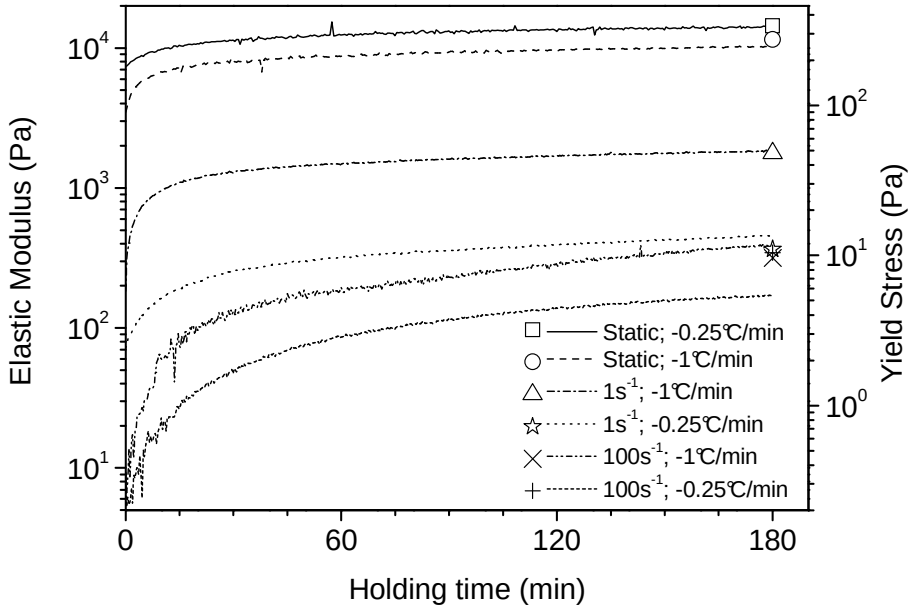

Figure 7.15. Elastic modulus evolution during holding time after cooling at 0, 1 and 100 s^{-1} and for cooling rates of -1 and -0.25 °C/min with the respective yield stress measured in the sequence.

7.3.2.1 Hermetic cell test

In order to complete the analysis supporting that this augmentation in G' during holding time is not caused due to evaporation of light components of the oil, one test was made using a hermetic cell in the rheometer. This cell provides a closed ambient to the sample, avoiding the escape of any light component. The hermetic cell consists of a cylinder of 28 mm diameter, where the oil sample is charged and the geometry used to shear the oil is mounted. Once assembled, the cell presents only one opening, normally used for controlling the internal pressure with a selected gas. Nitrogen is normally used for pressurizing crude oil without disturbing its properties due to the gas low solubility in oil. The geometry used to impose the oscillatory deformations was a vane.

The oil was cooled in the cell from 60 °C to 4 °C at -0.5 °C/min. Slower cooling rate was used for helping the oil sample temperature homogenization, since the cell contains a bigger volume of oil than in plan-plan experiments. The oscillation frequency was 10 Hz and amplitude was set to 5% deformation for having a good sensibility. The same setup was used with the plate-plate geometry for comparison.

Figure 7.16 presents the comparison between normalized G’ (G’ divided by the highest G’ value of the curve) obtained with those two measuring systems during the holding time after the cooling process. The result shows a higher relative elastic modulus increase in the hermetic cell. The gel formed in cell also develops its elastic modulus with time in a similar way to the open sample in plate-plate geometry.

Part of the G’ initial evolution in the cell during the holding time may be due to a transient thermal effect. If the oil sample has not an homogeneous temperature distribution, part of the fluid may be still cooling even if the cell’s internal wall has already reached 4 °C. For investigating

that possibility, the sample effective thermal profile was estimated by numerically calculating the transient heat diffusion in the oil inside the cell. The cooling rate imposed in this experiment was assumed to be the internal wall temperature of the cell, which was used as a boundary condition in the calculation. Figure 7.17 shows the calculated average temperature during the holding time after cooling.

When the wall of cell reached 4 °C at the end of the cooling period, the bulk average temperature of the fluid was still at 7 °C. It took around 15 min to get under 4.5 °C. But after 30 min of holding time, for example, the fluid average temperature is already below 4.1 °C. The relative G' evolution from that point until the end of the test, at 240 min, is similar in both curves. So, even in a closed atmosphere, the fluid structure evolves with time, increasing its solid-like characteristic.

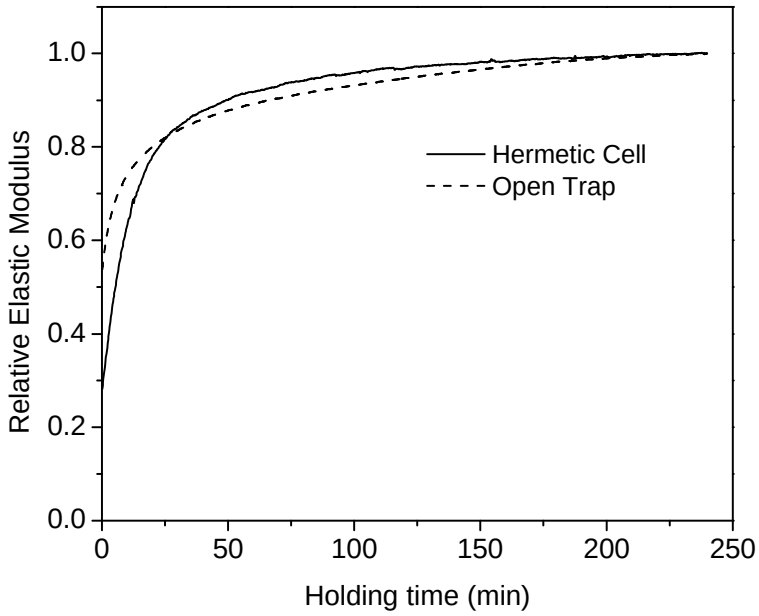

Figure 7.16. Comparison between relative elastic moduli – G' divide by highest measured G' value– during the holding time at 4°C obtained with conventional plan-plan geometry with simple cover and hermetic cell equipped with vane geometry.

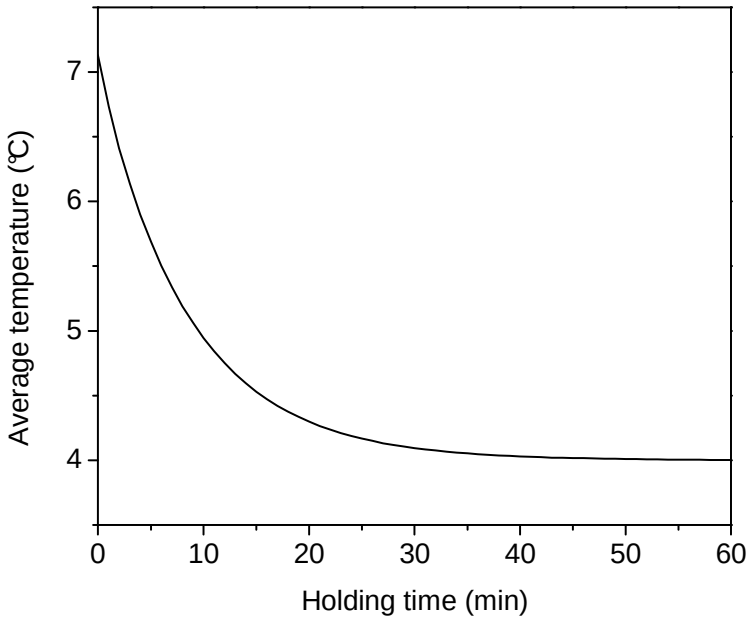

Figure 7.17. Average temperature calculated for the fluid inside a vane-cylinder geometry with external cylinder cooling from 60 °C to 4 °C at -0.5 °C/min. The time in the abscissa starts counting when the external cylinder reaches 4 °C.

7.3.2.2 Influence of phase change kinetics

The time dependence of the liquid-solid phase change process could also play a role on that evolution. If the phase change still happens during the holding time, the appearance of new wax crystals could also influence the fluid structure evolution. In order to evaluate the phase change time scale at the end of the cooling process a DSC test was set. An oil sample was charge in a DSC capsule and cooled at -1 °C/min from 80 to 4 °C. The principle is to observe the exothermic heat flux from the capsule at the end of the cooling. If there is no heat flux at constant temperature, it means that there is no phase change taking place.

Figure 7.18 shows the measured heat exothermic flux curve with time from the sample. At the experiment time of 86 minutes the 4 °C was achieved, and then let constant. That point is marked by a sudden drop in the heat flux, because no more sensible heat needs to be extracted to cool the fluid. Although, there is still some heat flux at constant temperature coming from the sample, for around 3 min after the 4 °C was achieved.

That residual heat flux indicates that the phase change, i.e. the wax solidification, lasts for approximately 3 min after the oil achieves a constant temperature subsequent to cooling. Thus, any change in the fluid rheological properties beyond those few minutes does not come from the phase change phenomenon.

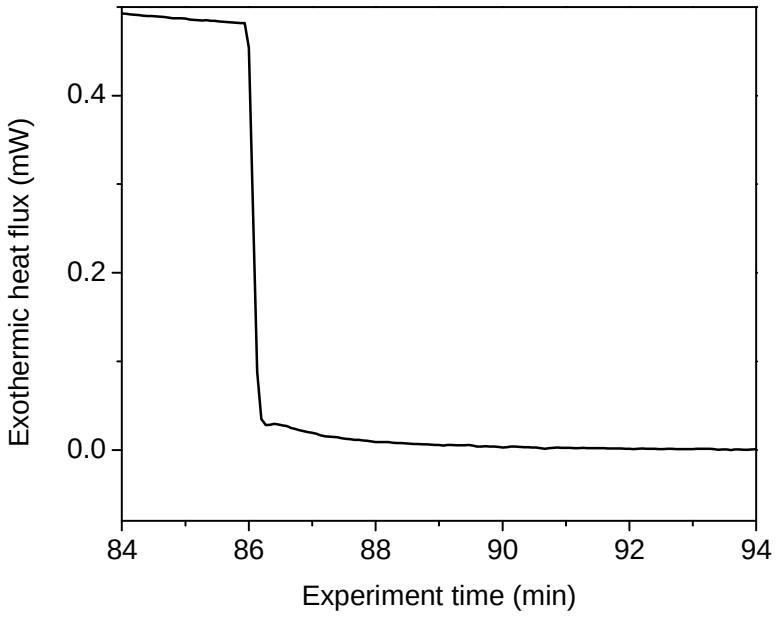

Figure 7.18. Heat flux measured in DSC experiment. At 86 min the sample reaches 4 °C. A residual heat flux was still measured for approximately 3 min.

The long evolution time of waxy oils gel structure may have its origins on any internal rearrangements, aggregations or forces equilibration (Visintin et al [77], Lopes-da-Silva and Coutinho [32]). It is an important phenomenon that promotes the yield stress and elastic modulus increase during holding time.

7.4 Correlating yield stress to cooling parameters

7.4.1 Evaluating main cooling parameters

From the tendencies observed in the experimental data presented in this chapter, some relationships can be drawn between the yield stress and the cooling parameters. The main interest in building such correlations is the determination of the yield stress field in the pipeline after a shut-in.

It was seen that the yield stress value reflects the influence of the measurement temperature, cooling rate, holding time, shear rate while cooling and the temperature limit between dynamic and static cooling.

However, some of those parameters, or some combinations of parameters, have minor influence on the yield stress. Here, the objective is to keep the global perspective of the yield stress magnitude, developing relations to capture the most significant variations.

Under that point of view, some simplifications can be made regarding the measurements presented in this chapter. As cooling rates are expected to be low in real pipeline cases (as report Van Engelen et al. [22]) and, for crude oil A, the yield stress did not present a clear variation with the cooling rate for values slower than -0.5 °C/min, the influence of the cooling rate will not be taken into account. Moreover, experiments showed that the magnitude of the

shear rate applied while the sample is cooling at low cooling rates do not play a major role in the yield stress value determination.

On the other hand, it is of major importance to know whether the cooling was under shear or at rest. Thus, the temperature limit between dynamic and static cooling should be an important parameter. As well as the temperature at which the yield stress is measured.

For low cooling rate cases, it may take days to achieve thermal equilibrium with the ambient. Thus, taking into account holding times at rest after cooling of some hours should not be a major concern. Nevertheless, for crude oil A, important evolutions in the structure state were measured during that period. Therefore, instead of accounting for the yield stress evolution with the holding time after cooling, only the final yield stress value after the holding time will be considered. It means that the yield stress values measured after the holding time will be considered as the final product of the cooling process.

7.4.2 Correlating the yield stress for static cooling

The first relation to be done is between the yield stress for static cooling conditions and the final cooling temperature. Here, a correlation depending only on the temperature will be employed, without accounting for the cooling rate, as did Zhao et al. [82]. The reason for that choice relies on the behavior showed in Figure 7.5, where no clear tendency can be observed for cooling rates slower than -0.5 °C/min. Additionally, cooling rates in pipelines are expected to be much slower. Then, the oil yield stress after static cooling is given by

$$\tau_{c,static} = \tau_{ref}\left[1 - Inf\left\{1, \frac{T - T_{ref}}{WAT - T_{ref}}\right\}\right]^{C_1} \tag{7.1}$$

where C_1 is a constant parameter, τ_{ref} is the yield stress measured at the temperature T_{ref} and the $Inf\{\}$ function assumes the lowest value of its arguments. Thus, if the temperature is above the WAT, the oil yield stress is zero.

The yield stress calculated by the equation above represents the fluid yield stress at the end of the static cooling period. Next, the material structure state evolution during the holding time, that increases the yield stress, should be added to the value predicted by Eq. (7.1). That can be done using a gel structure evolution kinetic equation as Eq. (2.23). However, for practical interests, considering the data measured for crude oil A, after the holding time of one hour, or even three hours, the gel structure development has practically ended. Thus, given the similarity of the shifting in the G' vs. temperature curve during the holding time (see Figure 7.13), the parameters of Eq. (7.1) can be directly fitted to the yield stress data measured after the holding time.

Therefore, Eq. (7.1) can be fitted to the data of Figure 7.13, assuming τ_{ref} as the value at the end of the holding time: 224 Pa. So, the corresponding T_{ref} is 4 °C. The value of the parameter C_1 that provides the best fitting to the data in Figure 7.13 is 4. The comparison between the yield stress data and the fitting provided by Eq. (7.1) is presented in Figure 7.19.

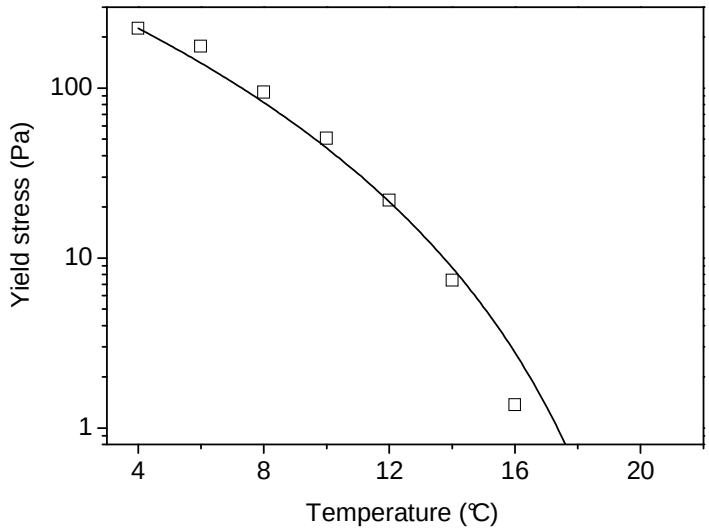

Figure 7.19. Symbols are the yield stress after cooling rate of -1 °C/min and holding time of 20 min and the line represents the respective fitting given by Eq. (7.1).

As the cooling process of -1 °C/min and holding time of 20 min is not the most critical condition for a pipeline restart in terms of gel strength, it would be interesting basing Eq. (7.1) on more critical conditions. Those could be, for example, -0.25 °C/min and holding time of 180 min, as shows Figure 7.5. It corresponds to a yield stress of 336 Pa, that could be used as τ_{ref} in Eq. (7.1).

7.4.3 General yield stress correlation

For the mixed cooling, the behavior exhibited in Figure 7.10 can be fitted by a power-law in function of T_{stop} (the limit temperature between dynamic and static cooling) limited by the higher and lower yield stresses. Those limiting yield stresses correspond to the completely static (τ_{stat}) and dynamic (τ_{dyn}) cases in Figure 7.10. For slow cooling rates, as -0.25 °C/min, the influence of shear rate magnitude while cooling is negligible.

However, in order to keep the yield stress description with respect to the cooling rate of -1 °C/min and holding time of 20 min, the power-law fitting for mixed and dynamic cooling processes will be applied to the curve corresponding to 100 s^{-1} (circles) of Figure 7.9. That allows a complete description of that cooling scenario since almost all the fitting parameters of the rheological models in Chapter 6 were based on that condition.

Thus, the yield stress at the reference temperature T_{ref} may be written as

$$\tau_{c,T_{ref}} = \tau_{dyn,T_{ref}} + \left(\tau_{stat,T_{ref}} - \tau_{dyn,T_{ref}}\right)\left(Inf\left\{1, \left[\frac{T_{stop} - T_{ref}}{WAT - T_{ref}}\right]\right\}\right)^{C_2} \quad (7.2)$$

where the best fitting valued for coefficient C_2 is 1.58 for the reference temperature of 4 °C. The presence of the *Inf{}* function assures that if the limit temperature between dynamic and static cooling is above the WAT, then it is equivalent to a static cooling condition. Figure 7.20 presents

the comparison between the correlation given by Eq. (7.2) and yield stress measurements already presented in Figure 7.9.

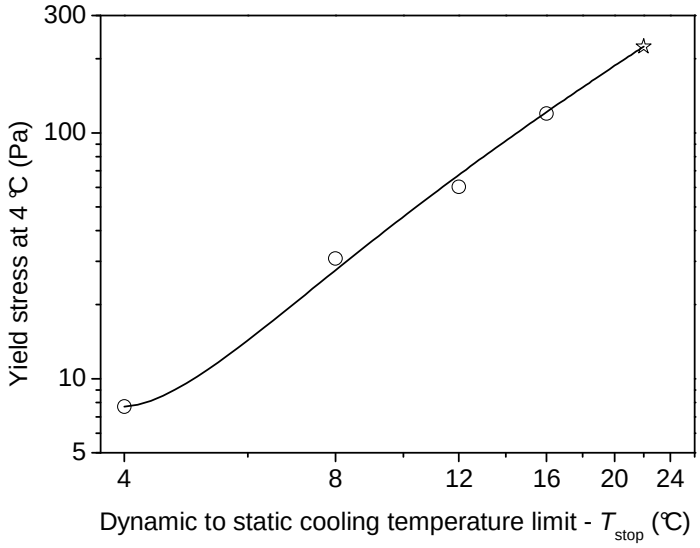

Figure 7.20. Comparison between yield stress predictions of Eq. (7.2) (line) and measured values (symbols) for mixed cooling condition of -1 °C/min and holding time of 20 min.

Thus, assuming that the yield stress after dynamic cooling presents the same behavior with the temperature as for static cooling, the yield stress can be correlated to the main cooling parameters by substituting the expression above for $\tau_{c,T_{ref}}$ in Eq. (7.1):

$$\tau_c = \tau_{c,T_{ref}}(T_{stop})\left[1 - Inf\left\{1, \frac{T - T_{ref}}{WAT - T_{ref}}\right\}\right]^{C_1} \tag{7.3}$$

where $\tau_{c,T_{ref}}$ is given by Eq. (7.2).

The Eq. (7.3) encapsulates the description the yield stress filed in a pipeline after the shut-in for a given flow and temperature history.

7.5 Conclusions

This chapter showed that different measurements techniques may be applied to measure a waxy crude oil yield (or critical) stress. Due to its simplicity and similarity to the flow restart simple deformation history, the low shear rate test was the preferred method for measuring the yield stress.

Comprehensive yield stress measurements evaluated the influence of cooling rate, shear rate while cooling and holding time after cooling in that property. Crude oil A did not show a specific trend of yield stress magnitude with the cooling rate for static cooling condition, except for the -1 °C/min cases where yield stress was systematically lower. For cooling under shear, the tendency observed is that slower the cooling rate, lower the yield stress. Moreover, slower the

cooling rate, lower is the influence of the shear rate magnitude. This last remark is also valid for mixed cooling cases. During the holding time at rest, the yield stress of crude oil A increased. However, it did not change the trends observed for the other cooling parameters.

For static cooling conditions the oil-gel elastic modulus measured by small amplitude oscillatory tests showed to be proportional to the yield stress. That is a useful relation because helps reducing the number of experiments for mapping the yield stress. However, for mixed cooling conditions and lower yield stresses after dynamic cooling, the proportionality between those two properties is not so clear. Thus, this approximation should be used with attention, depending on the application case.

The observations above allowed developing a simple mathematical correlation between the yield stress and the main cooling parameters. That correlation allows describing the yield stress field in a pipeline at the flow restart moment.

CHAPTER 8

PIPELINE FLOW RESTART

8.1 Introduction

The aim of this chapter is to present a complete pipeline flow restart case, applying the ColdStart Methodology with the improvements that were developed in this work. This case study is an interesting exercise, that allows having a global view of the flow restart problem in a real case scale.

The case under analysis was chosen to be as similar as possible to a real crude oil exporting pipeline Additionally, it should also present a range of flow properties that require modeling several oil-gel structure states conditions. Thermal boundary conditions, for example, were chosen to create static and mixed cooling conditions during pipeline shut-in.

The crude oil A is the fluid used in this restart flow study. That waxy crude oil is represented by the model proposed in Chapter 6. Unfortunately, there is no experimental data available in order to perform a comparative and more conclusive analysis. Even with some available data on flow restart in the literature (see Paso [44] for a reference list), it would be necessary to have access to the samples used in those studies in order to characterize them and find the proper parameters of the rheological model. Hence, the analysis presented in this chapter is an exercise focused on pipeline flow conditions, providing a complete description of the simulation of a pipeline flow restart with gelled oil.

The pipe flow model in which the rheological model was implemented is the StarWaCS code, property of IFP Energies nouvelles. The Houska model was already implemented in that code. Thus, a new version of StarWaCS code was created with the implementation of the rheological model developed in Chapter 6. As the objective here is not to analyze the employed numerical methods, discussions about the parameters related to the solution algorithm are let in a second plan.

The general methodology use to solve the pipeline restart flow case is discussed in the next section. Then, section 8.3 presents the numerical implementation of the rheological model in the Finite Volume method framework of StarWaCS. Section 8.4 presents each step of the flow restart calculation and its results. The last section of this chapter summarizes the conclusions of this exercise.

8.2 Discussion on the applied methodology

The methodology used to solve the flow restart case presented in this chapter is entirely based on the ColdStart methodology, introduced in Section 2.5.3. The idea behind that method is to obtain a detailed rheological description of the oil-gel in the pipe at the flow restart moment. It is done by calculating the fluid flow and thermal histories (see section 2.5.1) in order to evaluate their influence in the yield stress. Additionally, those histories should be taken into account in

the description of the oil-gel destructuring flow characteristics through the use of an appropriate rheological model.

The description of the flow history starts by knowing the pipeline steady state flow conditions. Here, for simulating the steady state flow, the oil was modeled by a Herschel-Bulkley model with parameters that vary with the temperature. Those parameters are presented in Section 6.9. For a given temperature, the HB model represents the oil flow curve. It implicitly assumes that cooling rates are low and the oil behaves as flowing in an equilibrium state at that temperature. The simulation results shall confirm that cooling rates are low and support such hypothesis.

The steady state temperature at each position in the pipe correspond to the limit of the dynamic cooling condition (T_{stop}). Before the pipeline shut-in, the oil was cooled under shear and after the shut-in the oil is statically cooled. Thus, the oil that was flowing at a temperature above the WAT at the shut-in moment will have its wax crystals formed at rest, during the static cooling phase after shut-in. The other pipe regions will be subjected to a mixed cooling. Figure 8.1 presents an example of a mixed cooling condition. For that particular position in the pipe at the shut-in moment, the oil cooled under shear until a temperature T_{stop} below the WAT. Then, after the shut-in, the cooling was at rest, what allows a stronger gel state development.

The original ColdStart Methodology does not take into account the gel structure development during the holding time at rest and constant temperature. If the oil that is being analyzed presents important structure development during the holding time, as it is indeed the case of crude oils A and B, it should be taken into account in the yield stress field determination.

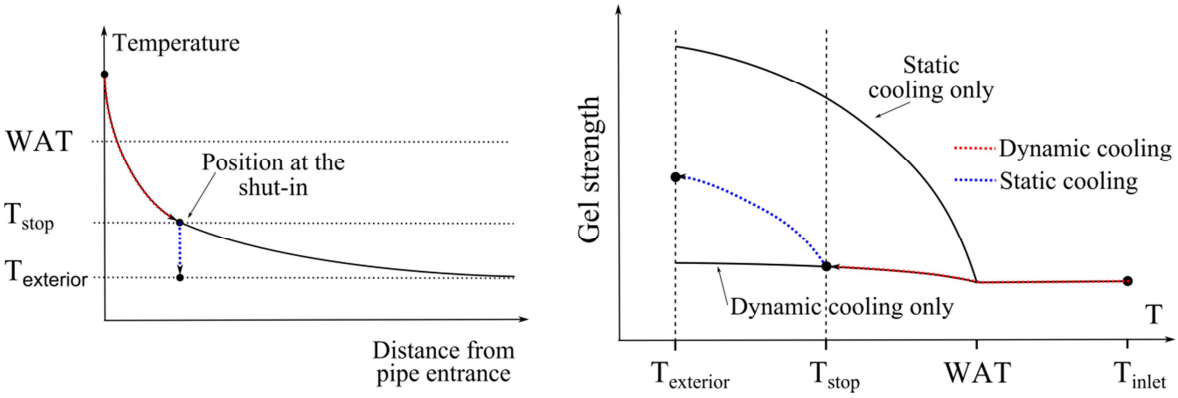

Figure 8.1. Scheme of gel strength evolution for different cooling histories. The oil is dynamic cooled until an intermediate temperature T_{stop} below the WAT, what prevents the development of a strong gel. Then, the oil finishes its cooling process at rest until achieving $T_{exterior}$. The dynamic part of the cooling corresponds to the pipe steady state flow while the static cooling happens after the shut-in.

However, modeling the transient process of structure evolution during the holding time may not be necessary in all cases. In fact, it strongly depends on the oil itself. As it was seen in Section 7.3.2, most of the structure development happened during the first two or three hours after temperature equilibration. Hence, if the flow shutdown takes longer than that, there is no need to calculate the kinetics of that process. Only the final yield stress value, at the end of the holding time is required. Besides, at the end of cooling at low cooling rates, the oil structure state did not show important evolution.

The yield stress field at the restart moment was estimated based on the measurements presented in the previous chapter. Thus, the yield stress correlations for different cooling parameters presented in Section 7.4 were used to construct the initial yield stress field for the flow restart simulation based on the calculated thermal and flow histories.

Next, in the flow restart simulation, the oil-gel is pushed out of the pipe by a different incoming fluid. In practical cases, there is interest in using a low viscosity Newtonian fluid as pushing fluid in order to avoid further gelling problems. Here, the heating of the oil-gel by the incoming fluid will not be considered. That assumption shall not affect the oil-gel plug that is pushed out of the pipe, but will prevent a proper estimation of the pipeline cleaning by the incoming fluid. The difficulty of simulating the cleaning process is in the correct representation of the oil-gel rheological response to the temperature increase during the destructuring flow. Doing an analog representation as in the cooling phase would not be valid, since the Wax Disappearance Temperature – WDT – is not expected to be the same as the WAT (see Ji et al. [27] and Rønningsen et al. [54], for example). As it was not among the objectives of this work, the destructuring flow while heating will not be simulated here.

The next section discusses the modifications done in the StarWaCS code for implementing this new rheological model.

8.3 Model numerical implementation

The StarWaCS code solves the Navier-Stokes equations system, with appropriate simplifications for the pipeline flow scenario, as described by Wachs et al. [79]. It features a Volume-of-Fluid (VOF) method to track the interface between the incoming and outgoing fluids. The momentum equation is solved only for the axial direction, where the velocity vector component in that direction is calculated and it is allowed to vary in both axial and radial directions. Advection in the radial direction is not considered in that equation. The pressure field is allowed to vary only the axial direction, i.e. it is one-dimensional. The mass balance equation is pre-integrated in the pipe cross-section. The Finite Volume method is used to discretize the equations system. A TVD (Total Variation Diminishing) interpolation scheme is used for the advective terms.

The augmented Lagrangian algorithm solves the viscoplastic problem and the compressible Stokes problem (see Vinay [73]). The advantage of the augmented Lagrangian method is that it handles the discontinuities in the derivative of the rheological models and characterizes the unyielded fluid zones by an exact zero shear rate. It is done by applying a transformation to the Navier-Stokes equations which introduces Lagrange's multipliers to the system. Thus, according to the implementation of this method in the StarWaCS code, when the shear stress is below the yield stress value, the shear rate is precisely zero. On the other hand, this is an inconvenient for the viscoelastic solid behavior represented by Eq. (6.8), which accounts for a shear rate in the solid regime.

In this work, as the shear rates in the solid regime are expected to be very low, the numerical implementation of the rheological model will account only for the elastic behavior of the solid. The discontinuity in the shear stress at the solid-liquid transition caused by this simplification is not expected to be important in pipeline flow restart cases, due to the inlet pressure increase rate (see section 8.4.1).

In the StarWaCS code framework, the rheological model must provide two variables to the momentum equation: The yield stress and the apparent viscosity. The former is compared with the fluid instantaneous shear stress to decide whether there is flow or not. If it flows, the apparent viscosity is then used in the friction terms and, consequently, as a parameter for the velocity field determination.

The Houska model, originally implemented in StarWaCS, calculates the yield stress and apparent viscosity in function of the structure parameter λ. This parameter is calculated by a transport equation, which advects λ with the flow and calculates its variations according to the build-up and break-down terms (see Eq. (2.6)). So, the flow history is taken into account by the λ parameter.

The rheological model developed in this work, presented in Eqs. (6.8) - (6.13), also needs to have some of its parameters advected in order to take the flow history into account. In this model, the description of the fluid rheological properties requires three transport equations. First, Eq. (6.10), that is valid for a closed system, must be written for a control volume frame. That is done by taking the viscosity η and the shear rate material derivatives instead of simple time derivatives:

$$\frac{D\eta}{Dt} = -\frac{1}{t_0} Sup\{0; (\eta - \eta_{ref})\}_{\dot{\gamma}} + \alpha \frac{D\dot{\gamma}}{Dt} \frac{\partial \eta_{ref}}{\partial \dot{\gamma}}\bigg|_{\gamma} \tag{8.1}$$

where the material derivative operator is given by $\frac{D}{Dt} = \frac{\partial}{\partial t} + w\frac{\partial}{\partial z}$, with w being the fluid axial velocity.

As η_{ref} depends on the deformation, the deformation field must also be tracked. The transport equation of the deformation γ is given by

$$\frac{D\gamma}{Dt} = \dot{\gamma} \tag{8.2}$$

While the oil-gel is in the solid state, as the shear rate is considered to be zero, the algorithm sets the deformation value as the corresponding elastic solid deformation, given by $\gamma = \tau/G$. The elastic shear modulus G is given by τ_c/γ_c. The critical stress τ_c is an input value, depending on the flow history, given as initial condition to the flow restart calculation. The material critical deformation γ_c is considered to be a constant value, estimated from rheometric tests. While in the solid state, since deformation rate is considered to be zero, the shear stress can be calculated from a local static force balance assuming incompressible flow $\tau = r(dp/dz)/2$, where r is the radius and dp/dz the pressure gradient in the axial direction.

The solid-liquid transition is characterized here by a deformation higher than the critical value, i.e. $\gamma > \gamma_c$. Once that limit is reached, the flow (continuous deformation) starts and the momentum equation requires an apparent viscosity value. At this point, the solution algorithm calculates the first apparent viscosity as being η_{ref}, according to Eq. (6.11).

However, Eq. (6.11) predicts the viscosity with respect to the fluid structure state to which it was fitted. The values of the parameters of Eq. (6.11), presented in Table 6.1 in Section 6.6, were fitted to data from experiments starting from static cooling conditions. It means that in order to apply that expression to other cooling conditions, as mixed or dynamic cooling (where the critical stress and the following liquid viscosity are lower), without changing its parameters, an

equivalent deformation must be calculated in function of the corresponding critical stress (as presented in Section 6.8) so that the right viscosity value can be predicted for the corresponding structure state.

After the solid-liquid transition, according to Eqs. (6.9) and (6.11), it is required that $\tau_c = \tau_{0,eq} + \tau_0 {\gamma_c}^{-m}$. In this rheological model, the parameters $\tau_{0,eq}$ and τ_0 are constants for the given temperature, whatever the cooling history. So, if the critical stress is not the one obtained from the cooling history to which the model was fitted, an equivalent deformation that fulfills the condition above must be used as the first deformation value for calculating the first viscosity value from Eq. (6.11).

Thus, at solid-liquid transition, the liquid initial deformation is calculated by $\gamma = \left[(\tau_c - \tau_{0,eq})/\tau_0\right]^{-1/m}$. It is equivalent to horizontally translate the original model prediction curve as already shown in Figure 6.9. That equivalent deformation value is in fact the initial condition for Eq. (8.2) when the liquid regime starts.

Finally, the critical stress is also advected, by solving the following equation.

$$\frac{D\tau_c}{Dt} = 0 \tag{8.3}$$

In StartWaCS code, the solution of a transport equation is very efficient. Since the time step is limited by the CFL limit, the explicitly solved TVD scheme presents robust and precise solutions (see Vinay [73]).

8.3.1 Solution algorithm

The general solution algorithm employed in a flow restart simulation may be summarized as follows:

1. Variables and fluid properties initialization. The initial yield stress field is calculated from Eq. (7.3).
2. Calculate the strain field solving Eq. (8.2) and set $\gamma = |\tau|/G$ where $\gamma < \gamma_c$, where the shear stress is calculated by $\tau = r(dp/dz)/2$.
3. Calculate the yield stress field advection solving Eq. (8.3);
4. For the control volumes where $\gamma \geq \gamma_c$, calculate the viscosity field solving Eq. (8.1). If in the previous time step $\gamma < \gamma_c$, calculate the equivalent deformation that matches the yield stress $\gamma = \left[(\tau_c - \tau_{0,eq})/\tau_0\right]^{-1/m}$ and inform the momentum equation that this control volume is now a liquid, by considering its apparent viscosity instead of its yield stress;
5. Solve the VOF transport equation;
6. Update Pressure-Velocity matrix coefficients;
7. Solve the Pressure-Velocity equations system and update the Lagrange's multipliers;
8. Check convergence of the pressure and velocity fields and Lagrange's multipliers. If not converged, return to step 2;
9. Calculate the temperature field;
10. Advance the time step and go to step 2 while the final time is not achieved;

8.4 Flow restart calculation

8.4.1 Boundary conditions, fluid properties and domain discretization

The pipeline of this case study has an internal diameter of 12 in. Its length is 10 km. This configuration could be used, for example, in crude oil transportation from an offshore production unit to another storage or treatment facility. The pipe is considered to be horizontal, with external temperature of 4 °C. The pipe wall is composed by steel and an insulation layer of thickness 1 in (thermal conductivity of 0.4 W/(mK)).

The crude oil A is the waxy oil used in this case. Its temperature at the pipe entrance is fixed at 35 °C. The outlet pressure is kept constant, at 1 bar. The inlet pressure in steady state operation is 3 bar. This differential pressure value was chosen in order obtain laminar flow at the pipe section where the oil achieves the WAT of 22 °C. So, rheological effects are not hidden by turbulence. Moreover, in order to keep the case simple, with a straightforward analysis of the rheological effects, the flow is considered to be incompressible.

The incoming fluid has a constant viscosity of 0.01 Pa.s and the same density as crude oil A.

The pipe is discretized by a staggered grid. The structured mesh has 20 control volumes in the axial direction, with uniform size distribution, and 15 control volumes in the radial direction, with an exponential size distribution. Figure 8.2 illustrates the discretization used. A very simple mesh refinement study was done by solving one case with a two times more refined mesh in the axial direction, since 500 m long control volumes may *a priori* seem too coarse.

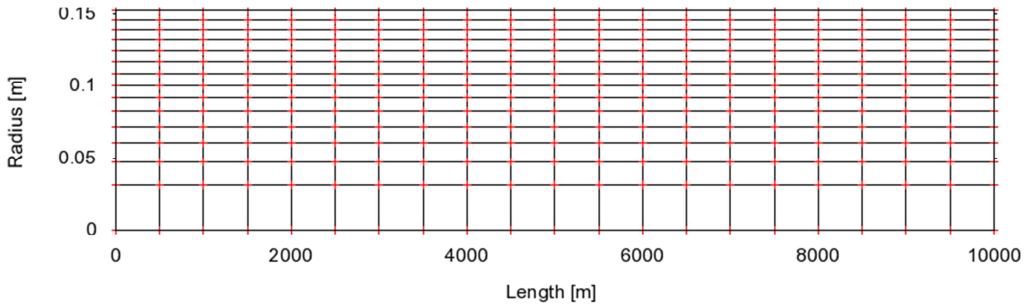

Figure 8.2. Pipe discretization mesh showing the control volumes and mesh nodes in red.

8.4.2 Steady state flow

After entering the pipe at 35 °C, the oil cools while flowing, loosing heat to the pipe wall. As its temperature decreases, the apparent viscosity increases, changing the velocity profile from the classical parabolic profile obtained for uniform viscosity in the pipe section. That will slow the oil layers that are closer to the wall and increase the viscosity heterogeneity in the pipe section.

The temperature field in steady state is shown in Figure 8.3. The dark line marks the iso-temperature of 22 °C, which is the WAT of crude oil A. The average temperature at the exit is 22.7 °C, i.e. an averaged cooling rate of -0.05 °C/min, since the fluid average velocity is 0.68 m/s. While the outlet temperature at the pipe center is still close to 35 °C, the minimum temperature is 10 °C.

If the cooling rate is locally calculated, values are even lower. Taking the stream line at radius 0.12 m, the fluid takes about 30 h to travel through the pipe and loses about 17 °C (difference from 35 °C at the entrance to 18 °C at the exit). Thus, the overall cooling rate at that stream line is -0.01 °C/min.

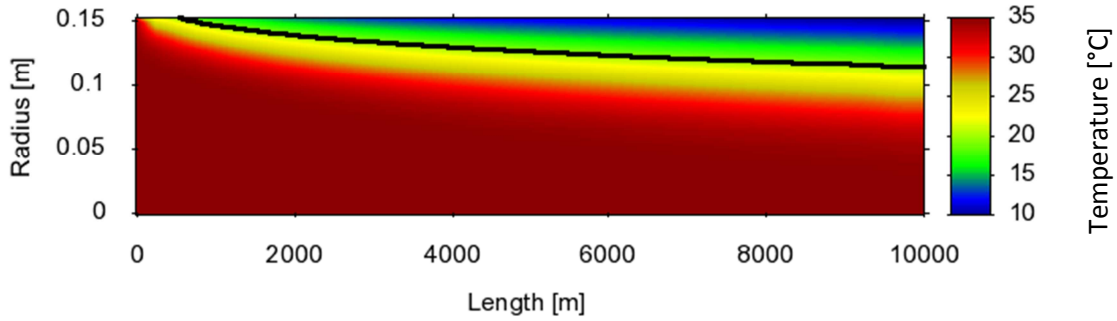

Figure 8.3. Steady state temperature field in the pipe. The dark line marks where the temperature is equal to the WAT of crude oil A, i.e. the iso-temperature of 22 °C.

The velocity profile calculated at the entrance is parabolic, obtained from laminar flow solution. The Reynolds number at the pipe entrance, based on the radial averaged apparent viscosity, is approximately 5300, falling to 4000 at 800 m downstream, where the transition to laminar flow may begin and the flow is completely laminar (Reynolds number lower than 2100) at 1300 m from the entrance. At the pipe exit the Reynolds number is 220.

Figure 8.4 shows the velocity profile evolution along the pipe. A slowing velocity layer can be observed close to the pipe wall. As the average velocity must remain constant, since the flow rate is a constant imposed value at the pipe inlet, at the pipe center the velocity increases, doubling its value. This kind of flow development is the opposite from what would be expected if there were not heat transfer effects. If temperature was constant, the higher shear stress close to the wall would induce high shear rate in that region and consequently lower apparent viscosity, in a shear thinning fluid.

Finally, the flow reduces its velocity close to the pipe wall due to its lower temperature and higher apparent viscosity at low shear rate.

If a wax deposition model was employed, it would predict the paraffinic species migration towards the wall due to the radial temperature gradient. With a higher paraffin concentration in that low shear rate region, it would be reasonable to expect a further increase of the viscosity and perhaps an effectively zero velocity zone due to the high paraffin crystals concentration.

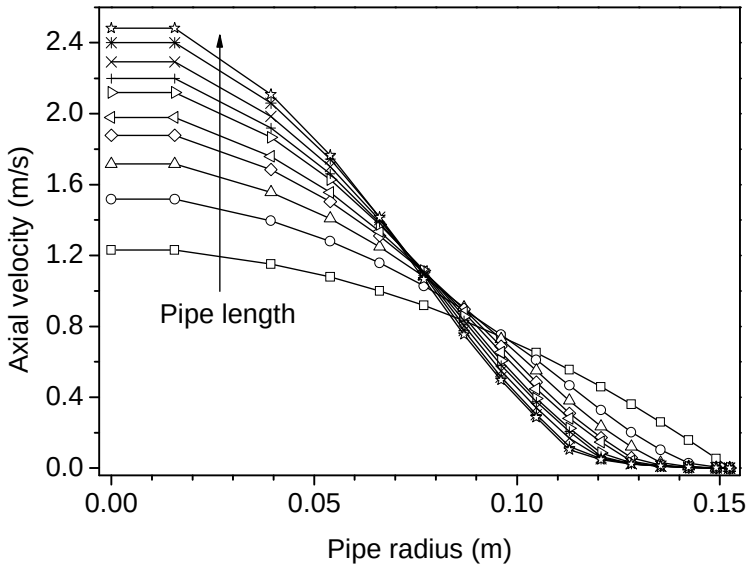

Figure 8.4. Steady state velocity profiles along pipe. Squares correspond to the pipe entrance and the stars to the exit.

8.4.3 Pipeline shut-in

Numerically, the pipeline shut-in is done by setting the entrance velocity to zero. So, instantaneously the flow stops and the remaining of the cooling process happens with the fluid at rest.

Figure 8.5 presents the section average temperature evolution during the 7 days that follow the shut-in (also called cool down time). Until achieving 5 °C at the third day, the average cooling rate was approximately -0.4 °C/h. Then, more 4 days were needed to lose 1 °C.

Flow restart can be predicted at any time after the shut-in. Here, however, complete simulations will be done only with respect to the 7 days after shut-in case. This is because the rheological model parameters were estimated only for the temperature of 4 °C. Employing the same parameters for higher temperatures shall not be valid.

Nevertheless, the minimum differential pressure required to restart the flow can be calculated once a valid yield stress field is set as the simulation initial condition. For calculating the restart pressure value only, it is not necessary to simulate the destructuring flow beyond the critical deformation, since incompressible flow is considered here.

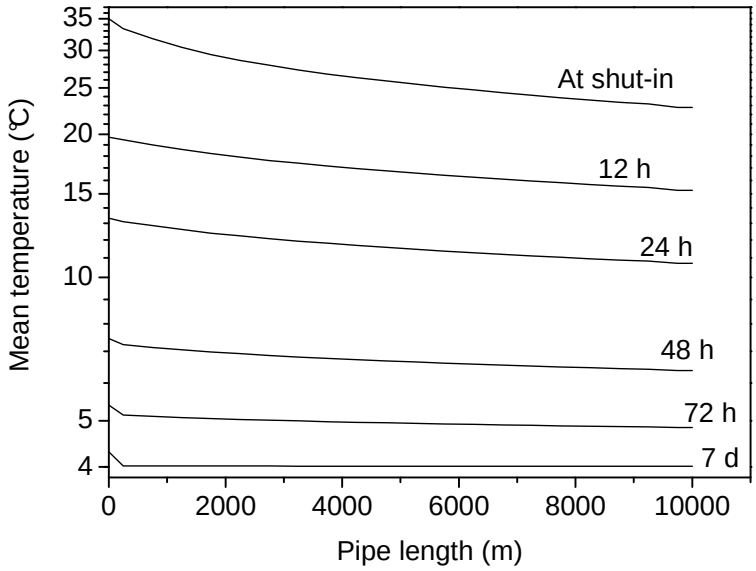

Figure 8.5. Section average temperature evolution during static cooling after the shut-in.

8.4.4 Yield stress field prediction

According to the temperature field at the shutdown moment, i.e. the steady state temperature showed in Figure 8.3, the oil at the exterior of the region delimited by the iso-temperature of 22 °C (i.e. oil close to the pipe wall) will achieve the equilibrium temperature of 4 °C by a mixed cooling process. That shall give rise to a lower yield stress in that region than in the region where the fluid cools down at rest when below the WAT.

The yield stress field at the restart flow moment may be calculated using Eq. (7.3), which is the result of systematic yield stress measurements presented in the previous chapter. The calculated values after 7 days at rest are presented in Figure 8.6. The temperature field at steady state flow presented in Figure 8.3 was used as the input parameter T_{stop} in Eq. (7.3).

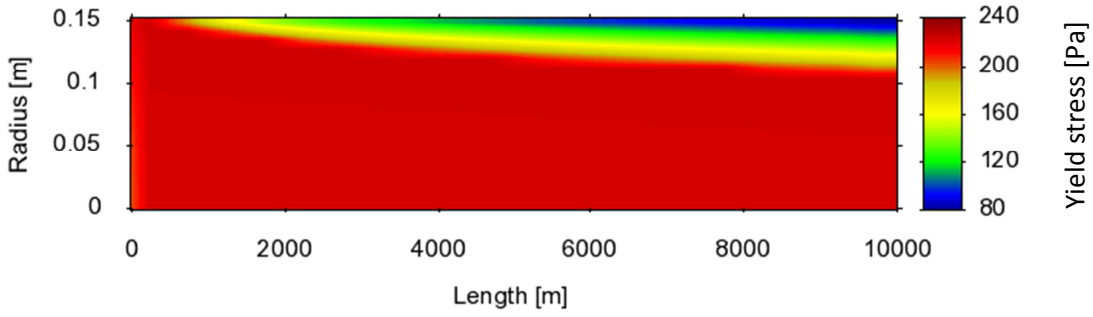

Figure 8.6. Yield stress field used as initial condition of the flow restart simulation, 7 days after the shut-in.

It is interesting to observe that the fluid which presented the higher viscosity during the steady state flow gave rise to the lower yield stress at the restart moment. That is the result of the shear below the WAT, which prevents high yield stress development.

The yield stress field at the flow restart moment can be used to obtain an estimative of the minimum required differential pressure to restart the flow. An integral static force balance provides the following expression for the differential pressure:

$$\Delta P = \frac{2}{R}\int_{z_i}^{z_f} \tau_c(R)dz \tag{8.4}$$

where R is the pipe radius and z_i and z_f are the initial and final axial coordinates.

Thus, the minimum differential pressure to restart the flow for the yield stress field in Figure 8.6 is 161 bar. This minimum pressure is 2 orders of magnitude higher than the steady state pressure drop (3 bar). That estimative does not account for dynamics effects, like the oil compressibility that contributes for lowering that value. On the other hand, recalling the maximum shear stress values measured for different imposed shear rates tests (Figure 5.2), an additional pressure shall be provided to effectively increase the shear rate after overcoming the yield stress. The data in Figure 5.2 show that for starting the flow with an imposed shear rate of 0.1 s^{-1}, the required shear stress is about 35% higher than the yield stress.

This kind of analysis is useful for assessing the restart pressure order of magnitude with simple flow calculations done until this point. However, critical cases shall require a complete flow restart dynamic calculation, in order to reduce the incertitude over that estimative.

8.4.4.1 Restart pressure sensitivity to shut-in duration

The yield stress correlation to cooling parameters given by Eq. (7.3) also allows calculating the yield stress field for intermediate temperatures during the oil cooling. Here, the intermediate temperature fields presented in Figure 8.5 are used as input parameters for the temperature T in Eq. (7.3). It allows estimating the yield stress field for different shut-in periods. Figure 8.7 presents the temperature fields and Figure 8.8 the respective yield stress fields calculated at 12, 24, 48, and 72 h after the pipeline shut-in.

For 12 h after the shut-in, it can be seen that the temperature close to the pipe center line is still higher than the WAT. Thus, the yield stress in that region is zero because the fluid behavior is Newtonian (see Figure 8.8). Therefore, the minimum differential pressure to restart the flow is zero, since the pipe is not completely blocked. In this case there is no meaning in using Eq. (8.4) to calculate the restart pressure, because that integral analysis only accounts for the yield stress at the walls.

The 24 h case is similar, although the temperature is not above the WAT through all the pipe center line, the developed yield stress is still close to zero. Hence, the gel shall be easily broken at the restart moment by the shear stress close to the pipe center.

In the 48 and 72 h cases, it is expected that the gel breaks close to the pipe wall, since the yield stress is lower than at the center. Restart pressure estimated by Eq. (8.4) are 126 and 148 bar, respectively.

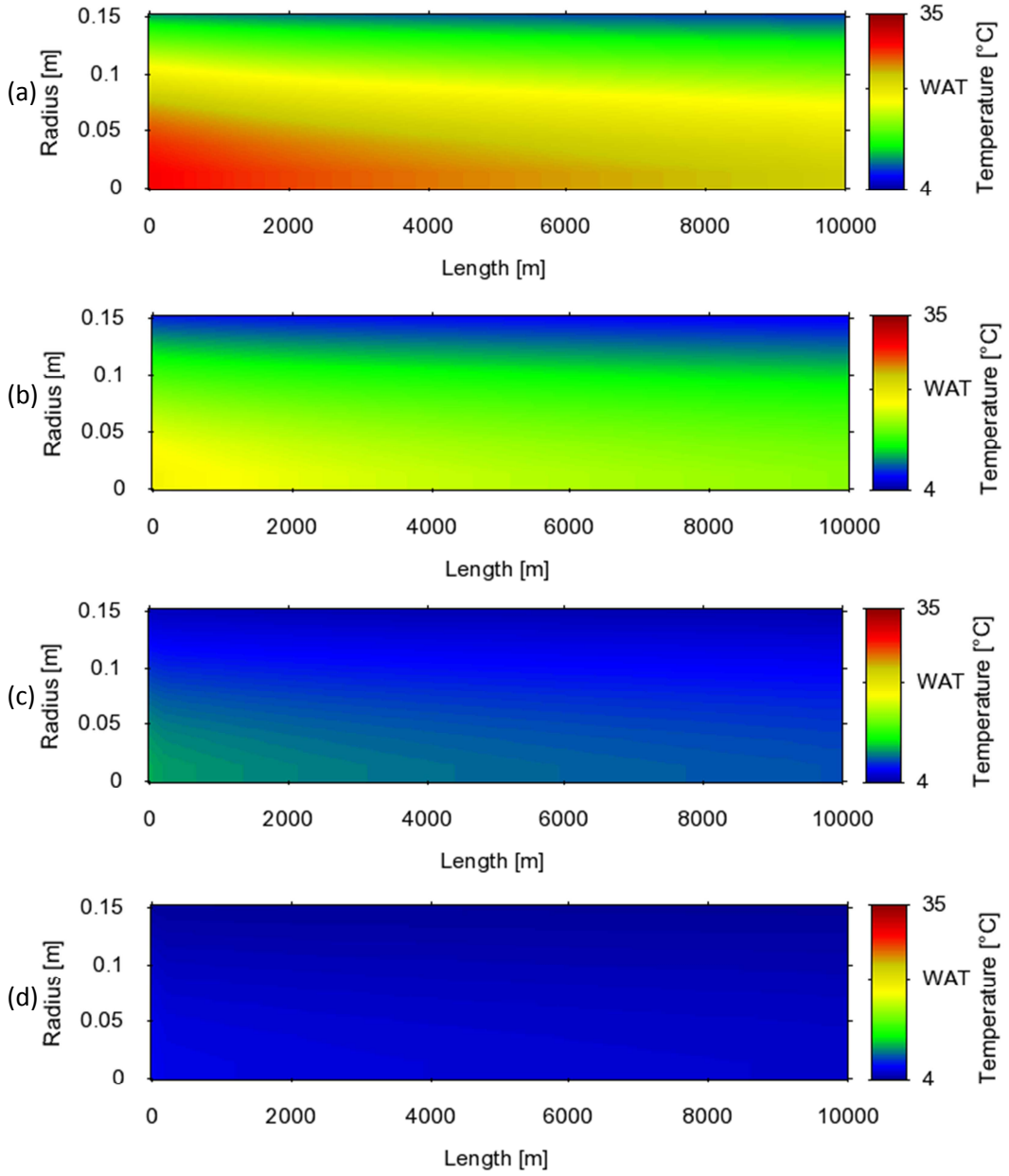

Figure 8.7. Temperature fields for (a) 12, (b) 24, (c) 48 and (d) 72 h after the shut-in.

The image sequence in Figure 8.8 shows that the yield stress takes more time to increase close to the pipe center because the temperature is still high. But while it cools down, at rest, the gel at the center will be stronger than close to the wall. Hence, there is a transition of the gel breakage zone from the pipe center towards the wall as the cool down time increases.

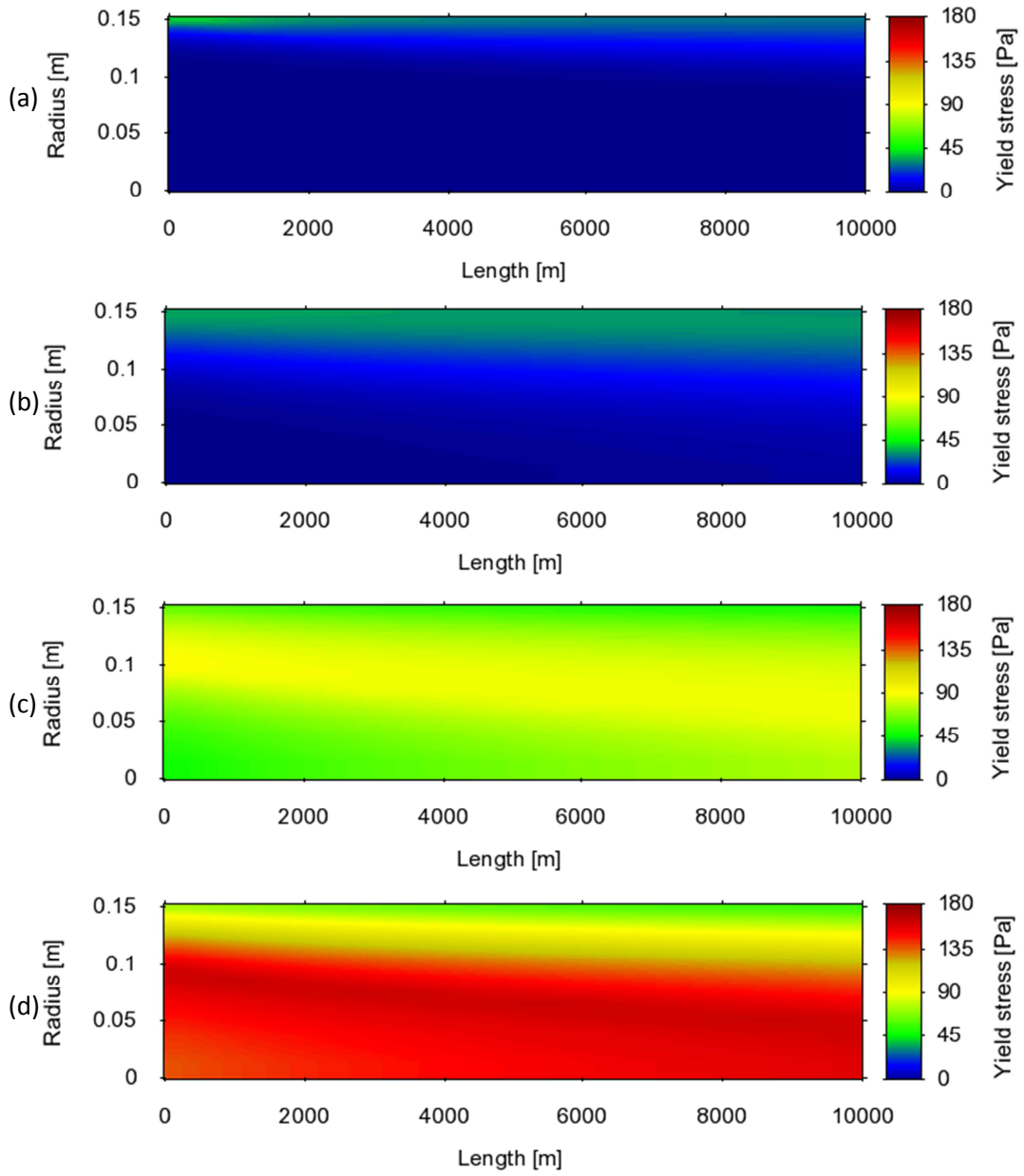

Figure 8.8. Yield stress fields calculated using the respective temperature fields of Figure 8.7. (a) 12, (b) 24, (c) 48 and (d) 72 h after the shut-in.

If the pipe inlet pressure is increased with time, the minimum differential pressure required to restart the flow is said to be achieved at the moment when a continuous broken gel path ($\gamma > \gamma_c$) is formed between the pipe inlet and outlet. Figure 8.9 compares that minimum differential pressure calculated by the two-dimensional simulation of StarWaCS code and the value estimated by the integral analysis (Eq. (8.4)), which accounts only for the fluid yield stress at the pipe wall.

In a first moment, while the gel is broken through the pipe center, Eq. (8.4) overestimates the required differential pressure to restart the flow. But for a flow restart at around 42 h of cool down time the gel breakage starts happening at the pipe wall and the predictions of both calculation methods superimpose. The exact position of the gel breakage front inside the pipe,

where the shear stress becomes higher than the yield stress, may be difficult to predict without a detailed two-dimensional analysis of the yield stress field.

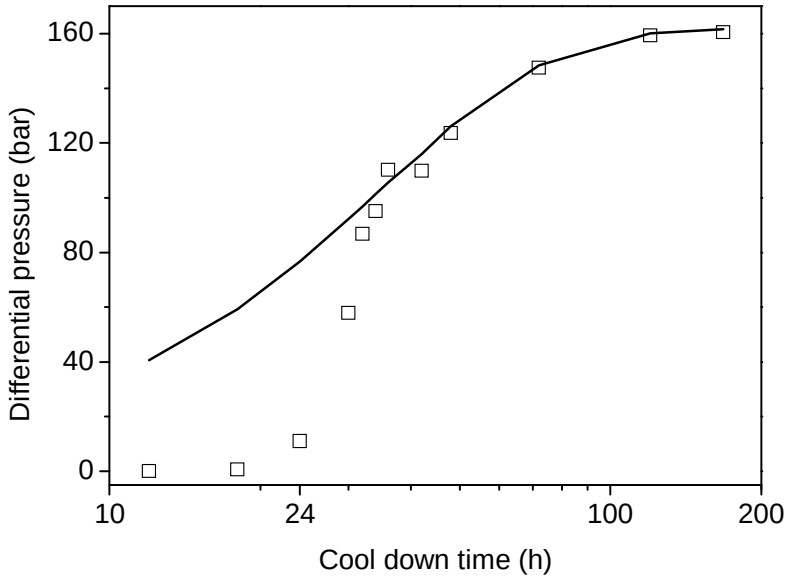

Figure 8.9. Comparison between the differential pressure required to restart the flow calculated by StarWaCS code (symbols) and by Eq. (8.4) (line).

Figure 8.10 presents the comparison between a theoretical shear stress field and the yield stress at three pipe sections also for 36 h after the shut-in. The difference between the yield stress at the different pipe sections reflects the temperature evolution. For the radial positions lower than approximately 0.12 m, the yield stress increases towards the pipe exit, since temperature gets lower in the same direction. For near-wall positions, the yield stress close to the pipe entrance is much higher because that region is being statically cooled when below the WAT. Further downstream pipe sections present mixed cooling at close to the wall, what limits the yield stress development. However, for the cool down time of 36 h the region closer to the pipe wall has lower temperature and therefore higher yield stress than the pipe center.

With the higher gel strengthening during the cool down time in the low radii region, for a restart 48 h after the shut-in, the oil-gel will break mostly at the wall, thus with a minimum restart pressure in accordance with the integral force balance prediction given by Eq. (8.4).

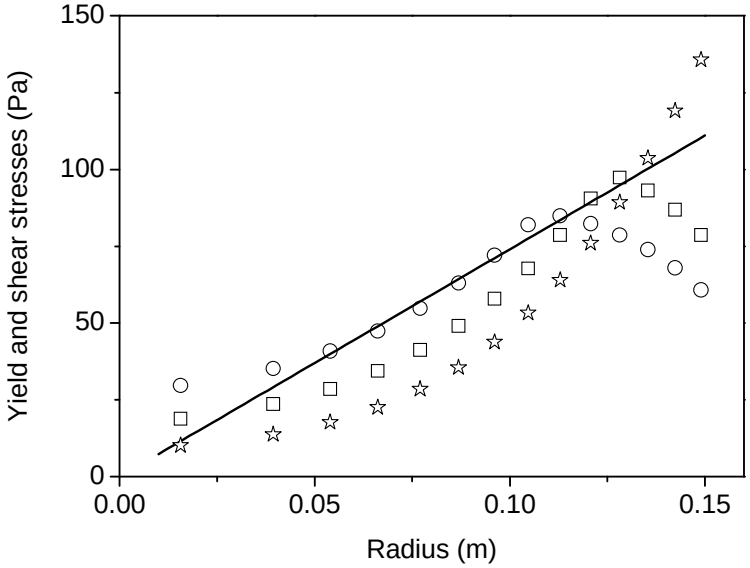

Figure 8.10. Comparison between an theoretical imposed shear stress (line) and the gel yield stress at (stars) 250, (squares) 3750 and (circles) 9750 m from pipe entrance 36 h after the shut-in.

8.4.5 Flow restart results

8.4.5.1 Restart pressure

The flow restart simulation after 7 days of the shut-in event was performed in two parts. In the first part, the inlet boundary condition is set to an increasing pressure ramp. At the flow start moment, the corresponding inlet pressure is the minimum restart pressure. Then, the pressure keeps increasing and the flow rate increases until achieving the same value of the pipeline steady state condition. At that point, the inlet boundary condition is switched to constant imposed flow rate. Next, the destructuring flow continues, the oil-gel is pushed out of the pipe and the inlet pressure reduces while the low viscosity incoming fluid front advances.

The oil temperature after 7 days at rest is close to the ambient temperature, 4 °C. Thus, the yield stress field presented in Figure 8.6 was the initial condition of this simulation. Figure 8.11 presents the differential pressure (imposed pressure ramp) and the calculated flow rates evolution with time until achieving 178 m^3/h, which is the flow rate at the pipeline steady state operation. The differential pressure at the flow restart moment is approximately 161 bar.

The initial gel breakage happens at the pipe wall, where the yield stress is lower and the shear stress higher. Next, the flow evolves with the development of shear layer close to the wall and an internal oil-gel plug, i.e. non-sheared material. That plug is pushed out of the pipe while the incoming fluid front moves forward.

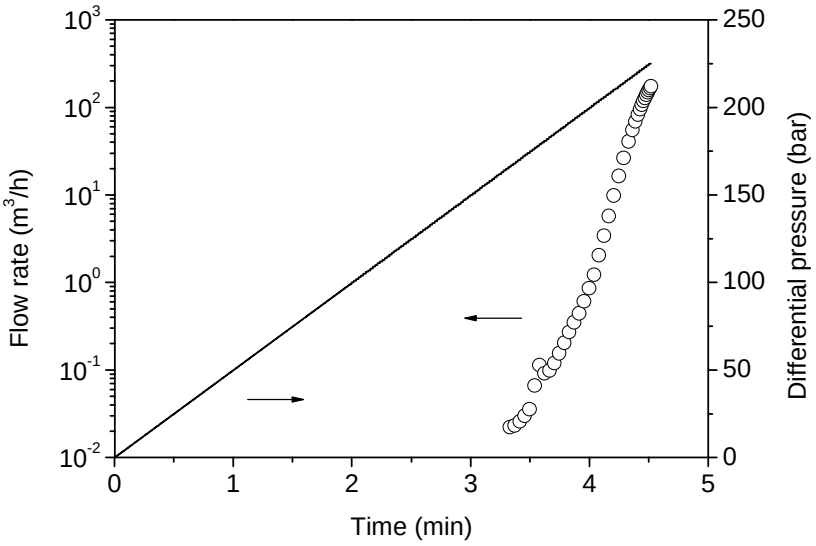

Figure 8.11. Pipe differential pressure (line) and flow rate (circles) evolution with time, until achieving the steady state flow rate of 178 m^3/h.

In this second part of the flow restart simulation the pipe inlet boundary condition is changed from the imposed pressure ramp to constant flow rate. Thus, the inlet pressure becomes a calculated variable.

Figure 8.12 presents the evolution with time of the calculated pipeline differential pressure, until the incoming fluid breakthrough, which happened at approximately 235 min. The continuous line was calculated with 20 control volumes in the axial direction and the dashed line with the double of that value, 40 control volumes. The two curves are superimposing. It shows that predictions obtained with the coarser mesh are already reasonable, even if it is known that 500 m long control volumes may induce numerical diffusion despite the interpolation function accuracy. Additionally, some oscillation in the calculated differential pressure can be observed at different positions of both curves, probably of numerical origin.

At the moment of the boundary condition switch from increasing pressure to constant flow rate, the differential pressure acting on the pipe drops immediately, since there is no more acceleration with time. Then, the differential pressure decreases slowly, as a result of the destructuring flow and the oil-gel expulsion by the incoming fluid.

The observed pressure peak is a result of the imposed boundary condition. If the differential pressure increase is limited to 165 bar, i.e. just above the minimum required value (161 bar), the flow will also restart, but the flow rate increase will take longer. Figure 8.13 shows the flow rate behavior for such condition. It takes about 5 min to reach the operational flow rate value, instead of 1 min for the previous case. That is an important maximal pressure reduction for just 4 min more waiting for the flow rate increase.

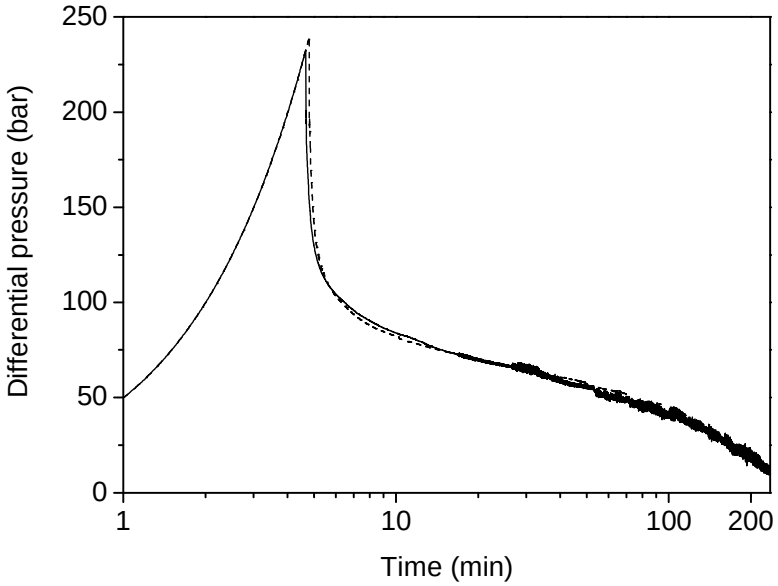

Figure 8.12. Pipeline differential pressure evolution with time until the incoming fluid reaches the pipe exit. The continuous line was obtained with 20 control volumes in the axial direction and the dashed line with 40 control volumes.

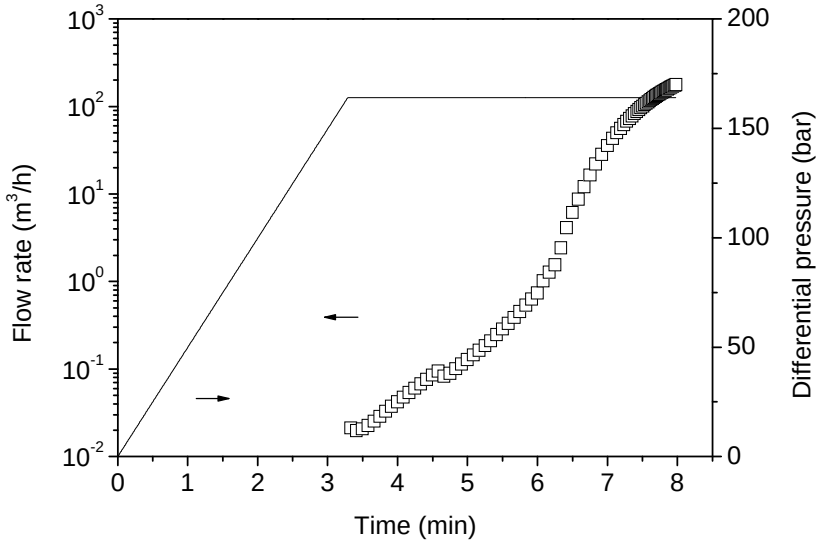

Figure 8.13. Flow rate evolution (symbols) for an increasing differential pressure (line) limited to 165 bar.

8.4.5.2 Gelled oil expulsion

As the incoming fluid enters the pipe, it pushes out the oil-gel. Its lower viscosity makes the incoming fluid flow preferentially at the pipe center, away from the wall where the higher viscosity oil shall flow with lower velocity. The objective here is not to develop a complete study

of fluid displacement, but just highlight some interesting features of the rheological behavior observed in the flow restart simulation.

Figure 8.14 shows the oil-gel velocity field at different moments during its displacement by the incoming fluid, represented in gray. It is possible to see that the oil-gel plug flows at uniform velocity and all the shear happens in a thin layer close to the pipe wall. This heterogeneous velocity field in the cross-section after the flow restart is a similar result to the measured velocity profile in the large Couette cell using the MRI: Due to the heterogeneous stress field, only part of the oil-gel was broken and the shear was limited to a given fluid layer (see Figure 4.17).

As the incoming fluid enters in the pipe, a layer of oil is formed between the advancing front and the pipe wall. The oil in that region was initially sheared, but will remain in the pipe due to its higher viscosity compared to the incoming fluid.

The oil-gel is also destructured due to the normal stress component. This component can be higher than zero due the velocity gradient in the pipe axial direction. It can be observed In Figure 8.14(c) that the interface between the two fluids starts to advance faster at the pipe center. It seems to penetrate the oil-gel plug. Since the yield stress of the oil-gel plug has not changed since the beginning of its displacement and the shear stress field decreases with time (due to pressure decrease, see Figure 8.16), there is no physical reason for this evolution of the interface in the region between the incoming fluid and oil-gel (solid) plug. The oil-gel plug formed after the structure break in the region close to the wall will not be further destructured. Hence, numerical diffusive effects, cumulative in time, are likely the origin of the non-flat shape of the interface. As a result, in the steady state solution, showed in Figure 8.14(d), the interface presents a conical shape beyond 6,000 m from the pipe entrance, overestimating the remaining oil-gel quantity. The use of even finer mesh sizes shall reduce numerical diffusion effects.

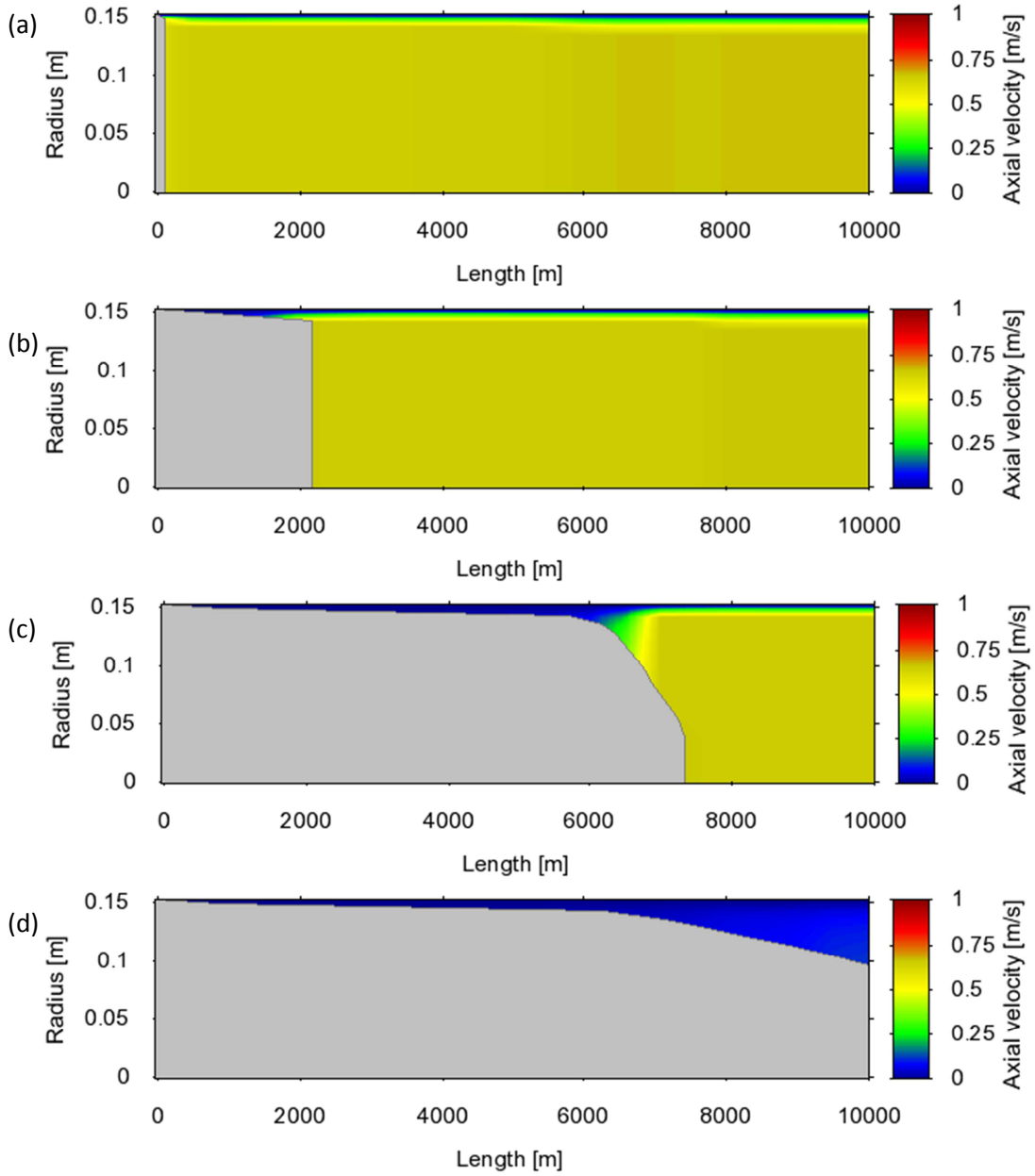

Figure 8.14. Oil velocity fields while being displaced by the incoming fluid, represented in gray, at different simulation times: (a) 5 min; (b) 60 min; (c) 180 min and; (d) steady state.

Nonetheless, that remaining oil-gel quantity is overestimated also because the thermal effects on the oil-gel rheology are not taken into account in this simulation. Figure 8.15, shows the oil-gel temperature increase due to the incoming fluid that enters the pipe at 35 °C. It can be seen that the thin oil-gel sheared layer between the incoming fluid front and the pipe wall is heated to a temperature close to the WAT. It should reduce the oil viscosity in that region, contributing to the pipe cleaning process.

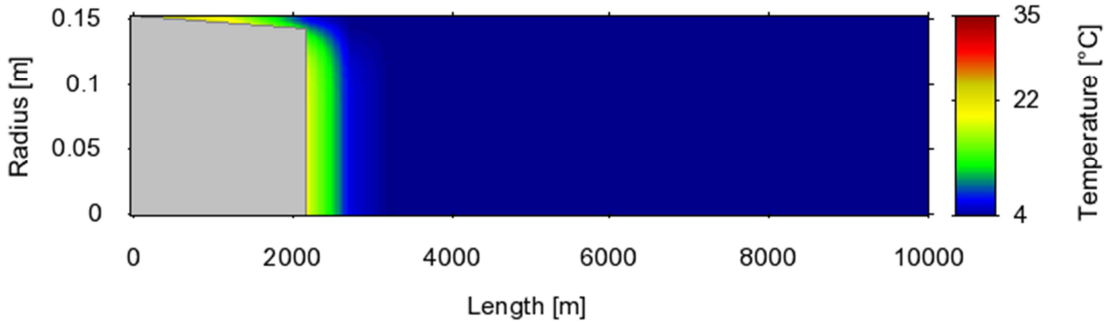

Figure 8.15. Oil-gel temperature field at the simulation time of 60 min. The incoming fluid is represented in gray.

The pipeline pressure profile during the gel expulsion phase is presented in Figure 8.16. The difference between the profiles at 5 and 60 min shows the important differential pressure decrease (already shown in Figure 8.12). Moreover, the pressure drop decreases with time in the oil-gel plug. Consequently, the shear stress also decreases and no further breakage is possible. The oil-gel plug continues with the same shape from the initial structure break. The incoming fluid front can be noticed by the curve slope change.

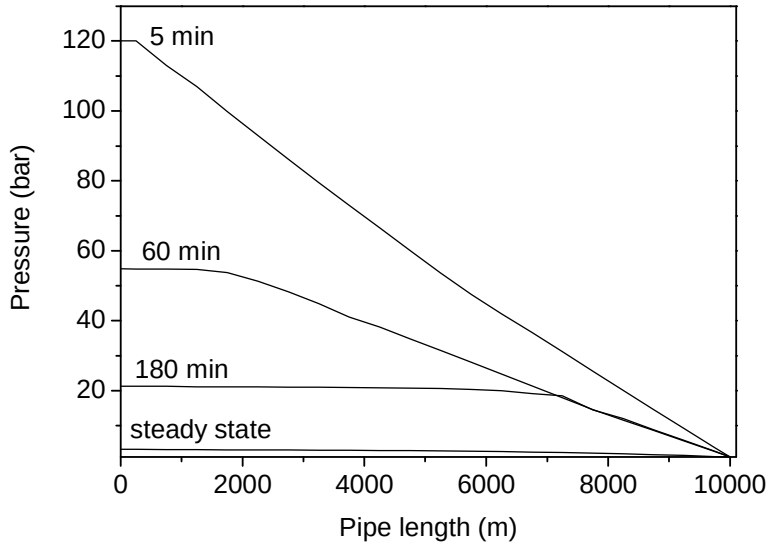

Figure 8.16. Pressure profile evolution during the oil-gel expulsion by the incoming fluid.

It is also interesting noting that the pressure drop in the oil-gel plug region at 60 and 180 min are approximately the same. It means that after 60 min the sheared layer between the oil-gel plug and the pipe wall is close to its equilibrium state.

8.5 Conclusions

The solution of a complete flow restart case allowed applying all the knowledge developed in this work. The complexity of the application scenario exposed the difficulty in dealing with all the physical parameters involved in the flow restart, from the steady state flow until the oil-gel displacement after the restart.

The ColdSart methodology showed to be consistent, providing a guideline for gathering all the information required for reconstructing the yield stress field in the pipe at the flow restart moment. Next, the implementation of the proposed model in a code that already runs the Houska model was straightforward. Adding more transport equations practically did not increase the calculation time, since most of the computing time is spent solving the pressure-velocity system.

The steady state simulation results showed that the velocity profile downstream is not the classical parabolic profile for laminar flow with uniform viscosity in the pipe section. The thermal-dependent rheological parameters resulted in a low velocity in the near wall region and higher velocity at the pipe center. That simulation also showed that cooling rates are low, -0.05 °C/min based on averaged values.

After the pipeline shut-in, the cooling process takes one week to achieve thermal equilibrium with the ambient, for the analyzed conditions. During that period, the yield stress first increases close to the wall, where the fluid is colder. But, the yield stress development in that region is limited, because it was sheared while cooling below in WAT during the steady state flow before the shut-in. At the pipe center the cooling process below the WAT happens with the fluid at rest, allowing the development of a higher yield stress when the temperature decreases. However, at the pipe center the temperature decrease is slower than close to the wall. Thus, the yield stress takes more time to develop in that region.

Consequently, the minimum restart pressure is practically zero if the flow is restarted in the first day after the shut-in. After 48 h, the minimum pressure is the same as the value obtained by an integral force balance on the entire oil-gel plug, since the gel is broken at the pipe wall from that cool down time on.

The destructuring flow simulation using the rheological model proposed here shows that, if pressure is kept at the same order of magnitude of the first gel breakage, the flow rate increase is fast, taking less than 5 min. The oil-gel is pushed out by the incoming fluid as plug. The shear in the oil-gel is located in a thin fluid layer close to the wall.

It would be interesting to compare this simulation results to field data, mainly to check its accuracy in terms of differential pressure and incoming fluid breakthrough prediction. Laboratory scale tests should also be of great value for evaluating the overall calculation methodology and simulation results.

CHAPTER 9

GENERAL CONCLUSIONS

This thesis has studied the rheological behavior of waxy oils, having the flow restart of long subsea pipelines as main application scenario. The focus of this work has been on the development of a better description of that rheological behavior at the different phases of a pipeline flow restart in order to improve the prediction of flow properties.

The literature review has indicated the need for more data (qualitative and quantitative) on the transient flow of gelled waxy crude oils. The interaction between wax crystals, that are at the origin of non-Newtonian and time-dependent rheological properties when the oil is below its WAT, is strongly affected by thermal and flow histories.

The qualitative rheological behavior was first analyzed using MRI-rheometry tests. This technique allows measuring local flow data, which associated with stress measurement provide information on the effective fluid properties, independently of possible flow heterogeneities. Different cooling histories were investigated using an equivalent model waxy oil, with macroscopic behavior analogous to waxy crude oils. Those tests have revealed that the time-dependent behavior of a waxy oil is not the same as in classical thixotropy. In waxy oils, the destructuring flow has important irreversible effects.

For a sample that was cooled under a given flow condition, there is an irreversible structure break each time the fluid is sheared at a new maximum historical shear rate. As long as the fluid is not heated and cooled again, its flow curve is determined by the maximum shear rate experienced by the fluid. The irreversible structure break caused by the new maximum shear rate promotes important reduction of the fluid apparent viscosity. But classical thixotropic behavior is present when the fluid flows with a shear rate below its cooling shear rate or the maximum shear rate it has ever experienced. In this condition, slow and relatively small recoveries of apparent viscosity were measured.

Moreover, it was found that if steady state flow is achieved at a given shear rate and if that is the maximum shear rate experienced by the fluid since its cooling, the waxy oil rheological behavior is independent of the flow history. It means that if the oil was already sheared at that maximum shear rate while cooling or if it cooled at rest and was sheared only afterwards at constant temperature, the resulting rheological behavior is the same.

Despite the original and enlightening conclusions that the MRI-rheometry tests allowed using the model waxy oil, more interesting measurements would be done if temperature control and torque measurement systems were integrated to the MRI apparatus. The measurement of the instantaneous flow curve evolution of real crude oils under controlled temperature would largely increase the quality of the data and reduce the number of experiments, with respect to conventional rheometric tests.

In a second phase of this work, rheometrical tests of destructuring flows of two waxy crude oils were performed and analyzed in details. The destructuring flows measured at constant shear

rate values have showed that, for a series of tests starting from the same initial state, the destructuring rate does not depend on the shear rate but evolves only with the deformation. A higher shear rate allows achieving the steady state flow faster because it deforms the material faster.

When the waxy crude oil is submitted to shear rate step changes during the destructuring flow, it presents different responses according to its structure state. For a strong structure state (low deformations) the response is close to that of HB fluid, i.e. instantaneous shear rate changes are followed by instantaneous viscosity changes. For lower structure states (high deformations) the instantaneous viscosity changes are less important and a progressive viscosity decrease is observed after an increasing step in shear rate, as in a thixotropic material response. But if the shear rate decreases, a progressive increasing viscosity is not observed or it is too small with respect to the instantaneous viscosity increase.

The waxy oil response to shear rate changes evolves with the destructuring flow until steady state flow is achieved. At equilibrium, decreasing the shear rate does not change the viscosity of the previous equilibrium state, a small restructuration is observed only at low shear rates, as $0.1\ s^{-1}$. For increasing shear rate, departing from a steady state condition to a value that overcome the maximum historical shear rate, only progressive viscosity reduction is observed, without instantaneous viscosity changes.

Those observed rheological characteristics were translated into a rheological model. The development of that mathematical model was focused on capturing the global behavior measured with the analyzed waxy crude oils. Thus, the proposed model is based on a constitutive equation as that of a Newtonian fluid, but with variable apparent viscosity. The viscosity evolution during the destructuring flow is calculated by a differential equation taking into account the current flow condition and its history.

The proposed model has showed good quality predictions of the two waxy crude oils rheological behaviors in complex flow histories, not used in the fitting process of the model parameters. Those tests are flow restart tests with imposed shear stress, imposed shear rate up-and-down ramps and constant shear rate followed by a ramp down during the destructuring flow where a yield stress is still present.

The good predictions of the transient rheological response to complex flows show that major physical phenomena are integrated in the model. Nevertheless, some additional features could be considered depending on the application. Waxy crude oils exhibiting non-Newtonian characteristics during the ramp down departing from an equilibrium state would benefit of a more complete constitutive equation than the one proposed here: $\tau = \eta\dot{\gamma}$. Furthermore, if classical thixotropic effects are stronger, an additional reversible structure evolution should be considered. That could be possibly done by adding a structure parameter with a kinetic equation. Experiment procedure should be improved as well in order to evaluate those reversible evolutions.

Next, a comprehensive study of the yield stress in function of flow and temperature histories was realized. It allowed correlating the yield stress with selected cooling parameters. Keeping in mind the scenario of long subsea pipelines (essentially low cooling rates), those selected yield stress parameters are the final cooling temperature and the limit temperature between shearing and static phases of the cooling process. Parameters related to the oil itself are also required, as

the yield stresses after static and dynamic cooling conditions and the WAT. Describing the yield stress in function of parameters of the cooling process is an important step for the flow restart calculation since it defines the yield stress field in the pipe at the restart moment.

Accurately modeling the yield stress in function of the oil cooling history remains a challenging task. The correlation presented here is application-oriented. A more phenomenological solid model accounting for different solid structure states would be an interesting approach.

Finally, the developed correlation for the yield stress and the proposed rheological model were applied in a case study of flow restart numerical simulation of a real scale pipeline. That exercise provided a global view of the methodology used to solve the problem, from the steady state flow to the gelled oil destructuring flow simulations. The implementation of the proposed rheological model with its auxiliary equations in a control volume method framework was also discussed. Flow restart calculations of a case study in function of pipeline shut-in duration have showed that an increase of the minimum required pressure to restart the flow can be expected only after almost 24 h after the shutdown. After 48 h the oil-gel is expected to start flowing by the structure breakdown in the near-wall region. In a simulation of flow restart seven days after the shut-in, where the oil-gel is pushed out of the pipe by an incoming fluid, the near-wall breakdown gives rise to an oil-gel plug flow, with shear located only in a fluid layer close to the wall.

Generally speaking, it cannot be said that the conclusions of this work are valid for any waxy crude oil, since there are many differences between oils produced from different regions in the world. But the same qualitative tendencies of the rheological behavior could be expected, as they origin is in the basic interaction between wax crystals and liquid matrix. Moreover, the methodology of the study develop here is itself a useful guideline for evaluating the rheological behavior of other waxy oils. The successful overall agreement of the developed model with experimental data has showed that the main physical behavior at different flowing conditions were captured.

As an outlook for future developments, some investigations aiming for a better representation of the application scenario can be suggested. First, the heating during the oil destructuring flow shall change its rheological parameters. A better modeling of the waxy oils rheological response to the heat process would increase the accuracy of pipe cleaning predictions, the last stage of the flow restart. Moreover, heating pipes development would benefit from a study of the yield stress behavior of a waxy crude oil that was cooled and then heated again, with the objective of reducing the minimum required pressure to restart the flow.

Another interesting improvement would be the evaluation and modeling of the rheological behavior of gelled water-in-oil emulsions. The main application scenario would be petroleum production flowlines, from subsea wells to topside facilities, for example. The water droplets interaction with the wax crystals network adds complexity to the system, with more parameters to be evaluated, as water content and droplets size distribution. Those improvements should be integrated to more sophisticated pipe flow models, accounting for multiphase flows and the oil thermodynamic behavior, for example.

Challenging production environments require more accurate models. The new rheological description of waxy crude oils presented in this thesis contributes for improving predictions of complex flows. Future developments accounting for additional physical phenomena shall

increase the model accuracy, allowing more reliable projects and opening new perspectives for offshore petroleum production systems architectures.

Published Papers and Conferences

Published papers

R. Mendes, G. Ovarlez, G. Vinay and P. Coussot. “Modeling the rheological behavior of waxy crude oils as a function of flow and temperature history”. Journal of Rheology 59, 2015, 703-732.

R. Mendes, G. Ovarlez, G. Vinay and P. Coussot. “Reversible and irreversible destructuring flow in waxy oils: An MRI study”. Journal of Non-Newtonian Fluid Mechanics, in press, published online in 2014.

Oral presentations in conferences

Presentation “Flow behavior of waxy oils: From local rheology to pipelines” at the 9th Annual European Rheology Conference, Karlsruhe, 2014.

Presentation “Local Rheology Analysis of Waxy Oils” at the international conference Viscoplastic Fluids: From Theory to Application, Rueil-Malmaison, 2013.

REFERENCES

[1] D. J. Abdallah and R. G. Weiss, “n-Alkanes gel n-alkanes (and many other organic liquids)”. Langmuir 16, 2000, 352-355.

[2] A. Ahmadpour and K. Sadeghy, “Start-up flows of Dullaert–Mewis viscoplastic-thixoelastic fluids: A two-dimensional analysis”. Journal of Non-Newtonian Fluid Mechanics 214, 2014, 1-17.

[3] L. A. Alcazar-Vara, J. A. Garcia-Martinez, E. Buenrostro-Gonzalez, “Effect of asphaltenes on equilibrium and rheological properties of waxy model systems”. Fuel 93, 2012, 200-212.

[4] M. G. Cawkwell and M. E. Charles, “Characterization of Canadian artic thixotropic gelled crude oils utilizing an eight-parameter model”. Journal of Pipelines, 1989, 251-264.

[5] C. Chang, D. V. Boger, Q. D. Nguyen, “The yielding of waxy crude oils”. Ind. Eng. Chem. Res. 37, 1998, 1551-1559.

[6] C. Chang, Q. D. Nguyen, H. P. Rønningsen, “Isothermal start-up of pipeline transporting waxy crude oil”. Journal of Non-Newtonian Fluid Mechanics 87, 1999, 127-154.

[7] P. Coussot, A. I. Leonov and J. M. Piau, “Rheology of concentrated dispersed systems in low molecular weight matrix”. Journal of Non-Newtonian Fluid Mechanics 46, 1993, 179-217.

[8] P. Coussot, Q. D. Nguyen, H. T. Huynh and D. Bonn, “Viscosity bifurcation in thixotropic, yielding fluids”. Journal of Rheology 46(3), 2002, 573-589.

[9] P. Coussot, “Rheometry of pastes, suspensions, and granular materials: Applications in industry and environment”. John Wiley & Sons, Inc., Hoboken, NJ, 2005.

[10] P. Coussot, H. Tabuteau, X. Chateau, L. Tocquer, and G. Ovarlez, “Aging and solid or liquid behavior in pastes”. Journal of Rheology 50, 2006, 975-994.

[11] P. Coussot, “Rheophysics of pastes: A review of microscopic modelling approaches”. Soft Matter 3, 2007, 528-540.

[12] M. R. Davidson, Q. D. Nguyen, C. Chang, H. P. Rønningsen, “A model for restart of a pipeline with compressible gelled waxy crude oil”. Journal of Non-Newtonian Fluid Mechanics 123, 2004, 269-280.

[13] M. R. Davidson, Q. D. Nguyen, H. P. Rønningsen, “Restart model for a multi-plug gelled waxy oil pipeline”. Journal of Petroleum Science and Engineering 59, 2007, 1-16.

[14] C. J. Dimitriou, G. H. McKinley, R. Venkatesan, “Rheo-PIV analysis of the yielding and flow of model waxy crude oils”. Energy Fuels 25(7), 2011, 3040-3052.

[15] C. J. Dimitriou and G. H. McKinley, “A comprehensive constitutive law for waxy crude oil: A thixotropic yield stress fluid”. Soft Matter 10, 2014, 6619-6644.

[16] J. Ding, J. Zhang, H. Li, F. Zhang and X. Yang, “Flow behavior of Daqing waxy crude oil under simulated pipelining conditions”. Energy Fuels 20, 2006, 2531-2536.

[17] M. Dirand, V. Chevallier, E. Provost, M. Bouroukba, D. Petitjean, “Multicomponent paraffin waxes and petroleum solid deposits: Structural and thermodynamic state”. Fuel 77(12), 1998, 1253-1260.

[18] K. Dullaert and J. Mewis, “Stress jumps on weakly flocculated dispersions: Steady state and transient results”. Journal of Colloid and Interface Science 287, 2005, 542-551.

[19] K. Dullaert, and J. Mewis, “A structural kinetics model for thixotropy”. Journal of Non-Newtonian Fluid Mechanics 139, 2006, 21–30.

[20] C. Ekweribe, F. Civan, H. S. Lee, P. Singh, “Effect of system pressure on restart conditions of subsea Pipelines”. SPE 115672, 2008.

[21] H. El-Gendy, M. Alcoutlabi, M. Jemmett, M. Deo, J. Magda, R. Venkatesan, A. Montesi, “The propagation of pressure in a gelled waxy oil pipeline as studied by particle imaging velocimetry”. AIChE 58, 2012, 302.

[22] G. P. Van Engelen, C. L. Kaul, B. Vos, H. P. Aranha, “Study of flow improvers for transportation of bombay high crude oil through submarine pipelines”. Journal of Petroleum Technology, 1981, 2539-2544.

[23] M. C. Garcia, L. Carbognani, A. Urbina, M. Orea, “Correlation between oil composition and paraffin inhibitors activity”. SPE 49200, 1998.

[24] I. Hénaut and F. Brucy, “Description rhéologique des bruts paraffiniques gélifiés”. In *Congès du Groupe Français de Rhéologie*, 2001.

[25] I. Hénaut, O. Vincké, F. Brucy, “Waxy crude oil restart: Mechanical properties of gelled oils“. SPE 56771, 1999.

[26] M. Houska, “Engineering aspects of the rheology of thixotropic liquids”. Ph.D. thesis, Faculty of Mechanical Eng., Czech Technical University of Prague-CVUT, Prague, 1981.

[27] H.-Y. Ji, B. Tohidi, A. Danesh, A. C. Todd, “Wax phase equilibria: Developing a thermodynamic model using a systematic approach”. Fluid Phase Equilibria 216, 2004 201-217.

[28] M. Kané, M. Djabourov, J. L. Volle, J. P. Lechaire, G. Frebourg, “Morphology of paraffin crystals in waxy crude oils cooled in quiescent conditions and under flow”. Fuel 82, 2003, 127-135.

[29] M. Kané, M. Djabourov, J. L. Volle, “Rheology and structure of waxy crude oils in quiescent and under shearing conditions”. Fuel 83, 2004, 1591-1605.

[30] H. S. Lee, P. Singh, W. H. Thomason, H. S. Fogler, “Waxy oil gel breaking mechanisms: Adhesive versus cohesive failure”. Energy Fuels 22, 2008, 480-487.

[31] M. Lin, C. Li, F. Yang, Y. Ma, “Isothermal structure development of Qinghai waxy crude oil after static and dynamic cooling”. Journal of Petroleum Science and Technology 77, 2011, 351-358.

[32] J. A. Lopes-da-Silva, J. A. P. Coutinho, “Analysis of the isothermal structure development in waxy crude oils under quiescent conditions”. Energy Fuels 21, 2007, 3612-3617.

[33] J. J. Magda, H. El-Gendy, K. Oh, M. D. Deo, A. Montesi and R. Venkatesan, “Time-dependent rheology of a model waxy crude oil with relevance to gelled pipeline restart”. Energy Fuels 23, 2009, 1311–1315.

[34] F. H. Marchesini, A. A. Alicke, P. R. de Souza Mendes, C. M. Ziglio, “Rheological characterization of waxy crude oils: Sample preparation”. Energy Fuels 26(5), 2012, 2566–2577.

[35] J. Mewis and N. J. Wagner, “Thixotropy”. Advances in Colloidal and Interface Science, 147-148, 2009, 214-227.

[36] S. Misra, S. Baruah, K. Singh, “Paraffin problems in crude oil production and transportation: A review”. SPE Production and Facilities 10, 1995, 50-54.

[37] P. C. F. Møller, J. Mewis, D. Bonn, “Yield stress and thixotropy: On the difficulty of measuring yield stresses in practice”. Soft Matter 2, 2006, 274-283.

[38] P. C. F. Møller, S. Rodts, M. A. J. Michel and D. Bonn, “Shear banding and yield stress in soft glassy materials”. Physical Review E 77, 2008.

[39] K. Oh and M. Deo, “Characteristics of wax gel formation in the presence of asphaltenes”. Energy Fuels 23, 2009, 1289-1293.

[40] Oh, K., M. Jemmett and M. Deo, “Yield behavior of gelled waxy oil: Effect of stress application in creep ranges”. Ind. Eng. Chem. Res. 48, 2009, 8950–8953.

[41] M. C. K. de Oliveira, R. M. Carvalho, A. B. Carvalho, B. C. Couto, F. R. D. Faria, R. L. P. Cardoso, “Waxy crude oil emulsion gel: Impact in flow assurance”. Energy Fuels 24, 2010, 2287-2293.

[42] G. M. Oliveira, L. L. V. Rocha, A. T. Franco, C. O. R. Negrão, “Numerical simulation of the start-up of Bingham fluid flows in pipelines”. Journal of Non-Newtonian Fluid Mechanics 165, 2010, 1114-1128.

[43] G. Ovarlez, S. Rodts, X. Chateau and P. Coussot, “Phenomenology and physical origin of shear localization and shear banding in complex fluids”. Rheol Acta 48, 2009, 831-844.

[44] K. G. Paso, “Comprehensive treatise on shut-in and restart of waxy oil pipelines”. Journal of Dispersion Science and Technology 35(8), 2014, 1060-1085.

[45] K. Paso, M. Senra, Y. Yi, A. M. Sastry, H. S. Fogler, “Paraffin polydispersity facilitates mechanical gelation”. Ind. Eng. Chem. Res. 44, 2005, 7242-7254.

[46] K. Paso, A. Silset, G. Sørland, M. A. L. Gonçalves, J. Sjöblom, “Characterization of the formation, flowability, and resolution of Brazilian crude oil emulsions”. Energy Fuels 23, (2009) 471-480.

[47] Patent US20060130563 (A1), “Method of determining paraffinic crude flow restart conditions”.

[48] J. R. A. Pearson, “Flow curves with a maximum”. Journal of Rheology 38, 1994, 309.

[49] D. A. Philips, I. N. Forsdyke, I. R. McCracken, P. D. Ravenscroft, “Novel approaches to waxy crude restart: Part 1: Thermal shrinkage of waxy crude oil and the impact for pipeline restart”. Journal of Petroleum Science and Technology 77, 2011, 237-253.

D. A. Philips, I. N. Forsdyke, I. R. McCracken, P. D. Ravenscroft, “Novel approaches to waxy crude restart: Part 2: An investigation of flow events following shut down”. Journal of Petroleum Science and Technology 77, 2011, 286-304.

[50] F. Pignon, A. Magnin and J. Piau, “Thixotropic colloidal suspensions and flow curves with minimum: Identification of flow regimes and rheometric consequences”. Journal of Rheology 40, 1996, 573.

[51] J. S. Raynaud, P. Moucheront, J. C. Baudez, F. Bertrand, J.P. Guibaud and P. Coussot, “Direct determination by nuclear magnetic resonance of the thixotropic and yielding behavior of suspensions”. Journal of Rheology 46, 2002, 709.

[52] C. A. Robertson, D. T. Liem, P. Singh, W. H. Thomason, “Practical application of flow assurance and production chemistry”. SPE 127334, 2010.

[53] S. Rodts, F. Bertrand, S. Jarny, P. Poullain, P. Moucheront, “Développements récents dans l’application de l’IRM à la rhéologie et à la mécanique des fluids”. C. R. Chimie, 7, 2004, 275-282.

[54] H. P. Rønningsen, B. Bjorndal, A. B. Hansen, W. B. Pedersen, “Wax precipitation from north sea crude oils. 1. Crystallization and dissolution temperatures, and newtonian and non-Newtonian flow properties”. Energy Fuels 5, 1991, 895-908.

[55] H. P. Rønningsen, “Rheological behaviour of gelled, waxy North Sea crude oils”. Journal of Petroleum Science and Engineering 7, 1992, 177-213.

[56] J. Sestak, M. E. Charles, M. G. Cawkwell, M, Houska, “Start-up of gelled crude oil pipelines”. Journal of Pipelines 6, 1987, 15-24.

[57] P. Singh, R. Venkatesan, H. S. Fogler, N. Nagarajan, “Formation and aging of incipient thin film wax-oil gels”. AIChE Journal 46(5), 2000, 1059-1074.

[58] S. P. Srivastava, H. Jyoti, K. M. Agrawal, G. C. Joshi, “Phase-transition studies in n-alkanes and petroleum-related waxes. A review”. The Journal of Physics and Chemistry of Solids 54(6), 1993, 639-670.

[59] P. R. de Souza Mendes, “Modeling the thixotropic behavior of structured fluids”. Journal of Non-Newtonian Fluid Mechanics 164, 2009, 66-75.

[60] P. R. de Souza Mendes, “Thixotropic elasto-viscoplastic model for structured fluids”. Soft Matter 7, 2011, 2471.

[61] P. R. de Souza Mendes, F. S-M. de Abreu Soares, C.M. Ziglio, M. Gonçalves, “Startup flow of gelled crudes in pipelines”. Journal of Non-Newtonian Fluid Mechanics 179-180, 2012, 23-31.

[62] P. R. de Souza Mendes, R. L. Thompson, “A unified approach to model elastoviscoplastic thixotropic yield-stress materials and apparent yield-stress fluids”. Rheol. Acta 52 (7), 2013, 673–694.

[63] G. Sun, J. Zhang, H. Li, “Structural behaviors of waxy crude oil emulsion gels”. Energy Fuels 28, 2014, 3718-3729.

[64] S. Suppiah, A. Ahmad, C. Alderson, K. Akbarzadeh, J. Gao, J. Shorthouse, I. A. Khan, C. Forde, A. Jamaluddin, “Waxy crude production management in a deepwater subsea environment”. SPE 132615, 2010.

[65] R. I. Tanner, “Engineering Rheology”. Oxford University Press, Oxford, 2000.

[66] H. Teng and J. Zhang, “Modeling the thixotropic behavior of waxy crude”. Ind. Eng. Chem. Res 52, 2013, 8079-8089.

[67] W. H. Thomasson, “Start-up and shut-in issues for subsea production of high paraffinic crudes”. OTC 11967, 2000.

[68] J. F. Tinsley, J. P. Jahnke, H. D. Dettman and R. K. Prud’home, “Waxy gels with Asphaltenes 1: Characterization of precipitation, gelation, yield stress, and morphology”. Energy Fuels 23, 2009, 2056-2064.

[69] R. Venkatesan, P. Singh, H. S. Fogler, “Delineating the pour point and gelation temperature of waxy crude oils”. SPE Journal 7(4), 2002.

[70] R. Venkatesan, J. A, Östlund, H. Chawla, P. Wattana, M. Nydén, J. S. Fogler, “The effect of asphaltenes on the gelation of waxy oils”. Energy Fuels 17, 2003, 1630-1640.

[71] R. Venkatesan, N. R. Nagarajan, K. Paso, Y. B. Yi, A. M. Sastry, H. S. Fogler, “The strength of paraffin gels formed under static and flow conditions”. Chemical Engineering Science 60, 2005, 3587-3598.

[72] R. Venkatesan and J. Creek, “Wax deposition and rheology: Progress and problems from an operator's view”. OTC 20668, 2010.

[73] G. Vinay, “Modélisation du redémarrage des écoulements de bruts paraffiniques dans les conduits pétrolières”. PhD. thesis, École des Mines de Paris, Paris, 2005.

[74] G. Vinay, A. Wachs, J. F. Agassant, “Numerical simulation of non-isothermal viscoplastic waxy crude oil flows”. Journal of Non-Newtonian Fluid Mechanics 128, 2005, 144-162.

[75] G. Vinay, A. Wachs, J. F. Agassant, “Numerical simulation of weakly compressible Bingham flows: The restart of pipeline flows of waxy crude oils”. Journal of Non-Newtonian Fluid Mechanics 136, 2006, 93-105.

[76] G. Vinay, A. Wachs, I. Frigaard, “Start-up transients and efficient computation of isothermal waxy crude oil flow”. Journal of Non-Newtonian Fluid Mechanics 143, 2007, 141-156.

[77] R. F. G. Visintin, R. Lapasin, E. Vignati, P. D'Antona, T. P. Lockhart, “Rheological behavior and structural interpretation of waxy crude oil gels”. Langmuir 21, 2005, 6240-6249.

[78] R. F. G. Visintin, T. P. Lockhart, R. Lapasin, P. D´Antona, “Structure of waxy crude oil emulsion gels”. Journal of Non-Newtonian Fluid Mechanics 149, 2008 34-39.

[79] A. Wachs, G. Vinay, I. Frigaard, “A 1.5D numerical model for the start up of weakly compressible flow of a viscoplastic and thixotropic fluid in pipelines”. Journal of Non-Newtonian Fluid Mechanics 159, 2009, 81-94.

[80] Y. Wang, and Q. Huang, “Evaluation of Measurement Methods of Waxy Crude Oil Thixotropy”. Journal of Dispersion Science and Technology 35(9), 2014, 1255-1263.

[81] Z. Yusof, C. C. Min, D. Sharma, Z. Baoli, S. Krishna, R. A. Elmutalib, “Pipeline restart of waxy crude for Greater Nile Petroleum Operating Company, GNPOC (Sudan)”. Multiphase Production Technology 12, 2005.

[82] Y. Zhao, L. Kumar, K. Paso, J. Safieva, M. Z. B. Sariman and J. Sjöblom, “Gelation behavior of model wax-oil and crude oil systems and yield stress model development”. Energy Fuels 26, 2012, 6323−6331.

[83] Y. Zhao, L. Kumar, K. Paso, H. Ali, J. Safieva and J. Sjöblom, “Gelation and breakage of model wax-oil systems: Rheological properties and model development”. Ind. Eng. Chem. Res. 51, 2012, 8123-8133.